

申 报	系列：教师系列
	科研为主型
	专业：畜牧
	职称：副教授

业绩成果材料

（申报人的业绩成果材料包括论文、科研项目、获奖以及其他成果等）

单 位（二级单位） 动物科学学院

姓 名 蔡柏林

材料核对人：

单位盖章：

核对时间：

华南农业大学制

目 录

一、教学研究业绩

1. 教学研究项目：关于华南农业大学 2024 年度校级教学改革项目的立项通知	1
---	---

二、科研项目

1. 主持的科研项目	
1.1. 主持：关于国家自然科学基金委员会——青年科学基金项目的资助计划书	3
1.2. 主持：关于农业生物育种国家科技重大专项子课题的任务书	11
1.3. 主持：关于国家重点研发计划子课题的任务书.....	21
1.4. 主持：关于 2024 年省级乡村振兴战略专项资金种业振兴行动项目的合同书及联合申报协议书	33
1.5. 主持：关于广东省自然科学基金-面上项目的合同书.	60
1.6. 主持：关于中国博士后科学基金面上资助一等资助项目的资助证书	71
1.7. 主持：关于广州市基础研究计划基础与应用基础研究项目（青年博士“启航”方向）的任务书	72
1.8. 主持：关于华南农业大学特定高校学科建设专项（人才引进类）课题的任务书	82
2. 主参的科研项目	
2.1. 主参：关于农业生物育种国家科技重大专项的课题任务书	88
2.2. 主参：关于 2023 年广州市农业科研项目的立项公示及实施方案	98
三、论文、著作等	
1. 检索证明	123

2. 以第一作者发表本专业论文情况

- 2.1. MYH1G-AS is a chromatin-associated lncRNA that regulates skeletal muscle development in chicken. 126
- 2.2. Long noncoding RNA ZFP36L2-AS functions as a metabolic modulator to regulate muscle development 151
- 2.3. LncEDCH1 improves mitochondrial function to reduce muscle atrophy by interacting with SERCA2..... 163
- 2.4. circPTPN4 regulates myogenesis via the miR-499-3p/NAMPT axis 179
- 2.5. LncEDCH1 g.1703613 T>C regulates chicken carcass traits by targeting miR-196-2-3p 194

3. 以通讯作者发表本专业论文情况

- 3.1. PPM1J regulates meat quality feature and glycerophospholipids composition in broiler by modulating protein dephosphorylation 208

四、科研成果

1. 知识产权

- 1.1. 专利授权证书：与鸡屠体性状相关的 CYP27A1 单核苷酸多态性分子标记及应用 219
- 1.2. 专利授权证书：与鸡屠体性状相关的 SERCA2 基因分子标记及其应用 220
- 1.3. 专利授权证书：一种应用于小白鸡青脚性状的分子检测方法及其应用 221
- 1.4. 专利授权证书：与鸡屠体性状相关的 CRELD1 基因分子标记及应 222

五、其他业绩

1. 指导学生学科竞赛

1.1. 第十七届“挑战杯”广东大学生课外学术科技作品竞赛 一等奖	223
2. 其他业绩	
2.1. Journal of Animal Science and Biotechnology 最佳 论文奖	224

一、教学研究业绩

1. 教学研究项目：关于华南农业大学2024年度校级教学改革项目的立项通知

学校概况 机构设置 师资队伍 人才培养 科学研究 社会服务 校园文化 对外交流 招生就业 学校标识 信息公开 来访预约

校内通知

所有通知 机关部处 教学单位 教辅/科研单位 群团/附属单位

首页

关于公示2024年度校级本科教学质量与教学改革工程项目拟立项名单的通知

来源单位及审核人： 编辑： 审核发布：本科生院（招生办公室） 发布时间：2024-07-29

各学院、部处、各单位：

根据《关于开展2024年度校级本科教学质量与教学改革工程项目申报工作的通知》精神,经项目负责人申报、所在单位推荐和学校组织专家评审等程序,拟立项“基于大湾区新能源汽车人才需求的智能网联技术课程改革”等121个项目为2024年度校级教学改革项目;拟立项“涉外法治人才培养实验班”等36个项目为2024年度校级质量工程项目;根据学校年度人才培养工作重点及本年度申报项目质量,拟立项“‘长基计划’下新文科历史学课程体系的改革与实践”等11个项目为2024年度“长基计划”教学质量和教学改革工程专项项目(经费由“长基计划”专业专项资金资助)。教改招标项目因不符合立项指南要求,不予立项。现予以公示,具体名单见附件。

公示期自2024年7月29日至8月3日。如有异议,请在公示期内以书面方式提交(附必要的证据材料,并署真实姓名),未署真实姓名或逾期者不予受理。

附件: [1. 华南农业大学2024年校级教学改革拟立项名单.xlsx](#)
[2. 华南农业大学2024年校级质量工程拟立项名单.xlsx](#)
[3. 华南农业大学2024年度校级“长基计划”教学质量和教学改革工程专项拟立项名单.xlsx](#)

联系人: 孙齐胜
电 话: 85288020 (15192666549)
地 址: 行政楼329
邮 箱: gjyj@scau.edu.cn

本科生院(招生办公室)
2024年7月29日

分享至:

最新动态

2024-11-27

关于做好2024届本科毕业生(12月批)毕业审核和学位授予资格审核...

2024-11-22

关于录入2024-2025学年度第一学期期末成绩的通知

2024-11-15

关于全国大学英语四、六级口语考试的通知

2024-11-14

关于我校2024年新文科实践创新大赛晋级校赛现场赛项目的公示

2024-11-13

关于公布2024-2025学年第一学期期末集中考试安排的通知

联系我们 地址: 广州市天河区五山华南农业大学 邮编: 510642 管理登录

序号	项目编号	项目类别	单位	项目名称	负责人	项目组成员
104	JG2024104	自筹项目	经济管理学院	数字化转型下的新文科经管类虚拟实验室建设改革探索	李巧璇	蔡键、何勤英、潘逵、宋冰洁
105	JG2024105	自筹项目	数学与信息学院、软件学院	就业创业课程教学内容优化与实践 ——基于大学生劳动法律风险应对能力提升的研究	张佳午	徐海婵、杨莹、张俊韬
106	JG2024106	自筹项目	生命科学学院	“慢就业”背景下基于 OBE 理念的大学生“就业+心理”课程体系改革研究	梁辰	方媛媛、梁春江、何晁毓、郭雪倩
107	JG2024107	自筹项目	公共管理学院	新文科背景下公共管理专业大数据课程建设的探索与实践	刘志明	贾海薇、游艳玲、张小娟
108	JG2024108	自筹项目	文博馆	高校农博馆传承农耕文化的路径探讨—— 以华南农业博物馆为例	刘峻嵘	王茹、刘明骞、李薇、陆炜斌
109	JG2024109	自筹项目	电子工程学院 (人工智能学院)	基于数字化评价的模电实验教学改革	殷惠莉	李震、薛秀云、孙道宗、张霞
110	JG2024110	自筹项目	动物科学学院	基于OBE教育理念的动物遗传学课程教学改革与实践	蔡柏林	张细权、聂庆华、黎镇晖、刘满清
111	JG2024111	自筹项目	数学与信息学院、软件学院	人工智能赋能《数理统计》课程混合教学的探索与实践	朱玲湘	陈银辉、利小玲、夏英俊
112	JG2024112	自筹项目	体育教学研究部	混合教学中线上线下教学一体化设计 ——以华南农业大学《空手道思政课程》为例	黄飞	邵东明、贾力运、于江杨、吕立
113	JG2024113	自筹项目	生命科学学院	新农科背景下《大学生职业生涯发展与就业力提升》课程思政设计与实践	郭雪倩	何晁毓、周毅、梁春江、申佐佐
114	JG2024114	自筹项目	人文与法学学院	习近平法治思想融入法学实践教学研究 ——以模庭课程为例	王琳	杜国明、刘万洪、易晓芸、肖蕙
115	JG2024115	自筹项目	图书馆	高校虚拟教研室建设与图书馆嵌入式服务研究	周立军	杨德惠、时卫锋、程燕峰、卢炳卫
116	JG2024116	自筹项目	林学与风景园林学院	高校学生会组织功能型团支部建设的探索与实践	喻凯	陈锐帆、王国辽、陈刚、解加米
117	JG2024117	自筹项目	生物质工程研究院	能源化学课程与教学内容改革与建设	钟家伟	魏国强、姚业成
118	JG2024118	自筹项目	文博馆	本科教学评估视域下高校试卷档案信息化管理新模式研究	叶小泮	陈国华、王敏虹、姜峥
119	JG2024119	自筹项目	植物保护学院	激发科研意识的思政教学在本科分子生物学课程教学中的应用	阮小蕾	饶雪琴、李鹏飞
120	JG2024120	自筹项目	动物科学学院	优化实践平台提高桑树学教学质量的改革探索	刘伟强	刘吉平、黄志君、易辉玉
121	JG2024121	自筹项目	艺术学院	农业院校影视动画专业助力乡村振兴战略的实践探索	刘瑞	刘红斌、辛珏、石娟娟、苏珊珊

二、科研项目

1.1. 主持：关于国家自然科学基金委员会——青年科学基金项目的资助计划书



项目批准号	32302728
申请代码	C1703
归口管理部门	
依托单位代码	51064208A0499-0932



国家自然科学基金
资助项目计划书
(包干制项目)

资助类别： 青年科学基金项目

亚类说明：

附注说明：

项目名称： ALKBH5介导lncRNA MSTRG. 14465可变剪接调控鸡骨骼肌发育的机制研究

资助经费： 30万元 执行年限： 2024.01-2026.12

负 责 人： 蔡柏林

通讯地址： 广东省广州市天河区五山华南农业大学

邮政编码： 510642 电 话： 13580356512

电子邮件： bolincai@scau.edu.cn

依托单位： 华南农业大学

联 系 人： 唐家林 电 话： 020-85280070

填表日期： 2023年08月25日



国家自然科学基金资助项目计划书填报说明 （包干制项目）

- 一、项目负责人收到《国家自然科学基金资助项目批准通知》（以下简称《批准通知》）后，请认真阅读本填报说明，参照国家自然科学基金相关项目管理办​​法和新修订的《国家自然科学基金资助项目资金管理办法》（以下简称《资金管理办法》，请查阅国家自然科学基金委员会官方网站首页“政策法规”栏目），按《批准通知》的要求认真填写和提交《国家自然科学基金资助项目计划书》（以下简称《计划书》）。
- 二、填写《计划书》时要科学严谨、实事求是、表述清晰、准确。《计划书》经国家自然科学基金委员会相关项目管理部门审核批准后，将作为项目研究计划执行、检查和验收的依据。
- 三、《计划书》各部分填写要求如下：
 - （一）简表：由系统自动生成。
 - （二）摘要及关键词：各类获资助项目都应当填写中、英文摘要及关键词。
 - （三）正文：
 1. 青年科学基金项目：如果《批准通知》所附“项目评审意见及修改意见表”中“修改意见”栏目没有修改要求的，只需选择“研究内容和研究目标按照申请书执行”即可；如果《批准通知》中上述栏目明确要求调整研究期限或研究内容等的，须选择“根据研究方案修改意见更改”并填报相关修改内容。
 2. 国家杰出青年科学基金项目和优秀青年科学基金项目按下列提纲撰写：
 - （1）研究方向；
 - （2）结合国内外研究现状，说明研究工作的学术思想和科学意义（限两个页面）；
 - （3）研究内容、研究方案及预期目标（限两个页面）；
 - （4）年度研究计划；
 3. 科技管理专项项目按下列提纲撰写：
 - （1）科技战略研究领域方向；
 - （2）结合该领域国内外研究现状及发展趋势，分析科学基金资助战略与政策（限两个页面）；
 - （3）研究内容、研究方案及预期目标（限两个页面）；
 - （4）年度研究与实践计划。
- 四、资助经费相关要求：
 1. 资助经费批准时不再区分直接费用和间接费用。
 2. 项目负责人在提交计划书时需签署承诺书，承诺尊重科研规律，弘扬科学家精神，遵守科研伦理道德和作风学风诚信要求，认真开展科学研究工作；承诺项目经费全部用于与本项目研究工作相关的支出，不得用于与本项目研究无关的支出。
 3. 项目负责人提交计划书时，无需编制项目预算。项目资金由项目负责人自主决



定使用，按照《资金管理办法》第九条规定的开支范围列支。有关管理费用的补助支出，由依托单位根据实际管理需要，在充分征求项目负责人意见基础上合理确定。绩效支出由项目负责人根据实际科研需要和相关薪酬标准自主确定，依托单位按照工资制度进行管理。其余用途经费无额度限制，由项目负责人根据实际需要自主决定使用。

4. 项目结题时，项目负责人根据实际使用情况编制项目经费决算，经依托单位财务、科研管理部门审核后，报自然科学基金委。依托单位应当在单位内部公开非涉密项目立项、主要研究人员、资金使用（重点是间接费用、外拨资金、结余资金使用等）、决算、大型仪器设备购置以及项目研究成果等情况，接受内部监督。
5. 自然科学基金委结合项目管理，对经费使用情况和依托单位管理情况定期开展抽查。



简表

项目负责人信息	姓 名	蔡柏林	性 别	男	出生年月	1992年10月	民 族	汉族
	学 位	博士			职称	副教授		
	是否在站博士后	否			电子邮件	bolincai@scau.edu.cn		
	电 话	13580356512			个人网页			
	工 作 单 位	华南农业大学						
	所 在 院 系 所	动物科学学院						
依托单位信息	名 称	华南农业大学					代码	51064208A0499
	联 系 人	唐家林			电子邮件	kycjkh@scau.edu.cn		
	电 话	020-85280070			网站地址	http://kjc.scau.edu.cn/		
合作单位信息	单 位 名 称							
项目基本信息	项 目 名 称	ALKBH5介导lncRNA MSTRG.14465可变剪接调控鸡骨骼肌发育的机制研究						
	资 助 类 别	青年科学基金项目				亚 类 说 明		
	附 注 说 明							
	申 请 代 码	C1703:家禽及其他经济动物种质资源与遗传育种学						
	基 地 类 别							
	执 行 年 限	2024.01-2026.12						
	资 助 经 费	30万元						



项目摘要

中文摘要:

作为基因组中极具数目的转录物，lncRNAs在鸡骨骼肌发育过程中发挥重要的调控作用。然而，关于骨骼肌发育相关lncRNA形成和表达的调控机理尚鲜有报道。整合前期MeRIP-seq、Iso-seq及RNA-seq结果并结合分子实验验证，申请人率先发现m6A去甲基化酶ALKBH5介导调节了lncRNA MSTRG.14465可变剪接的发生，但该过程的确切机制仍待探寻。本项目拟选定MSTRG.14465作为研究对象，综合利用MeRIP、SELECT和ChIRP等技术，系统揭示ALKBH5介导MSTRG.14465可变剪接的分子途径，并以MSTRG.14465不同剪接异构体互作调控RNA结合蛋白为切入点，深入探究由ALKBH5介导调节的MSTRG.14465不同剪接异构体对鸡骨骼肌发育的调控功能。预期成果将有助于更精细地理解鸡骨骼肌发育的表观遗传调控规律，并为鸡肉品质的改良提供理论依据。

Abstract:

As a large number of transcripts in the genome, lncRNAs play important roles in the regulation of chicken skeletal muscle development. However, the regulatory mechanism of the formation and expression of skeletal muscle development related-lncRNAs is still poorly understood. By analyzing our previous MeRIP-seq, Iso-seq and RNA-seq data and verified by molecular experiments, we were the first to discover that ALKBH5 (which is a m6A demethylase) mediated alternative splicing of lncRNA MSTRG.14465. But the exact mechanism of this process remains to be explored. Here, we plan to select MSTRG.14465 as the research object, and perform a series of molecular biology experiments to systematically reveal the molecular pathway of ALKBH5-mediated alternative splicing of MSTRG.14465. Furthermore, we try to investigate the molecular mechanism of chicken skeletal muscle development regulated by the interaction between ALKBH5-mediated different splicing isoforms of MSTRG.14465 and RNA binding proteins. The outcome of this project will help us to understand the epigenetic regulation process of skeletal muscle development more elaborate, and provide a molecular theoretical foundation for the improvement of muscle quality in chicken.

关键词(用分号分开): 鸡; 非编码RNA; m6A修饰; 可变剪接; 骨骼肌发育

Keywords(用分号分开): Chicken; Non-coding RNA; m6A modification; Alternative splicing; Skeletal muscle development



报告正文

研究内容和研究目标按照申请书执行。



国家自然科学基金项目负责人、依托单位承诺书

国家自然科学基金项目负责人承诺书

本人郑重承诺：我接受国家自然科学基金的资助，严格遵守中共中央办公厅、国务院办公厅《关于进一步加强科研诚信建设的若干意见》《关于进一步弘扬科学家精神加强作风和学风建设的意见》《关于加强科技伦理治理的意见》等规定，及国家自然科学基金委员会关于资助项目管理、项目资金管理等各项规章，在《计划书》填写及项目执行过程中：

（一）按照《批准通知》《国家自然科学基金资助项目计划书填报说明》的要求填写《计划书》，未自行降低、更改目标任务或约定要求，或缩减研究（研制）内容；

（二）树立“红线”意识，严格履行科研合同义务，按照《计划书》负责实施本项目（批准号：32302728），切实保证研究工作时间，按时报送有关材料，及时报告重大情况变动，不违规将科研任务转包、分包他人，不以项目实施周期外或不相关成果充抵交差；

（三）遵守科研诚信、科技伦理规范和学术道德，认真开展研究工作，对资助项目发表的论著和取得的科研成果按规定进行标注，不在非本项目资助的成果或其他无关成果上标注本项目批准号，反对无实质学术贡献者“挂名”，不在成果署名、知识产权归属等方面侵占他人合法权益，并如实报告本人及项目组成员发生的违背科研诚信要求的任何行为；

（四）尊重科研规律，弘扬科学家精神，严谨求实，追求卓越，反对浮夸浮躁、投机取巧，不人为夸大学术或技术价值，不传播未经科学验证的现象和观点；

（五）将项目资金全部用于与本项目研究工作相关的支出，并结合科研活动需要，科学合理安排项目资金支出进度；

（六）做好项目组成员的教育和管理，确保遵守以上相关要求。

如违背上述承诺，本人愿接受国家自然科学基金委员会和相关部门做出的各项处理决定。

项目负责人（签字）：

年 月 日

国家自然科学基金项目依托单位承诺书

我单位同意承担上述国家自然科学基金项目，将保证项目负责人及其研究队伍的稳定和研究项目实施所需的条件，严格遵守国家自然科学基金委员会有关资助项目管理、项目资金管理、科研诚信管理和科技伦理管理等各项规定，并督促实施。

依托单位（公章）

年 月 日



国家自然科学基金资助项目签批审核表

本 栏 目 由 自 然 科 学 基 金 委 填 写	科学处审查意见：	负责人（签章）： 年 月 日
	科学部审查意见：	负责人（签章）： 年 月 日

1.2. 主持：关于农业生物育种国家科技重大专项子课题的任务书

课题编号： 2023ZD0406401

农业生物育种重大项目 子课题任务书

子 课 题： 黄羽肉鸡种质资源的三维基因组景观研究

所属项目： 优质加工型肉鸡新品种设计与培育

所属课题： 种质资源优异性状挖掘及多组学解析

委托部门（甲方）： 华南农业大学

承担部门（乙方）： 华南农业大学

2023 年 9 月



填写说明

- 1、任务书为课题验收的依据，其各项内容应尽可能详细填写。
- 2、课题目标要强调形成主导品种（产品、装备）、主推技术、重要标准（规程规范）、决策支持方案、知识产权等；考核指标应具体、量化、可考核。按已提交的实施方案进行填报，不得私自减少任务指标。
- 3、经费的使用应严格按有关经费管理办法执行。
- 4、开户银行及账号应是课题参加单位计财部门的开户行和账号。
- 5、本任务书要求用 A4 纸、正文四号仿宋_GB2312。
- 6、任务书正式文本一式捌份。

课题名称		种质资源优异性状挖掘及多组学解析					
子课题名称		黄羽肉鸡种质资源的三维基因组景观研究					
所属项目		优质加工型肉鸡新品种设计与培育					
子经费预算		总需求 100 万元，其中中央财政专项资金需求 100 万元					
子课题周期节点		起始时间	2023 年 09 月		结束时间	2025 年 12 月	
		实施周期	共 28 个月		预计中期时间点	2024 年 12 月	
课题承担单位	单位名称	华南农业大学			单位法定代表人姓名	薛红卫	
	单位性质	大专院校			组织机构代码	124400004554165634	
	单位主管部门	广东省教育厅			隶属关系	省属	
	单位所属地区	广东省			地市（市、自治州、盟）	广州市天河区	
	通信地址	广东省广州市天河区五山路 483 号			邮政编码	510642	
	单位开户名称	华南农业大学					
	开户银行（全称）	中国工商银行股份有限公司广州五山支行			汇入地点	广东省广州市	
	银行账号	3602002609000310520			银行机构代码	102581000546	
课题负责人	姓 名	聂庆华	性 别	<input checked="" type="checkbox"/> 男 <input type="checkbox"/> 女		出生日期	1975-12-18
	证件类型	身份证	证件号码	342824197512182714			
	所在单位	华南农业大学					
	最高学位	<input checked="" type="checkbox"/> 博士 <input type="checkbox"/> 硕士 <input type="checkbox"/> 学士 <input type="checkbox"/> 其他					
	职 称	<input checked="" type="checkbox"/> 正高级 <input type="checkbox"/> 副高级 <input type="checkbox"/> 中级 <input type="checkbox"/> 初级 <input type="checkbox"/> 其他				职务	副院长
	电子邮箱	nqinghua@scau.edu.cn		移动电话		13922195759	
子课题承担单位	单位名称	华南农业大学	单位法定代表人姓名	薛红卫			
	单位性质	华南农业大学	组织机构代码	124400004554165634			
	单位主管部门	广东省教育厅	隶属关系	省属			

	单位所属地区	广东省	地市（市、自治州、盟）	广州市天河区		
	通信地址	广东省广州市天河区五山路 483 号	邮政编码	510642		
	单位开户名称	华南农业大学				
	开户银行（全称）	中国工商银行股份有限公司广州五山支行	汇入地点	广东省广州市		
	银行账号	3602002609000310520	银行机构代码	102581000546		
子课题 负责人	姓 名	蔡柏林	性 别	<input checked="" type="checkbox"/> 男 <input type="checkbox"/> 女	出生日期	1992-10-09
	证件类型	身份证	证件号码	440111199210094218		
	所在单位	华南农业大学				
	最高学位	<input checked="" type="checkbox"/> 博士 <input type="checkbox"/> 硕士 <input type="checkbox"/> 学士 <input type="checkbox"/> 其他				
	职 称	<input type="checkbox"/> 正高级 <input checked="" type="checkbox"/> 副高级 <input type="checkbox"/> 中级 <input type="checkbox"/> 初级 <input type="checkbox"/> 其他			职务	无
	电子邮箱	bolincai@scau.edu.cn	移动电话	13580356512		

一、子课题的研究主要内容

收集我国黄羽肉鸡特色地方种质资源，利用 Hi-C 测序技术，系统揭示黄羽肉鸡不同种质资源胸肌组织的染色质三维结构景观，解析黄羽肉鸡种质资源三维基因组遗传多样性。

二、子课题的主要考核指标

- (1) 挖掘肉鸡肌肉生长的候选基因或分子标记 8-10 个；
- (2) 发表论文 1 篇。

三、子课题实施计划		
2023 年 09 月 至 2024 年 06 月	任务:	收集我国黄羽肉鸡特色地方种质资源, 采集各品种 8 周龄胸肌组织并记录 18 周龄宰前活重、屠体重和胸肌重的数据。
	考核指标:	获得至少 15 个黄羽肉鸡地方种质资源的肌肉发育相关的表型数据。
	成果形式:	研究报告。
2024 年 07 月 至 2024 年 12 月	任务:	利用 Hi-C 技术, 获得高质量的不同种质资源胸肌组织的三维基因组数据。
	考核指标:	鉴定与肉鸡肌肉生长的候选基因或分子标记 3-5 个。
	成果形式:	研究报告。
2025 年 01 月 至 2025 年 06 月	任务:	分析不同种质资源胸肌组织染色质 A / B 隔室和拓扑结构域的差异, 并明确导致染色质结构差异的遗传变异。
	考核指标:	鉴定与肉鸡宰前活重、屠体重和胸肌重等重要经济性状相关的候选基因或分子标记 5 个。
	成果形式:	研究报告。
2025 年 07 月 至 2025 年 12 月	任务:	相关数据整理和论文撰写、发表
	考核指标:	发表论文 1 篇
	成果形式:	论文 (课题第一标注) 。

四、参加人员名单								
	姓 名	单 位	年龄	性别	职称/职务	责任分工	手机号	邮箱
主持人	蔡柏林	华南农业大学	31	男	副教授	课题负责人，指导分工，数据分析，课题总结。	13580356512	bolincai@scau.edu.cn
参加人								

1520

五、年度经费预算表

序号	预算科目名称	金额（万元）
	(1)	(2)
1	一、中央财政专项资金	100
2	（一）直接费用	83.34
3	1. 设备费	0
	（1）购置设备费	0
	（2）设备试制/改造/租赁费	0
4	2. 业务费	62.50
5	3. 劳务费	20.84
6	（二）间接费用（自动计算）	16.66
7	二、其他来源资金	0
8	三、合计	100

六、共同条款

签约各方共同遵守《国务院办公厅关于改革完善中央财政科研经费管理的若干意见》（国办发[2021]32号）等有关规定。

- 1.课题经费要专款专用，不得挪作它用。经费的使用要严格按照有关规定执行。若经费超支，由乙方自筹解决，但不得因此影响课题的执行。
2. 甲方根据相关规定，监督乙方经费的使用情况。凡不符合规定的开支，甲方负责提出调整意见。
3. 任务执行过程中，乙方如需调整任务，应根据有关规定，向甲方提出变更内容的申请报告，经甲方审核后逐级上报项目组织部门、科技部审定后实施。未接到正式批准书以前，双方须按原任务书履行，否则后果由自行调整的一方负责。
4. 乙方因某种原因（如：与可行性研究内容有出入、挪用经费、技术措施或某些条件不落实）致使计划无法执行，并要求中止任务，应视不同情况，部分或全部退还所拨经费；若乙方没有提出中止任务的要求，甲方根据调查情况有权提出中止任务的建议，经上报项目组织部门、科技部审核批准后执行。
- 5.乙方因不可抗力不能履行任务书规定的工作内容时，应及时通知甲方，并在合理期间内出具不能履行的证明。
- 6.乙方应保证课题负责人及主要承担人员的稳定，不得随意调换；如确需调换，应征得甲方同意，否则，由于人员安排问题造成课题不能正常实施，其损失由乙方负责。
- 7.课题承担单位要严格按本任务书履行承担的任务，并于每年年底前，提交课题年度执行情况总结、经费决算及下年度工作计划。如不能按期完成本年度计划指标，项目负责人会同项目执行委员会成员有权对项目进行审核、缓拨经费，直至停止合同，撤销课题处理。
8. 课题结束后，乙方应根据有关要求，向甲方提交验收申请，由甲方组织有关专家，依据任务书的内容对课题进行验收。
- 9.本课题形成的成果统一标注“农业生物育种重大项目”（编号 **2023ZD04064**）。
- 10.本任务书签订各方均负有相应责任。若有争议或纠纷时，按照有关规定处理。

七、合同签约各方

甲方（委托方）：

华南农业大学

（公章）



单位法人：（签章）

薛红已

课题负责人：（签字）

聂良奇

年 月 日

乙方（承担方）：

华南农业大学

单位（公章）



单位法人：（签章）

薛红已

子课题负责人：（签字）

李树

年 月 日

1.3. 主持：关于国家重点研发计划子课题的任务书

课题编号： 2022YFF1000201

国家重点研发计划 子课题任务书

子 课 题：蛋白质磷酸化修饰对鸡肉风味前体物质的调控研究

所属专项：农业生物重要性状形成与环境适应性基础研究

所属项目：鸡高产优质高抗性状形成的分子调控网络

所属课题：鸡产肉量及肉品质性状遗传基础及分子调控网络解析

委托部门（甲方）： 东北农业大学

承担部门（乙方）： 华南农业大学

2023 年 04 月



填写说明

- 1、任务书为课题验收的依据，其各项内容应尽可能详细填写。
- 2、课题目标要强调形成主导品种（产品、装备）、主推技术、重要标准（规程规范）、决策支持方案、知识产权等；考核指标应具体、量化、可考核。按已提交的实施方案进行填报，不得私自减少任务指标。
- 3、经费的使用应严格按有关经费管理办法执行。
- 4、开户银行及账号应是课题参加单位计财部门的开户行和账号。
- 5、本任务书要求用 A4 纸、正文四号仿宋_GB2312。
- 6、任务书正式文本一式六份，项目主持单位两份，课题主持单位两份，课题参与单位两份。



课题名称		鸡产肉量及肉品质性状遗传基础及分子调控网络解析					
子课题名称		蛋白质磷酸化修饰对鸡肉风味前体物质的调控研究					
所属项目		鸡高产优质高抗性状形成的分子调控网络					
所属专项		农业生物重要性状形成与环境适应性基础研究					
子课题经费预算		总需求 60 万元，其中中央财政专项资金需求 60 万元					
子课题周期节点		起始时间	2022 年 12 月		结束时间	2027 年 11 月	
		实施周期	共 60 个月		预计中期时间点	2025 年 05 月	
课题承担单位	单位名称	东北农业大学				单位法定代表人姓名	付强
	单位性质	大专院校				组织机构代码	122300004140017248
	单位主管部门	黑龙江省教育厅				隶属关系	地方
	单位所属地区	黑龙江省				地市（市、自治州、盟）	哈尔滨市香坊区
	通信地址	黑龙江省哈尔滨市香坊区长江路 600 号				邮政编码	150030
	单位开户名称	东北农业大学					
	开户银行（全称）	中国银行股份有限公司哈尔滨香坊支行			汇入地点	黑龙江省哈尔滨市	
	银行账号	171450715430			银行机构代码	104261003401	
课题负责人	姓 名	李辉	性 别	<input checked="" type="checkbox"/> 男 <input type="checkbox"/> 女		出生日期	1963-06-01
	证件类型	身份证	证件号码	650103196306013254			
	所在单位	东北农业大学					
	最高学位	<input checked="" type="checkbox"/> 博士 <input type="checkbox"/> 硕士 <input type="checkbox"/> 学士 <input type="checkbox"/> 其他					
	职 称	<input checked="" type="checkbox"/> 正高级 <input type="checkbox"/> 副高级 <input type="checkbox"/> 中级 <input type="checkbox"/> 初级 <input type="checkbox"/> 其他				职务	农业农村部鸡遗传育种重点实验室主任
	电子邮箱	lihui@neau.edu.cn		移动电话		13359991416	
子课题	单位名称	华南农业大学		单位法定代表人姓名		刘雅红	



承担单位	单位性质	大专院校		组织机构代码		124400004554165634	
	单位主管部门	广东省		隶属关系		省属	
	单位所属地区	广东省		地市(市、自治州、盟)		广州市天河区	
	通信地址	广东省广州市天河区五山路 483 号		邮政编码		510642	
	单位开户名称	华南农业大学					
	开户银行(全称)	中国工商银行股份有限公司广州五山支行		汇入地点		广东省广州市	
	银行账号	3602002609000310520		银行机构代码		102581000546	
子课题负责人	姓 名	蔡柏林	性 别	<input checked="" type="checkbox"/> 男 <input type="checkbox"/> 女	出生日期	1992-10-09	
	证件类型	身份证	证件号码	440111199210094218			
	所在单位	华南农业大学					
	最高学位	<input checked="" type="checkbox"/> 博士 <input type="checkbox"/> 硕士 <input type="checkbox"/> 学士 <input type="checkbox"/> 其他					
	职 称	<input type="checkbox"/> 正高级 <input checked="" type="checkbox"/> 副高级 <input type="checkbox"/> 中级 <input type="checkbox"/> 初级 <input type="checkbox"/> 其他			职务	无	
	电子邮箱	bolincai@scau.edu.cn		移动电话	13580356512		



一、课题的简述

本课题旨在利用 4D-磷酸化修饰蛋白质组、TMT 标记定量蛋白质组、非靶向代谢组等多组学测序技术，系统探究蛋白质磷酸化修饰对鸡肉风味前体物质形成的调控机制，预期成果可为鸡肉品质的遗传改良提供理论依据。

二、子课题的主要考核指标

- (1) 挖掘调控肉鸡高产和优质性状形成的候选基因 1-2 个，其中重要新基因 1 个；
- (2) 发表高水平论文 1 篇；
- (3) 授权国家发明专利 1 项。



三、子课题的研究主要内容

联合 4D-磷酸化修饰蛋白质组、TMT 标记定量蛋白质组、非靶向代谢组等多组学测序技术，挖掘参与鸡肉风味前体物质形成的蛋白质磷酸化修饰标记，构建关键磷酸化修饰蛋白-代谢物调控网络，系统阐明蛋白质翻译后修饰调控肉鸡优良肉质性状形成的遗传基础和调控机制。



四、子课题实施计划		
2022 年 12 月 至 2023 年 05 月	任务:	比较黄羽肉鸡和快大型白羽肉鸡的肌纤维特性和肉质性状差异
	考核指标:	获得各品种至少 10 个个体的肌纤维类型组成和肉品质物理特性数据
	成果形式:	研究报告
2023 年 06 月 至 2023 年 11 月	任务:	分析导致不同肉鸡品种肉风味差异的风味前体组成及相关调控基因
	考核指标:	鉴定影响不同肉鸡品种肉风味组成的风味前体物质至少 10 种, 构建相关基因-风味前体网络至少 5 个
	成果形式:	研究报告
2023 年 12 月 至 2024 年 05 月	任务:	联合 4D-磷酸化修饰蛋白质组和 TMT 标记定量蛋白质组技术挖掘参与不同肉鸡品种肉风味形成的蛋白质磷酸化标记
	考核指标:	获得相关蛋白质磷酸化标记和候选基因至少 2 个
	成果形式:	研究报告
2024 年 06 月 至 2024 年 11 月	任务:	细胞水平鉴定相关蛋白质磷酸化标记和候选基因对肉风味前体形成的调控作用
	考核指标:	获得与肉风味前体物质相关的重要新基因 1 个
	成果形式:	研究报告
2024 年 12 月 至 2025 年 05 月	任务:	活体水平明确相关蛋白质磷酸化标记和候选基因的作用功能
	考核指标:	阐明相关蛋白质磷酸化标记和候选基因的分子功能
	成果形式:	研究报告
2025 年 06 月	任务:	探究相关蛋白质磷酸化标记和候选



至 2025 年 11 月		基因的分子作用途径
	考核指标:	综合揭示相关蛋白质磷酸化标记和候选基因调控风味前体组成的作用机理
	成果形式:	研究报告
2025 年 12 月 至 2026 年 05 月	任务:	相关数据整理和论文撰写
	考核指标:	发表高水平论文 1 篇
	成果形式:	论文 (课题第一标注)
2026 年 06 月 至 2026 年 11 月	任务:	开发与风味前体物质相关的分子标记
	考核指标:	建立与风味前体物质相关的分子标记 1 个, 申请国家发明专利 1 项
	成果形式:	专利申请受理书
2026 年 12 月 至 2027 年 05 月	任务:	国家发明专利审查
	考核指标:	获授权国家发明专利 1 项
	成果形式:	授权国家发明专利
2027 年 06 月 至 2027 年 11 月	任务:	整理相关项目成果、撰写结题报告
	考核指标:	结题报告 1 份
	成果形式:	结题报告



五、参加人员名单								
	姓名	单位	年龄	性别	职称/职务	责任分工	手机号	邮箱
主持人	蔡柏林	华南农业大学	31	男	副教授	课题负责人, 指导分工, 数据分析, 课题总结。	13580356512	bolincai@scau.edu.cn
参 加 人								



六、年度经费预算表

序号	预算科目名称	金额（万元）
	(1)	(2)
1	一、中央财政专项资金	60
2	(一) 直接费用	48
3	1. 设备费	0
	(1) 购置设备费	0
	(2) 设备试制/改造/租赁费	0
4	2. 业务费（材料费、测试化验加工费、燃料动力费、出版/文献/信息传播/知识产权事务费）	32.4
5	3. 劳务费（会议/差旅/国际合作交流费、劳务/专家咨询费、其他支出）	15.6
6	(二) 间接费用（自动计算）	12
7	二、其他来源资金	0
8	三、合计	60



七、共同条款

签约各方共同遵守《国务院办公厅关于改革完善中央财政科研经费管理的若干意见》（国办发[2021]32号）等有关规定。

1. 课题经费要专款专用，不得挪作它用。经费的使用要严格按照有关规定执行。若经费超支，由乙方自筹解决，但不得因此影响课题的执行。
2. 甲方根据相关规定，监督乙方经费的使用情况。凡不符合规定的开支，甲方负责提出调整意见。
3. 任务执行过程中，乙方如需调整任务，应根据有关规定，向甲方提出变更内容的申请报告，经甲方审核后逐级上报项目组织部门、科技部审定后实施。未接到正式批准书以前，双方须按原任务书履行，否则后果由自行调整的一方负责。
4. 乙方因某种原因（如：与可行性研究内容有出入、挪用经费、技术措施或某些条件不落实）致使计划无法执行，并要求中止任务，应视不同情况，部分或全部退还所拨经费；若乙方没有提出中止任务的要求，甲方根据调查情况有权提出中止任务的建议，经上报项目组织部门、科技部审核批准后执行。
5. 乙方因不可抗力不能履行任务书规定的工作内容时，应及时通知甲方，并在合理期间内出具不能履行的证明。
6. 乙方应保证课题负责人及主要承担人员的稳定，不得随意调换；如确需调换，应征得甲方同意，否则，由于人员安排问题造成课题不能正常实施，其损失由乙方负责。
7. 课题承担单位要严格按本任务书履行承担的任务，并于每年年底前，提交课题年度执行情况总结、经费决算及下年度工作计划。如不能按期完成本年度计划指标，项目负责人会同项目执行委员会成员有权对项目进行审核、缓拨经费，直至停止合同，撤销课题处理。
8. 课题结束后，乙方应根据有关要求，向甲方提交验收申请，由甲方组织有关专家，依据任务书的内容对课题进行验收。
9. 本课题形成的成果统一标注“国家重点研发计划经费资助”（编号**2022YFF1000201**）；；SCI论文第一标注（National Key R&D Program of China, Grant No. 2022YFF1000201）。
10. 本任务书签订各方均负有相应责任。若有争议或纠纷时，按照有关规定处理。



八、合同签约各方

甲方（委托方）：
东北农业大学
(公章)



单位法人:



课题负责人: (签字)

2023 年 4 月 23 日

李辉

乙方（承担方）：
华南农业大学

单位 (公章)



单位法人: (签章)

刘雅红

子课题负责人: (签字)

李辉

2023 年 4 月 11 日



1.4. 主持：关于2024年省级乡村振兴战略专项资金种业振兴行动项目的合同书及联合申报协议书

合同编号：2024-XPY-07-001

2024年省级乡村振兴战略专项资金 种业振兴行动项目



合 同 书

项目名称：优质小型白羽肉鸡育繁推一体化示范
项目管理单位（甲方）：广东省农业农村厅
项目牵头承担单位（乙方）：广东广弘种业科技有限公司
项目推荐(主管)单位(丙方)：河源市农业农村局
项目负责人：聂庆华 联系电话：13922195759
项目联系人：李恒丰 联系电话：15920448694

广东省农业农村厅制



第一条 为保障 2024 年省级乡村振兴战略专项资金种业振兴行动项目顺利实施，按时保质保量完成项目任务，根据《中华人民共和国民法典》《广东省省级财政专项资金管理办法（修订）》（粤府〔2023〕34 号）、《广东省农业农村厅种业振兴行动专项资金管理办法（试行）》等文件有关规定，经甲、乙、丙三方协商一致，签署本合同书。

第二条 甲方的权利义务：本合同履行过程中，甲方有权对乙方项目的实施情况和资金到位、使用情况进行监督、检查，提出改进要求。

第三条 乙方的权利义务：

1. 按财政资金管理规定，对甲方核拨的资金做到专款专用，单独列账，并随时配合甲方进行监督检查。

2. 认真填写本合同书附件 1《项目任务书》，《项目任务书》的内容应与乙方的《项目申报书》保持一致。

3. 严格按照本合同书及附件 1《项目任务书》的要求及时完成项目建设内容，项目实施完成后，按照本合同附件 2《验收报告》模版要求提交验收报告。

4. 按照《广东省农业农村厅种业振兴行动专项资金管理办法（试行）》规定，按期（每年 6 月 30 日、12 月 31 日）向甲方、丙方书面报告项目实施进展及资金使用情况等内容。

5. 乙方需保留与所有参与单位的合作实施协议和相关财务凭证，并向甲方备案。

第四条 丙方的权利义务：

1. 为乙方项目实施提供必要的条件保障。

2. 负责对项目承担单位的实施条件、能力以及财务管理规范进行审查，对推荐项目的实施场地、申报材料等进行真实性审核，并监督项目实施、资金预算执行情况。

3. 协助甲方完成对财政资金投资 500 万元（含）以上【科研项目财政资金在 200 万元（含）以上】项目验收等工作；负责完成对财政资金投资 500 万元以下（科研项目财政资金 200 万元以下）项目验收工作，并及时向甲方报告情况。

第五条 本项目资金不得用于以下方向：1. 行政事业单位基本支出；2. 各项奖金、津贴、福利补助、职工工资、奖励绩效等；3. 企业担保金和弥补企业亏损；4. 修缮楼堂馆所以及建造职工住宅；5. 弥补单位预算支出缺口和偿还债务；6. 购买交通工具及通讯设备；7. 形成地方政府债务的支出；8. 购买理财产品、发放借款及平衡预算等。

第六条 项目验收。项目验收及结果处理严格执行《广东省农业农村厅专项资金项目验收管理办法（试行）》（粤农农办〔2023〕73 号）的规定。乙方应在项目完成后 3 个月内，提出验收申请。申请验收除了规定材料外，还应该提交项目审计报告或者经费决算表，其中财政专项资金 50 万元以下的项目，需提交由项目承担单位财务部门出具的经费决算表，财政专项资金 50 万元（含）以上的项目，需提交由项目承担单位委托会计师事务所出具的审计报告。对财政资金投资 500 万元（含）以上【科研项目财政资金在 200 万元（含）以上】的项目，及乙方直接向甲方申报的项目，由甲方负责组织验收；对财政资金投资 500 万元以下（科研项目财政资金 200 万元以下）的项目，由项目推荐（主管）单位（丙方）负责验收，验收单位向甲方提交验收材料，甲方对验收材料进行审核确认。

第七条 在履行本合同的过程中，如出现相关政策法规重大改变等不可抗力情况，甲方有权对所核拨经费的数量和时间进行相应调整。因非不可抗力因素导致的项目未履行或未履行完毕，或因乙方责任造成项目不能继续开展的，甲方有权终止项目合同，收回尚未使用和使用不符合规定的财政经费。

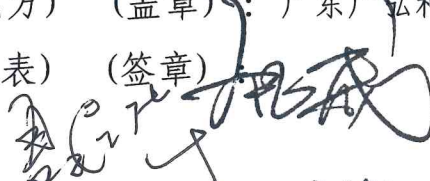

第八条 在履行本合同的过程中，乙方发现可能导致项目整体或部分失败的情形时，应及时通知甲方，并采取适当措施减少损失，没有及时通知并采取适当措施，致使损失扩大的，应当就扩大的损失承担责任。

第九条 实施项目所获得的科技成果(项目成果)归属、成果转让和实施技术成果所产生的经济利益的分享，按照国家和广东省有关规定执行。项目研究成果应向省农业农村厅进行登记、备案，对外发布前应征求省农业农村厅的意见。

第十条 本合同在履行过程中发生的任何争议，由甲乙丙三方友好协商解决。

第十一条 本合同未尽事宜，各方同意按照《广东省省级财政专项资金管理办法(修订)》(粤府〔2023〕34号)、《广东省农业农村厅种业振兴行动专项资金管理办法(试行)》履行。

项目管理单位(甲方) (盖章): 广东省农业农村厅
法定代表人(或授权代表) (签章): 
签订日期: 2025年2月17日

项目牵头承担单位(乙方) (盖章): 广东广弘种业科技有限公司
法定代表人(或授权代表) (签章): 
项目负责人(签章): 
签订日期: 2025年1月17日

乙方推荐(主管)单位(丙方) (盖章): 河源市农业农村局
法定代表人(或授权代表) (签章): 
签订日期: 年 月 日

附件 1

项目任务书

填写说明

一、本项目任务书由乙方填写。

二、本项目任务书所列内容应实事求是填写，表达要明确、严谨。对填写不符合要求的，或填报内容出现虚报夸大、不切实际的，将退回项目承担单位修改。

三、项目任务书规定的项目考核指标、建设内容和绩效目标必须依据《项目申报书》填写，应遵循明确、量化、可考核的原则，其中技术指标应明确项目完成时达到的关键技术参数及预期可以形成的发明专利、标准、新技术、新产品、新装置、论文、专著等的数量。项目申报指南对项目技术、经济和成果等指标有明确要求的，应符合项目申报指南的要求，相关专项管理办法有特别规定的，应符合相关规定。

四、《项目申报书》及申报指南是本项目任务书填报的重要依据，项目任务书填报不得修改考核指标、绩效目标、资金预算等内容。《项目申报书》、申报指南和本项目任务书将共同作为项目过程管理、综合绩效评价（验收）和监督评估的重要依据。

五、省财政资金支出的预算计划应按照国家及省相关规定执行。

六、表格栏目不够可自行增加。

一、目的及意义

主要说明项目的建设目的、研究价值和意义。

鸡肉是世界肉类消费体系中的重要组成部分。在当前全球经济低迷和通货膨胀的大背景下，消费者对“低价格”且“高品质”的动物产品的消费需求与日俱增。统计数据显示，2023 年全球肉鸡产量达 10238.9 万吨，相较于 2022 年增长 54.9 万吨。我国肉鸡产业经过 40 多年的高速发展，肉鸡产量常年位居全球前四。2023 年我国肉鸡产量占比全球产量近 14%，位居全球第三，仅次于美国和巴西。随着我国和世界范围内社会经济环境的优化和改善，加上我国肉鸡父母代后备种鸡的存栏量充裕，将进一步拉动我国肉鸡的消费总量，有利于我国肉鸡产业的进一步发展。

我国肉鸡产业主要是以黄羽肉鸡、白羽肉鸡和小型白羽肉鸡三大类型组成，已逐步形成“三分天下”的发展格局，以满足国内外不同消费者的市场需求。近年来，小型白羽肉鸡产业的扩张势头迅猛，持续占据了大份额的快速型黄羽肉鸡消费市场。传统的小型白羽肉鸡是指以快大型白羽肉鸡（科宝，罗斯等）作为父系，高产商业蛋鸡（海兰褐等）作为母系杂交配套而成的肉鸡，具有生长速度快、饲料转化效率高、屠宰性能优异、胴体外观良好等优势，在“活禽屠宰，冰鲜上市”的消费市场大背景下具有得天独厚的优势，快速获得了市场消费者的青睐。《全国肉鸡遗传改良计划（2014-2015）》文件中早已提出要规范小型白羽肉鸡制种技术，保障种鸡质量，改善群体疫病净化和生物安全水平，并培育出专用新品种（配套系），完善良种繁育体系。而《全国肉鸡遗传改良计划（2021-2035 年）》再次强调了将小型白羽肉鸡产业视为肉鸡产业发展的重要方向，通过品种培育、市场拓展和产业链完善等措施，推动产业的持续发展。

我国广东省的“无鸡不成宴”的岭南特色饮食文化一直在持续推动当地肉鸡产业的发展，拥有的国家肉鸡核心育种场和品种（配套系）超过全国总数的一半，一直处于我国肉鸡育种和生产的领先地位，其种业技术创新和新品种（配套系）的培育能力直接影响到我国肉鸡产业在未来市场的竞争力和可持续发展。尽管我省在肉鸡品种创新方面已取得显著进展，但在小型白羽肉鸡新品种（配套系）的培育和推广应用上仍有众多问题。由于我省小型白羽肉鸡产业存在种源混杂、制种不规范、饲养管理手段差等现场，导致市场上的小型白羽肉鸡产品存在性能不稳定、抗病力差、均匀度低等问题，不能满足当前消费市场优质畜禽肉产品日益增长的需求。

结合目前小型白羽肉鸡产业存在的问题和产业发展大背景，本项目结合我省肉鸡产业的现况和发展优势，紧紧围绕《广东省种业振兴行动实施方案》和《广东省现代畜牧业发展“十四五”规划》的种业攻坚战略部署，通过依托“农业部鸡遗传育种与繁殖重点实验室”、“畜禽育种国家地方联合工程研究中心”和“广东省畜禽遗传育种工程技术研究中心”等多个省部级科研平台，组建优质小型白羽肉鸡新品种培育及推广应用研发团队进行产学研联合攻关，针对屠体性状、饲料转化率、繁殖性能、肉品质和抗病力等重要经济性状开展基于精准表型测定和基因组分子水平的综合性遗传评估，利用组学技术开展上述复杂性状的遗传解析和拮抗分子机制研究；同时，通过整合传统育种手段、分子标记辅助选育、全基因组选择育种技术和多性状平衡育种技术等方法，构建优质小型白羽肉鸡新品种复合育种技术体系，提高选种的精确性和效率，突破优质小型白羽肉鸡新品种（配套系）的选育和开发推广，进一步提升广东小型白羽肉鸡在全国的种源优势和影响力。

二、项目建设内容

详细说明项目建设内容（项目需求或项目建设任务，包含项目参与单位的建设内容）。

（一）项目（课题）牵头承担单位

1. 单位名称：广东广弘种业科技有限公司

项目（课题）负责人：聂庆华

2. 研究开发内容（或推广内容）：

（1）基于育种软件开展信息化育种技术研发

建立利用育种云计算系统开展智能化表型测定、育种值自动化估算、精准选种选配和种鸡种蛋管理的信息化育种技术，实现育种数据的云端呈现；通过智能化、信息化、自动化领域技术交叉融合的方法，实现核心育种群表型的精准测定，为优质小型白羽肉鸡育种提供数据支撑；稳步推行“业财一体化”，从纸质记录升级到电子信息化，从系统上了解并监管整个饲养过程的存栏情况、物料、成本等，提高管理效能。

（2）优质小型白羽肉鸡新品种（配套系）培育

调研分析现阶段小型白羽肉鸡的产业情况，面对市场需求，确立小型白羽肉鸡品种重点生产性能的育种目标；围绕育种目标，收集筛选具有优异特性的育种素材，根据专门化品系的特点，利用配套系平衡制种方法，开展专门化品系之间的配合力测定；联合科研院校进行深度产学研合作，结合传统育种方法和现代分子育种技术、全基因组选择技术，采用三系配套的杂交方式，同时持续开展禽白血病和鸡白痢净化工作，培育具有“高效、优质、抗病力强、屠宰性能优”等特点的优质小型白羽肉鸡新品种（配套系）。

（3）优质小型白羽肉鸡新品种（配套系）的产业化推广

对培育出的新品种（配套系）开展父母代和商品代鸡的生长发育规律以及关键饲养技术与集成，制定相应的配套系饲养管理技术规范，通过采取适合的“公司+农户”、“公司+养殖公司”或其他产业化形式等，结合不同区域对品种的消费需求，多元化推广新品种；根据新品种（配套系）特色经济性状，进一步开发下游特色加工产品，增加产品品类及用户需求，从而达到拓宽销售渠道，提高市场占有率的效果，实行产、供、销一体化，延长产业链，共同抵御市场风险。

（二）项目（课题）参与单位

1. 单位名称：华南农业大学

2. 研究开发内容（或推广内容）：

（1）优质小型白羽肉鸡胫色、肤色和快慢羽分子检测技术的开发
探究专门化品系中胫色、肤色和快慢羽性状的遗传规律；建立小型白羽肉鸡胫色和肤色的评价鉴定标准；利用全基因组关联分析并结合转录组、代谢组等多组学测序方法，定位与胫色、肤色和快慢羽性状相关的遗传变异；开发适用于小型白羽肉鸡胫色、肤色和快慢羽性状选育的有效分子标记。

（2）优质小型白羽肉鸡肉质风味的鉴定及评价
分析培育出的新品种（配套系）的肉质特性（pH 值、剪切力、系水力、色泽和肌肉脂肪含量）；利用代谢组和脂质组测序技术，探究培育出的新品种（配套系）的肌肉代谢物组成；比较社会同类产品，建立小型白羽肉鸡肉质风味的评价体系。

（3）全基因组选择育种技术研发及标准化个体育种值评估流程建立
以生长速度、饲料转化效率、繁殖等肉鸡重要经济性状为重点，开展时间序列表型性状和阈性状全基因组选择研究；综合 GBLUP 模型和基于多种贝叶斯方法、神经网络等统计模型或深度学习策略，建立针对特定/重点性状的遗

传评定模型，获得最优预测策略和最优标记组合，提高育种值估计准确性；搭建整合表型、基因分型到遗传评估的表型-基因型-个体遗传评估的标准化个体育种值评估流程。

备注：项目建设内容（项目需求或项目建设任务）按《项目申报书》内容填写。

三、项目绩效目标

主要说明项目实施后，预期达到的目标和产生的效果，相关表述应量化。

（一）总体目标

本项目针对传统小型白羽肉鸡配套系肉质不理想、性能不稳定、均匀度差、料肉比有待提升等突出问题，开发适用于小型白羽肉鸡胫色、肤色、快慢羽、料肉比、生长速度、肉质等性状的检测方法和分子选育标记，突破难度性状选育困难的瓶颈；创新生长速度、饲料转化效率、繁殖等时间序列表型性状和阈性状全基因组选择技术，建立表型-基因型-个体遗传评估的标准化个体育种值评估流程；加速“高效、优质、抗病力强、屠宰性能优”的优质小型白羽肉鸡新品种（配套系）培育，提升我国肉鸡育种水平。

（二）总体考核指标

1、开发适用于小型白羽肉鸡胫色、肤色、快慢羽等性状选育的分子标记 3-4 个；

2、搭建针对专门化品系的表型-基因型-个体遗传评估的标准化个体育种值评估流程 1 套；

3、培育优质小型白羽肉鸡新品种（配套系）1 个，每套父母代母鸡 66 周龄提供雏鸡 200 只以上，商品代 49 日龄上市公母平均体重达 2.0 千克、公母平均料肉比在 1.65 以内

4、新品种（配套系）每年推广商品代肉鸡 1 亿羽以上；

5、发表学术论文 2-3 篇，申请国家发明专利 2-3 件。

（三）各任务目标及考核指标

1、小型白羽肉鸡重点性状的鉴定评价及分子标记开发

建立肤色、肉质等难度量性状的测定体系和评价标准，开发适用于小型白羽肉鸡胫色、肤色、快慢羽等性状选育的分子标记 3-4 个，发表学术论文 1-2 篇，申请国家发明专利 2-3 件。

2、全基因组选择育种技术研发及标准化个体育种值评估流程建立

开发基于低深度测序的全基因组高通量基因分型技术，解决育种成本的卡脖子问题；构建专门化品系的大规模参考群体，创新基因组选择选种、选配技术，解决选种准确性的关键问题；以生长速度、饲料转化效率、繁殖等肉鸡重要经济性状为重点，开展时间序列表型性状和阈性状全基因组选择研究。搭建针对专门化品系的表型-基因型-个体遗传评估的标准化个体育种值评估流程 1 套；发表学术论文 1-2 篇。

3、优质小型白羽肉鸡新品种（配套系）培育及产业化推广

建立规模化的表型-基因型信息数据库，结合全基因组选择技术，对各专门化品系持续选育，不断提高各品系的性能，优化并稳定各品系特点；以白羽肉鸡、高产蛋鸡以及黄羽肉鸡等专门化品系为素材，根据专门化品系的特点，利用配套系平衡制种方法，开展专门化品系之间的配合力测定；以市场需求为目标，采用三系配套的杂交方式，培育出高效、优质、抗病力强、屠宰性能优”的优质小型白羽肉鸡新品种（配套系）1 个，每套父母代母鸡 66 周龄提供雏鸡 200 只以上，商品代 49 日龄上市公母平均体重达 2.0 千克、公母平均料肉比在 1.65 以内；在全国范围内进行大规模产业化推广，新品种（配套系）每年推广商品代肉鸡 1 亿羽以上，使其成为我国市场份额占比大的核心品种。

四、项目进度安排

详细说明各阶段的工作内容和时间安排情况。

2025 年 01 月-2025 年 03 月 确立小型白羽肉鸡配套系的育种目标；收集和筛选具有优质特性的育种素材；开展配合力测定明确配套系的构成；持续开展禽白血病和鸡白痢的净化工作。

2025 年 04 月-2025 年 06 月 制定配套系饲养管理技术规范；建立优质小型白羽肉鸡胫色、肤色的评价和鉴定标准；定位与胫色、肤色和快慢羽表型相关的基因组变异；开展对于生长速度、饲料转化效率和繁殖性能的全基因组选择；分析新配套系的肉质风味特性。

2025 年 07 月-2025 年 10 月 结合细分市场需求，多元化推广新品种产品；开发适用优质小型白羽肉鸡胫色、肤色和快慢羽表型相关的分子检测方法；综合 GBLUP 和深度学习模型等建立遗传评定模型提高育种值估计的准确性；搭建标准化的个体育种值评估分析流程；建立优质小型白羽肉鸡肉质风味的评价体系。

2025 年 11 月-2025 年 12 月 培育出优质小型白羽肉鸡新配套系；根据品种的特色经济性状，进一步开发下游特色加工产品；评估育种改良进度；再次根据实际性能筛选种鸡进行小范围推广试验；正式面向市场推广示范；完成项目总结并进行验收。

备注：项目绩效目标按《项目申报书》内容填写。

五、项目主要合作、参与单位(含牵头承担单位)			
单位名称	单位性质	统一社会信用代码	通讯地址
广东广弘种业科技有限公司	企业	91441625MA56NPYJ76	河源市东源县顺天镇滑滩村 军民共建路 666 号
华南农业大学	高等院校	124400004554165634	广东省广州市天河区五山 路 483 号

六、项目组主要成员(含项目负责人)					
姓名	性别	身份证号	单位	职称/职务	电话
聂庆华	男	342824197512182714	广东广弘种业科技有限公司	正高级	13922195759
郑煦灿	男	440506198312160016	广东广弘种业科技有限公司	副高级	13923240706
蔡柏林	男	440111199210094218	华南农业大学	副高级	13580356512
甘建伉	男	440781198504158130	广东广弘种业科技有限公司	副高级	13824427951
张细权	男	440106196305161992	华南农业大学	高级	13922276891
李恒丰	男	445381199609150431	广东广弘种业科技有限公司	中级	15920448694
罗文	男	441481198806144150	华南农业大学	副高级	13710789890
曾庆强	男	44148119970219203X	广东广弘种业科技有限公司	其他	18318194480
黎镇晖	男	441225198704251033	华南农业大学	副高级	13560468254
苏皖中	男	340811198903095811	广东广弘种业科技有限公司	中级	13380042710
徐翌斌	男	430726199501161332	华南农业大学	其他	18819495186

严常燕	女	440981198708075426	广东广弘种业科技有限公司	副高级	15218928857
郭利金	女	445122199407140613	华南农业大学	其他	13660126276
温丽华	女	440103198208141244	广东广弘种业科技有限公司	初级	13516641504
詹惠娜	女	445122198303251242	华南农业大学	其他	15918500846
李国亮	男	440103198208141244	广东广弘种业科技有限公司	中级	15218935987
孔少芬	女	44120219970105152X	华南农业大学	其他	15813316895
张海艺	男	440981198310112258	广东广弘种业科技有限公司	初级	13928526200
杨大森	男	440981198109266837	广东广弘种业科技有限公司	其他	18777223837
周震	男	460103199903190011	华南农业大学	其他	18520734741
罗海燕	女	445381199511037828	广东广弘种业科技有限公司	中级	15521152928

七、资金使用预算

主要说明资金使用的范围或方向及资金使用进度安排(包含参与单位内容)。

项目(课题)承担单位资金分配预算明细表 金额单位: 万元

填表说明: 1. 单位类型为牵头承担单位、参与单位; 2. 组织机构代码指企事业单位国家标准代码, 单位若已三证合一请填写单位统一社会信用代码, 无组织机构代码的单位填写“000000000”。									
序号	单位名称	组织机构代码	单位类型	任务分工	负责人	合计	省级财政专项资金		其他渠道资金
							小计	其中: 间接费用	
	(1)	(2)	(3)	(4)	(5)	(6)	(7)	(8)	(9)
1	广东广弘种业科技有限公司	91441625MA56NPYJ76	企业	承担单位	聂庆华	625.00	325.00	0.00	300.00
2	华南农业大学	124400004554165634	高等院校	参与单位	蔡柏林	175.00	175.00	10.50	0.00
累计						800.00	500.00	10.50	300.00

预算汇总表 金额单位: 万元

序号	预算科目名称	合计		省级财政专项资金		其他渠道资金	
		——	其中: 推广示范资金	——	其中: 推广示范资金	——	其中: 推广示范资金
1	一、资金支出	800.00	0.00	500.00	0.00	300.00	0.00
2	(一) 直接费用	789.50	0.00	489.50	0.00	0.00	0.00
3	1. 设备费	0.00	0.00	0.00	0.00	0.00	0.00
4	2. 材料费	427.02	0.00	162.02	0.00	265.00	0.00
5	3. 测试化验加工费	232.60	0.00	222.60	0.00	10.00	0.00
6	4. 燃料动力费	50.00	0.00	25.00	0.00	25.00	0.00
7	5. 出版/文献/信息传播/知识产权事务费	22.76	0.00	22.76	0.00	0.00	0.00
8	6. 会议/差旅/国际合作交流费	20.22	0.00	20.22	0.00	0.00	0.00
9	7. 培训费	0.00	0.00	0.00	0.00	0.00	0.00
10	8. 劳务费	36.90	0.00	36.90	0.00	0.00	0.00
11	10. 专家咨询费	0.00	0.00	0.00	0.00	0.00	0.00
12	11. 基本建设费	0.00	0.00	0.00	0.00	0.00	0.00
13	(1) 房屋建筑物构建	0.00	0.00	0.00	0.00	0.00	0.00
14	(2) 专用设备购置	0.00	0.00	0.00	0.00	0.00	0.00

15	(3) 基础设施建设	0.00	0.00	0.00	0.00	0.00	0.00
16	(4) 大型修缮	0.00	0.00	0.00	0.00	0.00	0.00
17	(5) 信息网络建设	0.00	0.00	0.00	0.00	0.00	0.00
18	(6) 其他基本建设支出	0.00	0.00	0.00	0.00	0.00	0.00
19	12. 其他费用	0.00	0.00	0.00	0.00	0.00	0.00
20	(二) 间接费用	10.50	—	10.50	—	0.00	—
21	二、项目(课题)资金来源						
22	(一) 省级财政专项资金	500.00	0.00	300.00	0.00	/	0.00
23	(二) 其他渠道资金	300.00	0.00	/	0.00	300.00	0.00
24	1. 单位自筹资金	300.00	0.00	/	0.00	300.00	0.00
25	2. 其他资金	0.00	0.00	/	0.00	0.00	0.00

(一) 省级财政资金预算主要用途

1、材料费 162.02 万元，用于饲料、疫苗、分子生物学实验和细胞培养的试剂耗材、玻璃仪器、疾病净化试剂盒等。

2、测试化验加工费 222.60 万元，用于禽白血病检测、饲料及水源等相关检测、低深度基因组测定，超级计算机计算核时等。

3、燃料动力费 25.00 万元：用于鸡舍环境控制设备、相关检测设备等运行发生产生的可单独计量的水、电、气、燃料消耗费用。

4、出版/文献/信息传播/知识产权事务费 22.76 万元，用于课题成果的整理、发表和出版过程中需要支付的专利申请、软件著作权登记、论文编辑费和出版费、资料购买和打印、宣传手册定制、标准规程的制定等。

5、差旅费 20.22 万元，用于种鸡性能测定、样本采集、调查、示范、调研、学术交流等所产生的费用。

6、劳务费 36.90 万元，用于参与该项目的技术员工、研究生、博士后及科研人员等的费用劳务支出及临时工作人员的劳务支出。

7、间接费用 10.50 万元，用于项目期间单位管理成本。项目参与单位华南农业大学按规定收取 6%管理费，即 $175 \text{ 万} \times 0.06 = 10.5 \text{ 万元}$ 。

(二) 其他渠道资金预算主要用途

1、材料费 265.00 万元，用于饲料、疫苗、疾病净化试剂盒、消毒剂等。

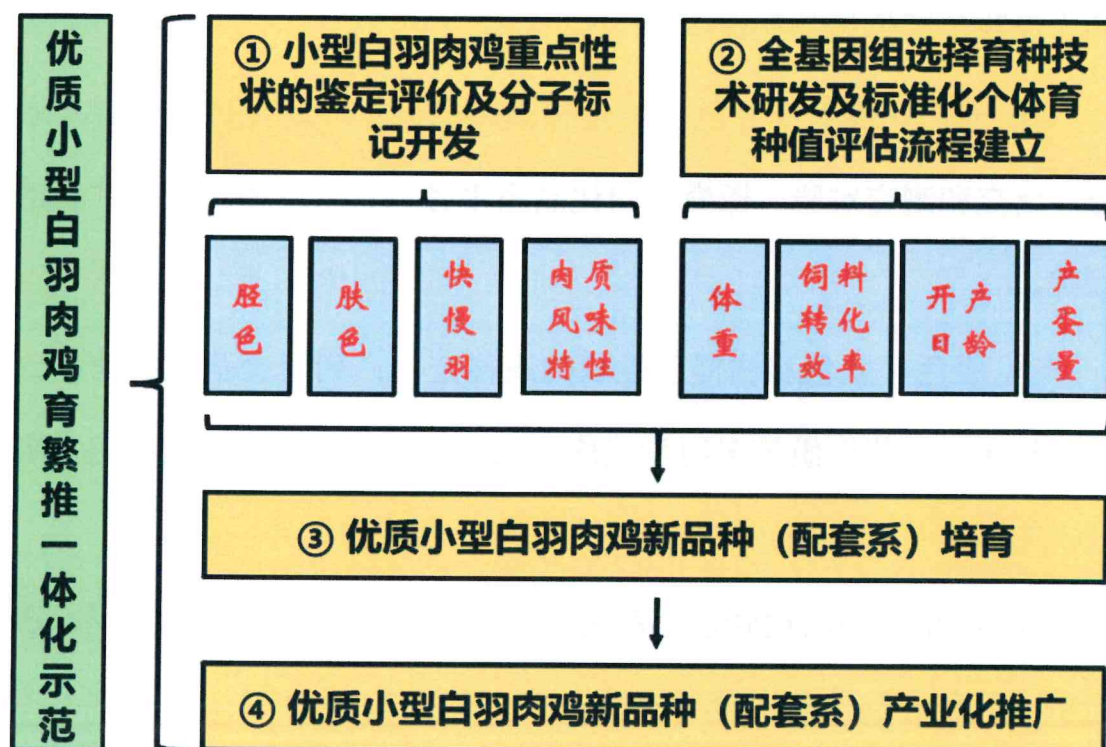
2、测试化验加工费 10.00 万元，用于禽白血病检测。

3、燃料动力费 25 万元：用于鸡舍环境控制设备、相关检测设备等运行发生产生的可单独计量的水、电、气、燃料消耗费用。

八、保障措施

说明围绕完成项目任务、目标所要采取的具体措施。

1. 技术方案



项目技术路线图

2. 具体措施

(1) 基于育种软件开展信息化育种技术研发

① 信息化育种平台的搭建：利用育种云计算系统开展智能化表型测定、育种值自动化估算、精准选种选配和种鸡种蛋管理，实现育种数据的云端呈现。

② 智能化数据的收集、利用：通过智能化、信息化、自动化领域技术交叉融合的方法，实现核心育种群表型的精准测定，为优质小型白羽肉

鸡育种提供数据支撑。

（2）优质小型白羽肉鸡胫色、肤色和快慢羽分子检测技术的开发

① 小型白羽肉鸡胫色和肤色的评价鉴定标准的建立：建立小型白羽肉鸡胫色的活体分级评价标准，利用色差仪结合液相色谱和拉曼光谱技术等实现肤色活体精准测定。

② 专门化品系中胫色、肤色和快慢羽性状的遗传规律分析：通过正交、反交和测交实验，探究专门化品系中胫色、肤色和快慢羽性状的遗传规律。

③ 胫色、肤色和快慢羽性状的遗传定位：利用全基因组关联分析并结合转录组、代谢组等多组学测序方法，定位与胫色、肤色和快慢羽性状相关的基因位点，挖掘影响上述表型形成的遗传变异。

④ 小型白羽肉鸡胫色、肤色和快慢羽性状的分子标记开发：在定位到的与胫色、肤色和快慢羽性状相关的基因位点基础上，结合群体验证，开发适用于小型白羽肉鸡胫色、肤色和快慢羽性状选育的有效分子标记。

（3）优质小型白羽肉鸡肉质风味的鉴定及评价

① 培育出的新品种（配套系）的肉质特性分析：利用电子 pH 值测定仪、剪切力测定仪等分析培育出的新品种（配套系）的肉质特性（pH 值、剪切力、系水力、色泽和肌肉脂肪含量）。

② 培育出的新品种（配套系）的肉质风味代谢物鉴定：联合代谢组和脂质组测序技术，探究培育出的新品种（配套系）的肌肉代谢物和脂肪酸组成。

③ 培育出的新品种（配套系）与社会同类产品肉质风味的比较：收集社会同类产品，比较分析培育出的新品种（配套系）与社会同类产品的肉质风味差异，建立小型白羽肉鸡肉质风味的评价体系。

（4）全基因组选择育种技术研发及标准化个体育种值评估流程建立

① 全基因组选择育种技术的研发：以生长速度、饲料转化效率、繁殖等肉鸡重要经济性状为重点，利用不同类型的多种参数模型（GBLUP、Bayesian B、深度学习等）开展时间序列表型性状和阈性状全基因组选择研究，建立针对特定/重点性状的最优遗传评定模型，提高育种值估计准确性。

② 标准化个体育种值评估流程的建立：完善育种表型组、基因组数据管理/存储系统，建立数据收储、解析与回馈规范；通过后裔成绩形成可监督学习和自进化的智能育种策略，建立整合表型、基因分型到遗传评估的表型-基因型-个体遗传评估的标准化个体育种值评估流程。

（5）优质小型白羽肉鸡新品种（配套系）培育

① 育种目标的确立：调研分析现阶段小型白羽肉鸡的产业情况，面对市场需求，确立小型白羽肉鸡品种重点生产性能的育种目标。

② 专门化品系的持续改良培育：围绕育种目标，收集筛选具有优异特性的育种素材；建立具有特色明显的专门化品系的规模化表型-基因型信息数据库，结合全基因组选择技术，对各专门化品系持续选育，不断提高各品系的性能，优化并稳定各品系特点。

③ 新品种（配套系）的创制：联合科研院校进行深度产学研合作，

结合传统育种方法和现代分子育种技术、全基因组选择技术，以白羽肉鸡、高产蛋鸡以及黄羽肉鸡等专门化品系为素材，根据专门化品系的特点，利用配套系平衡制种方法，开展专门化品系之间的配合力测定。采用三系配套的杂交方式，同时持续开展禽白血病和鸡白痢净化工作，培育出每套父母代母鸡 66 周龄提供雏鸡 200 只以上，商品代 49 日龄上市公母平均体重达 2.0 千克、公母平均料肉比在 1.65 以内的优质小型白羽肉鸡新品种（配套系）。

（6）优质小型白羽肉鸡新品种（配套系）的产业化推广

① 饲养管理技术规范的制定：对培育出的新品种（配套系）开展父母代和商品代鸡的生长发育规律以及关键饲养技术与集成，制定相应的新品种（配套系）饲养管理技术规范。

② 新品种（配套系）的多元化推广：通过采取适合的“公司+农户”、“公司+养殖公司”或其他产业化形式等，结合不同区域对品种的消费需求，多元化推广新品种。

③ 新品种（配套系）特色经济性状开发加工：根据新品种（配套系）特色经济性状，进一步开发下游特色加工产品，增加产品品类及用户需求，从而达到拓宽销售渠道，提高市场占有率的效果，实行产、供、销一体化，延长产业链，共同抵御市场风险。

3、组织方式和管理机制

本项目设有首席专家 1 人，负责项目的统筹工作，包括组织项目内容、

分配任务、管理经费、推动进度和监督进展等。由于管理性事务较为繁琐，因此需要成立首席专家管理办公室，并设立首席专家专职秘书岗位，以协助团队日常管理。

根据岗位性质和工作特点，设立了不同功能研究室。在项目启动后，项目负责人与各研发人员明确任务分配及完成要求，并按照制定的工作计划严格按时完成研究内容。此外，建立质量监督机制、绩效考评、评审制度和协商机制，并设置了知识产权专员，以将知识产权保护贯彻到项目实施全过程。项目进展自觉接受管理部门的监督管理，按要求汇总、报告项目执行情况，并确保成果内容真实可靠。为推动项目的顺利实施，还设立了专家组，由项目组负责人、骨干成员以及相关领域知名专家组成。该专家组定期开展项目进展会议，推动项目的研究进度和具体实施情况，并对项目的研究方案和技术问题等提供咨询。同时，定期以会议评审和现场检查相结合的方式对项目进度的评估，确保项目能够得到有效监督。此外，项目设立执行专家组，方便对具体工作进行讨论、决策和行动，确保研究内容的工作实施能够落到实处。通过建立科学规范、职责分明的协调机制，研究内容得以有效管理。

本项目联合广东广弘种业科技有限公司和华南农业大学，深化产学研校企合作，汇聚企业一线生产经营工作者和高校科研人员，建立了稳固的、长期的合作关系，共建创新平台，基地和联盟等。本项目在完成理论研究，品种培育和品种推广的同时，培养一批具有创造力，积极向上的研发队伍。在项目进行中，队伍在科学技术，团队合作，创新性，凝聚力等方面得到充分的锻炼和培养，将成为我国育种事业发展的重要力量。

联合申报项目协议书

甲方：广东广弘种业科技有限公司

注册地址：河源市东源县顺天镇滑滩村军民共建路 666 号

法定代表人：姚威

统一社会信用代码：91441625MA56NPYJ76

项目负责人：聂庆华

乙方：华南农业大学

注册地址：广东省广州市天河区五山

法定代表人：薛红卫

统一社会信用代码：124400004554165634

项目负责人：蔡柏林

甲方和乙方经友好协商决定联合申报 2024 年省级种业振兴行动专项资金 项目，项目名称：优质小型白羽肉鸡育繁推一体化示范，并达成如下合作协议：

第一条：项目研究工作详细分工：

甲方(主持方)：(1) 统筹项目整体的设计、实施、汇报和考核验收等；(2) 育种核心群和专门化品系的构建；(3) 优质小型白羽肉鸡新品种（配套系）培育；(4) 优质小型白羽肉鸡新品种（配套系）的产业化推广；(5) 基于育种软件开展信息化育种技术研发。

乙方(参与方)：(1) 优质小型白羽肉鸡胫色、肤色和快慢羽分子检测技术的开发；(2) 优质小型白羽肉鸡肉质风味的鉴定及评价；(3) 全基因组选择育种技术研发及标准化个体育种值评估流程建立。乙方（参与方）主要考核指标如下：(1) 开发适用于小型白羽肉鸡胫色、肤色、快慢羽等性状选育的分子标记 3-4 个；(2) 搭建针对专门化品系的表型-基因型-个体遗传评估的标准化个体育种值评估流程 1 套；(3) 发表论文 2-3 篇，其中高水平学术论文 1-2 篇；申请国家发明专利 2-3 件，获授权发明专利 1-2 件。

第二条：经费分配：

1、如果本申报项目获批立项，按政府下达的资助经费，甲方和乙方同意此经费分别按政府资助经费的甲方：65 %、乙方：35 % 进行分配。



2、甲方在收到 广东省农业农村厅 下达的资助经费后的一个月内将乙方所占经费支付给乙方指定帐户。乙方收到经费后应及时向甲方开具收据。

乙方账户信息：

账 户：华南农业大学

帐 号：3602002609000310520

开户行：广州工行五山支行

第三条：企业配套经费比例： 广东广弘种业科技有限公司配套人民币 300 万元。

第四条：知识产权归属及保密：

1. 项目实施过程中所产生的知识产权，优先执行任务下达单位的知识产权管理政策，在此前提下，作如下规定：

①各方独立完成的所有权归各自所有；两方共同完成的由双方共享，具体按照两方的贡献大小进行分配或双方另行商定。

②共同完成的项目成果的转让，须在两方同意的前提下进行，任何一方不得私自转让或许可实施。

2. 项目成果申报各级奖项，两方单位排名根据具体情况另行商定，人员排名原则上按贡献大小先后排名。

3. 两方在合作期间，对合作项目成果及相关技术负有保密义务。未经其他两方书面同意，均不得擅自将项目成果及相关技术以任何方式向任何第三方提供或透露。由泄密的内容而引起的一切法律纠纷和经济损失均由泄密方承担。上述保密义务，在本合同终止或解除之后仍需履行。

第五条：合作项目各方应严格遵守共同签订的合作协议书，除因不可抗拒的客观原因，不得中途撤销或中止合同。在合同期内，某方要求修改合同条款，须各方协商，书面确认后方能生效。

第六条：如合作方因各种原因无法履行合同条款时，由项目负责人报项目主管部门同意后，另寻合作者。

第七条：经批准中途退出合作的一方，应视具体情况将所余经费退回项目主持方，已用经费由项目负责人提出审查报告，报项目主管部门审批。

第八条：合作一方在工作进行中有问题不及时报告，影响项目整体的年度进展者，

项目负责人有权缓拨或停拨下一年度经费，并通报项目主管部门。如影响项目整体无法完成者，将承担相关责任，并报主管部门。

第九条：通知送达：

1. 根据本合同需要，任何一方向另一方发出的全部通知、文件往来及与本合同有关的通知、文件往来等，必须用书面形式，各方确认各自的合法有效送达地址及联系方式如下：

甲方通信地址：河源市东源县顺天镇滑滩村军民共建路 666 号

联系人：李恒丰

联系电话：15920448694

乙方通信地址：广州市天河区五山路华南农业大学动物科学学院新楼

联系人：詹惠娜

联系电话：15918500846

2. 前述联系信息适用于各方往来联系、书面文件送达及争议解决时法律文书送达。因联系方式和联系信息错误或拒收等原因导致无法妥收的，自交邮后第 5 日即视为送达。一方变更名称、地址、联系人、联系方式的，应当在变更后 3 日内及时书面通知其他两方当事人，其他两方当事人实际收到变更通知前的送达仍为有效送达。变更方未及时通知的，其他两方当事人按照变更前的信息进行送达的仍视为有效送达，因此产生的不利后果由变更方承担。

3. 本通知送达条款为独立条款，不受合同整体或其他条款的效力影响，始终有效。

第十条：争议解决

1. 因本合同以及本合同项下订单/附件/补充协议等（如有）引起或有关的任何争议，由合同各方协商解决。协商不成的，应向甲方和乙方所在地有管辖权的人民法院起诉。

第十一条：本协议自两方签字盖章之日起生效，至项目完成之日起终止；若合作申请未获资助，本协议自动废止。

第十二条：本协议一式陆份，两方各执贰份，具有同等法律效力。附件是合同有效组成部分，与本合同具有同等法律效力。

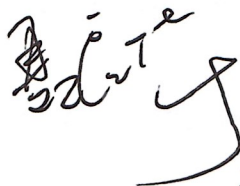
（以下签署页，无合同正文）

(本页为联合申报项目协议书之签署页，无合同正文)

甲方单位（盖章）：
广东广弘种业科技有限公司

乙方单位（盖章）：(4)
华南农业大学

项目负责人（签字）：



项目负责人（签字）



2024年10月13日

2024年10月13日

1.5. 主持：关于广东省自然科学基金-面上项目的合同书

广东省基础与应用基础研究基金项目任务书

受理编号：c23140500002700

项目编号：2023A1515010096

文件编号：粤基金字〔2023〕2号

广东省基础与应用基础研究基金项目
任务书

项目名称：ALKBH5介导lncRNA MYH1G-AS去甲基化调控鸡骨骼肌发育的功能与机制研究

项目类别：广东省自然科学基金-面上项目

项目起止时间：2023-01-01 至 2025-12-31

管理单位（甲方）：广东省基础与应用基础研究基金委员会

依托单位（乙方）：华南农业大学

通讯地址：广东省广州市天河区五山路483号

邮政编码：510642

单位电话：020-85283435

项目负责人：蔡柏林

联系电话：13580356512



（广东科技微信公众号）



（查看任务书信息）



（受理纸质材料二维码）

广东省基础与应用基础研究
基金委员会
二〇二〇年制

填写说明

一、项目任务书内容原则上要求与申报书相关内容保持一致，不得无故修改。

二、项目承担单位通过广东省科技业务管理阳光政务平台下载项目任务书，按要求完成签名盖章后扫描上传到广东省科技业务管理阳光政务平台。

三、签名盖章说明。请分别在单位工作分工及经费分配情况页、人员信息页、签约各方页等地方按要求签字或盖章，签章不合规或错漏将不予受理。其中，人员信息页要求所有参与人员本人亲笔签名，代签或印章无效，漏签将不予受理。

四、本任务书自签字并加盖公章之日起生效，各方均应负本任务书的法律责任，不应受机构、人事变动影响。

五、根据《广东省科学技术厅广东省财政厅关于深入推进省基础与应用基础研究基金项目经费使用“负面清单+包干制”改革试点工作的通知》（粤科规范字[2022]2号），2022年度及以后立项资助的全部省基金项目（包括省自然科学基金、省市联合基金、省企联合基金项目等）均适用“负面清单+包干制”，项目提交申请书和任务书时无需编制费用明细科目预算。

一、主要研究内容和要达到的目标

① 鸡骨骼肌不同类型肌纤维中由m6A修饰介导调控的lncRNA的筛查与分析（本部分研究内容已部分完成，详见研究基础）

分析7周龄杏花鸡胸大肌和比目鱼肌两组织的肌纤维类型组成和肌纤维横截面积。检测两组织的总体m6A RNA甲基化水平差异，并探究造成m6A甲基化水平差异的成因。联合RNA-seq和MeRIP-seq技术，挖掘在鸡不同类型肌纤维组织中由m6A修饰潜在介导调控的lncRNA分子，构建关键调控网络。

② m6A关键去甲基化酶ALKBH5介导调节MYH1G-AS RNA稳定性的验证

分析ALKBH5对MYH1G-AS上m6A位点修饰程度的调节作用；验证ALKBH5对MYH1G-AS的RNA稳定性及转录后表达的调节。明确介导调控MYH1G-AS m6A修饰的m6A阅读蛋白，并探究候选m6A阅读蛋白对MYH1G-AS的RNA稳定性及转录后表达的介导调控。

③ MYH1G-AS的鉴定及功能分析

扩增MYH1G-AS的完整全长序列，并探究其核酸序列结构。分析MYH1G-AS的亚细胞定位及其在鸡不同生长发育阶段和不同组织器官中的表达规律。鉴定MYH1G-AS中潜在开放阅读框（Open Reading Frame, ORF）的蛋白质编码潜力。构建MYH1G-AS过表达/干扰的细胞和活体模型，明确MYH1G-AS对成肌细胞增殖、分化以及鸡骨骼肌肌纤维类型转化和肌肉肥大/萎缩的调控作用。

④ MYH1G-AS与下游RNA结合蛋白互作调控鸡骨骼肌发育的系统研究

分析与MYH1G-AS特异性结合互作的RNA结合蛋白。验证候选RNA结合蛋白与MYH1G-AS的结合互作，并确定它们结合互作的核心区域。检测MYH1G-AS及候选RNA结合蛋白的表达关联。探究MYH1G-AS与下游RNA结合蛋白互作调控鸡骨骼肌发育的分子途径和信号通路。

二、项目预期获得的科研成果及形式

论文及专著情况	国家统计局源刊物以上刊物 发表论文（篇）		2		科技报告（篇）		1	
	其中被SCI/EI/ISTP收录 论文数（篇）		2		培养人才（人）		0	
	专著（册）		0		引进人才（人）		0	
专利情况(项)	发明专利		实用新型专利		外观设计专利		国外专利	
	申请	授权	申请	授权	申请	授权	申请	授权
	0	0	0	0	0	0	0	0


三、项目进度和阶段目标

(一) 项目起止时间： 2023-01-01 至 2025-12-31		
(二) 项目实施进度及阶段主要目标：		
开始日期	结束日期	主要工作内容
2023-01-01	2023-12-31	① 利用RNA-seq和MeRIP-seq技术，分析两组织中的lncRNA和mRNA的表达模式、全面剖析两组织中的RNA m6A修饰图谱。 ② 整合分析RNA-seq和MeRIP-seq测序数据，挖掘在鸡不同类型肌纤维组织中由m6A修饰潜在介导调控的lncRNA分子，构建关键调控网络。 ③ 分析ALKBH5介导的MYH1G-AS去甲基化对MYH1G-AS RNA稳定性和转录后表达水平的介导调控，并探究其调控机理。
2024-01-01	2024-12-31	① 分析MYH1G-AS的亚细胞定位和时空表达规律，鉴定MYH1G-AS的蛋白质编码潜力。 ② 构建MYH1G-AS的过表达/干扰鸡原代成肌细胞模型，分析MYH1G-AS对鸡原代成肌细胞增殖、分化的遗传调控。 ③ 申请人参加全国畜禽遗传标记学术研讨会，与相关领域专家进行学术交流并汇报研究进展。
2025-01-01	2025-12-31	① 通过慢病毒注射法构建MYH1G-AS的过表达/干扰活体模型，确定MYH1G-AS对鸡骨骼肌肌纤维类型转化和肌纤维横截面积变化的影响。 ② 验证MYH1G-AS与下游RNA结合蛋白的结合互作，并探究MYH1G-AS与候选RNA结合蛋白的表达关联。 ③ 整理实验数据，撰写及发表相关论文，提交项目总结和结题报告。

四、项目总经费及省基金委经费预算

1. 省基金委经费下达总额： （大写）壹拾万圆整；（小写 ）10万元；					
2. 省基金委经费年度下达计划：					
年度	2023 年	年	年	年	年
经费(万元)	10.00				

五、人员信息

项目负责人								
姓名	证件号码	年龄	性别	职称	学历	在项目中承担的任务	所在单位	签名
蔡柏林	440111199210094218	31	男	未取得	博士研究生	项目负责人	华南农业大学	

项目组主要成员								
姓名	证件号码	年龄	性别	职称	学历	在项目中承担的任务	所在单位	签名
聂庆华	342824197512182714	48	男	教授	博士研究生	m6A修饰介导调控的lncRNA的挖掘	华南农业大学	
徐海平	430425198109284787	42	女	副研究员	博士研究生	MYH1G-AS的分析鉴定	华南农业大学	徐海平
马曼婷	460031199310164424	30	女	未取得	硕士研究生	ALKBH5介导调节MYH1G-AS稳定性的验证	华南农业大学	马曼婷
孔少芬	44120219970105152X	26	女	未取得	本科	MYH1G-AS的分子功能分析	华南农业大学	孔少芬
周震	460103199903190011	24	男	未取得	本科	MYH1G-AS的分子功能分析	华南农业大学	周震
袁荣帅	370783199510296731	28	男	未取得	本科	MYH1G-AS的作用机制研究	华南农业大学	袁荣帅

六、工作分工及财政经费分配

承担/参与单位名称 (盖章)	工作分工	省级财政科技资金分配 (万元)
华南农业大学	作为项目依托单位，监督及管理项目的实施	10.00
	合计	10.00

七、任务书条款

第一条 甲方与乙方根据《中华人民共和国民法典》及国家有关法规和规定，按照《广东省科学技术厅关于广东省基础与应用基础研究基金（省自然科学基金、联合基金等）项目管理的实施细则（试行）》《广东省省级科技计划项目验收结题工作规程（试行）》等规定，为顺利完成（2023）年ALKBH5介导lncRNA MYH1G-AS去甲基化调控鸡骨骼肌发育的功能与机制研究专项项目（文件编号：粤基金字〔2023〕2号）经协商一致，特订立本任务书，作为甲乙双方在项目实施管理过程中共同遵守的依据。

第二条 甲方的权利义务：

1. 按任务书规定进行经费核拨的有关工作协调。
2. 根据甲方需要，在不影响乙方工作的前提下，定期或不定期对乙方项目的实施情况和经费使用情况进行检查或抽查。
3. 根据《广东省科研诚信管理办法(试行)》等规定对乙方进行科技计划信用管理。

第三条 乙方的权利义务：

1. 确保落实自筹经费及有关保障条件。
2. 按任务书规定，对甲方核拨的经费实行专款专用，单独列账，并随时配合甲方进行监督检查。
3. 经费使用按照广东省级财政科研项目经费使用等有关规定进行管理。
4. 项目依托单位应制定经费使用“负面清单+包干制”内部管理制度并报甲方备案。
5. 使用财政资金采购设备、原材料等，按照《广东省实施〈中华人民共和国招标投标法〉办法》有关规定，符合招标条件的须进行招标。
6. 项目任务书任务完成后，或任务书规定的任务、指标及经费投入等提前完成的，乙方可提出验收结题申请，并按甲方要求做好项目验收结题工作。
7. 若项目发生需要终止结题的情况，乙方须提出终止结题申请，并按甲方要求做好项目终止结题工作。
8. 在每年规定时间内向甲方如实提交上年度工作情况报告，报告内容包含上年度项目进展情况、经费决算和取得的成果等。
9. 按照国家和省有关规定，提交科技报告及其他材料。
10. 利用甲方的经费获得的研究成果，项目负责人和参与者应当注明获得“广东省基础与应用基础研究基金（英文：Guangdong Basic and Applied Basic Research Foundation）（项目编号）”资助或作有关说明。
11. 乙方要恪守科学道德准则，遵守科研活动规范，践行科研诚信要求，不得抄袭、剽窃他人科研成果或者伪造、篡改研究数据、研究结论；不得购买、代写、代投论文，虚构同行评议专家及评议意见；不得违反论文署名规范，擅自标注或虚假标注获得科技计划（专项、基金等）等资助；不得弄虚作假，骗取科技计划（专项、基金等）项目、科研经费以及奖励、荣誉等；不得有其他违背科研诚信要求的行为。
12. 确保本项目开展的研究工作符合我国科技伦理管理相关规定。

第四条 在履行本任务书的过程中，如出现广东省相关政策法规重大改变等不可抗力情况，甲方有权对所核拨经费的数量和时间进行相应调整。

第五条 在履行本任务书的过程中，当事人一方发现可能导致项目整体或部分失败的情形时，应及时通知另一方，并采取适当措施减少损失，没有及时通知并采取适当措施，致使损失扩大的，应当就扩大的损失承担责任。

第六条 本项目技术成果的归属、转让和实施技术成果所产生的经济利益的分享，除双方另有约定外，按国家和广东省有关法规执行。

第七条 根据项目具体情况，经双方另行协商订立的附加条款，作为本任务书正式内容的一部分，与本任务书具有同等效力。

第八条 本任务书一式三份，各份具有同等效力。甲、乙方及项目负责人各执一份，三方签字、盖章后即生效，有效期至项目结题后一年内。各方均应负任务书的法律责任，不应受机构、人事变动的影响。

第九条 乙方必须接受甲方聘请的本项目任务书监理单位的监督和管理。监理单位按照甲方赋予的权利对本项目任务书的履行进行审核、进度调查，对项目任务书变更、经费使用情况进行监督管理及组织项目验收。

说明：1. 本任务书中，凡是当事人约定无需填写的内容，应在空白处划（/）。

2. 委托代理人签订本任务书的，应出具合法、有效的委托书。

八、本任务书签约各方

管理单位（甲方）：	广东省基础与应用基础研究基金委员会（盖章）
法定代表人（或法人代理）：	曾路（盖章）
2023 年 02 月 14 日	
依托单位（乙方）：	华南农业大学（盖章）
法定代表人（或法人代理）：	刘雅红（盖章）
联系人（项目主管）姓名：	倪慧群（盖章）
Email: kjcgxk@scau.edu.cn	
电话: 020-85283435 / 15920301530	
开户单位名称：	华南农业大学
开户银行名称：	广东广州工行五山支行
开户银行帐号：	3602002609000310520
2023 年 3 月 3 日	
联系人（项目负责人）姓名：	蔡柏林（签名）
Email: bolincai@scau.edu.cn	
电话: 13580356512	
2023 年 2 月 22 日	

1.6. 主持：关于中国博士后科学基金面上资助一等资助项目的资助证书



1.7. 主持：关于广州市基础研究计划基础与应用基础研究项目（青年博士“启航”方向）的任务书

任务书编号：2024A04J0172

广州市科技计划项目 任务书

项目名称：ATP2A2调控鸡肉风味前体组成的作用研究

承担单位：华南农业大学

项目负责人：蔡柏林

计划类别：基础研究计划

专题名称：2024年度基础与应用基础研究专题

支持方向：青年博士“启航”项目

组织单位：华南农业大学

起止时间：2024-01-01 至 2025-12-31

主管处室：基础研究处

广州市科学技术局制

二〇二四年

填写说明

1. 任务书甲方为广州市科学技术局；乙方为项目承担单位；丙方为项目组织单位。

2. 任务书基于项目申报书转换而成，请按照“广州科技大脑”提示在线填写核实，若存在不填写内容的栏目，请用“无”表示；任务书中的单位名称应为规范全称，并与单位公章一致。

3. 乙方与合作单位的合作协议自动从项目申报书中读取，如需变化调整，须待任务书签订后，按要求及时办理重大变更。

4. 乙方完成项目任务书在线填写，依次提交丙方和甲方审核确认后，按要求登录“穗好办”APP完成电子签章。不具备电子签章条件的单位，经与业务主管处室沟通对接后，可下载电子版项目任务书用A4纸双面打印装订签章；一式六份报甲方和丙方签章，其中甲方两份丙方两份，项目承担单位和项目负责人各一份。

5. 涉密项目请在“广州科技大脑”下载项目任务书模板，按保密要求离线填写报送。

6. 项目申报书是项目任务书填报的重要依据，未经甲方许可，乙方不得修改考核指标，调整主要研究内容。项目任务书将作为项目实施管理、验收结题和监督评估的重要依据。

7. 项目任务书中的“备注”，包括重要的必须补充的内容。

8. “广州科技大脑”是项目管理过程中重要通知和文书的电子送达平台。为确保电子送达渠道畅通，乙方和项目负责人应及时更新维护“广州科技大脑”的单位和个人信息。

9. 根据相关要求，项目涉及人体临床研究的，项目需经医学伦理委员会审查通过并在任务书附件栏上传相关佐证材料。

一、项目基本信息

项目 基本 信息	项目名称	ATP2A2调控鸡肉风味前体组成的作用研究
	申请市财政科技经费	5(万元)
	研究期限	2（年）
项目 摘要	骨骼肌是动物体内最大的组织，其生长发育与畜禽的产肉量和肉质风味有着紧密的联系。申请人前期研究发现，ATP2A2调控鸡肌发生过程，且ATP2A2的表达水平与甘油磷脂、赖氨酸、次黄嘌呤等肉风味前体物质的含量显著相关，提示其参与鸡肉风味前体物质形成的遗传调控。本项目拟联合多组学测序技术并结合分子生物学实验验证，系统探究ATP2A2对鸡肉风味前体物质形成的调控作用，预期成果可为鸡肉品质的改良提供理论依据。	

二、项目单位情况

项目 承担 单位	单位名称	华南农业大学	统一社会信用代码	124400004554165634
	注册时间	1952-01-01	单位类型	高等院校
	注册地址	广东省广州市天河区五山路483号		
	办公地址	广东省广州市天河区五山路483号		
	联系人	姓名	倪慧群	
		手机号码	13711345768	
		电子邮箱	kjcgxk@scau.edu.cn	
	开户银行	广东广州工行五山支行		
	开户户名	华南农业大学		
银行账号	3602002609000310520			

三、项目负责人信息

姓名	蔡柏林	证件类型	身份证
证件号码	440111199210094218	性别	男
出生日期	1992-10-09	民族	汉族
国籍	中国	学历	博士研究生
学位	博士	学位授予国家 (或地区)	中国
职务	无	职称	无
所学专业	遗传学	手机号码	13580356512
办公电话	020-86241895	电子邮箱	bolincai@scau.edu.cn

四、项目经费信息

本项目总投入：¥（5）万元，其中，市财政科技经费：¥（5）万元，自筹经费：¥（0）万元。

经费下达计划			
资金来源	小计	市财政科技经费	自筹经费
2024	5	5	0
总计	5	5	0

（单位：万元）

注：本专题纳入“包干制”，市财政科技经费按市科技计划项目经费“包干制”相关规定执行。

五、预期代表性成果

项目负责人在项目实施期内，以该项目作为资助项目获得以下5种情形之一且经费使用符合规定的，由组织单位审核后通过验收。

（一）项目实施期内，以第一作者/通讯作者发表论文1篇或以上（须标注资助项目编号）；

（二）项目实施期内，以第一完成人申请或授权专利、软件著作权1项或以上；

（三）项目实施期内，获省级以上科技计划项目或人才项目支持1项或以上；

（四）项目实施期内，获省级以上科技奖励（含列入获奖团队成员名单）1项或以上；

（五）项目实施期内，获得职称晋升。

六、备注

专题补充约定条款：

甲方对未履行勤勉尽责义务的相关责任主体，自作出处理结论之日起，依照法律法规规定或任务书约定实施惩戒5年，取消相关责任主体申报市科技计划项目、申领市科技计划项目经费的资格。

预期代表性成果需在实施期内获得。

项目承担单位（乙方）及项目负责人承诺书

承诺书

本单位/本人作为广州市科技计划项目承担单位/项目负责人，将严格遵守广州市科技计划管理相关规定，严格履行自身责任，加强对项目组人员及合作单位的管理，在此郑重承诺：

（一）确保与本项目有关的全部材料真实、合法、有效，未侵犯其他方知识产权等权利，不存在多头申报、重复申报行为；

（二）严格遵守《广州市科技创新条例》《广州市科技计划项目管理办法》《广州市科技计划项目经费管理办法》《广州市科技计划科技报告管理办法》等相关规定，实施项目和经费管理；

（三）严格遵守国家、省、市关于科研诚信和科技伦理的有关法律、法规，相关政策以及各项规定，加强项目实施过程中的科研诚信及科技伦理管理，恪守科研道德准则。

如有违反，本单位/本人愿意接受相关部门做出的各项处理决定，包括但不限于终止项目、停拨经费、核减经费、追回经费，取消一定期限广州市科技计划项目申报资格，记入科研失信行为数据库，将不良行为向社会公开等。

项目承担单位：华南农业大学

日期：2023年12月14日

项目负责人：蔡柏林

日期：2023年12月14日

任务书签署

甲乙丙三方根据《广州市科技计划项目管理办法》《广州市科技计划项目经费管理办法》《广州市科技计划科技报告管理办法》等有关文件规定，以及有关法律、政策和管理要求，签署本任务书。

签订地点：广州市越秀区

广州市科学技术局（甲方）：广州市科学技术局
局项目经办人：蒋韬略 联系电话：83124150
责任处室负责人：麦胜文

2024年01月17日

项目承担单位(乙方): 华南农业大学
二级部门: 华南农业大学动物科学学院
项目负责人: 蔡柏林
项目经费汇入账号
账户名: 华南农业大学 账号: 3602002609000310520
开户银行: 广东广州工行五山支行
财务负责人: 肖斐

2023年12月14日

组织单位（丙方）：华南农业大学
项目经办人：倪慧群

2023年12月15日

1.8. 主持：关于华南农业大学特定高校学科建设专项（人才引进类）课题的任务书

特定高校学科建设专项（人才引进类）

项目（课题）任务书

项目名称： 国猪免疫代谢特征形成的机制解析

课题名称： 鸡肉风味前体物质形成的遗传调控研究

项目起止时间： 2024 年 01 月 01 日 至 2025 年 12 月 31 日

管理单位（甲方）： 华南农业大学

依托学院（乙方）： 动物科学学院

课题负责人（丙方）： 蔡柏林 联系电话： 13580356512

课题联系人： 蔡柏林 联系电话： 13580356512

华南农业大学
二〇二二年制

一、研究计划

（一）主要研究内容及创新点

主要研究内容：联合4D-磷酸化修饰蛋白质组、TMT标记定量蛋白质组、非靶向代谢组等多组学测序技术，挖掘参与鸡肉风味前体物质形成的蛋白质磷酸化修饰标记，构建关键磷酸化修饰蛋白-代谢物调控网络，系统阐明蛋白质翻译后修饰调控肉鸡优良肉质性状形成的遗传基础和调控机制。

创新点：骨骼肌由不同类型肌纤维组成。肌肉中不同类型的肌纤维具有不同的特性，对肌肉品质具有重大影响。水溶性化合物包括糖、氨基酸、肌酸、肌肽和核苷酸等物质，是决定肉类风味的主要风味前体物质。深入解析骨骼肌肌纤维发育及风味前体物质产生的分子机制，对肉鸡肌肉品质性状的遗传改良具有重大指导意义和现实意义。本项目通过深入探究蛋白质磷酸化调控骨骼肌肌纤维发育，影响风味前体物质产生的分子机制，研究结果将有助于加快揭示鸡肉品质形成的分子机理。

（二）拟开展的研究在国际国内同领域所处的地位

翻译后修饰是蛋白质动态反应和相互作用的一个重要分子基础，是增加蛋白质组多样性的关键机制。新近研究发现，翻译后修饰可通过调节肌肉组织中蛋白质的结构和功能，对畜禽肉品质具有重要的调控作用。当前，尽管已有利用组学技术挖掘参与骨骼肌肌纤维发育及风味前体物质产生的蛋白质磷酸化修饰，但其中确切的遗传调控机制仍鲜有研究。本项目拟联合多组学测序技术，系统探究蛋白质磷酸化修饰对鸡肉风味前体物质形成的遗传基础和调控机制，属同领域领先地位。

（三）开展的研究对提升我国相关领域科技创新能力和发展战略性新兴产业等的主要作用

我国是禽类生产和消费大国，畜禽产品提供我国居民摄入蛋白质总量和热量的40-50%。保证畜禽产品高效优质的生产是决定我国食物供给、社会稳定以及国家安全的重要基础。习近平总书记指出，“树立大食物观，要从更好满足人民美好生活需要出发”，保障肉产品供应，不仅要“吃得饱”，更要“吃得好”。因此，如何提高鸡肉品质俨然成为当前家禽遗传育种的研究重点。本项目聚焦挖掘蛋白质磷酸化修饰对鸡肉风味前体物质形成的遗传基础和调控机制，相关研究结果将为鸡肌肉品质的遗传改良提供分子理论依据。

（四）科研组织管理、国内外合作设想

科研组织管理：建立明确的项目组织管理形式，定期召开会议研究和交流总结项目的进度及完成情况。严格依据国家相关法规，财务会计管理制度和单位内部控制制度，对项目经费支出实行详细预算控制和辅助会计核算，确保了资金专款专用。

国内外合作设想：项目实施期间积极参加国际/国内学术会议，与领域专家交流请教。

（五）个人能力提升、人才培养和团队建设

个人能力提升：扎实基础科学研究，结合生产一线需求，助力“产学研”协调发展争取职称晋升。同时，在符合国家政策规定和申报条件的情况下，每年积极申报“国家优青”、“万人计划青年拔尖人才”等国家级、省部级人才项目。

人才培养和团队建设：积极申报硕士研究生导师、博士研究生导师等岗位，按学校、学院规定培养或协助培养研究生。协助团队做好“农业农村部鸡遗传育种与繁殖重点实验室”、“广东省农业动物基因组学与分子育种重点实验室”、“广东省家禽品种测定站”等重点实验室平台的建设。

二、预期考核目标（参照人才引进合同指标填报）

1. 发表SCI论文1篇；
2. 申请国家发明专利1项。

三、经费预算

直接费用	经费额	用途说明
(1) 设备费	0.00	/
(2) 材料费	1.50	用于项目研究过程中所需的各种实验动物、实验试剂、实验耗材等的采购
(3) 测试化验加工外协费	30.00	在项目研究过程中支付给外单位的检验、测试、化验及加工等费用
(4) 燃料动力费	0.00	/
(5) 差旅费/会议费/国际合作与交流费	0.00	/
(6) 出版/文献/信息传播/知识产权事务费	0.00	/
(7) 劳务费	3.50	研究生劳务费
(8) 专家咨询费	0.00	/
(9) 直接费用其他支出	0.00	/
合计	35.00	/
其他需说明的情况：无。		

四、签约各方

管理单位（甲方）： 华南农业大学（盖章）

科研部门负责人（签章）：



2024年12月3日

依托学院： 动物科学学院（盖章）

学院负责人：（签字）

项目负责人：（签字）



2024年12月04日

课题负责人（丙方）：

本人承诺由特定高校学科建设专项（Specific university discipline construction project）经费资助产出的相关科研成果，发表论文等成果将标注项目资助编号“2023B10564001”。

（签字）

2024年12月2日

2.1. 主参：关于农业生物育种国家科技重大专项的课题任务书

课题编号：2023ZD0406401

密 级：公开

科技创新 2030—重大项目
课题任务书

课题名称	种质资源优异性状挖掘及多组学解析
所属项目名称：	优质加工型肉鸡新品种设计与培育
所属重大项目：	农业生物育种重大项目
重大项目实施管理机构：	农业农村部科技发展中心
课题牵头承担单位：	华南农业大学（公章）
课题负责人：	聂庆华
执行期限：	2023 年 9 月至 2025 年 12 月

中华人民共和国科学技术部制

2023 年 9 月

填写说明

- 一、任务书甲方即项目牵头承担单位，乙方即课题承担单位。
- 二、任务书通过“国家科技计划管理信息系统公共服务平台”，按照系统提示在线填写。
- 三、任务书中的单位名称，请按规范全称填写，并与单位公章一致。
- 四、任务书要求提供乙方与所有参加单位的合作协议，需对原件进行扫描后在线提交。
- 五、任务书中文字须用宋体小四号字填写。
- 六、凡不填写内容的栏目，请用“无”表示。
- 七、乙方完成任务书的在线填写，提交甲方审核确认后，用 A4 纸在线打印、签章后上传电子扫描件。
- 八、如项目下仅设一个课题，课题任务书只需填报课题基本信息表与课题预算部分。
- 九、涉密课题请在“国家科技计划管理信息系统公共服务平台”下载任务书的电子版模板，按保密要求离线填写、报送。一式八份报项目牵头承担单位签章，其中课题承担单位一份，课题负责人一份，作为项目任务书附件六份。
- 十、《项目申报书》和《项目任务书》是本任务书填报的重要依据，任务书填报不得降低考核指标，不得自行对主要研究内容作大的调整。《项目申报书》和《项目任务书》和本任务书将共同作为课题过程管理、综合绩效评价（验收）和监督评估的重要依据。

课题基本信息表

课题名称	种质资源优异性状挖掘及多组学解析						
课题编号	2023ZD0406401						
所属项目名称	优质加工型肉鸡新品种设计与培育						
项目编号	2023ZD04064						
所属重大项目	农业生物育种重大项目						
密级	<input checked="" type="checkbox"/> 公开 <input type="checkbox"/> 秘密 <input type="checkbox"/> 机密			单位总数	5		
课题成果技术就绪度	<input checked="" type="checkbox"/> 1.发现基本原理 <input checked="" type="checkbox"/> 2.形成技术方案 <input type="checkbox"/> 3.方案通过验证 <input type="checkbox"/> 4.形成单元并验证 <input type="checkbox"/> 5.形成分系统并验证 <input type="checkbox"/> 6.形成原型并验证 <input type="checkbox"/> 7.现实环境的应用验证 <input type="checkbox"/> 8.用户验证认可 <input type="checkbox"/> 9.得到推广应用						
课题成果应用的主要国民经济行业	农、林、牧、渔业 畜牧业						
课题的社会经济目标	一级目标 农林牧渔业发展 二级目标 畜牧业发展						
经费预算	课题总经费根据概算批复结果核定，课题年度经费按照项目任务书约定下达。配套经费不得低于项目任务书约定要求。						
课题周期节点	起始时间	2023 年 9 月		结束时间	2025 年 12 月		
	实施周期	共 28 个月		预计中期时间点	2024 年 12 月		
课题承担单位	单位名称	华南农业大学			单位法定代表人姓名	薛红卫	
	单位性质	大专院校			组织机构代码	124400004554165634	
	单位主管部门	广东省教育厅			隶属关系	地方	
	单位所属地区	广东省			地市（市、自治州、盟）	广州市天河区	
	通信地址	广东省广州市天河区五山路483 号			邮政编码	510642	
	单位开户名称	华南农业大学					
	开户银行（全称）	中国工商银行股份有限公司广州五山支行			汇入地点	广东省广州市	
	银行账号	3602002609000310520			银行机构代码	102581000546	
课题负责人	姓 名	聂庆华		性 别	<input checked="" type="checkbox"/> 男 <input type="checkbox"/> 女	出生日期	1975-12-18
	证件类型	身份证		证件号码	342824197512182714		
	所在单位	华南农业大学					

	最高学位	<input checked="" type="checkbox"/> 博士 <input type="checkbox"/> 硕士 <input type="checkbox"/> 学士 <input type="checkbox"/> 其他		
	职 称	<input checked="" type="checkbox"/> 正高级 <input type="checkbox"/> 副高级 <input type="checkbox"/> 中级 <input type="checkbox"/> 初级 <input type="checkbox"/> 其他		职务 副院长
	电子邮箱	nqinghua@scau.edu.cn	移动电话	13922195759
课题 联系 人	姓 名	蔡柏林	电子邮箱	bolincai@scau.edu.cn
	固定电话	020-85285702	移动电话	13580356512
	证件类型	身份证	证件号码	440111199210094218
课题 财务 负责 人	姓 名	肖斐	电子邮箱	xiaofei@scau.edu.cn
	固定电话	020-85288032	移动电话	13416122195
	证件类型	身份证	证件号码	362421198305040024
其他 参与 单位	序号	单位名称	单位性质	组织机构代码
	1	中国农业大学	高等学校	12100000400018162 G
	2	浙江省农业科学院	事业型研究单位	12330000470001585 G
	3	江苏省农业科学院	事业型研究单位	12320000466005284 8
	4	佛山科学技术学院	高等学校	1244060045607389X C
课题参 加人数	10人。其中：	高级职称 <u>7</u> 人，中级职称 <u>3</u> 人，初级职称 <u>0</u> 人，其他 <u>0</u> 人；		
		博士学位 <u>10</u> 人，硕士学位 <u>0</u> 人，学士学位 <u>0</u> 人，其他 <u>0</u> 人。		
课题 简介 (限 500 字以内)	本课题拟收集特色地方种质资源，摸清不同种质资源相关重要经济性状的表型特性。针对黄羽肉鸡生产效率低、腹脂率高、胴体品质差等问题，采用先进的多组学技术系统解析黄羽肉鸡饲料转化率、肌肉生长、腹脂沉积、胴体品质等重要经济性状的遗传调控规律，鉴定出影响上述性状的关键功能基因和位点，充分挖掘地方鸡种特异基因资源，建立黄羽肉鸡重要经济性状的表型-基因型信息数据库，为研发出适合黄羽肉鸡生产的平衡选育技术体系和方法提供理论依据，助力生产效率高、节粮、胴体品质好的屠宰加工型肉鸡新品种（系）的培育。			

填表说明：1.组织机构代码指企事业单位国家标准代码，单位若已三证合一请填写单位统一社会信用代码，无组织机构代码的单位填写“000000000”；
2.单位公章名称必须与单位名称一致；
3.单位开户名称应与单位名称一致，如有开户名称不一致等特殊情况，必须提供证明文件。

九、课题参加人员基本情况表

填表说明：1、专业技术职称：A、正高级 B、副高级 C、中级 D、初级 E、其他；
 2、投入本课题的全时工作时间（人月）是指在课题实施期间该人总共为课题工作的满月度工作量；累计是指课题组所有人员投入人月之和；
 3、课题固定研究人员需填写人员明细；
 4、是否有工资性收入：Y、是 N、否；
 5、人员分类代码：B、课题负责人 C、项目/课题骨干 D、其他研究人员；
 6、工作单位：填写单位全称，其中高校要具体填写到所在院系。

序号	姓名	性别	出生日期	证件类型	证件号码	专业技术职称	职务	最高学位	专业	投入本课题的全时工作时间（人月）	人员分类代码	在课题中分担的任务	是否有工资性收入	工作单位
1	聂庆华	男	1975/12/18	身份证	342824197512182714	正高级	副院长	博士	动物遗传育种与繁殖	14	B	种质资源优异性状挖掘及多组学解析	Y	华南农业大学动物科学学院
2	罗庆斌	男	1969/05/20	身份证	513101196905200034	副高级	无	博士	动物遗传育种与繁殖	9	C	种质资源优异性状挖掘及多组学解析	Y	华南农业大学动物科学学院
3	蔡柏林	男	1992/10/09	身份证	440111199210094218	副高级	无	博士	遗传学	9	C	种质资源优异性状挖掘及多组学解析	Y	华南农业大学动物科学学院
4	陈黎	女	1984/04/29	身份证	320324198404296564	副高级	无	博士	家禽遗传育种	9	C	种质资源优异性状挖掘及多组学解析	Y	浙江省农业科学院
5	顾天天	女	1993/10/29	身份证	320681199310293643	中级	无	博士	家禽遗传育种	9	C	种质资源优异性状挖掘及多组学解析	Y	浙江省农业科学院

十、课题信息表

序号：1—1 课题编号：2023ZD0406401 课题名称：种质资源优异性状挖掘及多组学解析

填表说明：单位类型为课题牵头单位或课题参与单位。					
序号	单位名称	纳税人识别号（统一社会信用代码）	单位类型	任务分工	研究任务负责人
	(1)	(2)	(3)	(4)	(5)
1	华南农业大学	统一社会信用代码 124400004554165634	课题牵头单位	黄羽肉鸡重要经济性状的表型-基因型数据库构建，黄羽肉鸡种质资源的三维基因组景观研究	聂庆华 蔡柏林
2	中国农业大学	统一社会信用代码 12100000400018162G	课题参与单位	利用基因组学鉴定黄羽肉鸡种质资源优异性状的特性	曲鲁江
3	浙江省农业科学院	统一社会信用代码 123200004660052848	课题参与单位	肉鸡生长及肉质性状遗传研究	陈黎
4	江苏省农业科学院	统一社会信用代码 123200004660052848	课题参与单位	多组学整合分析挖掘黄羽肉鸡腹腔脂肪沉积的关键基因和解析其遗传调控机制	雷明明
5	佛山科学技术学院	统一社会信用代码 1244060045607389XC	课题参与单位	多组学解析黄羽肉鸡饲料转化效率的遗传机制	陈丝宇

十一、相关附件

1. 乙方与参加单位有关协议（须加盖乙方与参加单位公章、法人签字签章；协议文件须扫描上传。如无参加单位，则不填）；

任务书签署

甲乙双方根据《国务院印发关于深化中央财政科技计划（专项、基金）管理改革方案的通知》（国发〔2014〕64号）、《国务院关于优化科研管理提升科研绩效若干措施的通知》（国发〔2018〕25号）、《国务院办公厅关于改革完善中央财政科研经费管理的若干意见》（国办发〔2021〕32号）、《科学技术活动违规行为处理暂行规定》（科学技术部令第19号）、《科技部 财政部关于印发〈中央财政科技计划（专项、基金等）监督工作暂行规定〉的通知》（国科发政〔2015〕471号）、《科技部 自然科学基金委关于进一步压实国家科技计划（专项、基金等）任务承担单位科研作风学风和科研诚信主体责任的通知》（国科发监〔2020〕203号）、《科技部、财政部、自然科学基金委关于进一步加强统筹国家科技计划项目立项管理工作的通知》（国科办资〔2022〕107号）等有关文件规定，以及有关法律、政策和管理要求，依据项目立项通知，签署本任务书。

同时，本单位和课题负责人郑重承诺：对本课题所有成果产出（包括但不限于新产品、新技术、标准、论文、专利等）的真实性、与项目（课题）的关联性等负责，将按要求落实科研作风学风和科研诚信主体责任；课题经费全部用于与本课题研究工作相关的支出，不截留、挪用、侵占，不用于与科学研究无关的支出；接受并积极配合相关部门的监督检查。如有违反，本单位和课题负责人以及相关成果产出者愿接受项目管理专业机构和相关部门做出的各项处理决定，包括但不限于终止课题执行、追回课题经费，取消一定期限国家科技计划项目（课题）申报资格，记入科研诚信严重失信行为数据库以及主要负责人接受相应党纪政纪处理等。

项目牵头承担单位（甲方）：

广东温氏南方家禽育种有限公司

法定代表人签字（签章）：



项目负责人签字（签章）：

张院平

2023年12月11日

课题牵头承担单位（乙方）：

华南农业大学

法定代表人签字（签章）：

薛红已



课题负责人签字（签章）：

王二平

2023年12月8日

首页

政务

办事

互动

服务

数据

请输入关键字

您现在的位置： 首页 > 政务 > 通知公告

政务

政府信息公开

今日头条

政务要闻

专项业务

通知公告

委托服务

农业法治

政策解读

建议提案办理

规划统计

信用信息双公示

权责清单

热点专题

关于2023年广州市农业科研项目资金安排计划的公示

来源： 科教处 时间： 2023-06-07 17:31:51 浏览次数： 1530

根据《广州市农业农村局关于开展 2023 年市级财政农业农村项目入库储备工作的通知》（穗农函〔2022〕345号）和《广州市农业农村局关于印发2023年市级财政农业科研项目遴选方案的通知》（穗农函〔2022〕548号）要求，经项目申报、处室初审、专家评审、局项目评审小组评审、局务会局党组会审议等程序，拟将《特色蔬菜种质资源保护与利用研究》等16个农业科研项目列入2023年广州市农业科研项目资金安排计划（附件）。现予以公示，公示时间为6月7日-6月13日。如有异议，可在公示期内向广州市农业农村局反映，并留下姓名和联系方式，以便必要时进一步听取意见。

联系人：刘显恩

联系电话：020-86392359

邮 箱：pengyl@gz.gov.cn

附件：2023年广州市农业科研项目资金安排计划

附件

2023年广州市农业科研项目资金安排计划

序号	项目名称	申报单位
一、种质资源收集、保护和利用		
1	特色蔬菜种质资源保护与利用研究	广州市农业科学研究院
2	梯面镇古茶树种质普查及保护	广州市花都区梯面镇 人民政府
二、开展种业基础研究		
3	家禽基因组大数据平台建设及品种鉴定分子方法研究	华南农业大学
4	基于第三代分子标记的农作物品种真实性鉴定技术研发与平台建设	广州市农业科学研究院
三、特色种业创新攻关和科技成果示范推广		
5	广州蔬菜新品种展示与推广	广州市农业科学研究院
6	现代蔬菜育种技术研究和新品种选育与示范	广州市农业科学研究院

7	植物组织培养工程研究中心建设	广州市农业科学研究院
8	特色鲜食玉米新品种创新与示范应用	广州市农业科学研究院
9	绿色优质高效水稻新品种选育及示范应用	广州市农业科学研究院
10	多年生稻品种引种试验示范	广州市农业科学研究院
11	高档花卉新品种选育研究与试验示范	广州花卉研究中心
12	红螯螯虾全雄育种材料的创制及应用	广州南沙华农渔业 研究院
13	鲜食玉米生物育种创新及新品种选育	仲恺农业工程学院
14	岭南优新水果新品种选育示范推广及配套设施升级改造	广州市果树科学研究所
15	加州鲈抗虹彩病毒优良品种选育与推广示范	广州南沙华农渔业 研究院
16	兜兰新种质创制与试验示范推广	广州花卉研究中心

 打印

分享到：  

[关于我们](#) | [网站地图](#) | [联系我们](#) | [网站申明](#) | [隐私安全](#) | [使用帮助](#)

广州市农业机械化技术推广站版权所有，未经授权禁止复制或建立镜像

主办单位：广州市农业农村局 运营维护及技术支持：广州市农业机械化技术推广站 访问人数统计：**4247797**

公安机关备案号：44011102001333 粤ICP备20004752号-1 网站标识码：4401000027



广州市农业农村局 2023 年市级财政农业 农村项目——实施方案

项 目 名 称：	家禽基因组大数据平台建设及品种鉴定 分子方法研究
申 报 单 位：	华南农业大学
项 目 负 责 人：	聂庆华
主 管 部 门：	广州市农业农村局
申 报 日 期：	2022 年 7 月 16 日

一、项目（课题）单位概况

（一）承担单位概况

华南农业大学是国家“双一流”建设高校，全国重点大学，广东省和农业部共建的“211工程”大学，广东省高水平大学重点建设高校，以农业科学、生命科学为优势，以热带亚热带区域农业研究为特色。学校共有101个本科专业，14个博士学位授权一级学科，1个博士专业学位类别，30个硕士学位授权一级学科，19个硕士专业学位类别。有国家“双一流”建设学科1个，ESI排名前1%学科12个，国家重点学科5个，国家重点（培育）学科1个，广东省重点学科17个，广东省重点建设学科10个，农业部重点学科5个和国家林草局重点学科3个。

学校师资力量雄厚。现有教职工3438人，其中专任教师2634人（正高级476人，副高级952人）；院士3人，国家级人才58人，省级人才107人；国家级教学名师3人，国家级教学团队4个；博士生导师320人，学术型硕士生导师895人，专业型硕士生导师1314人。

学校科研创新能力强。现有国家级科研平台9个，省部级科研平台104个，广东省高校特色新型智库3个。近五年来，获国家科学技术奖12项，实现国家科技进步、技术发明和自然科学三大奖全覆盖。

（二）人员状况

项目负责人：聂庆华，华南农业大学二级教授、博士生导师，国家特支计划科技创新领军人才，教育部新世纪优秀人才，国家重点研发计划重点专项首席科学家，“广东特支计划”畜禽种业自主创新团队负责人，畜禽育种国家地方联合工程研究中心副主任，广东省家禽业协会秘书长。先

后入选教育部新世纪优秀人才、科技部中青年科技创新领军人才以及万人计划科技创新领军人才。近年来承担国家自然科学基金国际（地区）合作与交流项目、国家自然科学基金-广东联合基金、广东特支计划本土创新创业团队等项目，主持广东省家禽品种测定站项目建设。近五年主持 1000 万元以上科研项目 3 个，研究成果“优质鸡分子改良方法建立及其在新品种培育中的应用”获得 2012 年广东省科技进步二等奖，“清远麻鸡安全、优质、生态养殖集成技术与示范”获得 2014 年广东省科技进步三等奖，“高档优质肉鸡新品种的培育与应用”获得 2018 年度广东省科技进步一等奖。创建了黄肤色、麻羽、矮小型等 6 项单基因的分子育种技术，快速解决了优质肉鸡整齐度差的缺点。在 *Cell Death Differ*、*J Pineal Res*、*J Cachexia Sarcopenia* 等高水平期刊发表 SCI 论文共计 50 余篇，其中影响因 10 分以上论文 4 篇；授权专利 8 件，制定肉鸡行业标准 2 项。参编《分子遗传学》《动物遗传学》2 部教材。

项目骨干 1：黎镇晖，博士，华南农业大学副研究员，硕士生导师。2017 年 7 月至 2020 年 12 月，在华南农业大学生物学流动站博士后从事鸡的肌肉生长发育研究工作，期间赴美国洛克菲勒大学访学一年。2021 年 1 月，以突出人才引进到华南农业大学动物科学学院工作。先后主持“十四五”国家重点研发计划项目子课题、国家自然科学基金青年项目、广东省基础与应用基础研究基金重点项目、中国博士后基金、广州市基础与应用基础研究项目等课题。以第一作者或通讯作者（含并列）在 *Journal of Pineal Research* (IF=12.936)、*Journal of Cachexia Sarcopenia and Muscle* (IF=12.911, ESI 高被引论文)、*Molecular Therapy - Nucleic Acids* (IF=10.18)等

期刊发表 SCI 论文 11 篇。授权专利 4 项，获得广东省农业推广奖二等奖等科研奖励。担任 Journal of Agricultural and Food Chemistry, Frontier in Genetics, Journal of Virology 等期刊审稿人。

项目骨干 2: 蔡柏林，博士，华南农业大学首聘副教授，主要从事肉鸡骨骼肌生长发育的遗传调控研究。先后主持“十四五”国家重点研发计划项目子课题、广东省自然科学基金-面上项目、中国博士后科学基金面上资助一等资助等省级及以上科研项目 4 项。以第一作者（含并列）在 Molecular Therapy-Nucleic Acids、Cell Death & Disease、Journal of Animal Science and Biotechnology 等著名期刊发表高水平 SCI 论文 7 篇，授权专利 2 件，参编专著 1 部。

项目骨干 3: 张细权，华南农业大学教授，动物遗传育种与繁殖专业博士，国家肉鸡产业体系岗位专家，兼任中国畜牧兽医学会畜禽遗传标记学分会理事长，家禽学分会副理事长，动物遗传育种分会常务理事，国家畜禽遗传资源委员会家禽专业委员会委员等学术职务，主要从事分子遗传与家禽育种研究，主持完成国家基金、973 课题、863 课题等各级课题近 20 多项，在 Poultry Science, Cell death and differentiation, Journal of Cachexia, Sarcopenia and Muscle, Cell death & disease, DNA research, BBA-gene regulatory mechanisms 等高水平期刊发表研究论文 342 篇，其中 SCI 收录超过 141 篇，13 项成果获得省部级以上科技奖励（其中 1 项国家奖, 1 项广东省一等奖），国务院特殊津贴获得者。

项目骨干 4: 张德祥，研究员，由华南农业大学动物科学学院下派到广东温氏集团南方家禽育种有限公司工作，任副总经理，主管优质鸡和番

鸭的育种。主持培育的“新兴矮脚黄鸡”，“新兴黄鸡Ⅱ号”二个优质肉鸡新品种在 2001 年通过国家品种审定，主持培育的“新兴竹丝鸡 3 号”，“新兴麻鸡 4 号”于 2007 年 7 月通过国家品种审定，主持培育的“天露黄鸡”，“天露黑鸡”于 2014 年通过国家品种审定，主持培育的“温氏青脚麻鸡 2 号”于 2015 年通过国家品种审定。主持的“新兴矮脚黄鸡品种的培育和推广”于 2004 年获全国农牧渔业丰收奖二等奖。主持的“天露黑鸡配套系的选育与推广”于 2015 年获得吴常信动物遗传育种生产与推广成果奖。主持的“育种新技术在新兴矮脚黄鸡配套系选育中的应用与推广”于 2014 年获得广东省农业技术推广奖一等奖。具有丰富的育种经验。

项目骨干 5: 罗庆斌，华南农业大学副教授，农学博士，硕士生导师。主要从事《养禽学》，《珍禽学》，《水禽学》等家禽生产专业课的教学工作及动物遗传育种与繁殖，动物健康养殖与安全生产学科的科研工作，研究方向为家禽健康养殖与安全生产，分子遗传与动物育种，现代畜禽育种与产业化。

项目骨干 6: 李红梅，华南农业大学副教授，任教以来多次获得优秀班主任奖，教学排名多次排名第一，获得学院青年教师教学大赛一等奖，教学十佳等荣誉奖。从教以来主持和参与各类项目 29 项。主持项目 8 项，主持国家自然科学基金委下达的青年基金 1 项，广东省人才项目 1 项,主持种质资源库子项目 2 项，主持横向课题 1 项（150 万），主持广东省畜禽地方品种保护与开发利用提升工程项目子课题一项（40 万）。主持科创中心项目 1 项（100 万），主持国家重点研发项目 1 项（50 万）。作为主

要人员参与国家自然科学基金面上项目 3 项。主要参与广东省公益项目 1 项。参与完成国家自然科学基金面上及重大项目 20 余项。广东省中国科学院全面战略合作项目一项。目前以第一作者和合作作者形式共发表 SCI 文章 30 余篇。第一作者或通讯作者 SCI 文章 11 篇，最高影响因子 8.886。合作前 3 作者 SCI 论文 1 篇（NATURE COMMUNICATIONS，1 区，影响因子 12.353.）。第一作者核心期刊 4 篇，合作 SCI 文章 19 篇。研究方向为家禽遗传育种与繁殖-抗病育种（三大肿瘤疾病和代谢疾病等抗病遗传机制研究）方向。

项目骨干 7: 罗文，博士，副教授，硕士生导师，广东省“特支计划”科技创新青年拔尖人才，《中国家禽》青年编委，广东省家禽专业委员会副主任委员。2016 年毕业于华南农业大学动物科学学院遗传学专业，获理学博士学位，随后留校任教，任职于动物科学学院动物遗传育种与繁殖系。2020 年 11 月赴香港中文大学访学一年。研究领域为家禽遗传育种，主要运用功能基因组学和生物信息学方法，研究家禽重要经济性状的遗传基础和互作规律，开发基于标记辅助选择和活体基因编辑工具递送系统的家禽育种新技术。主持国家自然科学基金 4 项（面上项目 2 项、青年项目 1 项、重点研发子课题 1 项），省部级项目 5 项。以第一作者或通讯作者在 Cell death and differentiation（IF=12.896）、Journal of Cachexia, Sarcopenia and Muscle（IF=12.88）、Cell death & disease（IF=9.624，2 篇）等高水平期刊发表论文 20 余篇。授权国家发明专利 10 件（第一发明人 7 件），实用新型专利 1 件。作为“高档优质肉鸡新品种的培育与应用”和“屠宰型高效优质肉鸡育种技术创新与应用”项目组主要成员，分别获广东省科技

进步一等奖和中国产学研合作创新成果一等奖。

项目骨干 8：郑茗，华南农业大学动物遗传育种与繁殖专业博士生。参与广东省科技计划项目 1 项，广州市科技计划项目 1 项，广东省现代农业产业技术体系创新团队项目 1 项，公开发表论文 10 篇，其中以第一/并列第一作者发表论文 2 篇，授权发明专利 6 件，获得软著 2 件，参编书籍 1 本，参与培育新品种（配套系）1 个。

（三）单位现有平台、基础设施和配套仪器设备、专业技术水平和组织管理能力等现有条件基础等内容，以及能够满足项目（课题）开展所需条件的说明。

负责该项目的家禽遗传育种课题组拥有猪禽种业全国重点实验室、畜禽育种国家地方联合工程研究中心、岭南现代农业科学与技术广东省实验室、广东省农业动物基因组学与分子育种重点实验室、农业农村部鸡遗传育种与繁殖重点实验室等多个国家及省部级科研平台，占地面积 2176 m²。

团队所在实验室拥有先进的仪器设备，其中 5 万元以上的相关仪器设备超过 50 件，实验设备资产超 4000 万元。包括超景深三维显微镜系统、活细胞工作站、生物分子相互作用系统、生物人工气候试验箱、分选型流式细胞仪、超速冷冻离心机、X-射线多晶粉末衍射仪、液相色谱仪/电感耦合质谱仪、超高效气相色谱仪、分子成像系统、DNA 测序装置、紫外分光光度仪、DNA 片段分析系统、多功能酶标仪、实时荧光定量 PCR 仪、电转仪、体视显微镜、核酸蛋白检测仪、荧光/化学发光成像系统、超净工作台、显微操作仪、蛋白纯化分析系统、酶联检测仪、全自动索氏抽提仪、全自动氨基酸分析仪、全自动生化分析仪、冰冻切片机、非接触式超声波

细胞破碎仪、PCR 仪等大中型仪器设备。

团队多年来应用分子生物学、细胞生物学、多组学现代育种技术等对鸡生长、饲料转化效率、繁殖、肉质等重要经济性状开展深入研究，取得了重要进展，在 Cell Death Differentiation、J Cachexia Sarcopenia Muscle 等发表论文 300 余篇，为肉鸡育种关键技术研发提供理论依据和科技支撑；研发出一批遗传改良关键核心技术广泛应用于品系选育和新品种培育中，目前团队参与培育 8 个配套系通过国家畜禽新品种审定。自 2008 年开始团队陆续开发创建了矮小型基因、隐性白、快慢羽、黄肤色、芦花等多项分子检测技术，累计为国内育种企业提供检测服务 12 万次，为我国黄羽肉鸡种业的发展和育种技术水平的提高做出重大贡献；近年来团队承担十四五国家重点研发计划项目、国家自然科学基金国际（地区）合作与交流项目、国家自然科学基金-广东联合基金、“广东特支计划”本土创新创业团队等多个国家省部级项目，主持建设全国第 3 家农业农村部广东省家禽品种测定站；制定肉鸡行业标准 2 项；获国家发明专利 19 件，软件著作权 1 项；获科技奖励 20 余项，其中主持的“高档优质肉鸡新品种的培育与应用”获 2018 年度广东省科技进步一等奖。

项目（课题）牵头承担单位基本情况表

填表说明：1. 组织机构代码指企事业单位国家标准代码，单位若已三证合一请填写单位社会信用代码，无组织机构代码的单位填写“000000000”； 2. 单位公章名称必须与单位名称一致； 3. 单位开户名称应与单位名称一致，如有开户名称不一致等特殊情况，必须提供证明文件。					
牵 头 承 担 单 位	单位名称	华南农业大学			
	单位类别	<input type="checkbox"/> 科研院所 <input checked="" type="checkbox"/> 大专院校 <input type="checkbox"/> 企业 <input type="checkbox"/> 其他			
	单位主管部门	广东省教育厅		隶属关系	地方
	单位组织机构代码	124400004554165634			
	单位法定代表人姓名	刘雅红			
	单位开户名称	华南农业大学			
	开户银行（全称）	广东广州工行五山支行	汇入地点	广东省广州市	
	银行账号	3602002609000310520	银行机构代码	102581000546	
	单位所属地区	广东省	广州市	天河（区）	
	电子邮箱	kjcgxk@scau.edu.cn			
	通信地址	广东省广州市天河区五山路483号			
	邮政编码	510642			
相 关 责 任 人	项目（课题）负责人	姓名	聂庆华		
		身份证号码	342824197512182714		
		工作单位	华南农业大学		
		电话号码	020-85285759	手机号码	13922195759
		电子邮箱	nqinghua@scau.edu.cn	邮政编码	510642
		通信地址	广州市天河区五山路483号华南农业大学动物科学学院		
	项目（课题）联系人	姓名	蔡柏林		
		电话号码	020-85285759	手机号码	13580356512
		传真号码			
		电子邮箱	bolincai@scau.edu.cn		
	财务负责人	姓名	肖斐		
		身份证号码	362421198305040024		
		电话号码	02085288032	手机号码	13416122195
		电子邮箱	xiaofei@scau.edu.cn		

项目（课题）成员基本情况表

填表说明：1. 人员分类：负责人、骨干、其他人员；
2. 职称分类：正高级、副高级、中级、初级、其他；
3. 固定人员需填写人员明细。

序号	姓名	身份证号码 (士官证、护照)	工作单位	技术职称	投入本项目(课题)的全 时工作时间 (人/月)	人员 分类
	(1)	(2)	(3)	(4)	(5)	(6)
1	聂庆华	342824197512182714	华南农业大学	正高级	8	项目主持人
2	黎镇晖	441225198704251033	华南农业大学	副高级	6	项目骨干
3	蔡柏林	440111199210094218	华南农业大学	副高级	8	项目骨干
4	张细权	440106196305161992	华南农业大学	正高级	6	项目骨干
5	张德祥	230106196711132039	华南农业大学	正高级	6	项目骨干
6	罗庆斌	513101196905200034	华南农业大学	副高级	6	项目骨干
7	李红梅	140303198012211247	华南农业大学	副高级	6	项目骨干
8	罗文	441481198806144150	华南农业大学	副高级	6	项目骨干
9	郑茗	44170219910224284X	华南农业大学	其他	8	项目骨干
固定人员合计				/	60	/
流动人员或临时聘用人员合计				/	0	/
累计				/	60	/

二、项目（课题）的立项必要性分析

（1）立项背景和意义

家禽消费在世界肉类消费市场具有及其重要的地位。根据联合国粮农组织的报告，2019 年以鸡肉为首的禽肉成为全球第一大肉类消费品，此后也一直稳定在第二，仅次于猪肉。我国具有全球最为丰富的家禽遗传资源，根据《中国畜禽遗传资源志 家禽志》记载，我国目前拥有 116 个鸡品种，34 个鸭品种，31 个鹅品种，3 个鸽品种，2 个鹌鹑品种，3 个火鸡品种。我国家禽遗传资源具有多元化的起源特点、受到多种生态因素的影响演变，从而具有极为丰富的生产力类型和多种优良性状。然而目前，随着畜禽产品冰鲜上市政策的推进，市场上出现许多不良商贩以其他家禽品种产品冒充优质家禽产品的情况出现，严重扰乱家禽消费市场以及广大消费者权益。此外，广大家禽育种企业以及养殖户对于摸清其所培育的品种是否血缘纯正也有迫切需求。更重要的是，随着家禽地方品种新遗传资源挖掘工作的持续推进，急需一种科技技术手段鉴别其是否具有新遗传资源的潜力，与现有家禽品种的遗传距离远近。

基于上述背景，本项目依托猪禽种业全国重点实验室、畜禽育种国家地方联合工程研究中心、岭南现代农业科学与技术广东省实验室、广东省农业动物基因组学与分子育种重点实验室、农业农村部鸡遗传育种与繁殖重点实验室等多个国家及省部级科研平台，以及多个省级保种场和省级现代农业产业园，打造华南地区地方家禽品种基因组大数据平台，实现品种鉴定技术的开发与示范推广应用。

（2）国内外相关情况

经历三年新冠肺炎疫情影响，全球家禽产业面临着雏鸡销售，饲料运输和毛鸡压栏等困难影响而损失惨重。但随着新冠疫情局势的逐步好转以及各国政府相关政策的开放，家禽产业的发展形式逐步好转，家禽产业供给侧逐步恢复，我国以及世界范围内对家禽产品的需要量依然巨大。家禽消费作为全球第二大肉类消费品，在世界肉类消费市场占据重要地位。2001 年以来全球肉类消费总量增长约 52%，其中红肉消费比例下降，白肉消费比例由 31% 增加至 42%，禽肉作为白肉消费的主要载体，消费比例也有所增长。家禽产品消费与国民经济和百姓生活关系密切。全球肉类和家禽价格整体上看一直在持续增长，全球肉类和家禽贸易量稳步提升，这与世界范围内人口的增长以及人民平均收入水平的增加有显著关系。未来如何让 90 亿人口吃饱吃好，是一个极其重要的话题，在其中家禽肉和禽蛋的供应将成为关键性的因素，其作为一种廉价而优质的动物蛋白来源，其稳定供应水平将成为解决全球人口食物来源的关键指标。

畜禽种质资源是维护国家农业安全的重要战略资源，是国家畜牧业稳定发展的基石。自家禽驯化以来，家禽的产肉性能和产蛋性能与日俱增，但随之也产生了许多问题。以家鸡为例，纵观全球肉鸡生产情况，目前以快大型白羽肉鸡为主，其生长和产肉速度是地方鸡种望尘莫及的，但这也导致了遗传多样性和肉品种风味等的大幅下降。我国是世界上家禽生物多样性最为丰富的大国之一，蕴藏着丰富的家禽遗传资源，是世界范围内家禽遗传资源的重要提供国。我国的地方家禽资源是不可复制的瑰宝，是维护国家家禽产业健康发展的重要战略资源，如何优质且高效地对地方家禽资源进行保护和开发利用近年来受到国内外学者的高度关注。我国需要基

于我们自主把握且拥有完整知识产权的地方家禽品种遗传资源来培育出适合中国市场的家禽消费产品，满足大众消费者的需要，做到禽肉消费的数量平衡和质量平衡。在家禽育种工作中，常规育种手段已经不能完全满足现代化家禽育种工作的需要，新的分子育种手段的研发和应用可以提高育种的精确度和效率。

目前，基于国内家禽产业存在育种素材以及消费产品品种混杂和血缘不清等问题，极大影响了家禽育种工作的进展以及消费者的消费信心，亟需相关技术和方法进行品种鉴别和血缘关系判定。因此，本项目旨在收集和整理华南地区地方家禽品种基因组数据构建家禽基因组大数据平台，开发基于基因组数据的血缘关系判定和品种鉴定和方法，对家禽的血缘关系和品种进行精准鉴定和判别，从而提高育种效率，缩短育种世代间隔，增加消费者对家禽产品的消费信心。

(3) 与华南地区农业领域相关规划级战略、学科发展的相关性

近年来，广东省政府高度重视畜禽种业发展，不断优化畜禽种业基地布局，不断升级优质良种的供给能力，持续推动广东省畜禽产业的转型升级和高质量发展，“强畜禽种业芯片”一直都是广东省政府的重要议事日程。2013年，广东省印发了《广东省畜禽遗传资源调查实施方案》并出版了《广东省地方畜禽遗传资源志》。2018年，广东省财政厅更是安排专项资金由华南农业大学承担建设广东省畜禽种质资源库，并搭建了相应的广东省畜禽遗传资源综合管理服务平台。2019年，广东省政府制定了《广东省畜禽种业振兴方案(2019-2023年)》，再次明确了要将广东省打造成为世界范围内的畜禽种业科技创新高地，建设畜禽种业强省。截至目前，广

东省已经逐步构建起完善的地方畜禽遗传资源保护和利用体系，新家禽遗传资源的挖掘工作也正在稳步开展。但目前广东省家禽遗传资源保护和利用工作仍存在良种繁育体系建设不完善、育种品种不明确、育种素材血缘混杂以及新家禽遗传资源的挖掘工作效率低等问题。因此，如何从根本上把握品种种质资源核心，成为了广东省家禽产业持续发展的重要问题。

本项目的实施，通过建立华南地区地方家禽品种基因组大数据平台，开发家禽血缘关系判定和品种鉴定技术，有助于提高育种效率，缩短育种世代间隔，培养出种源可靠且可追溯的家禽品种，满足人民大众对优质家禽产品的需求。

（4）所面向的华南地区经济社会发展需求

广东省是我国家禽的生产和消费大省，拥有粤港澳大湾区的广大市场。由于家禽具有独特的营养价值且价格适中，内需市场不断发展，消费市场空间巨大。从长远来看，广东省家禽产业仍然保持着整体上持续发展的基本态势。从历史来看，广东省家禽产业发展早，规模大，在全国家禽产业中占据龙头地位，已经形成了具有岭南特色的养殖模式和市场消费习惯。广东省人民群众内对家禽消费产品的需求巨大，如白切鸡、盐焗鸡、烤乳鸽、卤鸭、卤鹅等。极具岭南特色的家禽消费产品已经成为了广东岭南美食的招牌。但在家禽产业发展的过程中，品种是根本，对种质资源的把握程度从根本上决定了广东省家禽产业发展的高度。种业是畜禽产业发展的卡脖子工程，种业不强，整个行业都不会强，广东省家禽产业也是如此。目前广东省家禽产业和育种正处于转型升级和高质量发展的关键时期。建立家禽基因组大数据平台并实现推广应用，将有利于家禽育种工作的优质

高效进行，有利于提升消费者对家禽消费产品的自信心。基于此，本项目对广东省经济社会发展具有重要意义。

（5）预期解决的重大或关键科学问题

建成首个华南地区地方家禽品种基因组大数据平台，开发家禽血缘关系判别和品种鉴定的分子方法，研发相应品种的鉴定芯片，解决育种工作中以及市场销售过程中家禽品种血缘混杂的问题。

三、项目（课题）内容

（1）建设华南地区地方家禽品种基因组大数据平台

在网上数据库（如 NCBI、ensembl 等网站）和申请人所在课题组多年来积累的地方特色品种基因组数据的基础上，进一步利用全基因组重测序技术收集各保种场特色家禽基因组资源，综合构建一个区域化、本地化的华南地区地方家禽品种基因组大数据平台。实现对华南地区地方家禽品种基因组数据的收集、储存和整理。

（2）开发基于全基因组数据的亲缘关系鉴定技术

依托于内容 ① 建成的华南地区地方家禽品种基因组大数据平台，基于各品种家禽的全基因组重测序数据，通过遗传距离计算、聚类分析和群体结构分析等技术，开发可用于不同品种亲缘关系评估的技术方法。

（3）建立家禽品种鉴定技术并研发相应品种鉴定芯片

综合运用群体分化指数计算的技术方法，挖掘不同品种的特异性遗传标记，建立一套可用于家禽品种鉴别的分子鉴定技术。结合基于目标区间基因组序列液相捕获的精准定位测序分型技术，研发相应品种的液相鉴定

芯片。

四、项目（课题）立项的绩效目标

（一）总体目标

本项目针对“集中屠宰、冷链配送、生鲜上市”全面推行下，部分不法商贩以次充好、以假乱真，阻碍优质家禽养殖行业的高质量发展，这一产业问题，拟整合现有华南地区地方家禽品种基因组数据，收集各保种场特色家禽基因组资源，综合构建一个区域化、本地化的华南地区地方家禽品种基因组大数据平台，初步实现华南地区地方家禽品种基因组信息全覆盖。在此基础上，开发出适用于品种亲缘关系鉴定的新方法，建立可用于不同家禽品种鉴定的分子标记技术并研发相应品种鉴定芯片，实现对华南地区地方家禽品种基因组数据的收集、储存和应用，服务于家禽育种（养殖）企业、科研单位和相关政府部门。

（二）总体考核指标

① 建成华南地区地方家禽品种基因组大数据平台 1 个；② 开发适用于品种亲缘关系鉴定的技术 1 套；③ 建立可用于家禽品种鉴别的分子鉴定技术 1 项；④ 研发特定品种鉴定芯片 1 套。

（三）预期经济效益或社会影响

以清远麻鸡为例，正宗清远麻鸡年产量约为 5000 万只，但市场销售多达 2 亿只，以每只清远麻鸡单价为 50 元测算，总销售量达 100 亿元。以次充好、以假乱真的产品严重扰乱市场正常秩序，误导禽肉产品的消费，影响产业健康发展。本项目基于基因组重测序数据建立品种分子鉴定技术，可快速、科学地鉴定出目标样品是否为正宗清远麻鸡，为政府整顿清远麻

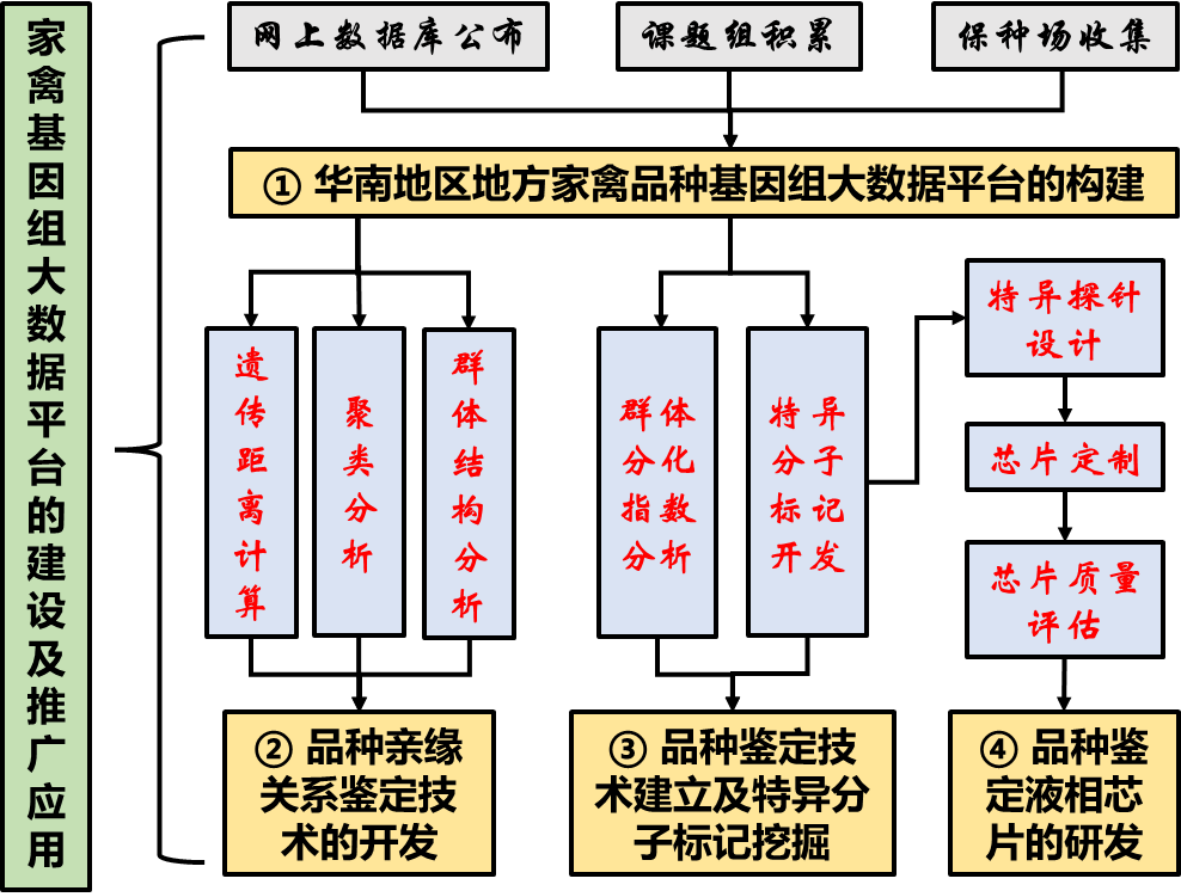
鸡市场提供了有效的技术手段。

此外，项目实施完成后，预计每年可为社会提供 10 次共 300 份样品的品种鉴定服务，助力华南地区地方家禽品种种质资源的保护和利用。

五、项目（课题）技术方案

（一）技术路线

1. 技术方案



项目技术路线图

2. 主要技术指标和参数分析

（1）华南地区地方家禽品种基因组大数据平台的建设

① 华南地区地方家禽品种基因组数据的收集：一方面，对网上数据

库（如 NCBI、ensembl 等网站）数据、课题组已有数据库进行收集；另一方面，利用全基因组重测序技术采集各保种场特色家禽基因组资源。

② 基因组数据的储存与整理：利用“天河二号”超级计算机系统储存收集到的各家禽品种基因组数据，进一步对数据进行分类整理。综合建成区域化、本地化的华南地区地方家禽品种基因组大数据平台。

（2）基于全基因组数据的亲缘关系鉴定技术的开发

① 各家禽品种基因组数据的参考基因组比对：利用基因组比对软件 BWA（比对算法为 `bwa mem` 默认参数），对过滤后获得的 Clean Reads 进行参考基因组比对。

② 各家禽品种基因组特异遗传变异位点的检测分析：基于比对后的 BAM 文件，利用 Picard-MarkDuplicates 去重。通过 GATK 检测单个样品全基因组中所有的潜在多态性 SNP 位点和 INDEL 位点，获得单样本 GVCF。使用 GATK-CombineGVCFs 命令合并待鉴定品种内和不同比较品种的 GVCF。对合并的 SNP 位点参照“ $QD < 2.0 \parallel FS > 60.0 \parallel MQ < 35.0 \parallel MQRankSum < -12.5 \parallel ReadPosRankSum < -8.0 \parallel DP > 6950$ ”条件进行初步过滤，最终获得待鉴定品种的高可信度特异遗传变异标记。

③ 遗传距离计算和聚类分析：利用 vcftools (0.1.17) 对含高可信度 SNP 位点的 VCF 进行 map 和 ped 文件构建。使用 PLINK (v1.90b3.46) 计算两次分析的样本间 IBS 遗传距离矩阵。利用 R (version 3.6.3) 对 IBS 遗传距离矩阵通过邻接法 (NJ) 进行构建进化树。最后使用 PLINK 进行 PCA 分析，并通过 R 进行主成分聚类的可视化。

(3) 家禽品种鉴定技术的建立

① 群体结构分析：利用 vcftools ($\text{missing rate} \leq 0.1$, $\text{MAF} \geq 0.05$) 对待鉴定品种的核基因组 SNP 位点进行阈值过滤。利用 Admixture 软件分析不同品种的群体结构。通过遍历 K 值计算，根据交叉熵最小值确定合适的 K 值，利用 R 软件对结果文件进行可视化。

② 群体分化指数分析：利用 vcftools 进行群体遗传分化 SNP 单点计算。取 0.25 作为 F_{st} 遗传分化阈值，分析待鉴定品种与各比较品种中的特异性位点。

③ 品种特异分子标记的挖掘：对上述获得的各比较组特异位点取交集处理，最终获得可用于鉴定待鉴定品种和各比较品种的专门化特异性位点。

(4) 品种鉴定芯片的研发

① 品种鉴定芯片的探针设计：基于上述获得的可用于鉴定待鉴定品种和各比较品种的专门化特异性位点设计合成相应的芯片探针。

② 品种鉴定芯片的定制：有偿委托相关生物技术公司定制基于目标区间基因组序列液相捕获的精准定位测序分型技术的液相芯片。

③ 芯片质量评估：选取与待鉴定品种具有不同梯度遗传距离的群体进行基因分型，评估研发的品种鉴定芯片的实用性。

(二) 预期的技术成果应用和价值

1. 技术成果的形式

本项目的技术成果主要通过数据库和数据平台构建、检测芯片、技术

方法、政府与企业服务次数和样品数量形式呈现。计划构建涵盖至少 15 个品种的 150 份测序数据的数据库平台 1 个；用于家禽亲缘关系鉴定的方法技术 1 套；用于家禽品种鉴别的分子鉴定技术 1 项；用于鉴定特定品种的液相芯片 1 套；每年可为社会提供 10 次共 300 份样品的品种鉴定服务。

2. 技术成果的预期价值（成果转移转化）

（1）华南地区地方家禽品种基因组大数据平台，有利于纷繁丰富的家禽基因组测序数据的归纳整合和处理，提高数据利用率。

（2）家禽亲缘关系鉴别和品种鉴定的技术方法，有利于育种企业和政府部门判断育种素材的可靠性，加快育种进展和提高新遗传资源的保护利用效率。

（3）鉴定特定家禽品种的检测芯片，有利于消费市场检测家禽产品的来源和血缘，减少假冒伪劣产品欺诈消费者的事件。

3. 技术应用前景及潜在交易市场

随着我国家禽产业的不断发展，我国家禽消费依然是我国乃至世界的第二大肉类消费品。但家禽消费因活禽交易管制和冰鲜上市政策的推进而自 2020 年不断下降，优质且高效地推进家禽新品种（配套系）的构建以及新遗传资源的挖掘势在必行。因此，基于全基因组大数据对家禽品种进行亲缘关系判别和品种鉴定，有利于家禽新品种（配套系）的精准选育，是我国家禽产业转型升级和高质量发展的推进器。本项目应用前景良好，潜在交易市场广大。

六、项目（课题）进度安排

2023.01.01 至 2023.03.31

家禽基因组数据的收集,主要通过三种方法收集家禽品种基因组数据:

- ① 通过网上数据库,如 NCBI、Ensemble 等网站收集家禽品种基因组数据;
- ② 整理课题组或兄弟单位已有的家禽基因组数据;
- ③ 保种场选取样品进行全基因组重测序。

2023.04.01 至 2023.06.30

通过遗传距离计算、聚类分析和群体结构分析等技术,建立基于全基因组数据的亲缘关系的鉴定方法。

2023.07.01 至 2023.09.30

挖掘不同品种的特异性遗传标记,建立一套可用于家禽品种鉴别的分子鉴定技术。基于上述遗传标记,研发相应品种的液相鉴定芯片。

2023.01.01 至 2023.12.30

液相鉴定芯片的测试和质量检测,对外提供家禽品种鉴定服务。

七、项目（课题）预算

项目（课题）预算汇总表

金额单位：100 万元

序号	预算科目名称	预算金额	测算依据及说明
1	（一）直接费用	94.00	
2	1. 材料费	15.60	购买分子生物试剂产生的费用。实验涉及DNA的抽提、PCR扩增等分子生物学实验。包括DNA抽提试剂盒、快速内切酶、定量PCR酶等。
3	2. 测试化验加工费	66.00	① 使用天河2号超级计算机所产生的核时费，0.1元/核，预计36万元； ② 全基因组重测序产生的费用，计划对200个样品进行深度为15X的全基因组重测序，0.15万元/样本，合计30万元
4	3. 出版/文献/信息传播/知识产权事务费	4.00	申请发明专利5项目，预计4万元。
5	4. 会议/差旅/国际合作交流费	3.00	采集样品产生的费用。省内采样5次，0.1万元/人/次，预计3万元。
6	5. 劳务费	5.40	本项目由1名博士、3名硕士承担，博士生活补贴0.15万元/人/月，预计1.8万元；硕士生活补贴0.1万元/人/月，预计3.6万元。合计5.4万元
7	（二）间接费用	6.00	
8	1. 管理费	6.00	用于依托单位的项目管理，按照总经费6%计算。
9	合计	100.00	申请财政预算总金额

八、市场、技术、政策风险分析及对策

华南地区地方家禽种质资源丰富，是我国重要的畜禽产品主产区和主销区。尽管在产业化方面全国领先，但始终存在种质资源混杂、丢失及灭绝等风险。本项目通过汇集、整合地方家禽基因组数据，区域化、本地化的华南地区地方家禽品种基因组大数据平台，并基于此开发用于家禽品种鉴别和亲缘关系远近的分子鉴定方法与技术，研发特定品种的鉴定芯片，有利于从源头上理清楚家禽品种来源和血缘组成，提高家禽的种源可靠性。本项目市场需求大，市场风险低。

项目团队为广东省畜禽种质资源库主要建设成员。资源库保存了广东省内外 45 个畜禽品种的遗传物质近 10 万份，覆盖清远麻鸡、惠阳胡须鸡、杏花鸡、中山沙栏鸡、怀乡鸡、阳山鸡等众多华南地区特色地方鸡种，存有丰富的地方品种 DNA 和 RNA 资源，试验样本储备丰富。团队成员具备扎实的样本采集和数据分析技能，故本项目不存在技术风险。

种业是国家战略性、基础性核心产业。畜禽良种对畜牧业发展的贡献率超过 40%，是提升畜牧业核心竞争力的重要体现。2022 年 2 月 11 日，中国政府网发布《国务院关于印发“十四五”推进农业农村现代化规划的通知》提出，“加强种质资源保护”，要求“启动农业种质资源精准鉴定评价，推进优异种质资源创制与应用，构建种质资源 DNA 分子指纹图谱库、特征库和农业种质资源数据库”。本项目深入贯彻习近平总书记重要指示精神，认真落实中央经济工作会议、中央农村工作会议部署，政策上不存在风险。

三、论文、著作等

1. 检索证明

SCAULIB202519205

检索证明

根据委托人提供的论文材料，委托人华南农业大学动物科学学院 蔡柏林 6 篇论文收录情况如下表。

序号	论文名称	发表刊物及发表的年月卷期/页码等	作者排名	论文等级	作者文中单位	收录情况	影响因子	中科院大类分区
1	MYH1G-AS is a chromatin-associated lncRNA that regulates skeletal muscle development in chicken	CELLULAR & MOLECULAR BIOLOGY LETTERS 出版年：2024 出版日期：JAN 4 卷期：29 1 页码：- 文献号：9 文献类型：Article	第一作者	T2 类	华南农业大学动物科学学院	SCI	IF2-year=10.2 IF5-year=9.4 (2024)	生物学 1 区 Top 期刊：否 (2023)
2	Long noncoding RNA ZFP36L2-AS functions as a metabolic modulator to regulate muscle development	CELL DEATH & DISEASE 出版年：2022 出版日期：APR 21 卷期：13 4 页码：- 文献号：389 文献类型：Article	第一作者	T2 类	华南农业大学动物科学学院	SCI	IF2-year=9.0 IF5-year=9.2 (2022)	生物学 1 区 Top 期刊：是 (2022)
3	LncEDCH1 improves mitochondrial function to reduce muscle atrophy by interacting with SERCA2	Molecular Therapy-Nucleic Acids 出版年：2022 出版日期：MAR 8 卷期：27 页码：319-334	并列第一作者（排第一）	T2 类	华南农业大学动物科学学院	SCI	IF2-year=8.8 IF5-year=8.4 (2022)	医学 1 区 Top 期刊：是 (2022)

		文献类型: Article						
4	circPTPN4 regulates myogenesis via the miR-499-3p/NAMPT axis	JOURNAL OF ANIMAL SCIENCE AND BIOTECHNOLOGY 出版年: 2022 出版日期: FEB 14 卷期: 13 1 页码: - 文献号: 2 文献类型: Article	第一作者	T2 类	华南农业大学 动物科学学院	SCI	IF2-year=7.0 IF5-year=7.3 (2022)	农林科学 1 区 Top 期刊: 是 (2022)
5	LncEDCH1 g.1703613 T>C regulates chicken carcass traits by targeting miR-196-2-3p	POULTRY SCIENCE 出版年: 2024 出版日期: MAR 卷期: 103 3 页码: - 文献号: 103412 文献类型: Article	并列第一作者 (排名第二)	T2 类	华南农业大学 动物科学学院	SCI	IF2-year=4.2 IF5-year=4.5 (2024)	农林科学 1 区 Top 期刊: 是 (2023)
6	PPM1J regulates meat quality feature and glycerophospholipids composition in broiler by modulating protein dephosphorylation	NPJ SCIENCE OF FOOD 出版年: 2024 出版日期: NOV 7 卷期: 8 1 页码: - 文献号: 89 文献类型: Article	共同通讯作者	T2 类	华南农业大学 动物科学学院	SCI	IF2-year=7.8 IF5-year=7.0 (2024)	农林科学 1 区 Top 期刊: 否 (2023)

说明: 论文等级和中科院大类分区按《华南农业大学学术论文评价方案(试行)》划分。

报告免责声明:如未盖章,报告无效



华南农业大学图书馆SCAU LIB202519205

RESEARCH ARTICLE

Open Access



MYH1G-AS is a chromatin-associated lncRNA that regulates skeletal muscle development in chicken

Bolin Cai^{1,2}, Manting Ma^{1,2}, Rongshuai Yuan^{1,2}, Zhen Zhou^{1,2}, Jing Zhang³, Shaofen Kong^{1,2}, Duo Lin^{1,2}, Ling Lian⁴, Juan Li⁵, Xiquan Zhang^{1,2} and Qinghua Nie^{1,2*}

*Correspondence:
nqinghua@scau.edu.cn

¹ State Key Laboratory of Livestock and Poultry Breeding, Guangdong Laboratory for Lingnan Modern Agriculture, College of Animal Science, South China Agricultural University, Guangzhou, China

² Guangdong Provincial Key Lab of Agro-Animal Genomics and Molecular Breeding, Key Laboratory of Chicken Genetics, Breeding and Reproduction, Ministry of Agriculture and Rural Affairs, National-Local Joint Engineering Research Center for Livestock Breeding, Guangzhou, China

³ Randall Centre of Cell and Molecular Biophysics, Faculty of Life Sciences and Medicine, New Hunt's House, King's College London, Guy's Campus, London, UK

⁴ National Engineering Laboratory for Animal Breeding and MOA Key Laboratory of Animal Genetics and Breeding, College of Animal Science and Technology, China Agricultural University, Beijing, China

⁵ Key Laboratory of Bio-Resources and Eco-Environment of Ministry of Education, College of Life Sciences, Sichuan University, Chengdu, China

Abstract

Background: Skeletal muscle development is pivotal for animal growth and health. Recently, long noncoding RNAs (lncRNAs) were found to interact with chromatin through diverse roles. However, little is known about how lncRNAs act as chromatin-associated RNAs to regulate skeletal muscle development. Here, we aim to investigate the regulation of chromatin-associated RNA (MYH1G-AS) during skeletal muscle development.

Methods: We provided comprehensive insight into the RNA profile and chromatin accessibility of different myofibers, combining RNA sequencing (RNA-seq) with an assay for transposase-accessible chromatin with high-throughput sequencing (ATAC-seq). The dual-luciferase reporter assay and chromatin immunoprecipitation (ChIP) assay were used to analyze the transcriptional regulation mechanism of MYH1G-AS. *ALKBH5*-mediated MYH1G-AS *N*⁶-methyladenosine (m⁶A) demethylation was assessed by a single-base elongation and ligation-based qPCR amplification method (SELECT) assay. Functions of MYH1G-AS were investigated through a primary myoblast and lentivirus/cholesterol-modified antisense oligonucleotide (ASO)-mediated animal model. To validate the interaction of MYH1G-AS with fibroblast growth factor 18 (FGF18) protein, RNA pull down and an RNA immunoprecipitation (RIP) assay were performed. Specifically, the interaction between FGF18 and SWI/SNF-related matrix-associated actin-dependent regulator of chromatin subfamily A member 5 (SMARCA5) protein was analyzed by coimmunoprecipitation (Co-IP) and a yeast two-hybrid assay.

Results: A total of 45 differentially expressed (DE) lncRNAs, with DE ATAC-seq peaks in their promoter region, were classified as open chromatin-associated lncRNAs. A skeletal muscle-specific lncRNA (MSTRG.15576.9; MYH1G-AS), which is one of the open chromatin-associated lncRNA, was identified. MYH1G-AS transcription is coordinately regulated by transcription factors (TF) SMAD3 and SP2. Moreover, SP2 represses *ALKBH5* transcription to weaken *ALKBH5*-mediated m⁶A demethylation of MYH1G-AS, thus destroying MYH1G-AS RNA stability. MYH1G-AS accelerates myoblast proliferation



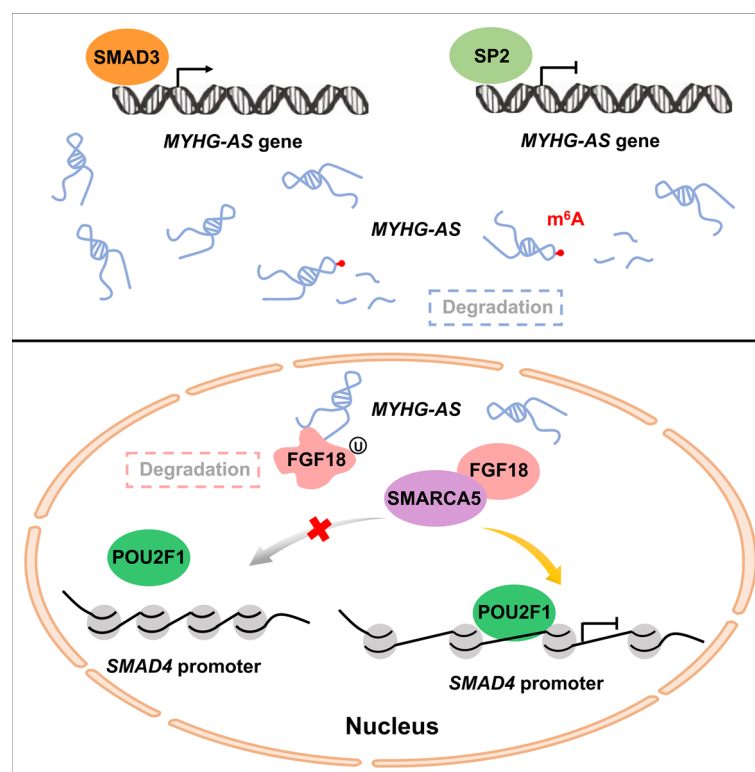
© The Author(s) 2024. **Open Access** This article is licensed under a Creative Commons Attribution 4.0 International License, which permits use, sharing, adaptation, distribution and reproduction in any medium or format, as long as you give appropriate credit to the original author(s) and the source, provide a link to the Creative Commons licence, and indicate if changes were made. The images or other third party material in this article are included in the article's Creative Commons licence, unless indicated otherwise in a credit line to the material. If material is not included in the article's Creative Commons licence and your intended use is not permitted by statutory regulation or exceeds the permitted use, you will need to obtain permission directly from the copyright holder. To view a copy of this licence, visit <http://creativecommons.org/licenses/by/4.0/>.

but restrains myoblast differentiation. Moreover, MYH1G-AS drives a switch from slow-twitch to fast-twitch fibers and causes muscle atrophy. Mechanistically, MYH1G-AS inhibits FGF18 protein stabilization to reduce the interaction of FGF18 to SMARCA5, thus repressing chromatin accessibility of the *SMAD4* promoter to activate the *SMAD4*-dependent pathway.

Conclusions: Our results reveal a new pattern of the regulation of lncRNA expression at diverse levels and help expound the regulation of m⁶A methylation on chromatin status.

Keywords: Chromatin accessibility, lncRNA MYH1G-AS, m⁶A methylation, Skeletal muscle development

Graphical Abstract



Background

Skeletal muscle consists of heterogeneous myofibers that are indispensable for locomotion, energy regulation, and posture maintenance [1]. After birth, skeletal muscle development is mainly regulated by changes in the type and size of myofibers. Notably, skeletal muscle development has been found to be essential for animal growth and health.

DNA transcription is dependent on chromatin opening. Dynamic changes in chromatin accessibility, which affect the binding of DNA-binding proteins such as TFs and RNA polymerases, regulated gene expression [2]. Interestingly, changes in chromatin accessibility are found to be closely relative to skeletal muscle development [3, 4].

As the most numerous transcripts in the genome, noncoding RNAs (ncRNAs) play important roles in epigenetic regulation [5, 6]. Recently, various ncRNAs have been found to be physically associated with chromatin, which are defined as chromatin-associated ncRNAs. As one of the ncRNAs, lncRNAs, are widely involved in epigenetic regulation of skeletal muscle development [4, 7–9]. Currently, only a fraction of lncRNAs have been well authenticated; however, they appear to interact with chromatin through diverse roles [10].

Here, to authenticate lncRNAs relative to skeletal muscle development and explore their transcriptional regulation, RNA-seq and ATAC-seq were performed. Based on these results, lncRNA MSTRG.15576.9 [named myosin, heavy chain 1G (*MYH1G*)-antisense transcript (*MYH1G-AS*)], was found to act as an open chromatin-associated lncRNA coordinately regulated by TF SMAD3 and SP2. Meanwhile, *MYH1G-AS* RNA stability was enhanced by *ALKBH5*-mediated m⁶A demethylation. Functional analysis revealed that *MYH1G-AS* regulates myogenesis, drives a switch from slow-twitch to fast-twitch fibers, and causes muscle atrophy. Mechanistically, *MYH1G-AS* inhibits FGF18 protein stabilization to reduce the interaction of FGF18 to SMARCA5, thus repressing chromatin accessibility of the *SMAD4* promoter to activate the *SMAD4*-dependent pathway. In general, our research discovers a chromatin-associated lncRNA that adjusts chromatin accessibility to regulate skeletal muscle development.

Methods

Ethics statement

All animal experimental protocols were conformed to “The Instructive Notions with Respect to Caring for Laboratory Animals”, issued by the Ministry of Science and Technology of the People’s Republic of China and approved by the Institutional Animal Care and Use Committee at the South China Agricultural University (approval ID: 2021c007).

Animals and cells

Seven-week-old Xinghua female chickens, which were used for tissue separation, and 1-day-old chicks, which were used for animal experiment, were obtained from the Avian Farm of South China Agricultural University (Guangzhou, Guangdong, China).

Chicken primary myoblasts (CPMs) were isolated from the leg muscles of 11-embryonic-day-old chicken and cultured as previously described [11].

RNA-seq

RNA-seq was performed using the strand-specific library construction method as previously described [12]. The purified library products were sequenced using an Illumina HiSeq[™] 4000 and data were analyzed by Gene Denovo Biotechnology Co. (Guangzhou, China). For the reference genome mapping, the chicken genome GRCg6a was used. Raw data of RNA-seq were deposited in the Sequence Read Archive and Genome Sequence Archive (GSA) database under accession nos. PRJNA751251 and CRA008840.

ATAC-seq

ATAC-seq was performed as previously described [13]. The Illumina HiSeq™ 4000 was used to sequence purified products. Bioinformatics analyses were conducted by Gene Denovo Biotechnology Co. (Guangzhou, China). The raw data of ATAC-seq were deposited in the GSA database under accession no. CRA008861.

RNA extraction, cDNA synthesis, and real-time quantitative polymerase chain reaction (RT-qPCR)

RNA extraction, cDNA synthesis, and RT-qPCR was performed as previously described [14]. The primer pairs used for RT-qPCR and RT-PCR are listed in the Additional file 1: Table S1.

Rapid amplification of complementary DNA ends (RACE)

RACE was performed by using a SMARTer RACE cDNA Amplification Kit (Clontech, Osaka, Japan). The primers used for RACE are listed in the Additional file 1: Table S1.

RNA fluorescence in situ hybridization (FISH)

RNA FISH experiments were performed as previously described [11]. MYH1G-AS-specific FISH probes were modified by the cyanine dye Cy3.

Vector construction and RNA oligonucleotides

Six potential Open Reading Frames (ORFs) of MYH1G-AS were cloned into the pcDNA3.1-3xFlag-C vector to construct Flag fusion protein expression vectors. Sequences of potential ORFs of MYH1G-AS are listed in the Additional file 1: Table S2.

For pGL3 luciferase reporter vector construction, wild type or mutated MYH1G-AS, *ALKBH5*, and *SMAD3* promoter fragments were cloned into the pGL3-basic vector (Promega, WI).

The MYH1G-AS full-length sequence, *SMAD3* coding sequence (NM_204475.1), *SP2* coding sequence (XM_025143997.2), *FGF18* coding sequence (NM_204714.1), *SMARCA5* coding sequence (XM_015276722.3), and *POU2F1* coding sequence (NM_205472.1) were cloned into the pcDNA-3.1 vector (Promega, Madison, WI) to generate overexpression vectors.

The MYH1G-AS full-length sequence was cloned into the overexpression lentiviral vector (pLVX-mCMV-ZsGreen-IRES-Puro; Addgene, Cambridge, MA). A short hairpin RNA against MYH1G-AS was designed and cloned into the knockdown lentiviral vector (pLVX-shRNA2-Puro; Addgene, Cambridge, MA).

The antisense oligonucleotide (ASO) and cholesterol-modified ASO against MYH1G-AS were designed and synthesized by Guangzhou RiboBio (Guangzhou, Guangdong, China). The small interfering RNAs (siRNA) against *SMAD3*, *SP2*, *FGF18*, *SMARCA5*, *SMAD4*, and *POU2F1* were also designed and synthesized.

The primer pairs for vector construction and the sequence of oligonucleotides are presented in the Additional file 1: Tables S1 and S3.

For transient cell transfection, a Lipofectamine 3000 reagent (Invitrogen, Carlsbad, CA) was used.

Dual-luciferase reporter assay

Dual-luciferase reporter assays were performed as previously described [11, 15].

ChIP assay

A chromatin immunoprecipitation (ChIP) assay was performed as previously described [15]. The primer pairs used for ChIP-qPCR are presented in the Additional file 1: Table S1.

RNA dot blot, m⁶A RNA methylation quantification, and SELECT assay

Total RNA was denatured at 95 °C for 3 min and then dropped on a positively charged nylon membrane. Subsequently, crosslinking (2000 joules for 1 min) was performed by using a ultraviolet (UV) cross-linker. A specific m⁶A antibody (no. 56593S, 1:1000, Cell Signaling Technology, Boston) was used to detect the m⁶A methylation level

The EpiQuik[™] m⁶A RNA Methylation Quantification kit (Colorimetric; P-9005, Epi-gentek, NY) was used for a total RNA m⁶A RNA methylation quantification assay.

SELECT assays were performed by using a Epi-SELECT[™] m⁶A site-identification kit (R202106M-01, Epibiotek, Guangzhou, China). Relative SELECT products were calculated using the $2^{-\Delta\Delta C_t}$ method. The primers used for the SELECT assays are provided in the Additional file 1: Table S1.

5-ethynyl-2'-deoxyuridine (EdU), flow cytometry, and cell counting kit-8 (CCK-8) assay

EdU, flow cytometry, and CCK-8 assays were performed as previously described [14].

Immunofluorescence (IF) and immunoblotting

IF was performed by using anti-MyHC (B103, 2.5 µg/mL, DSHB, IA), anti-FGF18 (bs-9762R, 1:200, Bioss, Beijing, China), or anti-SMARCA5 (bs-12653R, 1:100, Bioss, Beijing, China) as previously described [16]. A tyramide signal amplification kit (G1226, Servicebio, Wuhan, China) was used for fluorescent double-label staining.

Immunoblotting was performed as previously described [16]. The primary antibodies used in this study were anti-FLAG (14793, 1:1000, Cell Signaling Technology, MA), anti-MYF5 (bs-6936R, 1:500, Bioss, Beijing, China), anti-MYOD1 (M6190, 1:1000, Merck, NJ), anti-MYOG (orb6492, 1:500, Biorbyt, Cambridge, UK), anti-MYH1A (F59, 0.5 µg/mL, DSHB, IA), anti-MYH7B (S58, 0.5 µg/mL, DSHB, IA), anti-FBXO25 (LS-C31927, 1.25 µg/mL, LifeSpan Biosciences, WA), anti-FGF18 (bs-9762R, 1:500, Bioss, Beijing, China), anti-SMARCA5 (bs-12653R, 1:500, Bioss, Beijing, China), anti-Myc (AM926, 1:1000, Beyotime, Shanghai, China), anti-SMAD4 (bs-23966R, 1:500, Bioss, Beijing, China), anti-phosphorylated (p-) SMAD2 (bs-3419R, 1:500, Bioss, Beijing, China), anti-p-SMAD3 (bs-3425R, 1:500, Bioss, Beijing, China), and anti-β-Tubulin (A01030, 1:10,000, Abbkine, Wuhan, China). The goat anti-mouse IgG HRP (A21010, 1:10,000, Abbkine, Wuhan, China) and the goat anti-rabbit IgG HRP (A21020, 1:10,000, Abbkine, Wuhan, China) were used as a secondary antibody. Stability of the β-tubulin protein was

judged by using other housekeeping genes (such as GAPDH and β -actin) (Additional file 1: Fig. S1). Raw images of western blot are shown in the Additional file 2.

Lentivirus production and animal model construction

Lentivirus production and viral titer determination were performed as previously described [14].

Two groups [(a) Lv-MYH1G-AS and Lv-NC and (b) Chol-ASO-MYH1G-AS and Chol-ASO-NC] were randomly divided from 1-day-old chick. In brief, three intramuscular doses of gastrocnemius muscle (at days 1, 7, and 14) were performed with lentivirus (10^6 titers) or cholesterol modified-ASO (40 nmol). The infected gastrocnemius muscle samples were collected 21 days after the first injection.

Mitochondrial DNA (mtDNA) content, mitochondrial membrane potential, and reactive oxygen species (ROS) concentration assay

mtDNA content, mitochondrial membrane potential, and ROS concentration were measured as previously described [8]. The primers used to quantify the amount of mtDNA are list in the Additional file 1: Table S1.

Central carbon metabolic profiling

A central carbon metabolic profiling assay was performed by using MYH1G-AS knock-down gastrocnemius samples ($n=7$) as previously described [8].

The Cluster3.0 software was used for metabolic hierarchical clustering analysis (HCA).

Metabolite and enzyme activities assays

The content of glycogen and enzyme activity of lactic dehydrogenase (LDH) and succinate dehydrogenase (SDH) were detected as previously described [8].

ATPase staining, immunohistochemistry (IHC), and hematoxylin and eosin (HE) staining

ATPase staining, IHC, and HE staining were performed as previously described [14]. For IHC, anti-MYH1A (F59, 1:100, DHSB, IA) and anti-MYH7B (S58, 1:300, DHSB, IA) were used to label the signal.

For the measurement of cross-sectional area (CSA) of the myofiber, at least 60 myofibers were randomly selected in each replicate. More than 360 myofibers in total were subjected to statistical analysis of the frequency distribution of fiber CSA.

RNA pull-down and RIP assays

RNA pull-down and RIP assays were performed as previously described [8]. For the RIP assay, the antibody anti-FLAG (14793, 1:50, Cell Signaling Technology, MA) was used.

Co-IP assay

Co-IP assays were performed by using the Immunoprecipitation Kit with Protein A + G Agarose Gel (P2197S, Beyotime, Shanghai, China). For Co-IP assays, anti-FLAG (14793, 1:50, Cell Signaling Technology, MA) and anti-Myc (AM926, 1:100, Beyotime, Shanghai, China) were used.

Yeast two-hybrid assay

A yeast two-hybrid assay was performed as described in the Yeast Protocols Handbook (Clontech, Japan). The *FGF18* coding sequence, except signal peptide, was cloned into the prey vector (pGBKT7, Clontech, Japan). For the prey vector construction, the *SMARCA5* coding sequence was cloned into the pGADT7 vector (Clontech, Japan).

Statistical analysis

In this study, each experiment was conducted at least three times, and the results appeared as mean \pm standard error of the mean (SEM). An independent sample *t*-test or analysis of variance (ANOVA), followed by Dunnett's test, were used to test the statistical significance of the data. The test type and *P*-values, when applicable, are presented in the figure legends.

Results

Dynamic transcriptional and chromatin accessibility landscapes of different myofibers in chicken

Heterogeneous myofibers are the primary components of skeletal muscle, with different metabolic and physiological characteristics [17]. Using ATPase staining, we found that the pectoralis major (PEM) entirely consists of fast-twitch fibers, while the soleus (SOL) has a higher proportion of slow-twitch myofibers (Fig. 1A). Analogously, immunohistochemical results showed that MYH1A (fast-twitch marker protein) was expressed in all myofibers of PEM, whereas MYH1A and MYH7B (slow-twitch marker protein) proteins were expressed in SOL (Fig. 1B), suggesting that there was a difference in myofiber composition between PEM and SOL.

To authenticate the lncRNAs relative to skeletal muscle development, RNA-seq was performed. In total, 2422 DE genes and 262 DE lncRNAs were identified between PEM and SOL (Fig. 1C–F; Additional file 3: Table S4, and Additional file 4: Table S5). These DE genes were enriched in biological processes including cellular process, metabolic process, and single-organism process and involved in pyruvate metabolism, regulation of actin cytoskeleton, and the cGMP-PKG signaling pathway, which are related to skeletal muscle development (Additional file 1: Fig. S2A, B). ATAC-seq was further performed to reveal the dynamic landscape of chromatin accessibility in different myofibers. Compared with SOL, higher mapping rates of peak to genome (0.77% in PEM and 0.33% in SOL) and more ATAC signals at the transcriptional start site (TSS) were found in PEM (Additional file 1: Fig. S3A, B), declaring that PEM has a greater chromatin accessibility. The genomic feature distribution showed that more than 67% of ATAC-seq peaks in PEM are in introns (36.29%) and promoters (30.98%), and the distance distribution of those peaks to TSS is relatively uniform (Fig. 1G, H). In SOL, nearly half of (44.89%) ATAC-seq peaks are enriched at promoters and concentrated in the 5' upstream of TSS (Fig. 1G–H). Furthermore, 7960 differential ATAC-seq peaks were discovered (Fig. 1I; Additional file 5: Table S6). Gene ontology (GO) enrichment analysis found that genes associated with differential peaks were mainly enriched in cellular

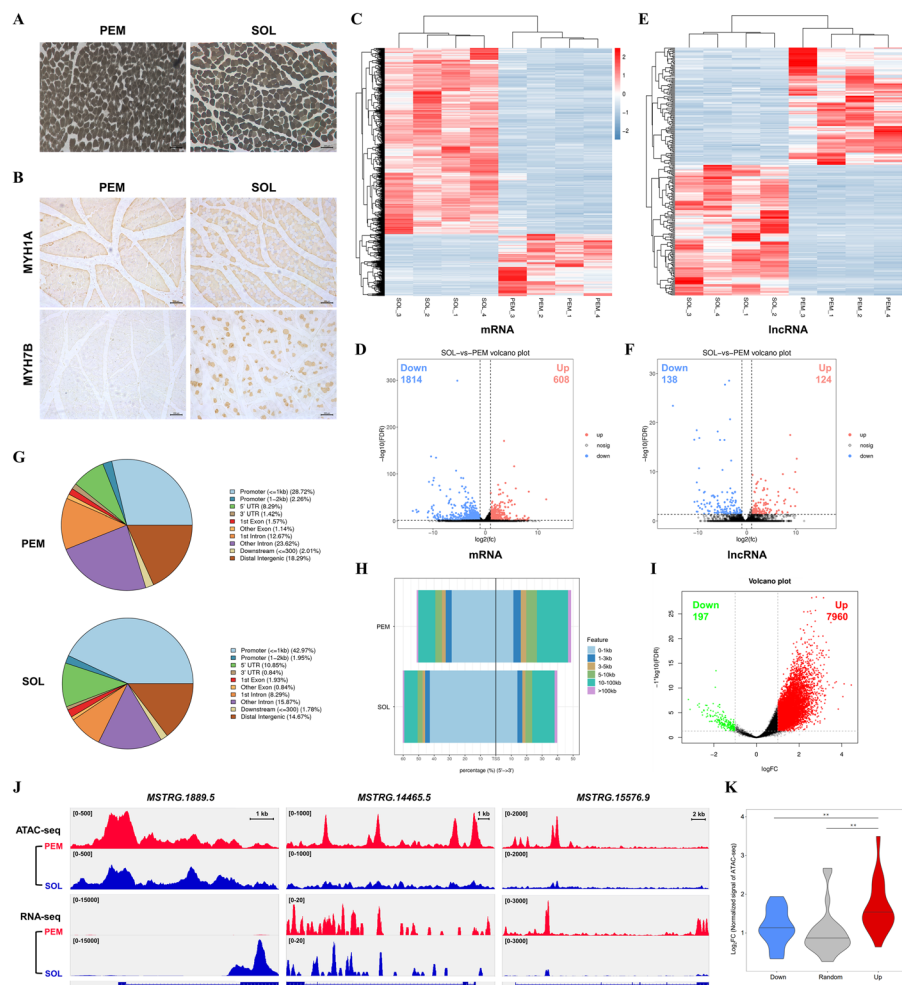


Fig. 1 Overview of transcriptome and chromatin accessibility profile in different myofibers. **A, B** ATPase staining (**A**) and IHC analysis (**B**) of PEM and SOL in 7-week-old Xinghua chicken. **C–F** Heatmaps (**C** and **E**) and volcano plots (**D** and **F**) of differentially expressed mRNAs (**C, D**) and lncRNAs (**E, F**). **G** Pie charts showing the distribution of ATAC-seq peaks across the genome. The different colors represent different genomic regions. **H** Accumulated barplot showing the feature distribution of ATAC-seq peaks around the TSS. **I** Volcano plots of differentially expressed ATAC-seq peaks. **J** Gene view of coverage of lncRNA and chromatin-accessibility footprint reads on selected genes. Gene structure is diagrammed at the bottom. **K** Violin plot showing the changes in ATAC-seq intensity around the TSS of open chromatin-associated lncRNAs and randomly selected nondifferentially expressed lncRNAs. Results are shown as mean \pm SEM. In panel **K**, the statistical significance of differences between means was assessed using an independent sample *t*-test. (** $P < 0.01$)

process, single-organism process, and metabolic process (Additional file 1: Fig. S2C). Moreover, these genes participated in the insulin signaling pathway, autophagy, and FoxO signaling pathway (Additional file 1: Fig. S2D).

A total of 45 DE lncRNAs, with DE ATAC-seq peaks in their promoter region (within 2 kb upstream of TSS), were classified as open chromatin-associated lncRNAs (Fig. 1J; Additional file 6: Table S7). Importantly, open chromatin-associated upregulated lncRNAs have a higher ATAC-seq intensity around the TSS (Fig. 1K), indicating that the change in chromatin accessibility leads to a change in lncRNA expression.

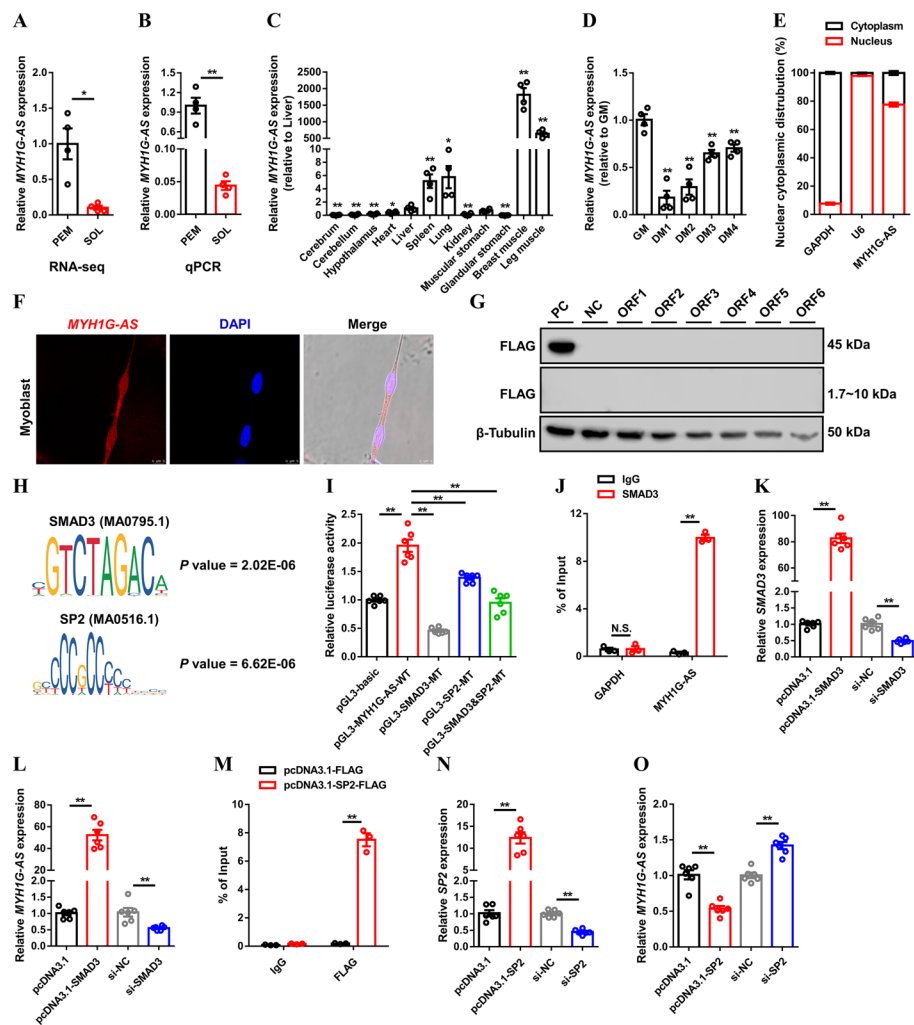


Fig. 2 MYH1G-AS is a skeletal muscle-specific lncRNA that is coordinately regulated by SMAD3 and SP2. **A, B** Relative MYH1G-AS expression in PEM and SOL of 7-week-old Xinghua chicken detected by RNA-seq (**A**) and qPCR (**B**). **C** Tissue expression profiles of MYH1G-AS. **D** Relative MYH1G-AS expression during CPM proliferation and differentiation. **E** The distribution of MYH1G-AS in the cytoplasm and nucleus of CPMs determined by qPCR. Glyceraldehyde-3-phosphate dehydrogenase (GAPDH) and U6 serve as cytoplasmic and nuclear localization controls, respectively. **F** RNA in situ hybridization of MYH1G-AS in CPM. Special FISH probes against MYH1G-AS were modified by Cy3 (red). The nucleus was stained by DAPI (blue). **G** Western blot analysis of the coding ability of MYH1G-AS. CPMs transfected with β -actin were used as a positive control (PC) and untransfected CPMs were used as a negative control (NC). **H** Significantly enriched TFs in MYH1G-AS upstream the ATAC-seq peak was predicted by MEME suite. **I** Transcriptional activity of MYH1G-AS upstream ATAC-seq peak. **J** ChIP analysis of the binding capacity of SMAD3 to the MYH1G-AS promoter. **K, L** Relative SMAD3 (**K**) and MYH1G-AS (**L**) expression after SMAD3 overexpression or interference. **M** ChIP analysis of the binding capacity of SP2 to MYH1G-AS promoter. **N, O** Relative SP2 (**N**) and MYH1G-AS (**O**) expression with SP2 overexpression or inhibition. Results are presented as mean \pm SEM. In panels A–D and I–O, statistical significance of differences between means was assessed using an independent sample *t*-test. (**P* < 0.05; ***P* < 0.01)

MYH1G-AS is a skeletal muscle-specific lncRNA that is coordinately modulated by SMAD3 and SP2

MYH1G-AS, which is one of the open chromatin-associated lncRNAs highly expressed in PEM (Fig. 1J, Fig. 2A, B; Additional file 6: Table S7), was selected as a candidate. First, RACE assay was performed to acquire a MYH1G-AS full-length sequence (Additional file 1: Fig. S4A). As an antisense transcript of *MYH1G*, MYH1G-AS was 1221 nt long and mainly conserved in Aves (Additional file 1: Fig. S4B, C). We further investigated the expression pattern of MYH1G-AS and found that MYH1G-AS was specifically highly expressed in skeletal muscle and downregulated during myogenic differentiation (Fig. 2C, D). A cell-fractionation assay and in situ RNA hybridization demonstrated that MYH1G-AS is mainly present in the nucleus (Fig. 2E, F). Moreover, the coding potential of MYH1G-AS was verified, and the result of western blotting suggested that MYH1G-AS was without protein-encoding potential (Fig. 2G).

The MEME suite was used to analyze a significant motif and predict its significantly enriched TFs in the MYH1G-AS upstream DE ATAC-seq peak. SMAD3 and SP2, which could potentially bind to the promoter of MYH1G-AS, were found (Fig. 2H). The dual-luciferase reporter assays showed that mutation of the SMAD3 potential binding site decreased the transcription activity of the MYH1G-AS promoter, while the transcription activity of the MYH1G-AS promoter was increased with mutation in the SP2 potential binding site (Fig. 2I). The binding of SMAD3 and SP2 to the MYH1G-AS promoter was also verified by ChIP assays (Fig. 2J and M). Furthermore, *SMAD3* overexpression strongly upregulated MYH1G-AS expression, while MYH1G-AS expression was reduced with *SP2* overexpression (Fig. 2K, L and N, O). On the contrary, *SMAD3* interference suppressed MYH1G-AS expression, while MYH1G-AS expression was promoted after *SP2* inhibition (Fig. 2K, L and N, O). Collectively, these data revealed that SMAD3 and SP2 coordinately regulate the transcription activity of MYH1G-AS.

ALKBH5-mediated m⁶A demethylation enhances RNA stability of MYH1G-AS

As the richest class of methylation modifications, m⁶A is well known to participate in multiple regulatory processes of RNA metabolism, widely regulating skeletal muscle development [18, 19]. Given that ALKBH5, which is a m⁶A demethylase, was highly expressed in PEM (Fig. 3A, B), we analyzed whether *ALKBH5* participates in the regulation of MYH1G-AS expression by mediating its m⁶A demethylation. As expected, *ALKBH5* overexpression induced m⁶A demethylation, whereas the m⁶A methylation level was upregulated with the *ALKBH5* interference (Fig. 3C–E). The potential m⁶A modification sites on MYH1G-AS were further predicted by using the SRAMP (<http://www.cuilab.cn/sramp>) software and verified by SELECT assays. A total of seven potential m⁶A modification sites were found, and the SELECT product at the 263 site was increased with *ALKBH5* overexpression (Fig. 3F and Additional file 1: Fig. S5A–G). Conversely, *ALKBH5* interference promoted the m⁶A methylation at the 263 site of MYH1G-AS (Fig. 3F). Moreover, *ALKBH5* overexpression facilitated the expression and RNA stability of MYH1G-AS, whereas MYH1G-AS expression was inhibited and MYH1G-AS RNA stability was destroyed after *ALKBH5* interference (Fig. 3G–I), suggesting that

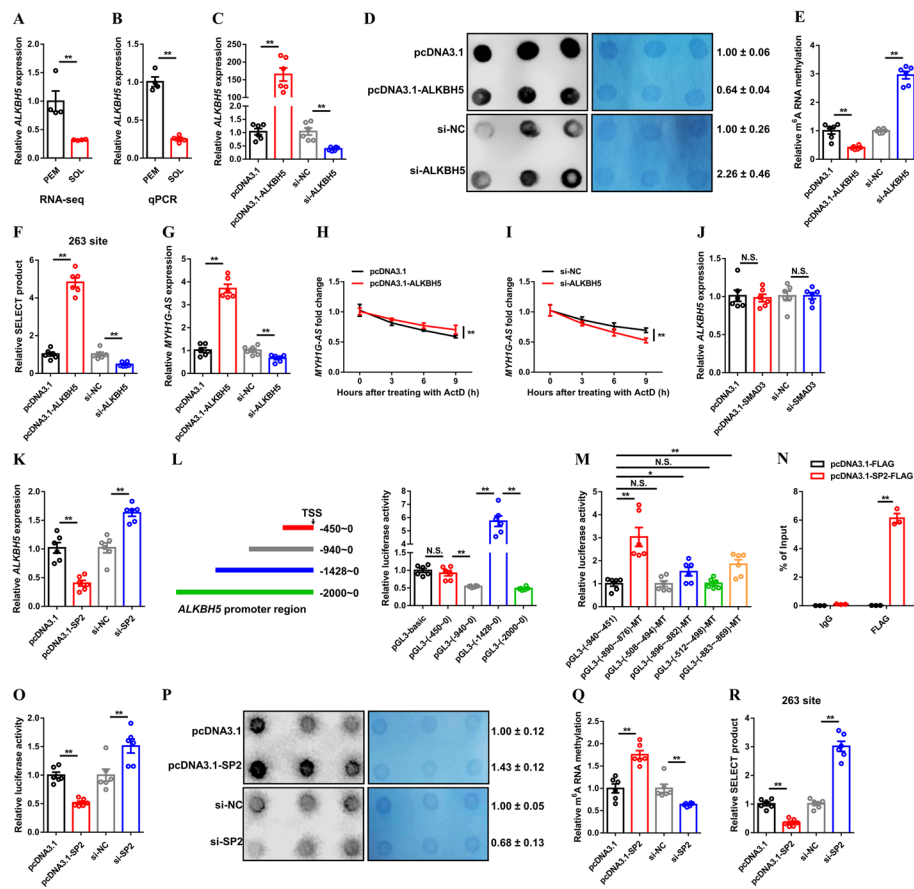


Fig. 3 ALKBH5-mediated m⁶A demethylation maintains RNA stability of MYH1G-AS. **A, B** Relative *ALKBH5* expression in PEM and SOL of 7-week-old Xinghua chicken detect by RNA-seq (**A**) and qPCR (**B**). **C–G** Relative *ALKBH5* expression (**C**), RNA dot blot assay (**D**), relative m⁶A methylation level (**E**), relative SELECT product at the 263 site of MYH1G-AS (**F**), and relative MYH1G-AS expression (**G**) after *ALKBH5* overexpression or interference. **H, I** MYH1G-AS RNA stability assay after *ALKBH5* overexpression (**H**) and inhibition (**I**). **J** Relative *ALKBH5* expression after *SMAD3* (**J**) and *SP2* (**K**) overexpression or interference. **L** Left: Schematic of four truncated *ALKBH5*-promoter constructs used for luciferase assays. Right: Dual-luciferase reporter assays of four reporter constructs. **M** The transcriptional activity of the *ALKBH5* core promoter region. **N** ChIP analysis of the binding capacity of SP2 to *ALKBH5* promoter. **O** The transcriptional activity of *ALKBH5* core promoter region after *SP2* overexpression or knockdown. **P–R** RNA dot blot assay (**P**), relative m⁶A methylation level (**Q**), and relative SELECT product at the 263 site of MYH1G-AS (**R**) with *SP2* overexpression or interference. Results are showed as mean ± SEM. In panels **A–C**, **E–O**, and **Q, R** statistical significance of differences between means was assessed using an independent sample *t*-test. (**P* < 0.05; ***P* < 0.01; NS, no significant difference)

ALKBH5 promotes MYH1G-AS expression by inducing m⁶A demethylation at the 263 site of MYH1G-AS.

TFs are well known to recognize specific motifs in promoters, thereby widely regulating the transcription and expression of its target genes. *ALKBH5* expressions were detected after *SMAD3* or *SP2* overexpression and interference. Overexpression or interference of *SMAD3* did not change the *ALKBH5* expression (Fig. 3J). Interestingly, *SP2* overexpression repressed *ALKBH5* expression, whereas *ALKBH5* expression was upregulated with *SP2* inhibition (Fig. 3K). To explore the potential binding site of *SP2* on the promoter of *ALKBH5*, promoter truncation experiments were performed. Luciferase activities in the −940 ~ 0 region and −2000 ~ 0 regions were significantly reduced (Fig. 3L), indicating that there are binding sites for silent elements between

– 940 to – 450 and – 2000 to – 1428 region. The potential binding sites for SP2 in these regions were further predicted by JASPAR (<https://jaspar.genereg.net/>) software and verified by several dual-luciferase reporter assays (Fig. 3M). The transcription activity of *ALKBH5* was improved with the mutation of the – 896 region to the – 869 (– 890 to – 876, – 896 to – 882 and – 883 to – 869) region (Fig. 3M), which is potential bound to SP2. The binding of SP2 was also confirmed by the ChIP assay (Fig. 3N). *SP2* overexpression suppressed *ALKBH5* transcription, whereas *ALKBH5* transcription was increased with *SP2* interference (Fig. 3O). Furthermore, *SP2* promoted m⁶A methylation and reduced SELECT product at the 263 site of MYH1G-AS (Fig. 3P–R and Additional file 1: Fig. S5H–M), which explains that *SP2* represses the transcription of *ALKBH5* to reinforce the inhibition of MYH1G-AS expression.

MYH1G-AS regulates myogenesis, drives a switch from slow-twitch to fast-twitch fibers, and causes muscle atrophy

To screen target genes regulated by MYH1G-AS and explore its potential functions, RNA-seq was performed after MYH1G-AS interference (Fig. 4A). In total, 213 genes were identified as being DE between the control group and MYH1G-AS interference CPMs ($P < 0.05$; $|FC| > 1.5$) (Fig. 4B; Additional file 7: Table S8). According to GO enrichment analysis, DE genes were mainly related to cellular processes, single-organism processes, and biological regulation (Additional file 1: Fig. S6A). KEGG pathway analysis indicated that cytokine–cytokine receptor interactions, signaling pathways regulating pluripotency of stem cells, and the TGF- β signaling pathway are the top three enriched pathways of those DE genes (Additional file 1: Fig. S6B).

Several genes, including *CDKN1A*, *CDKN1B*, *CCNG2*, *MYF5*, *MYF6*, *MYOD1* and *MYOG*, which are involved in cell cycle and myogenic differentiation, were found to be DE after MYH1G-AS interference (Fig. 4C). In addition, considering that MYH1G-AS was downregulated during myoblast differentiation (Fig. 1D), we study the function of MYH1G-AS in myogenesis. Cell cycle-inhibiting genes, such as *CDKN1A*, *CDKN1B*, and *CCNG2*, were upregulated with MYH1G-AS interference (Fig. 4D). EdU staining showed that MYH1G-AS interference decreased EdU incorporation and impeded proliferation of myoblasts (Fig. 4E, F). Moreover, flow cytometric analysis and CCK-8 assay showed that MYH1G-AS interference led to fewer S phase cells and downregulated myoblast viability (Fig. 4G, H). IF staining was further performed, and the result showed that MYH1G-AS inhibition increased the total areas of myotubes, increased the differentiation index, and induced the formation of myotubes (Fig. 4I–L). Besides, myoblast differentiation-related genes, such as *MYF5*, *MYF6*, *MYOD1*, and *MYOG*, were upregulated after MYH1G-AS interference (Fig. 4M, N). Conversely, opposite results were observed by MYH1G-AS overexpression (Additional file 1: Fig. S7A–L), illustrating that MYH1G-AS facilitates myoblast proliferation but hinders myogenic differentiation.

To verify the function of MYH1G-AS in vivo, cholesterol modified, ASO-mediated MYH1G-AS knockdown (Chol-ASO-MYH1G-AS) and lentivirus-mediated MYH1G-AS overexpression (Lv-MYH1G-AS) animal models were conducted (Fig. 5A and Additional file 1: Fig. S8A). MYH1G-AS knockdown increased mtDNA content and improved mitochondrial membrane potential (Fig. 5B, C), and ROS production was reduced with MYH1G-AS knockdown (Fig. 5D). Inversely, mtDNA content was decreased and

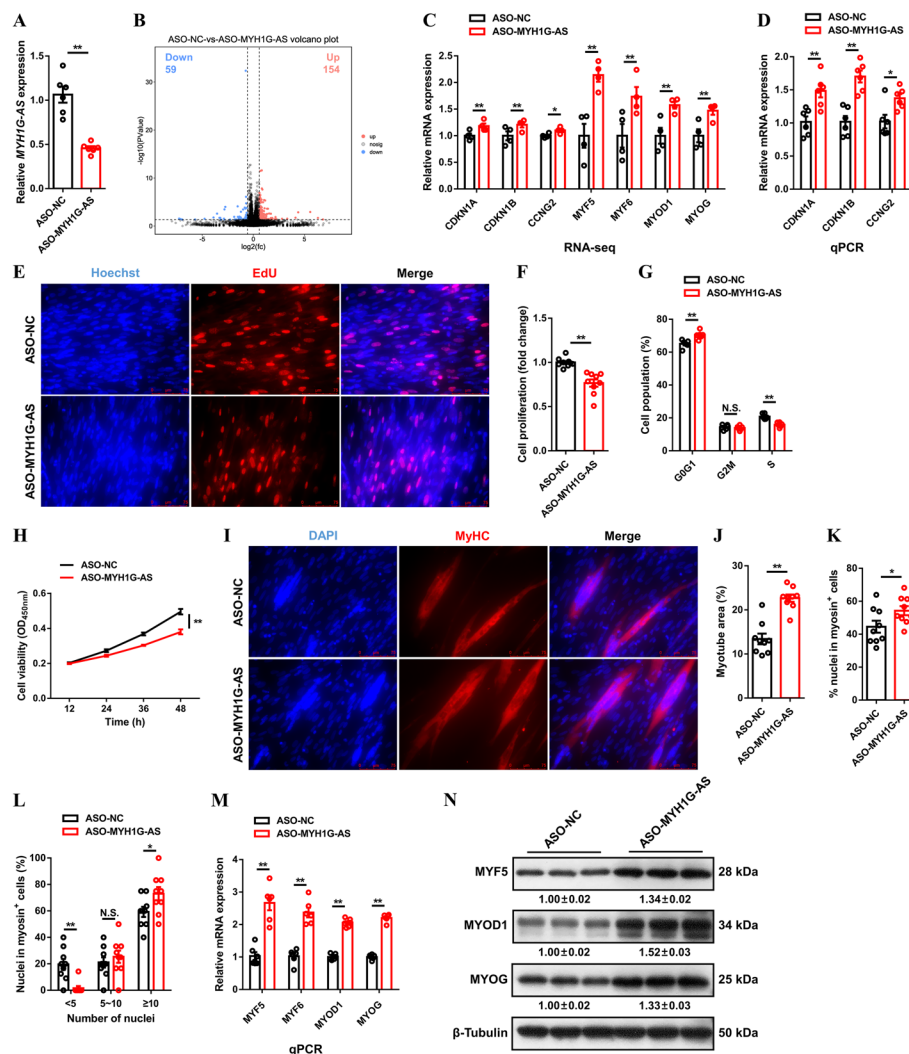


Fig. 4 MYH1G-AS facilitates myoblast proliferation but inhibits myogenic differentiation. **A** Relative MYH1G-AS expression with MYH1G-AS interference in CPMs. **B** Volcano plots of differentially expressed genes between the control group and MYH1G-AS interference. **C** Relative mRNA expressions of several differentially expressed genes after MYH1G-AS interference detected by RNA-seq. **D–M** Relative mRNA expressions of several cell cycle-inhibiting genes (**D**), EdU proliferation assay (**E**), proliferation rate of myoblasts (**F**), cell cycle analysis (**G**), CCK-8 assay (**H**), MyHC immunostaining (**I**), myotube area (**J**), differentiation index (**K**), myoblast fusion index (**L**), and relative mRNA (**M**) and protein (**N**) expression levels of myoblast differentiation marker genes with MYH1G-AS inhibition in vitro. In panel **N**, the numbers shown below the bands were folds of band intensities relative to the control. Band intensities were quantified by ImageJ and normalized to β -tubulin. Results are presented as mean \pm SEM. In panels **A**, **C**, **D**, **F–H**, and **J–M**, statistical significance of differences between means was assessed using an independent sample *t*-test. (* $P < 0.05$; ** $P < 0.01$)

mitochondrial function was impeded after MYH1G-AS overexpression (Additional file 1: Fig. S8B–D). Comparative metabolome analysis found that MYH1G-AS knock-down increased tricarboxylic acid cycle metabolite such as malic acid (Fig. 5E, F; Additional file 8: Table S9). The accumulation of glycogen was facilitated after MYH1G-AS knockdown (Fig. 5G). More importantly, results of immunohistochemistry and western blot showed that MYH1G-AS knockdown suppressed the MYH1A protein level but promoted the expression level of MYH7B protein, as well as aggrandized the CSA of

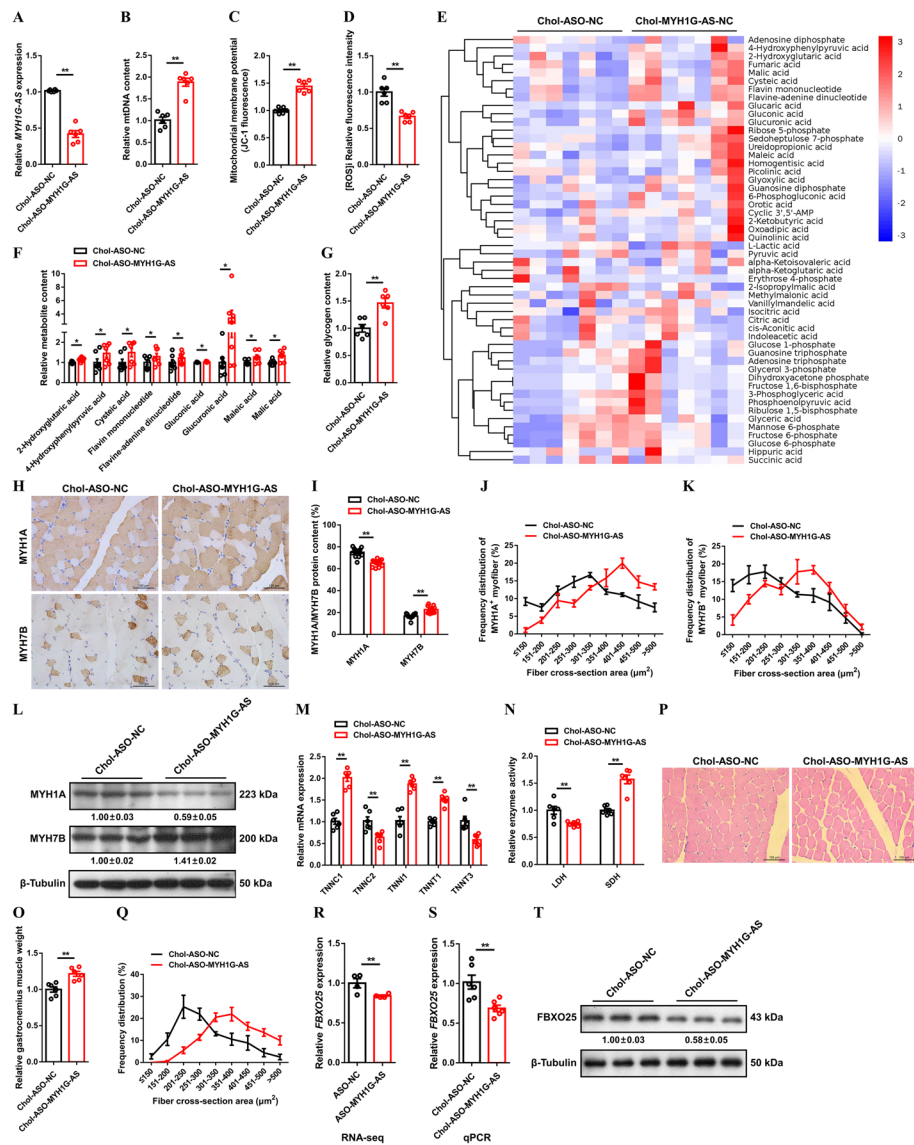


Fig. 5 MYH1G-AS modulates skeletal muscle metabolism to activate fast-twitch muscle phenotype and induces muscle atrophy. **A–D** Relative MYH1G-AS expression (**A**), relative mtDNA content (**B**), mitochondrial membrane potential (**C**), and intracellular ROS ([ROS]) (**D**) in gastrocnemius with MYH1G-AS knockdown. **E** HCA of metabolites in gastrocnemius after infected with Chol-ASO-MYH1G-AS or Chol-ASO-NC. The colors indicate the relative levels in control or MYH1G-AS knockdown group. **F** Relative metabolite content in MYH1G-AS knockdown gastrocnemius detected by central carbon metabolic profiling. **G–N** Relative glycogen content (**G**), IHC analysis (**H**), MYH1A/MYH7B protein content (**I**), frequency distribution of MYH1A⁺ (**J**) and MYH7B⁺ (**K**) myofiber CSA, relative protein expression of MYH1A and MYH7B (**L**), relative mRNA expression of several fast- and slow-twitch myofiber genes (**M**), relative enzymes activity of LDH and SDH (**N**), relative gastrocnemius muscle weight (**O**), H&E staining (**P**), and frequency distribution of fiber CSA (**Q**) in gastrocnemius with MYH1G-AS knockdown. **R** Relative mRNA expression of *FBXO25* after MYH1G-AS interference detected by RNA-seq. **S**, **T** Relative mRNA (**S**) and protein (**T**) expression of *FBXO25* after MYH1G-AS knockdown. In panel **L** and **T**, the numbers shown below the bands were folds of band intensities relative to control. Band intensities were quantified by ImageJ and normalized to β -tubulin. Results are shown as mean \pm SEM. In panels **A–D**, **F**, **G**, **I**, **M–O**, and **R**, **S**, the statistical significance of the differences between means was assessed using paired *t*-tests. (**P* < 0.05; ***P* < 0.01)

MYH1A⁺ and MYH7B⁺ myofibers (Fig. 5G–L). In addition, MYH1G-AS knockdown promoted expressions of slow-twitch myofiber genes, such as *TNNC1*, *TNNI1*, and *TNNT1*, and repressed expressions of fast-twitch myofiber genes, such as *TNNC2* and *TNNT3* (Fig. 5M). The activity of LDH was repressed while SDH activity was facilitated after MYH1G-AS knockdown (Fig. 5N). Opposite results were observed with MYH1G-AS overexpression (Additional file 1: Fig. S8E–L), indicating that MYH1G-AS suppresses mitochondria biogenesis to modulate skeletal muscle metabolism, thus activating the fast-twitch muscle phenotype.

Recent studies have found that muscle remodeling can induce muscle hypertrophy or atrophy by modulating muscle metabolism [20]. Here, muscle mass was increased and the CSA of myofibers were enlarged after MYH1G-AS knockdown (Fig. 5O–Q). Conversely, MYH1G-AS overexpression reduced gastrocnemius mass and lessened the size of myofibers (Additional file 1: Fig. S8M–O). The ubiquitin–proteasome system (UPS) is well known to regulate skeletal muscle atrophy [21, 22]. *FBXO25*, which is an ubiquitin E3 ligase involved in UPS, was found downregulated after MYH1G-AS interference (Fig. 5R). In vivo, MYH1G-AS knockdown repressed *FBXO25* expression, whereas *FBXO25* expression was promoted after MYH1G-AS overexpression (Fig. 5S, T and Additional file 1: Fig. S8P, Q). Given that MYH1G-AS induced atrophy of both fast-twitch and slow-twitch myofibers, we conclude that MYH1G-AS-induced muscle atrophy should be attributed to its regulation of *FBXO25*, rather than induced by myofiber remodeling.

MYH1G-AS binds with FGF18 to inhibit FGF18 protein stabilization

To clarify the molecular mechanism of MYH1G-AS, *MYH1G* expression was first examined. *MYH1G* mRNA was not changed with MYH1G-AS overexpression or knockdown (Additional file 1: Fig. S9A, B). Next, an RNA pull-down assay was performed. A total of 23 proteins were identified by mass spectrometry, suggesting they specifically bind to MYH1G-AS sense transcript (Fig. 6A; Additional file 9: Table S10). FGF18, which is a member of the fibroblast growth factor family, was found to be an endogenous interacting protein (Fig. 6B). A RIP assay was performed, which confirmed this special interaction (Fig. 6C). Only a full-length strand of MYH1G-AS could physically bind to FGF18 (Fig. 6D), hinting that the complete RNA structure is indispensable for their interaction. Similar to MYH1G-AS, cellular localization was confirmed by subcellular location annotation and IF staining (Fig. 6E and Additional file 1: Fig. S10A), explaining the interaction of MYH1G-AS and FGF18.

MYH1G-AS did not modulate *FGF18* mRNA expression (Additional file 1: Fig. S9C, D). Crucially, FGF18 protein expression was downregulated with MYH1G-AS overexpression, while FGF18 protein level was enhanced after MYH1G-AS knockdown (Fig. 6E, G). Furthermore, treatment with CHX (which is a protein biosynthesis inhibitor) decreased FGF18 protein expression (Fig. 6H). However, this degradation was relieved with MYH1G-AS knockdown (Fig. 6H). Proteasome inhibitor MG-132 was also used to elucidate the induction effect of MYH1G-AS on FGF18 protein degradation. As expected, the protein levels of FGF18 were upregulated, and the reduction of FGF18 protein levels with MYH1G-AS overexpression was rescued with MG-132 treatment (Fig. 6I). Given that MYH1G-AS induced *FBXO25* expression (Fig. 5R–T and

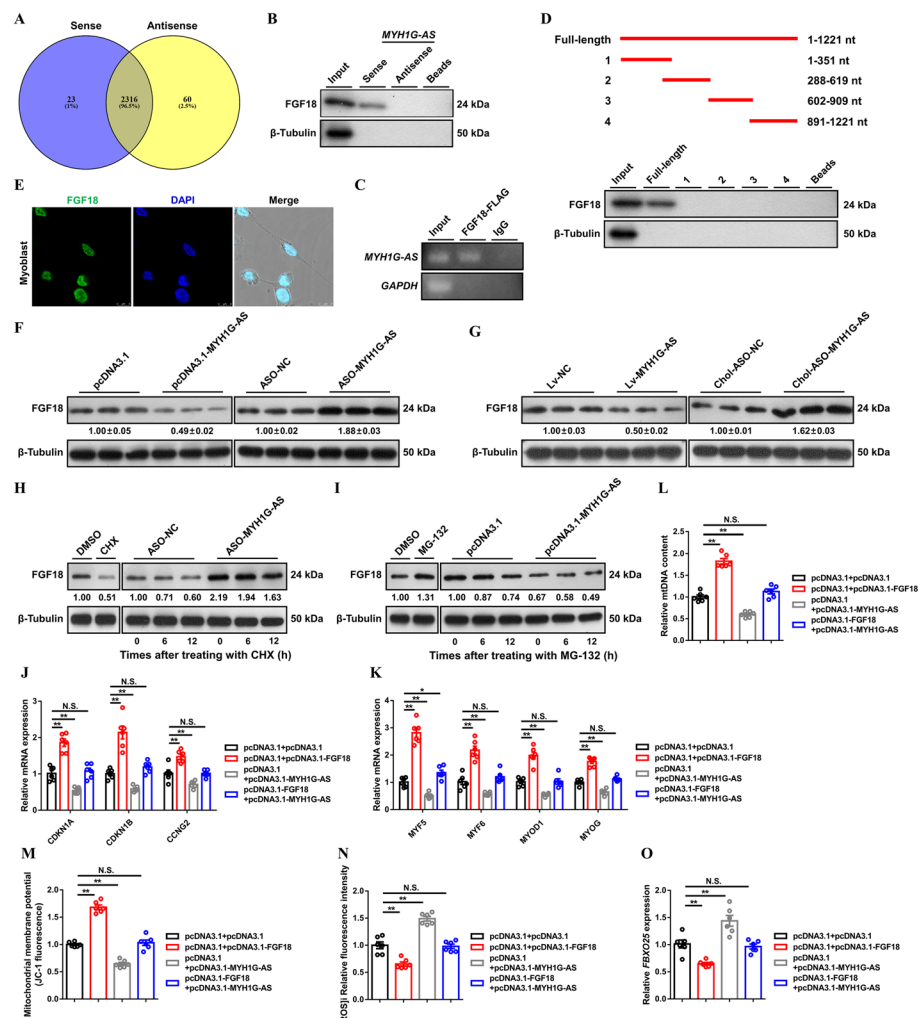


Fig. 6 MYH1G-AS interacts with FGF18 to destroy FGF18 protein stabilization. **A** Venn diagram showing the specific binding proteins of the MYH1G-AS sense strand or antisense strand. **B, C** The interaction of MYH1G-AS with FGF18 protein was determined by biotin-labeled RNA pull-down (**B**) and RIP (**C**) assays. **D** The binding of full-length and truncated MYH1G-AS with FGF18 protein was determined by RNA pull-down assay. **E** IF staining of FGF18 in CPM. **F, G** The protein expression level of FGF18 after MYH1G-AS overexpression or knockdown in vitro (**F**) and in vivo (**G**). **H** Left: FGF18 protein expression in myoblasts after dimethyl sulfoxide (DMSO) or cycloheximide (CHX; 25 µg/mL) treatment for 12 h. Right: FGF18 protein expression in the MYH1G-AS-knockdown myoblast was analyzed after incubation with CHX. **I** Left: FGF18 protein expression in myoblasts after DMSO or MG-132 (5 µmol/L) treatment for 12 h. Right: FGF18 protein expression in MYH1G-AS overexpressed myoblast was analyzed after incubated with MG-132. **J–O** Relative mRNA expressions of several cell cycle-inhibiting genes (**J**), relative mRNA expressions of myoblast differentiation marker genes (**K**), relative mtDNA content (**L**), mitochondrial membrane potential (**M**), [ROS]_i (**N**), and relative mRNA expressions of *FBXO25* (**O**) induced by the listed nucleic acids in CPMs. In panel **F–I**, the numbers shown below the bands were folds of band intensities relative to the control. Band intensities were quantified by ImageJ and normalized to β-tubulin. Results are presented as mean ± SEM. In panels **J–O**, the statistical significance of differences between means was assessed using an independent sample *t*-test. (**P* < 0.05; ***P* < 0.01)

Additional file 1: Fig. S8P, Q), we deduced that MYH1G-AS causes the ubiquitination of FGF18 to promote FGF18 degradation.

FGF18 was highly expressed in skeletal muscle (Additional file 1: Fig. S10B), and the expression level of *FGF18* increased gradually with myogenic differentiation (Additional

file 1: Fig. S10C). in vitro experiments were conducted to study the potential biological function of *FGF18* in myogenesis. An opposite result to MYH1G-AS was observed, suggesting that *FGF18* had an inverse biological function compared with MYH1G-AS (Additional file 1: Fig. S11A–R). Meanwhile, *FGF18* overexpression promoted expressions of cell cycle-inhibiting genes and myoblast differentiation-related genes, which neutralizes the effect of MYH1G-AS on myogenesis (Fig. 6J, K). The suppression of mitochondria biogenesis and promotion of *FBXO25* expression, which was induced by MYH1G-AS overexpression, were counteracted with *FGF18* overexpression (Fig. 6L–O), suggesting that *FGF18* mediates the function of MYH1G-AS.

MYH1G-AS reduces the interaction of FGF18 to SMARCA5, thereby promoting SMAD4 transcription and activating the SMAD4-dependent pathway

Considering that the molecular functional annotation of FGF18 is protein binding (Additional file 9: Table S10), Co-IP was performed to excavate its downstream interacting proteins. A total of 150 proteins were found to specifically interact with FGF18 by mass spectrometry (Additional file 10: Table S11). Among them, SWI/SNF-related matrix-associated actin-dependent regulator of chromatin subfamily A member 5 (SMARCA5), which belongs to the SWI/SNF family with remodeling activity [23, 24], was found. Co-IP and yeast two-hybrid assays confirmed the interaction between FGF18 and SMARCA5 (Fig. 7A–C). Nuclear localization of SMARCA5 was revealed by IF, which is similar to FGF18 (Fig. 7D). Moreover, Co-IP assays were further conducted after cotransfection with the FGF18-FLAG fusion expression vector and SMARCA5-MYC fusion expression vector, which also clearly stated that FGF18 specifically interacts with SMARCA5 (Fig. 7E). Neither MYH1G-AS nor *FGF18* could modulate the mRNA and protein expression of SMARCA5 (Additional file 1: Fig. S12A–F). Given that MYH1G-AS destroys the stabilization of FGF18 protein, we further explored whether MYH1G-AS hindered the interaction between FGF18 and the SMARCA5 protein. As expected, MYH1G-AS overexpression reduced the interaction between FGF18 and SMARCA5 by inhibiting FGF18 protein expression, whereas the interaction between FGF18 and SMARCA5 was heightened with MYH1G-AS interference (Fig. 7F).

SMAD family member 4 (SMAD4) is a pivotal signaling cascade of the TGF- β signaling pathway, which is widely involved in skeletal muscle development [25, 26]. Given that the TGF- β signaling pathway is one of the most enriched pathways in MYH1G-AS interference, myoblast and *SMAD4* was downregulated with MYH1G-AS inhibition (Fig. 7G and Additional file 1: Fig. S6B). We hypothesized that MYH1G-AS regulates *SMAD4* expression and modulates the *SMAD4*-dependent pathway. Both in vivo and in vitro, MYH1G-AS overexpression upregulated mRNA and protein expression of *SMAD4*, while *SMAD4* expression was suppressed with MYH1G-AS knockdown (Fig. 7H–K). Phosphorylated SMAD2 and SMAD3 have been reported to bind SMAD4 to participate in the TGF- β signaling pathway [27]. We also detected the phosphorylation levels of the SMAD2 and SMAD3 proteins after MYH1G-AS overexpression or knockdown. However, overexpression or interference of MYH1G-AS did not change the phosphorylation levels of the SMAD2 and SMAD3 proteins both in vitro and in vivo (Additional file 1: Fig. S13A, B). In view of MYH1G-AS reducing interaction of FGF18 to SMARCA5, which is a chromatin remodeler that can selectively mediate binding of distinct TFs [28],

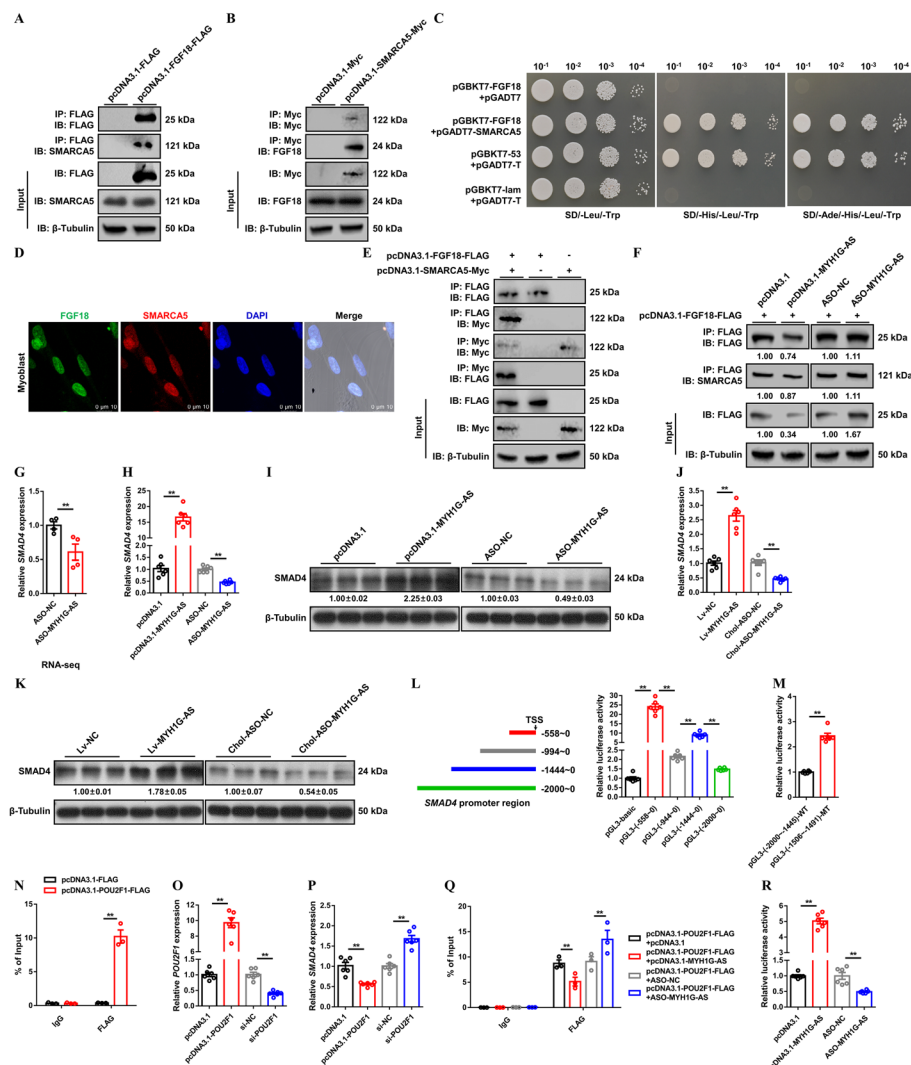
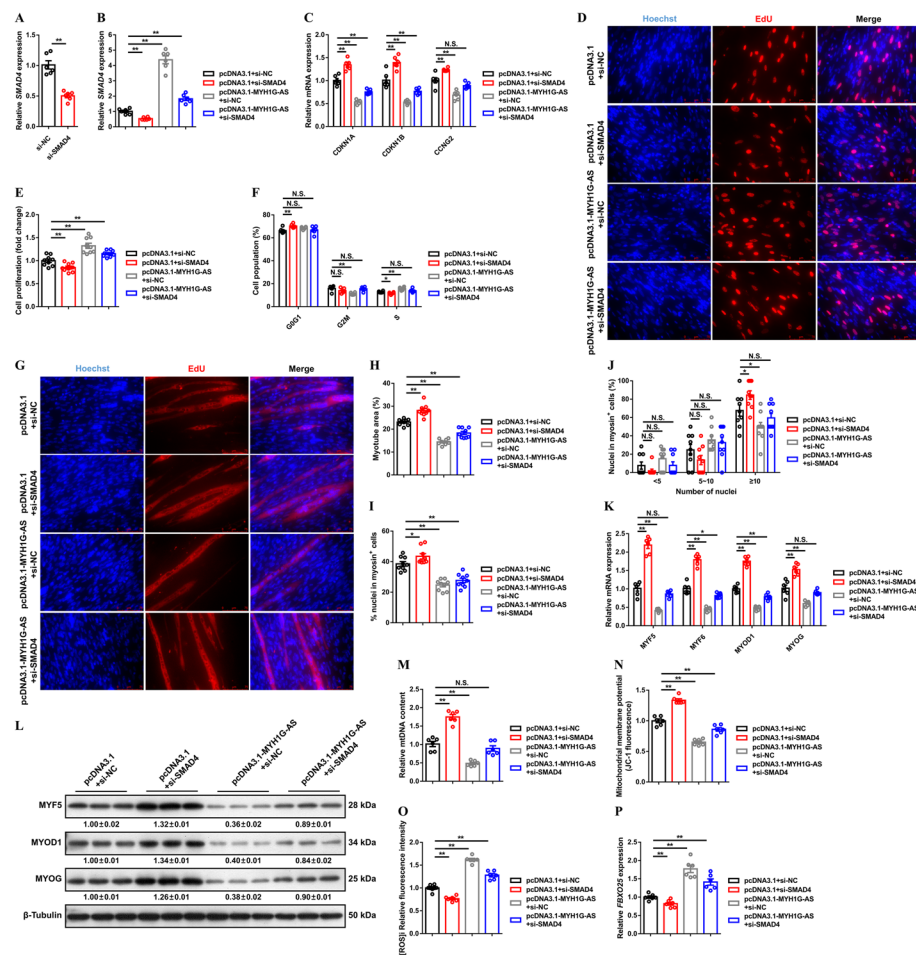


Fig. 7 MYH1G-AS reduces interaction of FGF18 to SMARCA5, thereby promoting the transcription and expression of *SMAD4*. **A** The binding of FGF18 to the SMARCA5 protein was determined by Co-IP assay. **B** The binding of SMARCA5 to the FGF18 protein was determined by Co-IP assay. **C** The interaction between FGF18 and the SMARCA5 protein was determined by the yeast two-hybrid system. **D** IF staining of SMARCA5 and FGF18 in CPM. **E** The interaction between FGF18 and the SMARCA5 protein was determined by Co-IP assay. **F** Co-IP assay after cotransfection with pcDNA3.1-FGF18-FLAG and the listed nucleic acids. **G** Relative *SMAD4* expression after MYH1G-AS interference detected by RNA-seq. **H–K** Relative mRNA (**H** and **J**) and protein (**I** and **K**) expression levels of *SMAD4* with MYH1G-AS overexpression or knockdown in vitro (**H**, **I**) and in vivo (**J**–**K**). **L** Left: Schematic of four truncated *SMAD4* promoter constructs used for luciferase assays. Right: Dual-luciferase reporter assays of four reporter constructs. **M** The transcriptional activity of *SMAD4* core promoter region. **N** ChIP analysis of the binding capacity of POU2F1 to the *SMAD4* promoter. **O**, **P** Relative *POU2F1* (**O**) and *SMAD4* (**P**) expression after *POU2F1* overexpression or knockdown. **Q** The transcriptional activity of the *SMAD4* core promoter region after MYH1G-AS overexpression or knockdown. **R** ChIP analysis of the binding capacity of POU2F1 to the *SMAD4* promoter with MYH1G-AS overexpression or knockdown. In panels **F**, **I**, and **K**, the numbers shown below the bands were folds of band intensities relative to control. Band intensities were quantified by ImageJ and normalized to β-tubulin. Results are shown as mean ± SEM. In panels **G**, **H**, **J**, and **L–R**, the statistical significance of differences between means was assessed using an independent sample *t*-test. (***P* < 0.01)



we further explored whether MYH1G-AS mediates the binding of TFs to the *SMAD4* promoter. First, promoter truncation experiments were performed and found that luciferase activities in the $-558 \sim 0$ region and $-1444 \sim 0$ region of the *SMAD4* promoter were promoted while luciferase activities in $-994 \sim 0$ region and $-2000 \sim 0$ region were restrained (Fig. 7L). Next, potential TF binding sites in transcriptional inhibitory regions of the *SMAD4* promoter were predicted by using gene-regulation (<http://gene-regulation.com>) and JASPAR software. The result showed that POU class 2 homeobox 1 (POU2F1) showed potential binding from the -1504 to -1493 region of the *SMAD4* promoter. Luciferase activities were increased with mutation of the POU2F1 binding site (Fig. 7M), suggesting that POU2F1 suppresses the transcription activity of *SMAD4*. The

binding of POU2F1 to the *SMAD4* promoter was also verified by ChIP assay (Fig. 7N). *POU2F1* overexpression suppressed *SMAD4* expression, whereas *SMAD4* expression was upregulated after *POU2F1* interference (Fig. 7O, P). MYH1G-AS overexpression impeded the binding of POU2F1 to the *SMAD4* promoter and upregulated transcription activity of *SMAD4*, whereas the interaction of POU2F1 to the *SMAD4* promoter was promoted and *SMAD4* transcription activity was inhibited after MYH1G-AS interference (Fig. 7Q, R). On the contrary, *FGF18* or *SMRACR5* overexpression repressed the expression and transcription activity of *SMAD4* and hindered the binding of POU2F1 to the *SMAD4* promoter; *SMAD4* expression and transcription activity were facilitated and binding of POU2F1 was reinforced after *FGF18* or *SMRACR5* interference (Additional file 1: Fig. S13C-L), indicating that MYH1G-AS reduces the interaction of FGF18 to SMARCA5 to hinder the binding of POU2F1 to the *SMAD4* promoter, thus promoting the transcription activity and expression of *SMAD4*.

Specific siRNA against *SMAD4* was used to study whether *SMAD4* mediates the molecular function of MYH1G-AS (Fig. 8A). *SMAD4* interference cancelled out the promoting effect of MYH1G-AS on *SMAD4* expression (Fig. 8B). *SMAD4* inhibition suppressed myoblast proliferation but promoted myogenic differentiation, which neutralized the regulation of MYH1G-AS in myogenesis (Fig. 8C–L). In addition, *SMAD4* interference rescued the inhibition of mitochondria biogenesis and attenuated upregulated expression of *FBXO25*, which were induced by MYH1G-AS overexpression (Fig. 8M–P). Altogether, these results hinted that *SMAD4* is required for the function of MYH1G-AS.

Discussion

Chromatin epigenome interaction, which functionally determines transcription and cell type, provides a powerful frame work for epigenetically classifying cellular sub-states [29]. During C2C12 differentiation, 385 DE lncRNAs, the transcription of which is determined by chromatin states around their transcriptional start sites, were found and identified as TF-lncRNA [30]. However, only the TF-lncRNA correlation network has been constructed, and the exact regulatory role has not been verified. To explore the genetic regulation during skeletal muscle development, we provide comprehensive insight into the transcriptome and chromatin accessibility in different myofibers. A total of 45 open chromatin-associated lncRNAs were found. Among them, MYH1G-AS, which is an antisense transcript of *MYH1G*, was found to be coordinately regulated by *SMAD3* and *SP2*.

As the most abundant RNA modification, m⁶A modification plays an important role in skeletal muscle development [19, 31]. However, *ALKBH5* is a well-known demethylase that has rarely been reported to regulate skeletal muscle development. In this study, *ALKBH5* was found to be highly expressed in fast-twitch myofibers. Moreover, *ALKBH5* modulated m⁶A demethylation of MYH1G-AS to maintain MYH1G-AS RNA stability, thus participating in the regulation of skeletal muscle development. Previous studies in mammals have found that multiple TFs can modulate *ALKBH5* transcription [32–34], but little is known in chicken. Here, we found *ALKBH5* transcription was repressed by *SP2*, indicated that *SP2* modulates m⁶A methylation to strengthen the suppression of MYH1G-AS expression.

Chromosome-associated RNA has been reported to be physically associated with chromatin and is widely involved in chromatin remodeling [10]. In this study, we found MYH1G-AS binds with FGF18 to inhibit FGF18 protein stabilization and reduce the interaction of FGF18 to SMARCA5, thus repressing chromatin accessibility and hindering the binding of POU2F1 to the *SMAD4* promoter. Notably, recent evidence has revealed that m⁶A modifications on chromatin-associated RNAs modulate chromatin accessibility and gene transcription [35, 36]. Here, we found that *ALKBH5*-mediated m⁶A demethylation enhances RNA stability of MYH1G-AS, which is a chromosome-associated lncRNA, and expands our understanding of the crosstalk between RNA modification and chromatin status.

It is well established that the TGF- β signaling pathway is widely involved in the regulation of cell growth, differentiation, and development [37–39]. As a family of signal transduction molecules, the SMAD family plays important roles in mediating the TGF- β signaling pathway [40–42]. *SMAD4* is the only member of the SMAD family with the common-mediator function. The receptor-regulated SMADs, such as SMAD2 and SMAD3, must combine with SMAD4 to form heterogenic complexes to exert their role in modulating the expression of their target genes [27]. Previous studies have reported cascading relationships among members of the SMAD family, but the expression regulation among members of the SMAD family remains poorly understood. In this study, we found MYH1G-AS regulated skeletal muscle development in vitro and in vivo through the *SMAD4*-dependent pathway. Given that MYH1G-AS, which is positively regulated by *SMAD3*, reduced interaction between FGF18 and SMARCA5 to remit the transcriptional inhibition of *SMAD4* by POU2F1, we concluded that *SMAD3* could promote *SMAD4* expression by mediating the transcription of MYH1G-AS. Our study presents a model for the expression regulation among members of the SMAD family and broadens insights into the interaction of cascade molecules in the TGF- β signaling pathway.

Conclusions

In summary, we identified a chromatin-associated lncRNA that regulates skeletal muscle development. Our results reveal a new pattern of the regulation of lncRNA expression at diverse levels and help expound the regulation of m⁶A methylation on chromatin status.

Abbreviations

ASO	Antisense oligonucleotide
ATAC-seq	Assay for transposase-accessible chromatin with high-throughput sequencing
CCK-8	Cell counting kit-8
ChIP	Chromatin immunoprecipitation
CHX	Cycloheximide
CPM	Chicken primary myoblast
CSA	Cross-sectional area
DE	Differentially expressed
EdU	5-ethynyl-2'-deoxyuridine
FGF18	Fibroblast growth factor 18
FISH	RNA fluorescence in situ hybridization
HE	Hematoxylin and eosin
IF	Immunofluorescence
IHC	Immunohistochemistry
KEGG	Kyoto Encyclopedia of Genes and Genomes
LDH	Lactic dehydrogenase
lncRNA	Long noncoding RNA
m ⁶ A	N ⁶ -methyladenosine

mtDNA	Mitochondrial DNA
ncRNA	Noncoding RNA
ORF	Open Reading Frame
PEM	Pectoralis major
POU2F1	POU class 2 homeobox 1
RACE	Rapid amplification of complementary DNA ends
RIP	RNA immunoprecipitation
RNA-seq	RNA sequencing
ROS	Reactive oxygen species
RT-qPCR	Real-time quantitative polymerase chain reaction
SDH	Succinate dehydrogenase
SELECT	Single-base elongation and ligation-based qPCR amplification method
SMAD4	SMAD family member 4
SMARCA5	SWI/SNF-related matrix-associated actin-dependent regulator of chromatin subfamily A member 5
SOL	Soleus
TF	Transcription factor
TSS	Transcriptional start site
UPS	Ubiquitin-proteasome system

Supplementary Information

The online version contains supplementary material available at <https://doi.org/10.1186/s11658-023-00525-x>.

Additional file 1: Table S1. Information of primers. **Table S2.** Sequences of potential ORFs of MYH1G-AS. **Table S3.** Oligonucleotide sequences in this study. **Fig. S1.** Relative β -Tubulin and GAPDH protein expression in myoblast proliferation (myoblast cultured in growth medium [GM]) and differentiation (myoblast cultured in differentiation medium from 1 to 5 day [DM1 to DM5; DM indicate differentiation day]) periods. The numbers shown below the bands were folds of band intensities relative to control. Band intensities were quantified by ImageJ and normalized to β -Tubulin. Data are expressed as a fold-change relative to the control. Results are presented as mean \pm SEM. **Fig. S2.** GO functions and KEGG pathways analysis of differentially expressed genes and ATAC-seq peaks between pectoralis major and soleus in 7-week-old Xinghua chicken. **(A, B)** GO functions **(A)** and KEGG pathways **(B)** analysis of differentially expressed genes between pectoralis major (PEM) and soleus (SOL) in 7-week-old Xinghua chicken. **(C–D)** GO functions **(C)** and KEGG pathways **(D)** analysis of differentially expressed ATAC-seq peaks between PEM and SOL in 7-week-old Xinghua chicken. **Fig. S3.** Heatmap of ATAC-seq signals at transcriptional start site. **(A)** Heatmap of ATAC-seq signals at transcriptional start site (TSS) in PEM samples. **(B)** Heatmap of ATAC-seq signals at TSS in SOL samples. **Fig. S4.** Characterization of MYH1G-AS. **(A)** Results of MYH1G-AS 3' RACE and 5' RACE. **(B)** The full-length sequence of MYH1G-AS. Coordinates are listed according to bGalGal1.mat.broiler.GRCg7b reference Annotation Release 106. **(C)** Conservative analysis of MYH1G-AS performed by using the NCBI's BLAST. A total of eighteen species, including *Anas platyrhynchos*, *Anser cygnoides*, *Apteryx mantelli mantelli*, *Aquila chrysaetos*, *Bos taurus*, *Coturnix japonica*, *Gallus gallus*, *Geospiza fortis*, *Homo sapiens*, *Meleagris gallopavo*, *Melospittacus undulatus*, *Mus musculus*, *Numida meleagris*, *Ovis aries*, *Pan troglodytes*, *Rattus norvegicus*, *Sus scrofa* and *Zebra finch* were used for Nucleotide BLAST. Top 5 most conservative results were listed above. **Fig. S5.** Prediction and identification of potential m⁶A modification sites on MYH1G-AS. **(A)** Potential m⁶A modification sites on MYH1G-AS were predict by using the SRAMP (<http://www.cuilab.cn/sramp>) software. **(B–G)** Relative single-base elongation and ligation-based PCR amplification method (SELECT) product at 250 **(B)**, 436 **(C)**, 495 **(D)**, 970 **(E)**, 1042 **(F)**, and 1116 **(G)** sites of MYH1G-AS after *ALKBH5* overexpression or interference. **(H–M)** Relative SELECT product at 250 **(H)**, 436 **(I)**, 495 **(J)**, 970 **(K)**, 1042 **(L)**, and 1116 **(M)** sites of MYH1G-AS after *ALKBH5* overexpression or interference. Results are presented as mean \pm SEM. In panels **B–M**, the statistical significance of differences between means was assessed using an independent sample t-test. (NS, no significant difference). **Fig. S6.** GO functions and KEGG pathways analysis of differentially expressed genes between control group and MYH1G-AS interference. **(A)** GO functions analysis of differentially expressed genes between control group and MYH1G-AS interference. **(B)** KEGG pathways analysis of differentially expressed genes between control group and MYH1G-AS interference. **Fig. S7.** Overexpression of MYH1G-AS promotes myoblast proliferation but inhibits myoblast differentiation. **(A–L)** Relative MYH1G-AS expression **(A)**, relative mRNA expressions of several cell cycle-inhibiting genes **(B)**, EdU proliferation assays **(C)**, proliferation rate of myoblasts **(D)**, cell cycle analysis ϵ , CCK-8 assays **(F)**, MyHC immunostaining **(G)**, myotube area **(H)**, differentiation index **(I)**, myoblast fusion index **(J)**, and relative mRNA **(K)** and protein **(L)** expression levels of myoblast differentiation marker genes with MYH1G-AS overexpression in vitro. In panel **L**, the numbers shown below the bands were folds of band intensities relative to control. Band intensities were quantified by ImageJ and normalized to β -Tubulin. Data are expressed as a fold-change relative to the control. Results are presented as mean \pm SEM. In panels **A, B, D–F**, and **H–K**, statistical significance of differences between means was assessed using independent sample t-test. (* $P < 0.05$; ** $P < 0.01$). **Fig. S8.** Overexpression of MYH1G-AS represses mitochondria biogenesis to drive the transformation of slow-twitch to fast-twitch myofiber and induces muscle atrophy. **(A–Q)** Relative MYH1G-AS expression **(A)**, relative mtDNA content **(B)**, mitochondrial membrane potential **(C)**, intracellular ROS ([ROS]) **(D)**, relative glycogen content **(E)**, immunohistochemistry analysis of MYH1A/MYH7B **(F)**, MYH1A/MYH7B protein content **(G)**, frequency distribution of MYH1A⁺ **(H)** and MYH7B⁺ **(I)** myofiber CSA, relative protein expression of MYH1A and MYH7B **(J)**, relative mRNA expression of several fast- and slow-twitch myofiber genes **(K)**, relative enzymes activity of LDH and SDH **(L)**, relative gastrocnemius muscle weight **(M)**, H&E staining **(N)**, frequency distribution of fiber CSA **(O)**, and relative mRNA **(P)** and protein **(Q)** expression of *FBXO25* in gastrocnemius with MYH1G-AS overexpression. In panel **J** and **Q**, the numbers shown below the bands were folds of band intensities relative to control. Band intensities were quantified by ImageJ and normalized to β -Tubulin. Data are expressed as a fold-change relative to the control.

Results are showed as mean \pm SEM. In panels **A–E**, **G**, **K–M**, and **P**, statistical significance of differences between means was assessed using independent sample *t*-test. (* $P < 0.05$; ** $P < 0.01$). **Fig. S9.** The mRNA level of *MYH1G* and *FGF18* didn't change with *MYH1G*-AS overexpression and knockdown both in vitro and in vivo. (**A–B**) Relative mRNA expression of *MYH1G* with *MYH1G*-AS overexpression and knockdown in vitro (**A**) and in vivo (**B**). (**C–D**) Relative mRNA expression of *FGF18* with *MYH1G*-AS overexpression and knockdown in vitro (**C**) and in vivo (**D**). Results are shown as mean \pm SEM. In all panels, statistical significance of differences between means was assessed using independent sample *t*-test. (NS, no significant difference). **Fig. S10.** The location and expression analysis of *FGF18*. (**A**) Subcellular location of *FGF18* protein annotated by UniProt Knowledgebase (<https://www.uniprot.org/>). (**B**) Tissue expression profiles of *FGF18*. The horizontal axis and vertical axis indicate different tissues and their relative expression values, respectively. (**C**) Relative *FGF18* expression during CPM proliferation and differentiation. Results are presented as mean \pm SEM. In panels **B–C**, statistical significance of differences between means was assessed using independent sample *t*-test. (* $P < 0.05$; ** $P < 0.01$). **Fig. S11.** *FGF18* inhibits myoblast proliferation, promotes myoblast differentiation, and facilitates mitochondria biogenesis. (**A–R**) Relative mRNA (**A**) and protein (**B**) expression levels of *FGF18*, relative mRNA expressions of several cell cycle-inhibiting genes (**C**), EdU proliferation assays (**D**), proliferation rate of myoblasts (**E**), cell cycle analysis (**F**), CCK-8 assays (**G–H**), MyHC immunostaining (**I**), myotube area (**J**), differentiation index (**K**), myoblast fusion index (**L**), relative mRNA (**M**) and protein (**N**) expression levels of myoblast differentiation marker genes, relative mtDNA content (**O**), mitochondrial membrane potential (**P**), intracellular ROS ([ROS]i) (**Q**), and relative *FBXO25* expression (**R**) with *FGF18* overexpression or interference in vitro. In panels **B** and **N**, the numbers shown below the bands were folds of band intensities relative to control. Band intensities were quantified by ImageJ and normalized to β -Tubulin. Data are expressed as a fold-change relative to the control. Results are showed as mean \pm SEM. In panels **A**, **C**, **E–H**, **J–M**, and **O–R**, statistical significance of differences between means was assessed using independent sample *t*-test. (* $P < 0.05$; ** $P < 0.01$). **Fig. S12.** Neither *MYH1G*-AS nor *FGF18* regulate the mRNA and protein expression of *SMARCA5*. (**A–D**) Relative mRNA (**A** and **C**) and protein (**B** and **D**) expression levels of *SMARCA5* after *MYH1G*-AS overexpression or interference in vitro (**A–B**) or in vivo (**C–D**). (**E–F**) Relative mRNA (**E**) and protein (**F**) expression levels of *SMARCA5* after *FGF18* overexpression or interference. In panels **B**, **D**, and **F**, the numbers shown below the bands were folds of band intensities relative to control. Band intensities were quantified by ImageJ and normalized to β -Tubulin. Data are expressed as a fold-change relative to the control. Results are presented as mean \pm SEM. In panels **A**, **C**, and **E**, statistical significance of differences between means was assessed using independent sample *t*-test. (NS, no significant difference). **Fig. S13.** *FGF18* and *SMARCA5* promotes the expression and transcription of *SMAD4*. (**A–B**) Protein expression levels of phosphorylated *SMAD2* and phosphorylated *SMAD3* after *MYH1G*-AS overexpression or interference in vitro (**A**) or in vivo (**B**). (**C–F**) Relative *SMAD4* mRNA expression (**C**), protein expression levels of *SMAD4*, phosphorylated *SMAD2* and phosphorylated *SMAD3* (**D**), the transcriptional activity of *SMAD4* core promoter region (**E**), and ChIP analysis of the binding capacity of *POU2F1* to *SMAD4* promoter (**F**) with *FGF18* overexpression or knockdown. (**G–L**) Relative mRNA (**G**) and protein (**H**) expression levels of *SMARCA5*, relative *SMAD4* mRNA expression (**I**), protein expression levels of *SMAD4*, phosphorylated *SMAD2* and phosphorylated *SMAD3* (**J**), the transcriptional activity of *SMAD4* core promoter region (**K**), and ChIP analysis of the binding capacity of *POU2F1* to *SMAD4* promoter (**L**) with *SMARCA5* overexpression or knockdown. In panels **A–B**, **D**, **H**, and **J**, the numbers shown below the bands were folds of band intensities relative to control. Band intensities were quantified by ImageJ and normalized to β -Tubulin. Data are expressed as a fold-change relative to the control. Results are presented as mean \pm SEM. In panels **C**, **E–G**, **I**, and **K–L**, statistical significance of differences between means was assessed using independent sample *t*-test. (* $P < 0.05$; ** $P < 0.01$).

Additional file 2: Raw images of Western blot.

Additional file 3: Table S4. Differential expression analysis of genes between pectoralis major and soleus in 7-week-old Xinghua chicken.

Additional file 4: Table S5. Differential expression analysis of lncRNAs between pectoralis major and soleus in 7-week-old Xinghua chicken.

Additional file 5: Table S6. Differential analysis of ATAC-seq peaks between pectoralis major and soleus in 7-week-old Xinghua chicken.

Additional file 6: Table S7. List of open chromatin-associated lncRNAs.

Additional file 7: Table S8. Differential expression analysis of genes between control group and *MYH1G*-AS interference in CPMs.

Additional file 8: Table S9. Comparative metabolome analysis of control group versus lncRNA *MYH1G*-AS knock-down gastrocnemius.

Additional file 9: Table S10. lncRNA *MYH1G*-AS specific binding proteins identified by RNA pull-down coupled to mass spectrometry.

Additional file 10: Table S11. *FGF18* specific interacting proteins identified by Co-IP coupled to mass spectrometry.

Acknowledgements

Not applicable.

Author contributions

Q.N. and X.Z. conceived and designed the study. B.C. performed the experiments, interpreted the data and wrote the paper. M.M., R.Y., Z.Z., J.Z., S.K., and D.L. performed the experiments. L.L., and J.L. interpreted the data. All authors read and approved the final manuscript.

Funding

This work was supported by the Natural Scientific Foundation of China (U1901206 and 32302728), National Key R&D Program of China (2021YFD1300100 and 2022YFF1000201), Local Innovative and Research Teams Project of Guangdong Province (2019BT02N630), China Agriculture Research System (CARS-41-G03), China Postdoctoral Science Foundation (2022M710052), and Guangdong Basic and Applied Basic Research Foundation (2021A151111069 and 2023A151010096).

Availability of data and materials

The datasets used and/or analyzed during the current study are available from the corresponding author on reasonable request.

Declarations

Ethics approval and consent to participate

All animal experimental protocols were conformed to “The Instructive Notions with Respect to Caring for Laboratory Animals” issued by the Ministry of Science and Technology of the People’s Republic of China, and approved by the Institutional Animal Care and Use Committee at the South China Agricultural University (approval ID 2021c007).

Consent for publication

Not applicable.

Competing interests

The authors declare that they have no competing interests.

Received: 16 May 2023 Accepted: 15 December 2023

Published online: 04 January 2024

References

1. Hawley JA, Lundby C, Cotter JD, Burke LM. Maximizing cellular adaptation to endurance exercise in skeletal muscle. *Cell Metab.* 2018;27:962–76.
2. Gottesfeld JM, Carey MF. Introduction to the thematic minireview series: chromatin and transcription. *J Biol Chem.* 2018;293:13775–7.
3. Yue J, Hou X, Liu X, Wang L, Gao H, Zhao F, et al. The landscape of chromatin accessibility in skeletal muscle during embryonic development in pigs. *J Anim Sci Biotechnol.* 2021;12:56.
4. Lv W, Jiang W, Luo H, Tong Q, Niu X, Liu X, et al. Long noncoding RNA lncMREF promotes myogenic differentiation and muscle regeneration by interacting with the Smarcat5/p300 complex. *Nucleic Acids Res.* 2022;50:10733–55.
5. Lee JT. Epigenetic regulation by long noncoding RNAs. *Science.* 2012;338:1435–9.
6. Cabili MN, Trapnell C, Goff L, Koziol M, Tazon-Vega B, Regev A, Rinn JL. Integrative annotation of human large intergenic noncoding RNAs reveals global properties and specific subclasses. *Genes Dev.* 2011;25:1915–27.
7. Hitachi K, Honda M, Tsuchida K. The functional role of long non-coding RNA in myogenesis and skeletal muscle atrophy. *Cells.* 2022;11:2291.
8. Cai B, Ma M, Zhang J, Wang Z, Kong S, Zhou Z, et al. lncEDCH1 improves mitochondrial function to reduce muscle atrophy by interacting with SERCA2. *Mol Ther Nucleic Acids.* 2022;27:319–34.
9. Cai B, Ma M, Zhang J, Kong S, Zhou Z, Li Z, et al. Long noncoding RNA ZFP36L2-AS functions as a metabolic modulator to regulate muscle development. *Cell Death Dis.* 2022;13:389.
10. Li X, Fu XD. Chromatin-associated RNAs as facilitators of functional genomic interactions. *Nat Rev Genet.* 2019;20:503–19.
11. Cai B, Ma M, Zhou Z, Kong S, Zhang J, Zhang X, et al. circPTPN4 regulates myogenesis via the miR-499-3p/NAMPT axis. *J Anim Sci Biotechnol.* 2022;13:2.
12. Zhang M, Zhao K, Xu X, Yang Y, Yan S, Wei P, et al. A peptide encoded by circular form of LINC-PINT suppresses oncogenic transcriptional elongation in glioblastoma. *Nat Commun.* 2018;9:4475.
13. Buenrostro JD, Giresi PG, Zaba LC, Chang HY, Greenleaf WJ. Transposition of native chromatin for fast and sensitive epigenomic profiling of open chromatin, DNA-binding proteins and nucleosome position. *Nat Methods.* 2013;10:1213–8.
14. Cai B, Li Z, Ma M, Zhang J, Kong S, Abdalla BA, et al. Long noncoding RNA SMUL suppresses SMURF2 production-mediated muscle atrophy via nonsense-mediated mRNA decay. *Mol Ther Nucleic Acids.* 2021;23:512–26.
15. Cai B, Li Z, Ma M, Wang Z, Han P, Abdalla BA, et al. Zhang X: lncRNA-Six1 encodes a micropeptide to activate Six1 in *Cis* and is involved in cell proliferation and muscle growth. *Front Physiol.* 2017;8:230.
16. Cai B, Ma M, Chen B, Li Z, Abdalla BA, Nie Q, et al. MiR-16-5p targets SESN1 to regulate the p53 signaling pathway, affecting myoblast proliferation and apoptosis, and is involved in myoblast differentiation. *Cell Death Dis.* 2018;9:367.
17. Bassel-Duby R, Olson EN. Signaling pathways in skeletal muscle remodeling. *Annu Rev Biochem.* 2006;75:19–37.
18. He PC, He C. m(6) A RNA methylation: from mechanisms to therapeutic potential. *Embo J.* 2021;40:e105977.
19. Li J, Pei Y, Zhou R, Tang Z, Yang Y. Regulation of RNA N(6)-methyladenosine modification and its emerging roles in skeletal muscle development. *Int J Biol Sci.* 2021;17:1682–92.
20. Braun T, Gautel M. Transcriptional mechanisms regulating skeletal muscle differentiation, growth and homeostasis. *Nat Rev Mol Cell Biol.* 2011;12:349–61.

21. Bodine SC, Latres E, Baumhueter S, Lai VK, Nunez L, Clarke BA, et al. Identification of ubiquitin ligases required for skeletal muscle atrophy. *Science*. 2001;294:1704–8.
22. Sandri M, Sandri C, Gilbert A, Skurk C, Calabria E, Picard A, et al. Foxo transcription factors induce the atrophy-related ubiquitin ligase atrogin-1 and cause skeletal muscle atrophy. *Cell*. 2004;117:399–412.
23. Kokavec J, Zikmund T, Savvulidi F, Kulvait V, Edelmann W, Skoultchi AI, et al. The ISWI ATPase Smarca5 (Snf2h) is required for proliferation and differentiation of hematopoietic stem and progenitor cells. *Stem Cells*. 2017;35:1614–23.
24. Ding Y, Wang W, Ma D, Liang G, Kang Z, Xue Y, et al. Smarca5-mediated epigenetic programming facilitates fetal HSPC development in vertebrates. *Blood*. 2021;137:190–202.
25. Zhu S, Goldschmidt-Clermont PJ, Dong C. Transforming growth factor-beta-induced inhibition of myogenesis is mediated through Smad pathway and is modulated by microtubule dynamic stability. *Circ Res*. 2004;94:617–25.
26. Watts R, McAinch AJ, Dixon JB, O'Brien PE, Cameron-Smith D. Increased Smad signaling and reduced MRF expression in skeletal muscle from obese subjects. *Obes (Silver Spring)*. 2013;21:525–8.
27. Attisano L, Wrana JL. Signal transduction by the TGF-beta superfamily. *Science*. 2002;296:1646–7.
28. Barisic D, Stadler MB, Iurlaro M, Schubeler D. Mammalian ISWI and SWI/SNF selectively mediate binding of distinct transcription factors. *Nature*. 2019;569:136–40.
29. Klemm SL, Shipony Z, Greenleaf WJ. Chromatin accessibility and the regulatory epigenome. *Nat Rev Genet*. 2019;20:207–20.
30. Qi X, Hu M, Xiang Y, Wang D, Xu Y, Hou Y, et al. LncRNAs are regulated by chromatin states and affect the skeletal muscle cell differentiation. *Cell Prolif*. 2020;53:e12879.
31. Yu B, Liu J, Zhang J, Mu T, Feng X, Ma R, et al. Regulatory role of RNA N(6)-methyladenosine modifications during skeletal muscle development. *Front Cell Dev Biol*. 2022;10:929183.
32. Guo X, Li K, Jiang W, Hu Y, Xiao W, Huang Y, et al. RNA demethylase ALKBH5 prevents pancreatic cancer progression by posttranscriptional activation of PER1 in an m6A-YTHDF2-dependent manner. *Mol Cancer*. 2020;19:91.
33. Song H, Feng X, Zhang H, Luo Y, Huang J, Lin M, et al. METTL3 and ALKBH5 oppositely regulate m6A modification of TFEB mRNA, which dictates the fate of hypoxia/reoxygenation-treated cardiomyocytes. *Autophagy*. 2019;15:1419–37.
34. Dong F, Qin X, Wang B, Li Q, Hu J, Cheng X, et al. ALKBH5 facilitates hypoxia-induced paraspeckle assembly and IL8 secretion to generate an immunosuppressive tumor microenvironment. *Cancer Res*. 2021;81:5876–88.
35. Liu J, Dou X, Chen C, Chen C, Liu C, Xu MM, et al. N(6)-methyladenosine of chromosome-associated regulatory RNA regulates chromatin state and transcription. *Science*. 2020;367:580–6.
36. Kan RL, Chen J, Sallam T. Crosstalk between epitranscriptomic and epigenetic mechanisms in gene regulation. *Trends Genet*. 2022;38:182–93.
37. Massague J, Blain SW, Lo RS. TGFbeta signaling in growth control, cancer, and heritable disorders. *Cell*. 2000;103:295–309.
38. Derynck R, Turley SJ, Akhurst RJ. TGFβ biology in cancer progression and immunotherapy. *Nat Rev Clin Oncol*. 2021;18:9–34.
39. Soomro A, Khajehei M, Li R, O'Neil K, Zhang D, Gao B, et al. A therapeutic target for CKD: activin A facilitates TGFβ1 profibrotic signaling. *Cell Mol Biol Lett*. 2023;28:10.
40. Derynck R, Zhang YE. Smad-dependent and Smad-independent pathways in TGF-beta family signalling. *Nature*. 2003;425:577–84.
41. Luo K. Signaling Cross Talk between TGF-β/Smad and Other Signaling Pathways. *Cold Spring Harb Perspect Biol*. 2017;9:a022137.
42. Yang X, Fan W, Huang R, Liu G. β-acetoxyisovaleryl alkannin (AAN-II) from *Alkanna tinctoria* promotes the healing of pressure-induced venous ulcers in a rabbit model through the activation of TGF-β/Smad3 signaling. *Cell Mol Biol Lett*. 2021;26:35.

Publisher's Note

Springer Nature remains neutral with regard to jurisdictional claims in published maps and institutional affiliations.

ARTICLE OPEN



Long noncoding RNA ZFP36L2-AS functions as a metabolic modulator to regulate muscle development

Bolin Cai^{1,2}, Manting Ma^{1,2}, Jing Zhang^{1,2}, Shaofen Kong^{1,2}, Zhen Zhou^{1,2}, Zhenhui Li^{1,2}, Bahareldin Ali Abdalla^{1,2}, Haiping Xu^{1,2}, Xiquan Zhang^{1,2}, Raman Akinyanju Lawal³ and Qinghua Nie^{1,2}✉

© The Author(s) 2022

Skeletal muscle is the largest metabolic organ in the body, and its metabolic flexibility is essential for maintaining systemic energy homeostasis. Metabolic inflexibility in muscles is a dominant cause of various metabolic disorders, impeding muscle development. In our previous study, we found lncRNA *ZFP36L2-AS* (for “*ZFP36L2*-antisense transcript”) is specifically enriched in skeletal muscle. Here, we report that *ZFP36L2-AS* is upregulated during myogenic differentiation, and highly expressed in breast and leg muscle. In vitro, *ZFP36L2-AS* inhibits myoblast proliferation but promotes myoblast differentiation. In vivo, *ZFP36L2-AS* facilitates intramuscular fat deposition, as well as activates fast-twitch muscle phenotype and induces muscle atrophy. Mechanistically, *ZFP36L2-AS* interacts with acetyl-CoA carboxylase alpha (ACACA) and pyruvate carboxylase (PC) to induce ACACA dephosphorylation and damaged PC protein stability, thus modulating muscle metabolism. Meanwhile, *ZFP36L2-AS* can activate ACACA to reduce acetyl-CoA content, which enhances the inhibition of PC activity. Our findings present a novel model about the regulation of lncRNA on muscle metabolism.

Cell Death and Disease (2022)13:389; <https://doi.org/10.1038/s41419-022-04772-2>

INTRODUCTION

As the largest tissue that comprises about 40% of the total body mass, skeletal muscle is a major player in regulating energy homeostasis and obesity progression [1–3]. A key metabolic feature of skeletal muscle is its plasticity, which is able to adjust fuel oxidation to fuel availability, called ‘metabolic flexibility’ [4, 5]. It’s well known that the metabolic regulation of skeletal muscle is pivotal for health and development, and loss of this flexibility is tightly associated with metabolic disorders such as obesity and muscle wasting [4, 6–8].

The maintenance of skeletal muscle mass is finely regulated by protein synthesis and catabolism [9]. Muscle atrophy refers to a decrease in muscle mass and fiber size and is characterized by enhanced protein degradation [10]. Muscle atrophy leading to muscle wasting seriously restricts animal development. Recently, muscle wasting has attracted many researchers’ attention, however, the molecular mechanisms that govern muscle atrophy remain largely unknown.

Protein-encoding genes only account for a small portion (2%) of the genome, and yet 70–90% of the genome is transcribed into long noncoding RNAs (lncRNAs) at some point during development [11]. lncRNAs are a new class of regulatory RNAs, commonly defined as transcribed RNAs of more than 200 nucleotides with low coding potential, are widely involved in gene expression regulation at the transcription, translation and epigenetic levels [12–16]. Although only a small number of functional lncRNAs have been well characterized to date, they seem to control major

biological processes impacting skeletal muscle development and muscle disorders [17–20].

White recessive rock (WRR) is a hypertrophic broiler chicken with a fast growth rate, which exhibits a different growth performance from Xinghua (XH) chicken (a lean Chinese native breed with a slow growth rate) [21, 22]. In our previous RNA-seq study (accession number GSE58755), we found lncRNA TCONS_00067025 (named *ZFP36* ring finger protein like 2 [*ZFP36L2*]-antisense transcript [*ZFP36L2-AS*]) differentially expressed between WRR (a fast growth rate broiler chicken) and XH chicken (a slow growth rate Chinese native breed) [22]. In the current study, functional studies demonstrated that *ZFP36L2-AS* inhibits myoblast proliferation but promotes myogenic differentiation in vitro. In vivo, *ZFP36L2-AS* represses fatty acid oxidation to facilitate intramuscular fat deposition, as well as activates fast-twitch muscle phenotype and induces muscle atrophy. Further mechanistic investigation revealed that *ZFP36L2-AS* interacts with acetyl-CoA carboxylase alpha (ACACA) and pyruvate carboxylase (PC) to induce ACACA activation and inhibit PC activity. Altogether, our studies uncover a functional lncRNA that modulates skeletal muscle development.

RESULTS

ZFP36L2-AS is a novel lncRNA associated with skeletal muscle development

Our previous RNA-seq study found a novel lncRNA (*ZFP36L2-AS*) was highly expressed in fast growth rate broilers (Fig. 1A, B) [22],

¹Lingnan Guangdong Laboratory of Modern Agriculture & State Key Laboratory for Conservation and Utilization of Subtropical Agro-bioresources, College of Animal Science, South China Agricultural University, Guangzhou 510642 Guangdong, China. ²Guangdong Provincial Key Lab of Agro-Animal Genomics and Molecular Breeding, and Key Laboratory of Chicken Genetics, Breeding and Reproduction, Ministry of Agriculture, Guangzhou 510642 Guangdong, China. ³The Jackson Laboratory, 600 Main Street, Bar Harbor, ME, US. ✉email: nqinghua@scau.edu.cn

Received: 6 May 2021 Revised: 17 March 2022 Accepted: 25 March 2022

Published online: 21 April 2022

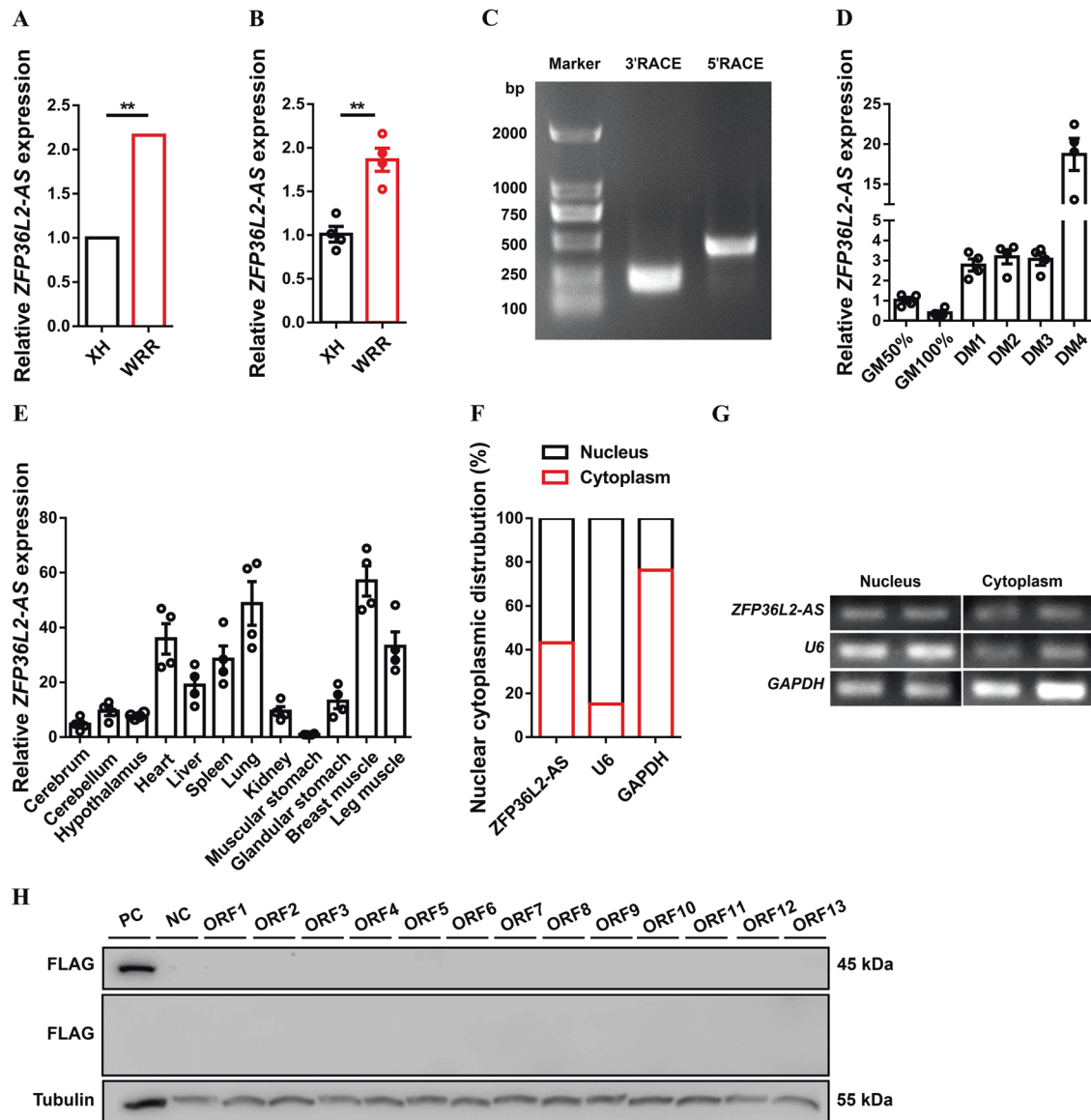


Fig. 1 Identification of lncRNA *ZFP36L2-AS*. **A, B** Relative *ZFP36L2-AS* expression in breast muscles of 7-week-old Xinghua (XH) chicken and White recessive rock (WRR) detected by RNA-seq (**A**) and qPCR (**B**). (**C**) Results of *ZFP36L2-AS* 3' RACE and 5' RACE. (**D**) Relative *ZFP36L2-AS* expression during CPM proliferation and differentiation. (**E**) Tissue expression profiles of *ZFP36L2-AS*. The horizontal axis and vertical axis indicate different tissues and their relative expression values, respectively. (**F, G**) The distribution of *ZFP36L2-AS* in the cytoplasm and nuclei of chicken primary myoblast (CPM) was determined by qPCR (**F**) and semi-qPCR (**G**). *GAPDH* and *U6* serve as cytoplasmic and nuclear localization controls, respectively. (**H**) Western blot analysis of the coding ability of *ZFP36L2-AS*. The potential ORFs of *ZFP36L2-AS* were cloned into the pcDNA3.1-3xFlag-C vector. CPMs transfected with β -actin were used as a positive control (PC) and untransfected CPMs were used as a negative control (NC). Results are presented as mean \pm SEM. In panels (**A, B**), statistical significance of differences between means was assessed using independent sample *t*-test. (* $P < 0.05$; ** $P < 0.01$).

implied that *ZFP36L2-AS* is probably associated with skeletal muscle development. To obtain the full-length of *ZFP36L2-AS*, 5' and 3' ends of this lncRNA were determined by RACE system (Fig. 1C). The Basic Local Alignment Search Tool (BLAST) of the National Center for Biotechnology Information (NCBI) showed that *ZFP36L2-AS* was an antisense transcript of *ZFP36L2* with 3,465 nt long, located at chromosome 3 from 25,089,365 to 25,092,829, and mainly conserved in Aves (Supplementary Fig. 1A and Table 1). *ZFP36L2-AS* was upregulated during myogenic differentiation, and highly expressed in breast and leg muscle (Fig. 1D, E). Compared with other muscle-resident cells, *ZFP36L2-AS* was highly expressed in myoblasts (Supplementary Fig. 1B). Furthermore, cell-fractionation assays demonstrated that *ZFP36L2-AS* was present

both in the cytoplasm and nucleus of chicken primary myoblast (CPM) (Fig. 1F, G). In order to verify the coding potential of *ZFP36L2-AS*, we further cloned 3xFLAG epitope tag in-frame with the C terminus of thirteen potential ORFs of *ZFP36L2-AS*. Crucially, western blot analysis indicated that *ZFP36L2-AS* was an lncRNA without protein-encoding potential (Fig. 1H).

***ZFP36L2-AS* inhibits myoblast proliferation but promotes myogenic differentiation**

Given that *ZFP36L2-AS* was decreased in myoblast proliferation and upregulated during myogenic differentiation (Fig. 1D), we performed overexpression and inhibition experiments to assess its effect in proliferation and differentiation of myoblast (Fig. 2A and

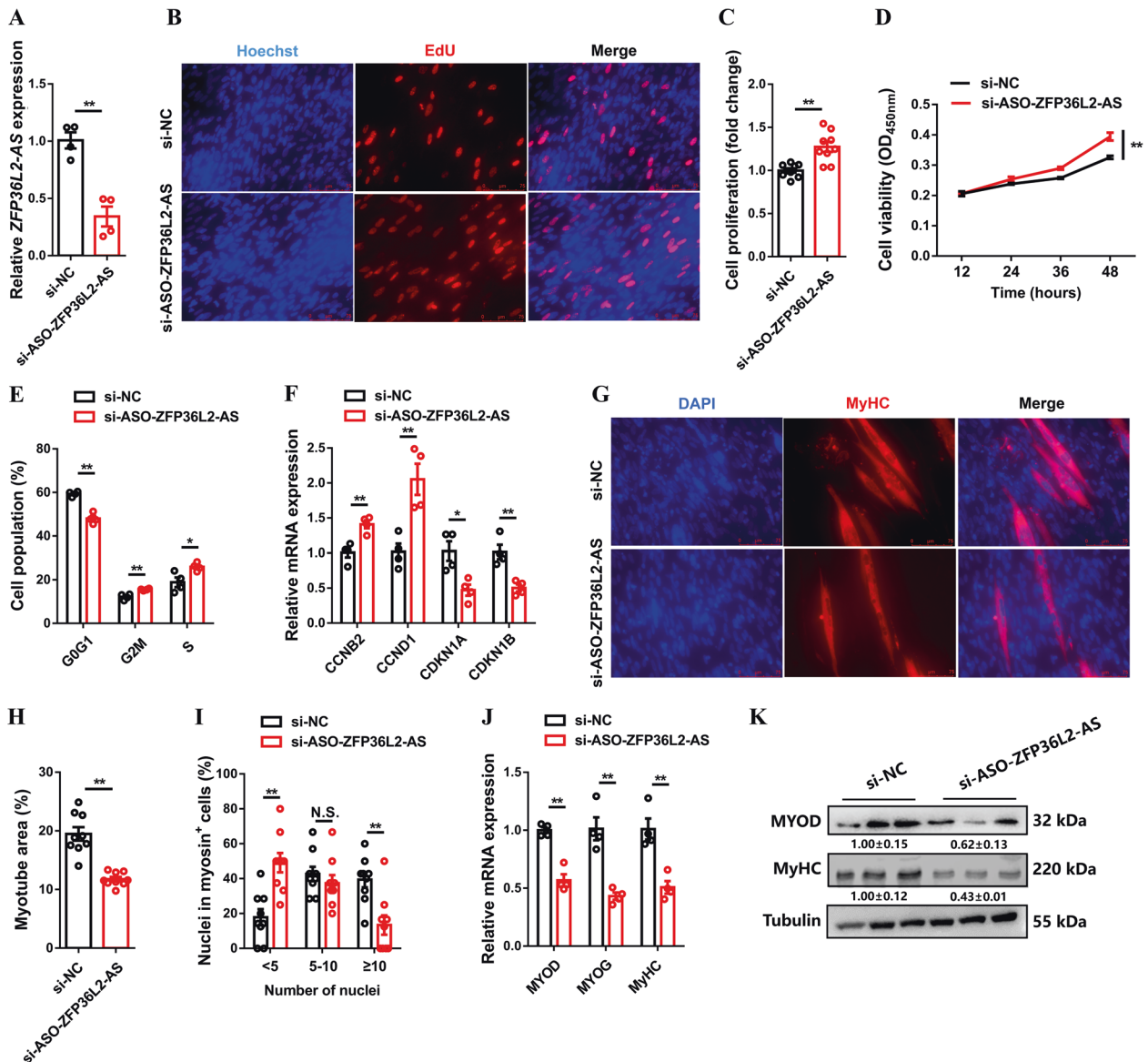


Fig. 2 IncRNA *ZFP36L2-AS* inhibits myoblast proliferation but promotes myoblast differentiation. **A** Relative *ZFP36L2-AS* expression with *ZFP36L2-AS* interference in vitro. **B** Proliferation of transfected CPMs was assessed by 5-ethynyl-2'-deoxyuridine (EdU) incorporation. **C** Proliferation rate of myoblasts after interference of *ZFP36L2-AS*. **D** CCK-8 assays were performed in CPMs with *ZFP36L2-AS* interference. **E** Cell cycle analysis of myoblasts after interference of *ZFP36L2-AS*. **F** Relative mRNA levels of several cell cycle genes with *ZFP36L2-AS* interference. **G–I** MyHC immunostaining (**G**), myotube area (%) (**H**), and myoblast fusion index (**I**) of CPMs transfected with *ZFP36L2-AS* interference. Cells were differentiated for 72 h after transfection. The nuclei were visualized with 4',6-diamidino-2-phenylindole (DAPI). **J, K** Relative mRNA (**J**) and protein (**K**) expression levels of myoblast differentiation marker genes from si-ASO-*ZFP36L2-AS* transfected CPMs. The numbers shown below the bands were folds of band intensities relative to control. Band intensities were quantified by ImageJ and normalized to β -Tubulin. Data are expressed as a fold-change relative to the control. Results are shown as mean \pm SEM. In panels (**A**, **C–F**, and **H–J**), statistical significance of differences between means was assessed using independent sample *t*-test. (**P* < 0.05; ***P* < 0.01; N.S. no significant difference).

Supplementary Fig. 2A). The 5-ethynyl-2'-deoxyuridine (EdU) staining and cell counting kit-8 (CCK-8) assay demonstrated that *ZFP36L2-AS* interference significantly increased EdU incorporation and promoted myoblast proliferation, whereas *ZFP36L2-AS* overexpression significantly inhibited the proliferation of myoblast (Fig. 2B–D and Supplementary Fig. 2B–D). Flow cytometric analysis showed that *ZFP36L2-AS* inhibition significantly reduced the number of cells that progressed to G0/G1 and increased the number of S phase cells (Fig. 2E). Conversely, *ZFP36L2-AS* overexpression resulted in a larger number of G0/G1 and fewer S phase cells (Supplementary Fig. 2E). Furthermore, inhibition of *ZFP36L2-AS* increased the expression of cell cycle-promoting

genes such as *CCNB2* and *CCND1*, while reduced cell cycle-inhibiting genes like *CDKN1A* and *CDKN1B* (Fig. 2F). And the opposite result was observed with *ZFP36L2-AS* overexpression (Supplementary Fig. 2F).

To further test whether *ZFP36L2-AS* functions in myogenic differentiation, immunofluorescence staining was performed after overexpression and inhibition of *ZFP36L2-AS*. *ZFP36L2-AS* inhibition significantly repressed myoblast differentiation and decreased the total areas of myotubes, while myotube formation was facilitated with *ZFP36L2-AS* overexpression (Fig. 2G–I and Supplementary Fig. 2G–I). In addition, the expressions level of myoblast differentiation marker genes, including *MYOD*, *MYOG*,

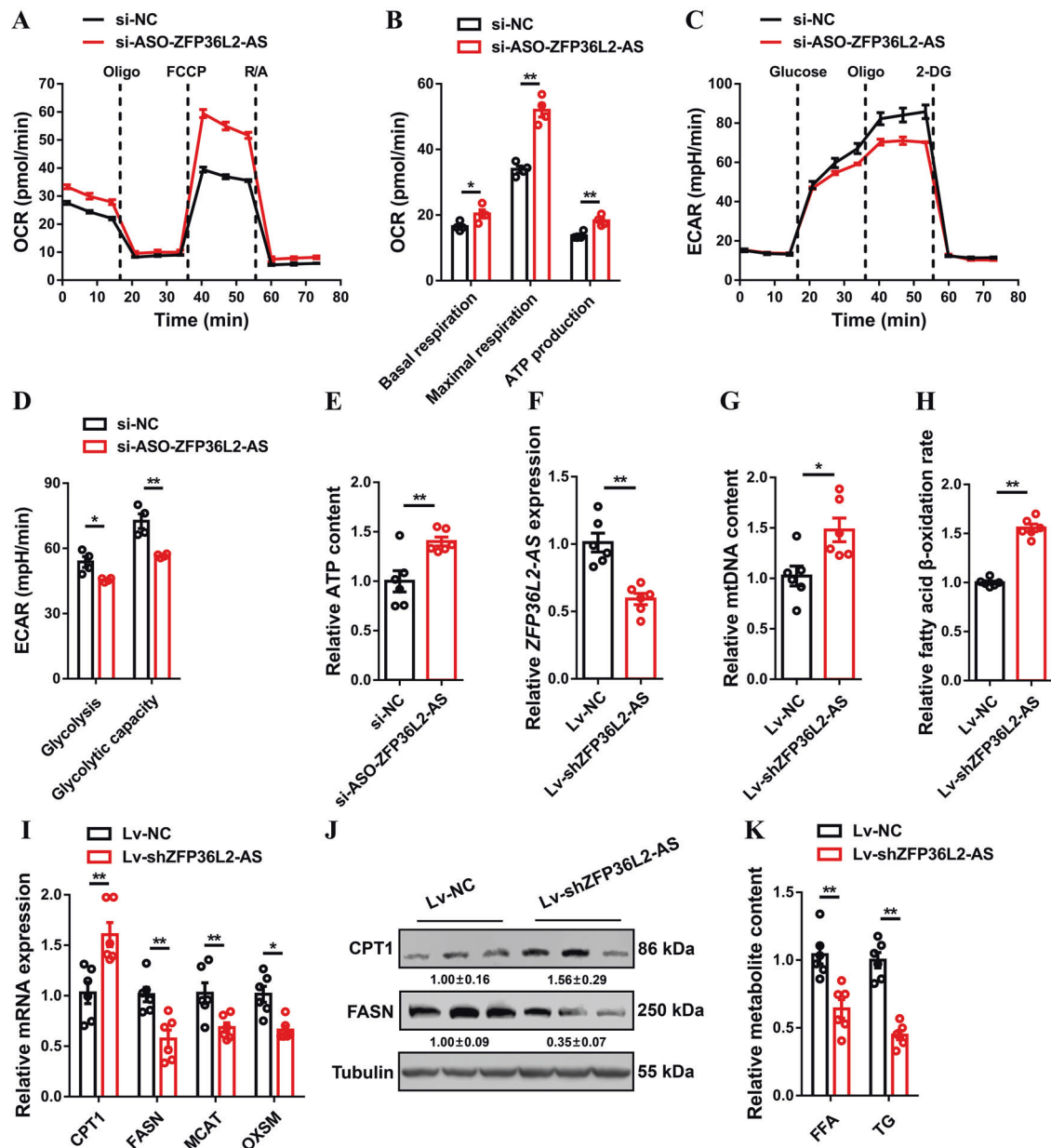


Fig. 3 IncRNA *ZFP36L2-AS* represses cellular respiration and fatty acid oxidation in skeletal muscle. **A, B** Oxygen consumption rate (OCR) (**A**), and basal respiration, maximal respiration, and ATP production (**B**) of myoblasts after interference of *ZFP36L2-AS*. (**C, D**) Extracellular acidification rate (ECAR) (**C**), and glycolysis and glycolytic capacity (**D**) of myoblasts with *ZFP36L2-AS* interference. **E** Relative cellular adenosine triphosphate (ATP) content with *ZFP36L2-AS* interference in CPMs. **F** Relative *ZFP36L2-AS* expression in gastrocnemius after infected with lentivirus-mediated *ZFP36L2-AS* knockdown (Lv-shZFP36L2-AS) or negative control (Lv-NC). **G** Relative mitochondrial DNA (mtDNA) content in *ZFP36L2-AS* knockdown gastrocnemius. (**H**) Relative fatty acid β -oxidation rate in gastrocnemius with *ZFP36L2-AS* knockdown. **I, J** Relative mRNA (**I**) and protein (**J**) expression levels of fatty acid oxidation or synthesis related-genes after infected with the indicated lentivirus. The numbers shown below the bands were folds of band intensities relative to control. Band intensities were quantified by ImageJ and normalized to β -Tubulin. Data are expressed as a fold-change relative to the control. **K** Relative free fatty acid (FFA) and triglyceride (TG) content in gastrocnemius with *ZFP36L2-AS* knockdown. Results are presented as mean \pm SEM. In panels (**B, D–I, and K**), statistical significance of differences between means was assessed using independent sample *t*-test. (**P* < 0.05; ***P* < 0.01).

and *MyHC* were significantly downregulated with *ZFP36L2-AS* interference (Fig. 2J, K). Conversely, overexpression of *ZFP36L2-AS* promoted their expression (Supplementary Fig. 2J, K).

***ZFP36L2-AS* decreases cellular respiration, fatty acid oxidation, and TCA cycle metabolites in skeletal muscle**

Cellular mitochondrial activities including oxygen consumption rate (OCR), basal and maximal mitochondrial respiration, and adenosine triphosphate (ATP) production were elevated with

ZFP36L2-AS interference, whereas *ZFP36L2-AS* overexpression facilitated glycolysis (Fig. 3A–D and Supplementary Fig. 3A–D), indicating that *ZFP36L2-AS* may be involved in cellular energy metabolism. Meanwhile, inhibition of *ZFP36L2-AS* increased ATP content in myoblast, while ATP content was decreased with *ZFP36L2-AS* overexpression in myoblasts (Fig. 3E and Supplementary Fig. 3E). Given that *ZFP36L2-AS* regulates cellular metabolism, we further detected the cellular ATP content in satellite cells after inhibition and overexpression of *ZFP36L2-AS* to explore whether

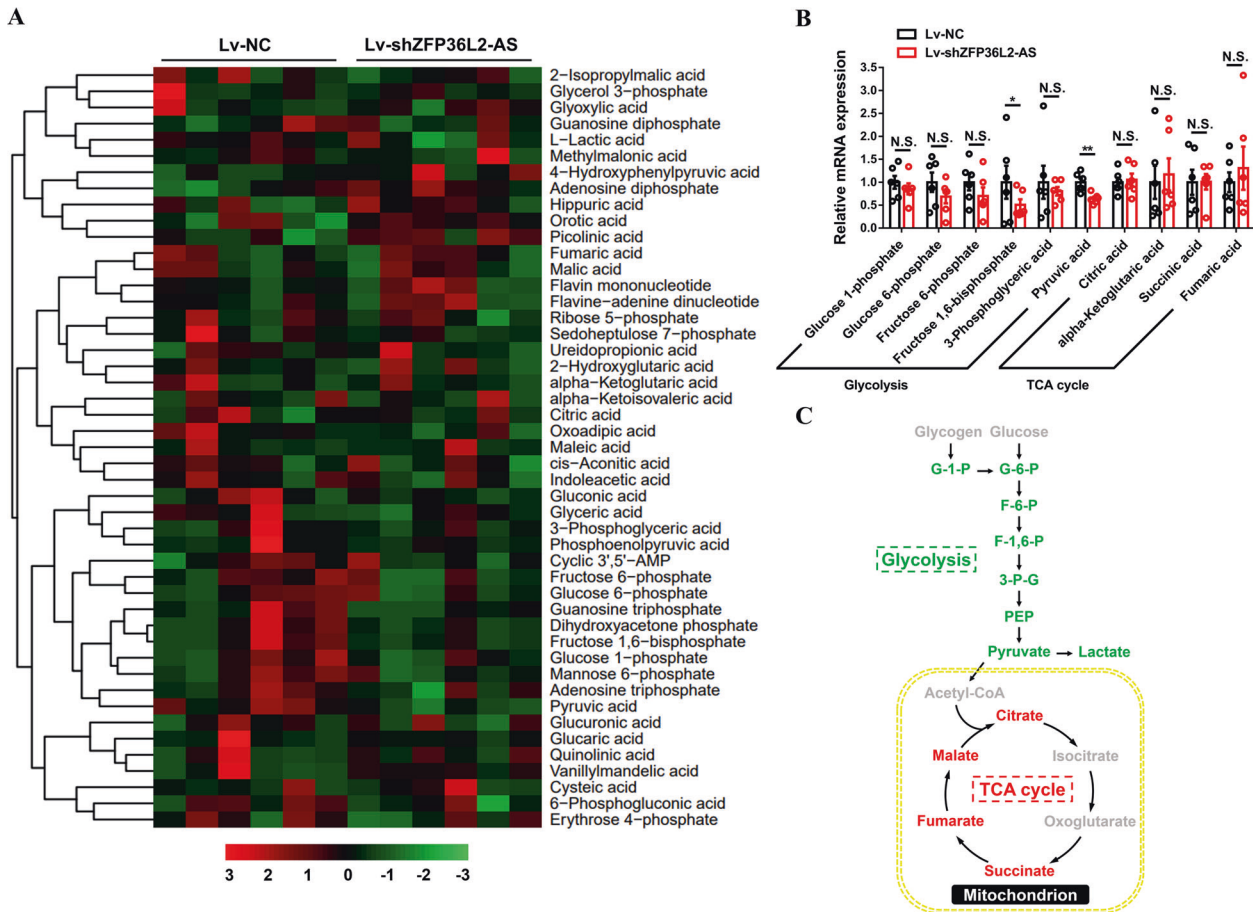


Fig. 4 Knockdown of lncRNA ZFP36L2-AS downregulates the TCA cycle. **A** Hierarchical clustering analysis (HCA) of metabolites in gastrocnemius after infected with Lv-shZFP36L2-AS or Lv-NC. The colors indicate the relative levels in lncRNA ZFP36L2-AS knockdown or control group. **B** Relative metabolite content of glycolysis and tricarboxylic acid (TCA) cycle in gastrocnemius with ZFP36L2-AS knockdown. **C** Schematic diagram of metabolic pathways of glycolysis and TCA cycle affected by ZFP36L2-AS knockdown in the gastrocnemius. Upregulated metabolites are shown in red, and the downregulated metabolites are shown in green. In panel (C), results are shown as mean \pm SEM, statistical significance of differences between means was assessed using independent sample t-test. (* $P < 0.05$; ** $P < 0.01$).

ZFP36L2-AS plays a metabolic regulatory role in satellite cells similar to that in myoblasts. The results shown that ZFP36L2-AS did not regulate cellular ATP content in satellite cells (Supplementary Fig. 4A, B), suggesting the function of ZFP36L2-AS in muscle metabolism mainly depends on its expression in myoblasts. To investigate the potential roles of ZFP36L2-AS in vivo, the gastrocnemius of 1-day-old chick was injected with adenovirus-mediated ZFP36L2-AS overexpression (Adv-ZFP36L2-AS) or lentivirus-mediated ZFP36L2-AS knockdown (Lv-shZFP36L2-AS) (Fig. 3F and Supplementary Fig. 3F). ZFP36L2-AS knockdown increased mitochondrial DNA content, which was potentially contribute to the acceleration of fatty acid oxidation (FAO) (Fig. 3G, H). In contrast, mitochondrial DNA content and fatty acid β -oxidation were reduced after overexpression of ZFP36L2-AS (Supplementary Fig. 3G, H). Besides, knockdown of ZFP36L2-AS upregulated the expression of FAO-related gene like CPT1, but downregulated key genes involved in fatty acid synthesis (such as FASN, MCAT and OXSM) and reduced intramuscular free fatty acid (FFA) and triglyceride (TG) content (Fig. 3I–K). Meanwhile, opposite results were showed with ZFP36L2-AS overexpression (Supplementary Fig. 3I–K).

Excessive lipid storage is often accompanied by changes in muscle metabolism [23–26]. To further study the regulation of ZFP36L2-AS on muscle metabolism, a comparative metabolome analysis was performed with ZFP36L2-AS knockdown in gastrocnemius. Hierarchical clustering analysis (HCA) based on

metabolite levels showed that several tricarboxylic acid cycle (TCA cycle) metabolites actually accumulate in ZFP36L2-AS knockdown gastrocnemius (Fig. 4A, B and Supplementary Table 2). On the contrary, ZFP36L2-AS knockdown significantly reduced glycolytic metabolites such as Fructose 1,6-bisphosphate and Dihydroxyacetone phosphate (Fig. 4A, B and Supplementary Table 2). Altogether, our results indicated that ZFP36L2-AS impairs mitochondrial respiration and FAO, leading to the accumulation of lipid metabolites, which elevates glycolysis as compensatory responses (Fig. 4C).

ZFP36L2-AS activates a fast-twitch gene expression profile concurrent with muscle atrophy

Skeletal muscle is comprised of heterogeneous myofibers that differ in their physiological and metabolic parameters [27]. Compared with fast-twitch (type II; glycolytic) myofibers, slow-twitch (type I; oxidative) myofibers have more myoglobin, more mitochondria, and higher activity of oxidative metabolic enzymes [28, 29]. In response to environmental demands, skeletal muscle can remodel by activating signaling pathways to reprogram gene expression to sustain muscle performance [27]. Given that knockdown of ZFP36L2-AS reduced the accumulation of glycolytic metabolites and upregulated oxidative metabolism in gastrocnemius (Fig. 4B, C), ZFP36L2-AS may function in the transformation of myofiber type by modulating muscle metabolism. As expected, glycogen content was increased and expression of glycogenolytic

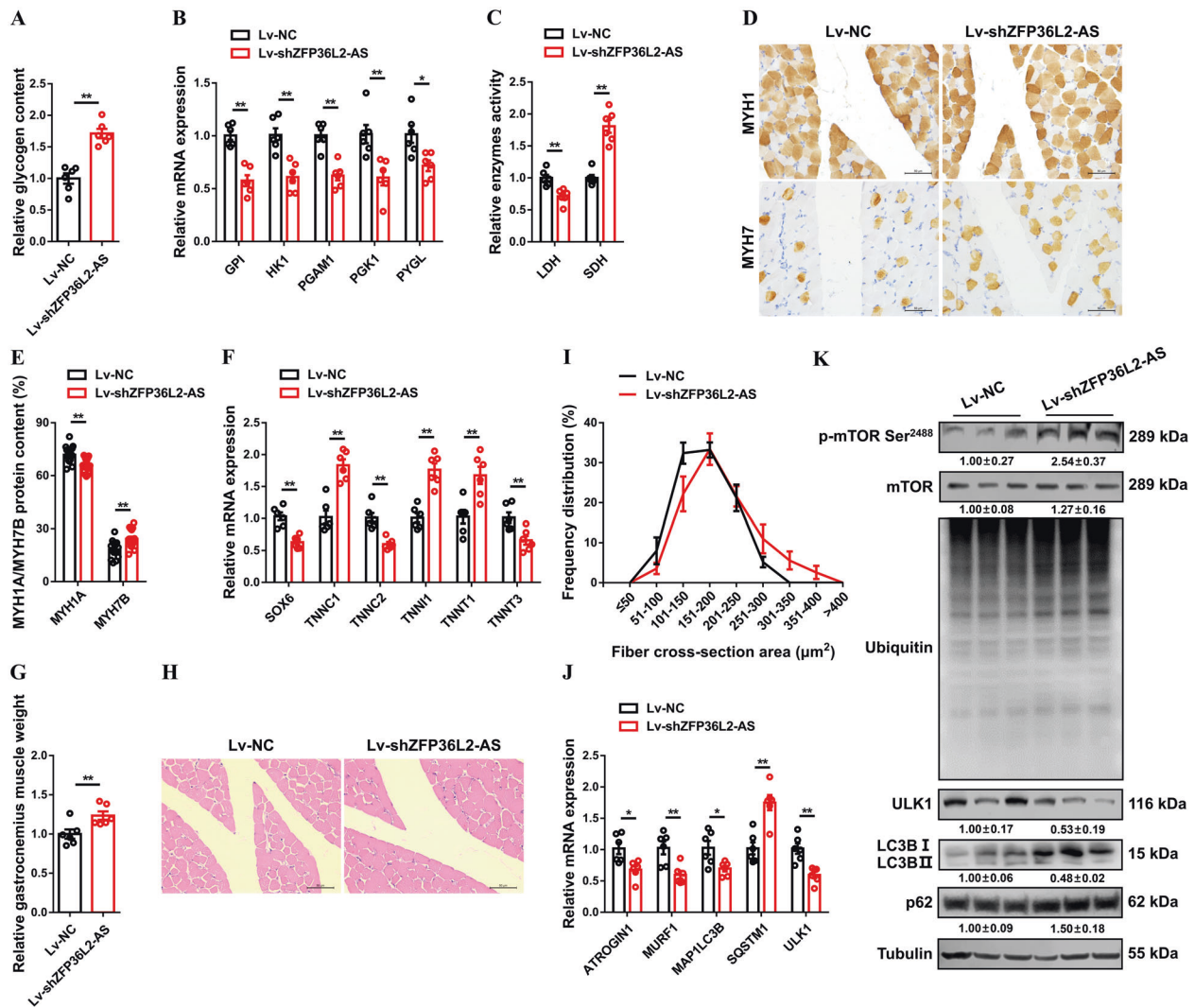


Fig. 5 IncRNA *ZFP36L2-AS* activates a fast-twitch gene expression profile concurrent with muscle atrophy. **A** Relative glycogen content in gastrocnemius with *ZFP36L2-AS* knockdown. **B** Relative mRNA expression levels of glycogenolytic and glycolytic genes in gastrocnemius after infected with the indicated lentivirus. **C** Relative enzymes activity of lactic dehydrogenase (LDH) and succinate dehydrogenase (SDH) in gastrocnemius infected with *ZFP36L2-AS* knockdown. **D, E** Immunohistochemistry analysis of MYH1/MYH7 (**D**) and MYH1/MYH7 protein content (**E**) of gastrocnemius after *ZFP36L2-AS* knockdown. **F** Relative mRNA expression levels of several fast-/slow-twitch myofiber genes with *ZFP36L2-AS* knockdown. **G** Relative gastrocnemius muscle weight after infected with the indicated lentivirus. **H, I** H&E staining (**H**) and frequency distribution of fiber cross-section area (CSA) (**I**) of transverse sections of gastrocnemius with *ZFP36L2-AS* knockdown. **J** Relative mRNA expression of the atrophy and autophagy-related genes in gastrocnemius after infected with the indicated lentivirus. **K** The protein expression levels of mTOR signaling after *ZFP36L2-AS* knockdown. The numbers shown below the bands were folds of band intensities relative to control. Band intensities were quantified by ImageJ and normalized to β -Tubulin. Data are expressed as a fold-change relative to the control. Results are presented as mean \pm SEM. In panels (A–C, E–G, and J), statistical significance of differences between means was assessed using independent sample *t*-test. (**P* < 0.05; ***P* < 0.01).

and glycolytic genes was downregulated with *ZFP36L2-AS* knockdown (Fig. 5A, B). Inversely, overexpression of *ZFP36L2-AS* reduced the accumulation of glycogen, as well as promoted expression of glycogenolytic and glycolytic genes (Supplementary Fig. 5A, B). *ZFP36L2-AS* knockdown suppressed the activity of lactic dehydrogenase (LDH) and enhanced the activity of succinate dehydrogenase (SDH), whereas *ZFP36L2-AS* overexpression elevated glycolytic capacity and decrease oxidative capacity of skeletal muscle (Fig. 5C and Supplementary Fig. 5C). More importantly, immunohistochemical results showed that *ZFP36L2-AS* knockdown suppressed MYH1A/fast-twitch protein level and promoted the expression level of MYH7B/slow-twitch protein (Fig. 5D, E). The expressions of multiple fast-twitch myofiber genes such as *SOX6*, *TNNC2* and *TNNT3* were significantly promoted, while slow-twitch myofiber genes like *TNNC1*, *TNNI1* and *TNNT1*

were inhibited with *ZFP36L2-AS* knockdown (Fig. 5F). On the contrary, *ZFP36L2-AS* overexpression upregulated fast-twitch protein level and expression of fast-twitch myofiber genes, drove the transformation of slow-twitch to fast-twitch myofibers (Supplementary Fig. 5D–F).

Muscle remodeling can also affect muscle mass; this is regulated by anabolic and catabolic signaling pathways, which induce muscle hypertrophy and muscle atrophy, respectively [30]. Here, *ZFP36L2-AS* knockdown increased muscle mass and elevated the proportion of large myofiber (> 200 μm^2) (Fig. 5G–I). Conversely, gastrocnemius mass was reduced and proportion of small myofiber (< 200 μm^2) was increased with overexpression of *ZFP36L2-AS* (Supplementary Fig. 5G–I), suggesting *ZFP36L2-AS* is involved in muscle atrophy. Mammalian target of rapamycin (mTOR) is a master growth regulator that senses and integrates

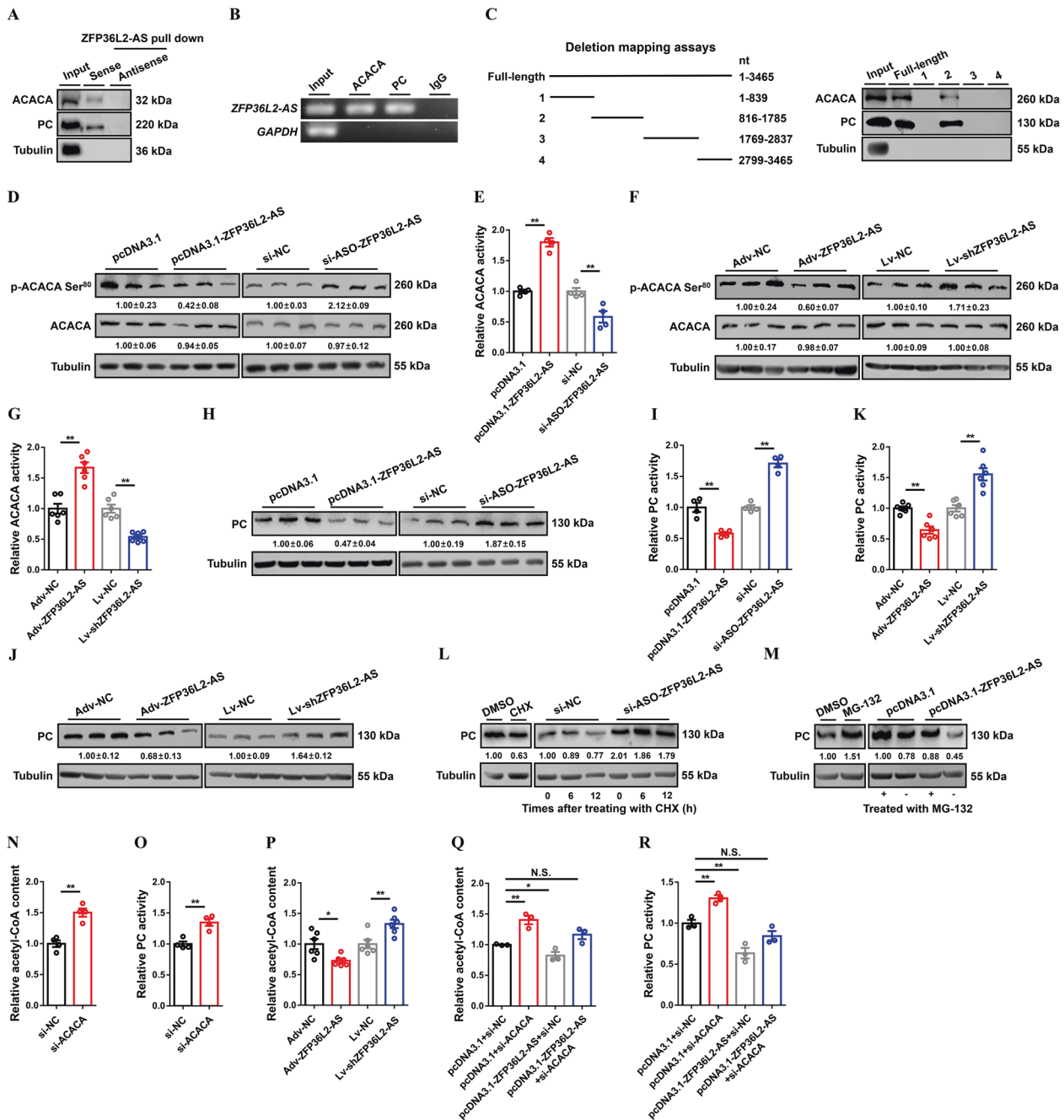


Fig. 6 IncRNA *ZFP36L2-AS* interacts with *ACACA* and *PC* to induce *ACACA* dephosphorylation and inhibit *PC* protein stabilization. **A, B** IncRNA *ZFP36L2-AS* interacts with *ACACA* and *PC* protein were determined by biotin-labeled RNA pull-down (**A**) and RIP (**B**). **C** The interaction of full-length and truncated *ZFP36L2-AS* with *ACACA* and *PC* protein was determined by RNA pull-down. **D–G** The protein expression levels of *ACACA* and phosphorylated *ACACA* (**D, F**), and relative *ACACA* activity (**E** and **G**) after *ZFP36L2-AS* overexpression or knockdown in vitro and in vivo. **H–K** The protein expression level of *PC* (**H, J**), and relative *PC* activity (**I, K**) after *ZFP36L2-AS* overexpression or knockdown in vitro and in vivo. **L** The protein expression level of *PC* in *ZFP36L2-AS* overexpressed myoblast was analyzed after incubated with the protein synthesis inhibitor cycloheximide (CHX; 25 µg/ml). **M** The protein expression level of *PC* in *ZFP36L2-AS* knockdown myoblast was analyzed after incubated with the proteasome inhibitor (MG-132; 5 µmol/L) for 12 h. **N, O** Relative acetyl-CoA content (**N**), and relative *PC* activity (**O**) with *ACACA* interference in vitro. **P** Relative acetyl-CoA content with *ZFP36L2-AS* overexpression or knockdown in vivo. **Q, R** Relative acetyl-CoA content (**Q**), and relative *PC* activity (**R**) induced by the listed nucleic acids. In panels (**D, F, H, J, L**), the numbers shown below the bands were folds of band intensities relative to control. Band intensities were quantified by ImageJ and normalized to β -Tubulin. Data are expressed as a fold-change relative to the control. Results are presented as mean \pm SEM. In panels (**E, G, I, K** and **N–P**), statistical significance of differences between means was assessed using independent sample *t*-test. In panels (**Q, R**), ANOVA followed by Dunnett's test was used. (**P* < 0.05; ***P* < 0.01; N.S., no significant difference).

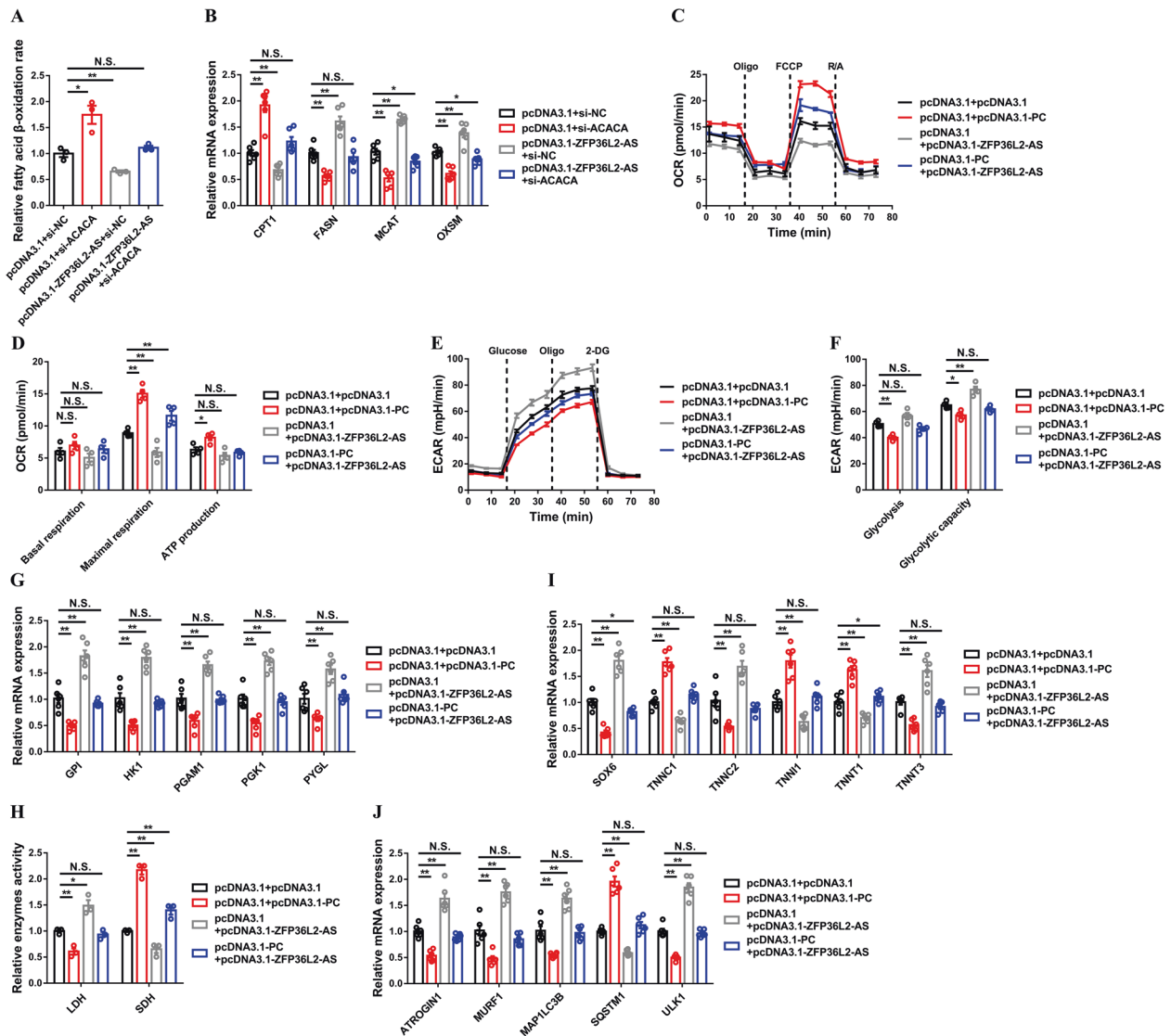


Fig. 7 ACACA and PC are required for the function of lncRNA ZFP36L2-AS. **A, B** Relative fatty acid β -oxidation rate (**A**), and relative mRNA levels of fatty acid oxidation or synthesis related-genes (**B**) after co-transfection with the listed nucleic acids in CPMs. **C–J** OCR (**C**), basal respiration, maximal respiration and ATP production (**D**), ECAR (**E**), glycolysis and glycolytic capacity (**F**), relative mRNA expression levels of glycolytic and glycolytic genes (**G**), relative enzymes activity of LDH and SDH (**H**), relative mRNA expression levels of several fast-/slow-twitch myofiber genes (**I**), and relative mRNA expression of the atrophy and autophagy-related genes (**J**) induced by the listed nucleic acids in CPMs. Results are shown as mean \pm SEM. In all panels, statistical significance of differences between means was assessed using ANOVA followed by Dunnett's test. (* $P < 0.05$; ** $P < 0.01$; N.S. no significant difference).

diverse nutritional and environmental cues, can resist muscle atrophy by inhibiting proteasomal degradation and autophagy [30–32]. To further explore the regulatory mechanism of ZFP36L2-AS on muscle atrophy, we assessed the mTOR signaling after ZFP36L2-AS overexpression and knockdown. ZFP36L2-AS knockdown facilitated Ser²⁴⁸⁸ phosphorylation of mTOR, thus inactivating ubiquitin-proteasome system (UPS) and autophagy-lysosomal system, while the mTOR signaling was inhibited with ZFP36L2-AS overexpression (Fig. 5J, K and Supplementary Fig. 5J, K), indicating that ZFP36L2-AS induces muscle atrophy by inhibiting the mTOR signaling.

ZFP36L2-AS interacts with ACACA and PC

Molecular decoy is one of the main molecular mechanisms for lncRNA to function. It refers to that lncRNA directly binds to RNA or protein molecules, thereby activating or blocking the role and signal pathway of these molecule [33]. To elucidate the mechanism by which ZFP36L2-AS regulates skeletal muscle

development, we attempted to identify its endogenous binding proteins by performing RNA pull-down coupled to mass spectrometry. Compared with the ZFP36L2-AS antisense group, a total of 141 proteins (protein score ≥ 19) were identified specifically bind to ZFP36L2-AS sense transcript (Supplementary Table 3). Gene ontology (GO) and Kyoto Encyclopedia of Genes and Genomes (KEGG) enrichment analysis found that these RNA binding proteins (RBPs) were mainly enriched in biological processes such as cellular process, metabolic process, cellular component organization or biogenesis, and biological regulation, as well as participated in biological processes including metabolic pathways, carbon metabolism, TCA cycle, pyruvate metabolism, glycolysis/gluconeogenesis and so on (Supplementary Fig. 6A, B). Acetyl-CoA carboxylase alpha (ACACA) and pyruvate carboxylase (PC) are members of biotin-dependent carboxylase, which are known to be widely involved in metabolic regulation [34–37], were found specifically bind to ZFP36L2-AS (Supplementary Table 3). To corroborate this result, we performed western blot analysis of

RNA pull-down samples, which validated the interaction of *ZFP36L2-AS* with ACACA and PC protein (Fig. 6A). Moreover, the specificity of these interactions was also verified with RNA immunoprecipitation (RIP) (Fig. 6B).

To further map the *ZFP36L2-AS* functional motifs corresponding to ACACA and PC binding, we conducted an in vitro RNA pull-down assay using a series of truncated *ZFP36L2-AS* fragments (Fig. 6C). This analysis revealed that nucleotides 816–1785 of *ZFP36L2-AS* are sufficient to interact with both ACACA and PC protein, while other *ZFP36L2-AS* truncated fragments could not (Fig. 6C). As the *ZFP36L2-AS* 816–1785 region is necessary for *ZFP36L2-AS*'s binding to ACACA and PC protein, we overexpressed the truncated fragment (816–1785 nt) and analyzed its impact on skeletal muscle development. Similar results to *ZFP36L2-AS* full-length overexpression were found (Supplementary Fig. 7A–F), implying that the interaction of *ZFP36L2-AS* with ACACA and PC protein may be a requisite for *ZFP36L2-AS* to function.

The function of *ZFP36L2-AS* partially depends on its regulation of ACACA and PC activity

With the observation that *ZFP36L2-AS* directly interacts with ACACA and PC, we further analyzed the effect of *ZFP36L2-AS* on ACACA and PC. Both in vitro and in vivo, the mRNA level of ACACA and PC were not changed with *ZFP36L2-AS* overexpression and knockdown (Supplementary Fig. 8A–D). Overexpression of *ZFP36L2-AS* significantly inhibited the phosphorylation level of ACACA protein and increased ACACA activity, whereas *ZFP36L2-AS* knockdown promoted ACACA phosphorylation and inactivated ACACA (Fig. 6D–G and Supplementary Fig. 7G, H), indicating that *ZFP36L2-AS* modulates the activity of ACACA by regulating ACACA phosphorylation. Next, we investigated the regulation of *ZFP36L2-AS* on the protein level and activity of PC. *ZFP36L2-AS* overexpression downregulated PC protein level and activity, while the protein level and activity of PC was increased with *ZFP36L2-AS* knockdown (Fig. 6H–K and Supplementary Fig. 7I, J). Cycloheximide (CHX) is a bacterial toxin that can inhibit protein biosynthesis. Treated with CHX decreased the expression of PC protein (Fig. 6L). However, *ZFP36L2-AS* knockdown relieved the decline of PC protein expression induced by CHX (Fig. 6L), suggesting that *ZFP36L2-AS* might promote the PC protein degradation. To further clarify the possible mechanism, the proteasome inhibitor MG-132 was used. MG-132 upregulated the protein levels of PC (Fig. 6M), suggesting that the inhibition of ubiquitin-proteasome pathway might ameliorate the degradation of PC. More importantly, MG-132 rescued the reduction of PC protein levels in *ZFP36L2-AS*-overexpressing myoblast (Fig. 6M). Overall, given that *ZFP36L2-AS* could modulate the ubiquitination level of total protein (Fig. 5K and Supplementary Fig. 5K), we infer *ZFP36L2-AS* induces the ubiquitination of PC to facilitate PC degradation, thereby inhibiting PC activity.

Acetyl-CoA is an allosteric activator of PC [38], has been found that can be catalyzed by ACACA to produce malonyl-CoA for fatty acid synthesis [39, 40], hinting that ACACA may affect the activity of PC by regulating acetyl-CoA. To verify this conjecture, ACACA was knockdown by specific siRNA (Supplementary Fig. 9A, B). As expected, ACACA knockdown increased acetyl-CoA content and enhanced the activity of PC (Fig. 6N, O). Similarly, *ZFP36L2-AS* knockdown augmented acetyl-CoA content, whereas the content of acetyl-CoA was reduced with overexpression of *ZFP36L2-AS* (Fig. 6P and Supplementary Fig. 7K). To further explore whether *ZFP36L2-AS* can reinforce the regulation of PC activity via ACACA, *ZFP36L2-AS* overexpression construct was co-transfected with ACACA specific siRNA. Partly, knockdown of ACACA abolished the downregulation of acetyl-CoA content and PC activity by *ZFP36L2-AS* overexpression (Fig. 6Q, R), demonstrated that *ZFP36L2-AS* can further enhance the inhibition of PC activity by activating ACACA.

Tissue expression profiles showed ACACA and PC highly expressed in breast and leg muscle (Supplementary Fig. 10A, D), implying that they may play an important role in skeletal muscle development. We further analyzed the expression of ACACA and PC during myoblast proliferation and differentiation. ACACA was slightly upregulated during myogenic differentiation, whereas the expression of PC was visibly decreased (Supplementary Fig. 10B, E). Moreover, subcellular location annotation showed that ACACA protein exists in nucleus and cytosol, while PC is localized in mitochondria (Supplementary Fig. 10C, F). To explore the potential biological functions of ACACA and PC in myogenesis, we performed a series of myoblast proliferation and differentiation assays. ACACA knockdown had similar results with PC overexpression, which promoted myoblast proliferation and inhibited myoblast differentiation (Supplementary Figs. 9C–L and 11A–L). In contrast, PC interference suppressed myoblast proliferation but facilitated myogenic differentiation (Supplementary Fig. 11M–X). Meanwhile, overexpression of PC promoted cellular mitochondrial respiration, whereas glycolytic capacity was increased with PC knockdown (Supplementary Fig. 12A–H).

Considering the expression and functional relationship between *ZFP36L2-AS* and ACACA and PC, we further determined the role of ACACA and PC on *ZFP36L2-AS*-mediated skeletal muscle development. Knockdown of ACACA improved fatty acid β -oxidation rate and upregulated the expression of *CPT1*, but downregulated key genes involved in fatty acid synthesis, which counteracts the inhibitory effect of *ZFP36L2-AS* on FAO (Fig. 7A, B). In addition, overexpression of PC rescued the suppression of cellular mitochondrial respiration induced by *ZFP36L2-AS* overexpression (Fig. 7C–F), as well as attenuates the activation of fast-twitch phenotype and muscle atrophy (Fig. 7G–J). Altogether, these results indicated that ACACA and PC are indispensable to the function of *ZFP36L2-AS*.

DISCUSSION

Myogenesis is a highly ordered process including myoblast proliferation and differentiation, myotube formation and maturity, and is controlled by a series of myogenic regulatory factors [30, 41–43]. After birth, the number of myofibers in animals is basically fixed, and their skeletal muscle development is mainly regulated by the composition and size of myofibers. Recently, it is becoming increasingly clear that a complex network of epigenetic regulators and lncRNAs plays an essential role in skeletal muscle development [17–20, 44]. In our previous RNA-seq data, we identified lncRNA *ZFP36L2-AS* was highly expressed in fast growth rate broilers. Here, we found *ZFP36L2-AS* was upregulated during myogenic differentiation and highly expressed in breast and leg muscle, indicating its potential role in muscle development. Gain- and loss-of-function analysis revealed that *ZFP36L2-AS* inhibited myoblast proliferation but promoted myoblast differentiation in vitro. In vivo, *ZFP36L2-AS* activated fast-twitch muscle phenotype and induced muscle atrophy.

Skeletal muscle is a structurally and metabolically plastic tissue that maintains systemic energy homeostasis in response to various metabolic stresses [26]. Metabolic inflexibility in muscles is a dominant cause of various metabolic disorders [5]. Notably, recent evidences have revealed that the maintenance of skeletal muscle mass is closely related to muscle metabolism [8]. In this study, we found that *ZFP36L2-AS* repressed cellular mitochondrial respiration and fatty acid oxidation in skeletal muscle, resulting in excessive deposition of intramuscular fat. In the meantime, *ZFP36L2-AS* elevated glycolytic capacity and decrease oxidative capacity of skeletal muscle, which inactivated mTOR signaling, leading to the activation of UPS and autophagy-lysosomal system and induced muscle atrophy. Given that *ZFP36L2-AS* facilitated intramuscular fat deposition and induced muscle atrophy, *ZFP36L2-AS* could be a novel therapeutic target for obesity and sarcopenia.

Post-transcriptional regulation is an important form for lncRNA to regulate gene expression and function. Notably, increasing studies revealed that lncRNAs can be widely involved in a variety of biological processes through interacting with RBPs [44–47]. ACACA is a key enzyme in the process of fatty acid biosynthesis and oxidation, whose Ser79 site phosphorylation would inhibit the enzymatic activity of ACACA to promote FAO [48, 49]. In this study, we found *ZFP36L2-AS* can interact with ACACA through its 816–1785 region, thus inducing ACACA dephosphorylation and facilitating intramuscular fat deposition. In addition, PC (an enzyme that converts pyruvate to oxaloacetate), who has been reported to function as a RBP [45], was also discovered to bind with *ZFP36L2-AS*. *ZFP36L2-AS* damaged PC protein stability and inhibited PC activity, which may be attributed to the induction of ubiquitination by *ZFP36L2-AS*. Interestingly, we found ACACA can reduce the activity of PC by consuming acetyl-CoA, demonstrating that the inhibitory effect of *ZFP36L2* on PC activity is partially ACACA-dependent.

Skeletal muscle is mainly composed of myofibers, which develop from myoblasts through a highly ordered biological process. In addition to myoblasts, skeletal muscle includes many muscle-resident cells such as blood cells, fibroblasts, preadipocytes, and satellite cells. Compared to other muscle-resident cells, we found that *ZFP36L2-AS* expression is more pronounced in myoblasts, blood cells and satellite cells. Since blood cells are mainly involved in oxygen transport and immune function of the body and *ZFP36L2-AS* regulates skeletal muscle development by mediating muscle metabolism, the function of *ZFP36L2-AS* in blood cells was not investigated in depth. On the other hand, inhibition and overexpression of *ZFP36L2-AS* did not change cellular ATP content in satellite cells, suggesting the expression of *ZFP36L2-AS* in satellite cells is not related to its role in muscle metabolism. Overall, the function of *ZFP36L2-AS* in muscle metabolism mainly depends on its expression in myoblasts, which contributes to its regulation of myogenesis and skeletal muscle development.

In summary, we identified lncRNA *ZFP36L2-AS* can interact with ACACA and PC to facilitate intramuscular fat deposition, as well as activate fast-twitch muscle phenotype and induce muscle atrophy (Supplementary Fig. 13). Our findings present a novel model about the regulation of lncRNA on muscle metabolism, and will contribute to the development of further research.

MATERIALS AND METHODS

Cell culture and transfection

Chicken primary myoblasts (CPMs) were isolated from the leg muscle of 11-day old chicken embryos and cultured as previously described [50]. To induce myogenic differentiation, growth medium was removed and replaced with differentiation medium (RPMI-1640 medium [Gibco, MD, USA] containing 2% horse serum after myoblasts achieving 90% cell confluence.

Fresh blood was collected from 14-day old chicken. After centrifugation at 1,500 × g, plasma was removed and blood cells were collected.

Chicken primary fibroblasts were isolated from the leg muscle of 10-day old chicken embryos. Fibroblasts were trypsinized and then collected by centrifugation as previously described [51]. Fibroblasts were cultured in Dulbecco's modified Eagle's medium (DMEM, Gibco, USA) supplemented with 10% (v/v) fetal bovine serum (FBS, Hyclone, USA) and 0.2% penicillin/streptomycin (Invitrogen, USA).

Chicken preadipocytes were isolated from 14-day old chicken as previously described [52], and cultured with DMEM/Ham's nutrient mixture F-12 (DMEM/F12) basic medium with 10% (v/v) FBS (Hyclone, USA) and 0.2% penicillin/streptomycin (Invitrogen, USA).

Chicken satellite cells were isolated from leg muscle of 15-day old chicken embryos and cultured as previously described [53].

All cells were cultured at 37 °C in a 5% CO₂ humidified atmosphere. And all transient transfections were performed using Lipofectamine 3000 Reagent (Invitrogen, USA) according to the manufacturer's instructions.

RNA extraction, cDNA synthesis and quantitative real-time PCR (qRT-PCR)

Total RNA was extracted using Trizol reagent (TaKaRa, Otsu, Japan) following the manufacturer's protocol. Nuclear and cytoplasmic RNA fractionation was performed by using the PARIS Kit (Ambion, Life Technologies, USA) as recommended by the supplier. cDNA synthesis for mRNA was carried out using the PrimeScript RT Reagent Kit with gDNA Eraser (Perfect Real Time) (TaKaRa, Otsu, Japan). Real-time qPCR assay was performed as described before [54]. And primers used for RT-PCR and qRT-PCR are listed in Supplementary Table 4.

5' and 3' rapid-amplification of cDNA ends (RACE)

5' and 3' RACE of *ZFP36L2-AS* was performed using SMARTer RACE cDNA Amplification Kit (Clontech, Osaka, Japan) according to the manufacturer's instructions. The gene-specific primers used for RACE were presented in Supplementary Table 4.

Plasmids construction and RNA oligonucleotides

For Flag fusion protein construction, thirteen ORFs of *ZFP36L2-AS* were amplified and subcloned into *HindIII* and *XhoI* restriction sites in the pcDNA3.1-3xFlag-C vector.

For overexpression vectors construction, the full-length sequence and 816–1785 nt of *ZFP36L2-AS* and *PC* coding sequence (NCBI Reference Sequence: NM_204346.1) were amplified and cloned into the pcDNA3.1 vector (Promega, Madison, WI, USA) by using the *NheI* and *HindIII* restriction sites.

For viral vectors constructed, the full-length sequence of *ZFP36L2-AS* was amplified, and then cloned into the adenoviral vector (pDC316-mCMV-ZsGreen; Addgene, Cambridge, MA, USA) between *NheI* and *HindIII* sites. Short hairpin RNA (shRNA) against *ZFP36L2-AS* was designed by Shanghai Hanbio Biotechnology Co., Ltd, and then subcloned into the pLVX-shRNA2-Puro vector (Addgene, Cambridge, MA, USA) by using the *BamHI* and *EcoRI* restriction sites.

The small interfering RNAs (siRNA) and antisense oligonucleotide (ASO) that were used for the specific knockdown of *ZFP36L2-AS* were designed and synthesized by Guangzhou RiboBio (Guangzhou, China). The siRNA against ACACA (NCBI Reference Sequence: NM_205505.1) and *PC* were also designed and synthesized.

The primers and oligonucleotide sequences used in this study are shown in Supplementary Tables 4 and 5.

Flow cytometry, 5-Ethynyl-2'-deoxyuridine (EdU) and cell counting kit-8 (CCK-8) assays

The experiments were performed as previously described [54]. In brief, the Cell Cycle Analysis Kit (Thermo Fisher Scientific, USA), C10310 EdU Apollo In Vitro Imaging Kit (RiboBio, China) and TransDetect Cell Counting Kit (TransGen, Beijing, China) were used for flow cytometry, EdU, and CCK-8 assay, as the manufacturer's protocol.

Immunoblotting and immunofluorescence (IF)

Western blots were performed as previously described [50]. The primary antibodies used were anti-FLAG (AF519, 1:1,000, Beyotime), anti-ACACA (PA5-17564, 1:1000, Thermo Fisher Scientific), anti-p-ACACA Ser⁸⁰ (orb315750, 1:500, Biorbyt), anti-PC (GTX132002, 1:500, GeneTex), anti-MYOD (ABP53067, 1:500, Abbkine), anti-MyHC (B103, 0.5 µg/ml, DHSB), anti-CPT1 (bs-23779R, 1:500, Bioss), anti-FASN (10624-2-AP, 1:200, Proteintech), anti-p-mTOR Ser²⁴⁸⁸ (#5536, 1:1000, CST), anti-mTOR (bs-1992R, 1:500; Bioss), Ubiquitin (#39361:1000, CST) anti-ULK1 (bs-3602R, 1:500; Bioss), anti-LC3B (NB100-2220, 2.0 µg/ml, Novus), anti-P62 (18420-1-AP, 1:1000, Proteintech) and anti-β-Tubulin (A01030, 1:10000, Abbkine). ProteinFind Goat Anti-Mouse IgG(H+L), HRP Conjugate (HS201-01, 1:1,000, TransGen) and ProteinFind Goat Anti-Rabbit IgG(H+L), HRP Conjugate (HS101-01, 1:500, TransGen) were used as a secondary antibody.

Immunofluorescence was performed using anti-MyHC (B103, 2.5 µg/ml, DHSB), as previously described [50]. A fluorescence microscope (DMI8; Leica, German) was used to capture three randomly selected fields to visualize the area labeled with anti-MyHC.

Mitochondrial respiration assay

The oxygen consumption rate (OCR) and extracellular acidification rate (ECAR) of transfected myoblasts were measured using Seahorse XF Cell Mito Stress Test Kit and Seahorse XF Glycolysis Stress Test Kit (Agilent

technologies, CA, USA) by a Seahorse XF96 Extracellular Flux Analyzer (Agilent technologies, CA, USA) following the manufacturer's protocol, respectively.

Adenovirus/Lentivirus production and transduction

To generate adenovirus, the recombinant adenoviral expression plasmid was co-transfected with pHBAΔ-BHGlox ΔE1,3Cre plasmid using Lipofectamine 3000 reagent. After amplification, acquired adenovirus were purified with a ViraBind™ Adenovirus Purification Kit (Cell Biolabs, USA). Lentivirus production was performed as previously described [54]. Viral titers were evaluated by a gradient dilution.

1-day-old female chicks were randomly divided into two groups (Adv-ZFP36L2-AS and Adv-NC, or Lv-shZFP36L2-AS and Lv-shNC; $n=30$), respectively. Chicks received two intramuscular doses of adenovirus (10^8 titers)/lentivirus (10^6 titers) in two different sites of the gastrocnemius. Thirteen days after the initial injection, chick gastrocnemius samples were collected from the above two groups.

Mitochondrial DNA (mtDNA) content and fatty acid oxidation (FAO) rate assay

Total DNA was extracted using the Tissue DNA Kit (D3396, Omega, GA, USA) according to the manufacturer's instructions. The amount of mitochondrial DNA was determined by quantification of cytochrome c oxidase subunit II (*COX2*). The nuclear-encoded β -globin gene was used as internal controls. Primers used in this study can be found in the Supplementary Table 4.

The mitochondria of myoblast and gastrocnemius was isolated using the Cell/Tissue Mitochondria Isolation Kit (C3601/C3606, Beyotime, China). After measuring the mitochondrial protein concentration, freshly isolated mitochondria were subjected to FAO rate assay with the Colorimetric Fatty Acid Oxidation Rate Assay Kit (HL50679, Haling, Shanghai, China), according to the manufacturer's protocol.

Central carbon metabolic profiling

ZFP36L2-AS knockdown gastrocnemius samples ($n=6$) were used for metabolites extraction, and then performed on HPLC-MS/MS analysis. The high-performance ion exchange liquid chromatography (HPLC) separation was carried out using an Thermo Scientific Dionex ICS-6000 HPLC System (Thermo Fisher Scientific, IL, USA). An AB SCIEX 6500 QTRAP + triple quadrupole mass spectrometer (AB Sciex, USA), equipped with an electrospray ionization (ESI) interface, was applied for assay development.

Metabolic hierarchical clustering analysis (HCA) was performed using Cluster3.0 software as previously described [24].

Hematoxylin and eosin (H&E) staining and immunohistochemistry (IHC)

H&E staining was performed using the Hematoxylin and Eosin Staining Kit (Beyotime, Shanghai, China) following the manufacturer's protocol. Immunohistochemistry was carried out using SP-POD Kit (SP0041, Solarbio, China) with primary antibodies included anti-MYH1 (F59, 1:100, DHSB) and anti-MYH7 (S58, 1:300, DHSB).

Metabolite and enzyme activities assays

Content of adenosine triphosphate (ATP), triglyceride (TG), free fatty acid (FFA), glycogen, and acetyl-CoA as well as enzyme activity of lactic dehydrogenase (LDH), succinate dehydrogenase (SDH), acetyl-CoA carboxylase (ACC) and pyruvate carboxylase (PC) in skeletal muscle were measured using commercially available kits (BC0305, BC0625, BC0595, BC0345, BC0980, BC0685, BC0955, BC0410 and BC0730, Solarbio, China) according to the manufacturer's instructions.

RNA pull-down assay

Ribo™ RNAmix-T7 biotin-labeled transcription kit (RiboBio, Guangzhou, China) was used to harvest biotinylated RNAs. RNA pull-down assays were performed with Pierce Magnetic RNA-Protein Pull-Down Kit (Thermo Fisher Scientific, IL, USA), according to the manufacturer's instructions. The eluted products were identified by mass spectrometry with a Q Exactive mass spectrometer (Thermo fisher) or western blot. Differentially expressed genes (DEGs) were subjected to enrichment analysis of Gene Ontology (GO) functions and Kyoto Encyclopedia of Genes and Genomes (KEGG) pathways.

RNA immunoprecipitation (RIP) assay

RIP assays were performed using the Magna RIP™ RNA-Binding Protein Immunoprecipitation Kit (Millipore, CA, USA) following the manufacturer's protocol. The antibodies used for RIP assays were anti-ACACA (PA5-17564, 1:50, Thermo Fisher Scientific) and anti-PC (GTX132002, 1:100, GeneTex).

Statistical analysis

In this study, all experiments were repeated at least three times, and results were represented as mean \pm SEM. Where applicable, the statistical significance of the data was tested using independent sample *t*-test or ANOVA followed by Dunnett's test. The types of tests and the *P* values, when applicable, are indicated in the figure legends.

DATA AVAILABILITY

All data generated or analysed during this study are included in this published article (and its supplementary information files). Additional data related to this paper may be available from the corresponding author on reasonable request.

REFERENCES

- Zurlo F, Larson K, Bogardus C, Ravussin E. Skeletal muscle metabolism is a major determinant of resting energy expenditure. *J Clin Invest*. 1990;86:1423–7.
- Rai M, Demontis F. Systemic nutrient and stress signaling via myokines and myometabolites. *Annu Rev Physiol*. 2016;78:85–107.
- Ibrahim A, Neinast M, Arany ZP. Myoblasts: muscle-derived metabolites with paracrine and systemic effects. *Curr Opin Pharm*. 2017;34:15–20.
- Goodpaster BH, Sparks LM. Metabolic flexibility in health and disease. *Cell Metab*. 2017;25:1027–36.
- Galgani JE, Moro C, Ravussin E. Metabolic flexibility and insulin resistance. *Am J Physiol Endocrinol Metab*. 2008;295:E1009–E1017.
- Stephen WC, Janssen I. Sarcopenic-obesity and cardiovascular disease risk in the elderly. *J Nutr Health Aging*. 2009;13:460–6.
- Buch A, Carmeli E, Boker LK, Marcus Y, Shefer G, Kis O, et al. Muscle function and fat content in relation to sarcopenia, obesity and frailty of old age-An overview. *Exp Gerontol*. 2016;76:25–32.
- Ferraro E, Pin F, Gorini S, Pontecorvo L, Ferri A, Mollace V, et al. Improvement of skeletal muscle performance in ageing by the metabolic modulator Trimetazidine. *J Cachexia Sarcopenia Muscle*. 2016;7:449–57.
- Sartorelli V, Fulco M. Molecular and cellular determinants of skeletal muscle atrophy and hypertrophy. *Sci Stke*. 2004;2004:re11.
- Jagoe RT, Goldberg AL. What do we really know about the ubiquitin-proteasome pathway in muscle atrophy? *Curr Opin Clin Nutr Metab Care*. 2001;4:183–90.
- Lee JT. Epigenetic regulation by long noncoding RNAs. *Science*. 2012;338:1435–9.
- Cabili MN, Trapnell C, Goff L, Koziol M, Tazon-Vega B, Regev A, et al. Integrative annotation of human large intergenic noncoding RNAs reveals global properties and specific subclasses. *Genes Dev*. 2011;25:1915–27.
- Wilusz JE, Freier SM, Spector DL. 3' end processing of a long nuclear-retained noncoding RNA yields a tRNA-like cytoplasmic RNA. *Cell*. 2008;135:919–32.
- Tsai MC, Manor O, Wan Y, Mosammaparast N, Wang JK, Lan F, et al. Long non-coding RNA as modular scaffold of histone modification complexes. *Science*. 2010;329:689–93.
- Wang KC, Yang YW, Liu B, Sanyal A, Corces-Zimmerman R, Chen Y, et al. A long noncoding RNA maintains active chromatin to coordinate homeotic gene expression. *Nature*. 2011;472:120–4.
- Lee JT, Bartolomei MS. X-inactivation, imprinting, and long noncoding RNAs in health and disease. *Cell*. 2013;152:1308–23.
- Wang S, Jin J, Xu Z, Zuo B. Functions and regulatory mechanisms of lncRNAs in skeletal myogenesis, muscle disease and meat production. *Cells*. 2019;8:1107.
- Luo H, Lv W, Tong Q, Jin J, Xu Z, Zuo B. Functional non-coding RNA during embryonic myogenesis and postnatal muscle development and disease. *Front Cell Dev Biol*. 2021;9:628339.
- Cai B, Ma M, Zhang J, Wang Z, Kong S, Zhou Z, et al. LncEDCH1 improves mitochondrial function to reduce muscle atrophy by interacting with SERCA2. *Mol Ther Nucleic Acids*. 2022;27:319–34.
- Ma M, Cai B, Jiang L, Abdalla BA, Li Z, Nie Q, et al. lncRNA-Six1 is a target of miR-1611 that functions as a ceRNA to regulate Six1 protein expression and fiber type switching in chicken myogenesis. *Cells*. 2018;7:243.
- Ouyang H, He X, Li G, Xu H, Jia X, Nie Q, et al. Deep sequencing analysis of miRNA expression in breast muscle of fast-growing and slow-growing broilers. *Int J Mol Sci*. 2015;16:16242–62.
- Li Z, Cai B, Abdalla BA, Zhu X, Zheng M, Han P, et al. LncIRS1 controls muscle atrophy via sponging miR-15 family to activate IGF1-PI3K/AKT pathway. *J Cachexia Sarcopenia Muscle*. 2019;10:391–410.

23. Lu Z, He X, Ma B, Zhang L, Li J, Jiang Y, et al. Chronic heat stress impairs the quality of breast-muscle meat in broilers by affecting redox status and energy-substance metabolism. *J Agric Food Chem*. 2017;65:11251–8.
24. Ding L, Yang X, Tian H, Liang J, Zhang F, Wang G, et al. Seipin regulates lipid homeostasis by ensuring calcium-dependent mitochondrial metabolism. *EMBO J*. 2018;37:e97572.
25. Li Q, Wang Y, Wu S, Zhou Z, Ding X, Shi R, et al. CircACC1 regulates assembly and activation of AMPK complex under metabolic stress. *Cell Metab*. 2019;30:157–73.
26. Yang X, Brobst D, Chan WS, Tse M, Herlea-Pana O, Ahuja P, et al. Muscle-generated BDNF is a sexually dimorphic myokine that controls metabolic flexibility. *Sci Signal*. 2019;12:eaau1468.
27. Bassel-Duby R, Olson EN. Signaling pathways in skeletal muscle remodeling. *Annu Rev Biochem*. 2006;75:19–37.
28. Schiaffino S, Reggiani C. Fiber types in mammalian skeletal muscles. *Physiol Rev*. 2011;91:1447–531.
29. Koutakis P, Weiss DJ, Miserlis D, Shostrom VK, Papoutsis E, Ha DM, et al. Oxidative damage in the gastrocnemius of patients with peripheral artery disease is myofiber type selective. *Redox Biol*. 2014;2:921–8.
30. Braun T, Gautel M. Transcriptional mechanisms regulating skeletal muscle differentiation, growth and homeostasis. *Nat Rev Mol Cell Biol*. 2011;12:349–61.
31. Zhao J, Brault JJ, Schild A, Cao P, Sandri M, Schiaffino S, et al. FoxO3 coordinately activates protein degradation by the autophagic/lysosomal and proteasomal pathways in atrophying muscle cells. *Cell Metab*. 2007;6:472–83.
32. Saxton RA, Sabatini DM. mTOR signaling in growth, metabolism, and disease. *Cell*. 2017;168:960–76.
33. Wang KC, Chang HY. Molecular mechanisms of long noncoding RNAs. *Mol Cell*. 2011;43:904–14.
34. Cheng T, Sudderth J, Yang C, Mullen AR, Jin ES, Mates JM, et al. Pyruvate carboxylase is required for glutamine-independent growth of tumor cells. *Proc Natl Acad Sci USA*. 2011;108:8674–9.
35. Fullerton MD, Galic S, Marcinko K, Sikkema S, Pulinilkunnil T, Chen ZP, et al. Single phosphorylation sites in Acc1 and Acc2 regulate lipid homeostasis and the insulin-sensitizing effects of metformin. *Nat Med*. 2013;19:1649–54.
36. Lin Z, Zhang B, Liu X, Jin R, Zhu W. Effects of chicory inulin on serum metabolites of uric acid, lipids, glucose, and abdominal fat deposition in quails induced by purine-rich diets. *J Med Food*. 2014;17:1214–21.
37. Cappel DA, Deja S, Duarte J, Kucejova B, Inigo M, Fletcher JA, et al. Pyruvate-carboxylase-mediated anaplerosis promotes antioxidant capacity by sustaining TCA cycle and redox metabolism in liver. *Cell Metab*. 2019;29:1291–305.
38. Adina-Zada A, Zeczycki TN, Attwood PV. Regulation of the structure and activity of pyruvate carboxylase by acetyl CoA. *Arch Biochem Biophys*. 2012;519:118–30.
39. Abu-Elheiga L, Jayakumar A, Baldini A, Chirala SS, Wakil SJ. Human acetyl-CoA carboxylase: characterization, molecular cloning, and evidence for two isoforms. *Proc Natl Acad Sci USA*. 1995;92:4011–5.
40. Cronan JJ, Waldrop GL. Multi-subunit acetyl-CoA carboxylases. *Prog Lipid Res*. 2002;41:407–35.
41. Buckingham M. Myogenic progenitor cells and skeletal myogenesis in vertebrates. *Curr Opin Genet Dev*. 2006;16:525–32.
42. Buckingham M, Rigby PW. Gene regulatory networks and transcriptional mechanisms that control myogenesis. *Dev Cell*. 2014;28:225–38.
43. Saccone V, Puri PL. Epigenetic regulation of skeletal myogenesis. *Organogenesis*. 2010;6:48–53.
44. Jin JJ, Lv W, Xia P, Xu ZY, Zheng AD, Wang XJ, et al. Long noncoding RNA SYISL regulates myogenesis by interacting with polycomb repressive complex 2. *Proc Natl Acad Sci USA*. 2018;115:E9802–E9811.
45. Ma MZ, Zhang Y, Weng MZ, Wang SH, Hu Y, Hou ZY, et al. Long noncoding RNA GCASPC, a target of miR-17-3p, negatively regulates pyruvate carboxylase-dependent cell proliferation in gallbladder cancer. *Cancer Res*. 2016;76:5361–71.
46. Kim J, Piao HL, Kim BJ, Yao F, Han Z, Wang Y, et al. Long noncoding RNA MALAT1 suppresses breast cancer metastasis. *Nat Genet*. 2018;50:1705–15.
47. Wang Z, Yang B, Zhang M, Guo W, Wu Z, Wang Y, et al. lncRNA epigenetic landscape analysis identifies EPIC1 as an oncogenic lncRNA that interacts with MYC and promotes cell-cycle progression in cancer. *Cancer Cell*. 2018;33:706–20.
48. Ha J, Daniel S, Broyles SS, Kim KH. Critical phosphorylation sites for acetyl-CoA carboxylase activity. *J Biol Chem*. 1994;269:22162–8.
49. Castle JC, Hara Y, Raymond CK, Garrett-Engle P, Ohwaki K, Kan Z, et al. ACC2 is expressed at high levels in human white adipose and has an isoform with a novel N-terminus [corrected]. *PLoS One*. 2009;4:e4369.
50. Cai B, Ma M, Chen B, Li Z, Abdalla BA, Nie Q, et al. MiR-16-5p targets SESN1 to regulate the p53 signaling pathway, affecting myoblast proliferation and apoptosis, and is involved in myoblast differentiation. *Cell Death Dis*. 2018;9:367.
51. Schmid C, Steiner T, Froesch ER. Preferential enhancement of myoblast differentiation by insulin-like growth factors (IGF I and IGF II) in primary cultures of chicken embryonic cells. *FEBS Lett*. 1983;161:117–21.
52. Zhang T, Zhang X, Han K, Zhang G, Wang J, Xie K, et al. Analysis of long non-coding RNA and mRNA using RNA sequencing during the differentiation of intramuscular preadipocytes in chicken. *PLoS One*. 2017;12:e0172389.
53. Bai C, Hou L, Li F, He X, Zhang M, Guan W. Isolation and biological characteristics of Beijing Fatty chicken skeletal muscle satellite cells. *Cell Commun Adhes*. 2012;19:69–77.
54. Cai B, Li Z, Ma M, Zhang J, Kong S, Abdalla BA, et al. Long noncoding RNA SMUL suppresses SMURF2 production-mediated muscle atrophy via nonsense-mediated mRNA decay. *Mol Ther Nucleic Acids*. 2021;23:512–26.

AUTHOR CONTRIBUTIONS

QN and XZ conceived and designed the study. BC and MM performed the experiments, interpreted the data and wrote the paper. JZ, SK, and ZZ performed the experiments. ZL, BAA, HX, and RAL interpreted the data. All authors read and approved the final manuscript.

FUNDING

This work was supported by the Natural Scientific Foundation of China (U1901206, 31802051 and 31761143014), Local Innovative and Research Teams Project of Guangdong Province (2019BT02N630), National Key R&D Program of China (2021YFD1300100), China Agriculture Research System (CARS-41-G03), Guangdong Basic and Applied Basic Research Foundation (2021A1515111069), and the Science and Technology Program of Guangdong province, China (2020B1212060060).

COMPETING INTERESTS

The authors declare no competing interests.

ETHICS

All animal experimental protocols were conformed to “The Instructive Notions with Respect to Caring for Laboratory Animals” issued by the Ministry of Science and Technology of the People’s Republic of China, and approved by the Institutional Animal Care and Use Committee at the South China Agricultural University (approval ID: 2020-C010).

ADDITIONAL INFORMATION

Supplementary information The online version contains supplementary material available at <https://doi.org/10.1038/s41419-022-04772-2>.

Correspondence and requests for materials should be addressed to Qinghua Nie.

Reprints and permission information is available at <http://www.nature.com/reprints>

Publisher’s note Springer Nature remains neutral with regard to jurisdictional claims in published maps and institutional affiliations.



Open Access This article is licensed under a Creative Commons Attribution 4.0 International License, which permits use, sharing, adaptation, distribution and reproduction in any medium or format, as long as you give appropriate credit to the original author(s) and the source, provide a link to the Creative Commons license, and indicate if changes were made. The images or other third party material in this article are included in the article’s Creative Commons license, unless indicated otherwise in a credit line to the material. If material is not included in the article’s Creative Commons license and your intended use is not permitted by statutory regulation or exceeds the permitted use, you will need to obtain permission directly from the copyright holder. To view a copy of this license, visit <http://creativecommons.org/licenses/by/4.0/>.

© The Author(s) 2022

2.3. *LncEDCH1* improves mitochondrial function to reduce muscle atrophy by interacting with SERCA2

Molecular Therapy

Nucleic Acids

Original Article



LncEDCH1 improves mitochondrial function to reduce muscle atrophy by interacting with SERCA2

Bolin Cai,^{1,2,5} Manting Ma,^{1,2,5} Jing Zhang,^{1,2} Zhijun Wang,^{1,2} Shaofen Kong,^{1,2} Zhen Zhou,^{1,2} Ling Lian,³ Jiannan Zhang,⁴ Juan Li,⁴ Yajun Wang,⁴ Hongmei Li,^{1,2} Xiquan Zhang,^{1,2} and Qinghua Nie^{1,2}

¹Lingnan Guangdong Laboratory of Modern Agriculture & State Key Laboratory for Conservation and Utilization of Subtropical Agro-bioresources, College of Animal Science, South China Agricultural University, Guangzhou, Guangdong 510642, China; ²Guangdong Provincial Key Lab of Agro-Animal Genomics and Molecular Breeding, Key Laboratory of Chicken Genetics, Breeding and Reproduction, Ministry of Agriculture, Guangzhou, Guangdong 510642, China; ³National Engineering Laboratory for Animal Breeding and MOA Key Laboratory of Animal Genetics and Breeding, College of Animal Science and Technology, China Agricultural University, Beijing 100193, China; ⁴Key Laboratory of Bio-Resources and Eco-Environment of Ministry of Education, College of Life Sciences, Sichuan University, Chengdu 610065, China

Skeletal muscle is a regulator of the body's energy expenditure and metabolism. Abnormal regulation of skeletal muscle-specific genes leads to various muscle diseases. Long non-coding RNAs (lncRNAs) have been demonstrated to play important roles in muscle growth and muscle atrophy. To explore the potential function of muscle-associated lncRNA, we analyzed our previous RNA-sequencing data and selected the lncRNA (*LncEDCH1*) as the research object. In this study, we report that *LncEDCH1* is specifically enriched in skeletal muscle, and its transcriptional activity is positively regulated by transcription factor SP1. *LncEDCH1* regulates myoblast proliferation and differentiation *in vitro*. *In vivo*, *LncEDCH1* reduces intramuscular fat deposition, activates slow-twitch muscle phenotype, and inhibits muscle atrophy. Mechanistically, *LncEDCH1* binds to sarcoplasmic/ER calcium ATPase 2 (SERCA2) protein to enhance SERCA2 protein stability and increase SERCA2 activity. Meanwhile, *LncEDCH1* improves mitochondrial efficiency possibly through a SERCA2-mediated activation of the AMPK pathway. Our findings provide a strategy for using *LncEDCH1* as an effective regulator for the treatment of muscle atrophy and energy metabolism.

INTRODUCTION

Skeletal muscle is the largest component in the body representing ~40% of body mass, and is an important regulator of the body's energy expenditure and metabolism.^{1–3} Abnormal regulation of skeletal muscle-specific genes leads to various muscle diseases such as sarcopenia, myosarcoma, and muscle metabolic disorder.^{4,5}

Muscle hypertrophy and atrophy are two opposing phenomena that are mechanistically linked.⁶ Muscle atrophy refers to a decrease in muscle mass and fiber size and is characterized by enhanced protein degradation.⁷ By contrast, muscle hypertrophy refers to an increase in muscle mass associated with increased intracellular RNA and protein synthesis and decreased protein degradation, and has been reported to be regulated by many pathways, such as mammalian target of rapamycin (mTOR), insulin-like growth factor, and AMP-activated

protein kinase (AMPK) pathways.^{8–10} Intracellular calcium ions (Ca^{2+}) are important signaling molecules involved in muscle contraction, secretion, and cell proliferation or death.^{11–14} Minor changes in the Ca^{2+} handling apparatus might result in major pathophysiological consequences in the skeletal muscle. Indeed, abnormal expression patterns of ion-regulatory proteins have been repeatedly reported in muscle atrophy.^{15–18}

Sarcoplasmic/ER calcium ATPase 2 (SERCA2), located in the ER, is a membrane transport protein that maintains a low cytosolic calcium level to ensure the physiological processes.¹⁹ A decrease in SERCA2 activity causes ER stress, which induces muscular dystrophies via mitochondrial dysfunction and generation of reactive oxygen species (ROS).¹⁶ Mitochondria and ER are physically and functionally interconnected to maintain cytosolic calcium homeostasis. In mitochondria, the homeostasis of calcium promotes the production of ATP and enhances the tricarboxylic acid (TCA) cycle. Meanwhile, mitochondrial dysfunction, which is induced by ER stress, can be fed back and further amplify ER stress.^{20–22}

Protein-encoding genes only account for a small portion (2%) of the genome, and the remainder is primarily transcribed into non-coding RNAs (ncRNAs).²³ Long non-coding RNAs (lncRNAs) are a new class of regulatory RNAs with a length of more than 200 nt that have been found in the cytoplasm and nucleus.^{24,25} Recent studies have demonstrated that lncRNAs have regulated multiple biological processes and participate in skeletal muscle development and muscle disorders.^{26–31}

Received 5 May 2021; accepted 7 December 2021;
<https://doi.org/10.1016/j.omtn.2021.12.004>

⁵These authors contributed equally

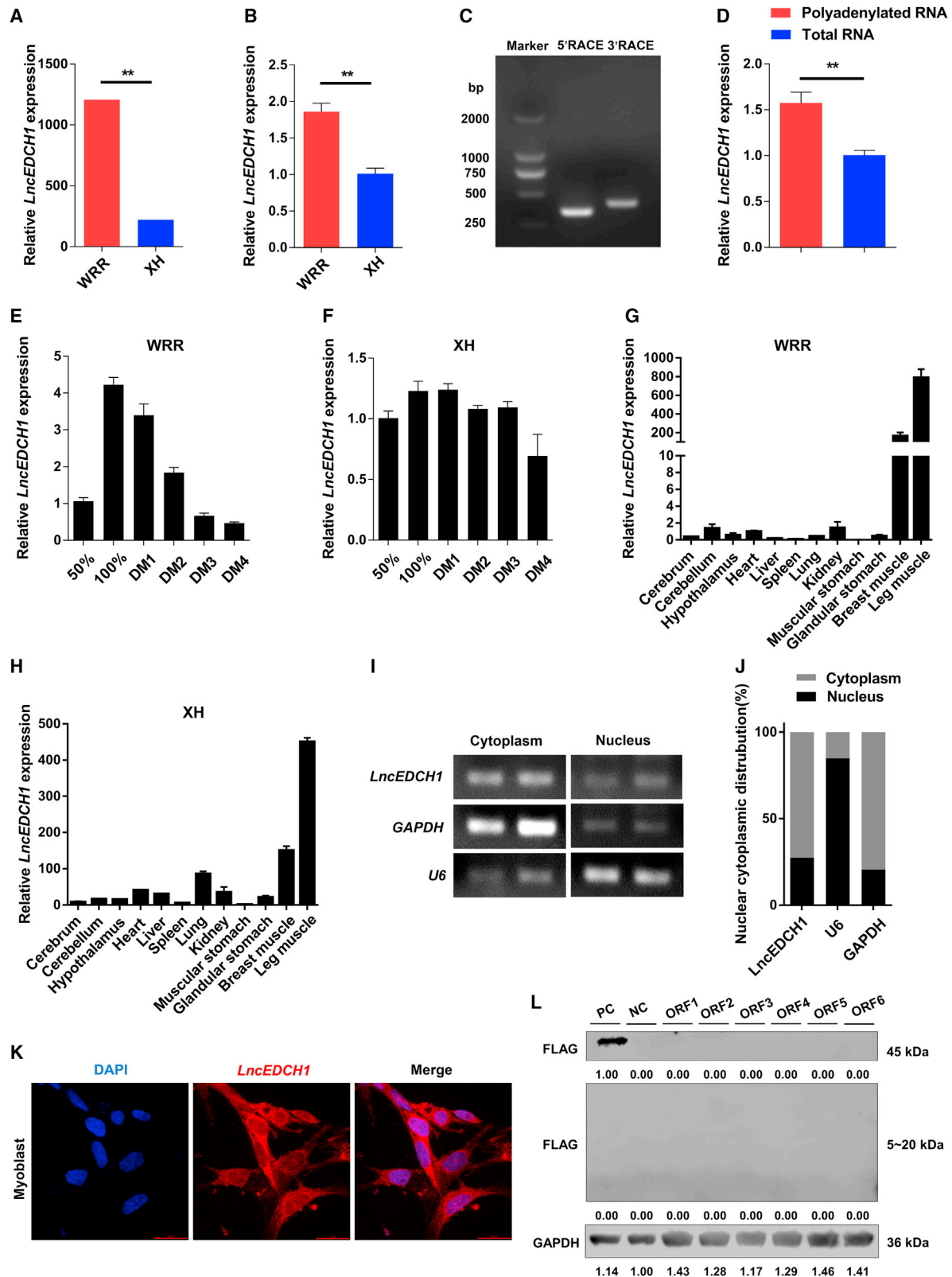
Correspondence: Hongmei Li, College of Animal Science, South China Agricultural University, Guangzhou 510642, Guangdong, China.

E-mail: hongmeili@scau.edu.cn

Correspondence: Qinghua Nie, College of Animal Science, South China Agricultural University, Guangzhou 510642, Guangdong, China.

E-mail: nqinghua@scau.edu.cn





In our previous RNA-sequencing (RNA-seq) analysis (accession number GEO: GSE58755), we screened out an lncRNA (TCONS_00059312, generated by epidermal differentiation protein containing cysteine histidine motifs 1 [*EDCH1*] gene, named *LncEDCH1*) differentially expressed in White recessive rock (a fast-growth-rate broiler chicken) and Xinghua chicken (a slow-growth-rate Chinese native breed).³² In this study, we found that *LncEDCH1* promotes the proliferation of myoblasts and inhibits myogenic differentiation, as well as reducing fat deposition, activating slow-twitch muscle phenotype, and alleviating muscle atrophy by activating the AMPK pathway and ameliorating mitochondrial efficiency. Further research found that *LncEDCH1* exerts its function by maintaining SERCA2 protein stability to increase SERCA2 activity. Our studies uncover a functional lncRNA whereby *LncEDCH1* may be a regulatory molecule for muscle disorders associated with calcium homeostasis.

RESULTS

LncEDCH1 is a muscle-associated lncRNA that is positively regulated by transcription factor SP1

To discover the potential function of muscle-associated lncRNA, we analyzed our previous RNA-seq data and found an lncRNA (*LncEDCH1*) highly expressed in hypertrophic broilers (Figures 1A and 1B).³² Rapid amplification of cDNA ends (RACE) was performed to identify the 5' and 3' ends of *LncEDCH1* (Figure 1C). The Basic Local Alignment Search Tool (BLAST) of the National Center for Biotechnology Information (NCBI) showed that *LncEDCH1* was 590 nt long, located at chromosome 25 from position 3,294,274 to 3,294,232, and 3,293,823 to 3,293,488, relatively conserved in *Meleagris gallopavo* and *Numida meleagris* (Table S1 and Figure S1). *LncEDCH1* was highly expressed in polyadenylated RNA, demonstrating that *LncEDCH1* is a polyadenylated lncRNA (Figure 1D). Moreover, *LncEDCH1* gradually decreased with the myogenic differentiation, and was enriched in breast and leg muscles (Figures 1E–1H). Cell-fractionation assays demonstrated that *LncEDCH1* is mainly present in the cytoplasm of chicken primary myoblasts (CPMs) (Figures 1I and 1J). A similar result was also confirmed by *in situ* RNA hybridization (Figure 1K). To further verify the coding potential of *LncEDCH1*, we cloned 3xFLAG epitope tag in-frame with the C terminus of six potential open reading frames (ORFs) of *LncEDCH1*. Subsequently, western blotting showed that *LncEDCH1* is a non-coding RNA without protein-encoding potential (Figure 1L).

To explore the mechanisms through which *LncEDCH1* is regulated at the transcriptional level, we conducted luciferase assays with four reporter constructs containing different fragments of the *LncEDCH1* promoter (located between –1,931 and +1 bp) (Figure S2A). The region between –1,931 and –1,591 bp had the highest transcriptional activity, which suggests that this region is the core promoter of *LncEDCH1* (Figure S1A). Furthermore, we predicted the transcription factors involved in regulating the transcriptional activity of *LncEDCH1* by bioinformatics analysis, and found that transcription factor SP1 specifically binds to the core promoter region (–1,923 to –1,912 bp) of *LncEDCH1* (Figure S2B). Compared with the mutated constructs, overexpression of *SP1* increased the luciferase activity of reporter constructs containing predicted SP1 binding sites (–1,931 to –1,591 bp) (Figure S2C). At the same time, *SP1* overexpression significantly increased the expression of endogenous *LncEDCH1* (Figure S2D). Collectively, these data revealed that *LncEDCH1* is positively regulated by the transcription factor SP1.

LncEDCH1 promotes proliferation and inhibits differentiation of myoblasts

Given that *LncEDCH1* was upregulated during myoblast proliferation (Figures 1E and 1F), we performed inhibition and overexpression experiments to assess its effect in proliferation and differentiation of myoblasts. *LncEDCH1* was successfully knocked down or overexpressed in CPMs (Figures 2A and S3A), as shown by the results of quantitative PCR (qPCR). Inhibition of *LncEDCH1* reduced cell-cycle-promoting genes such as *PCNA* while increasing the expression of cell-cycle-inhibiting genes (such as *CDKN1A* and *CDKN1B*) (Figure 2B). However, the opposite result was observed with *LncEDCH1* overexpression (Figure S3B). 5-Ethynyl-2'-deoxyuridine (EdU) and cell counting kit-8 (CCK-8) assays showed that interference of *LncEDCH1* decreases EdU incorporation and represses myoblast viability, whereas its overexpression promotes myoblast proliferation (Figures 2C–2E and S3C–S3E). Moreover, flow cytometric analysis revealed that *LncEDCH1* inhibition increases the number of cells that progressed to G₀/G₁ and reduces the number of S-phase cells. Conversely, *LncEDCH1* overexpression resulted in a fewer number of G₀/G₁ and greater number of S-phase cells (Figures 2F and S3F).

To further investigate the role played by *LncEDCH1* in myoblast differentiation, we performed immunofluorescence staining. *LncEDCH1* interference significantly facilitated myoblast differentiation and

Figure 1. Identification of *LncEDCH1*

(A and B) Relative *LncEDCH1* expression in breast muscles of 7-week-old Xinghua (XH) chicken and White recessive rock (WRR) detected by RNA-seq (A) (n = 1) and real-time qPCR (B) (n = 4). (C) Results of *LncEDCH1* 5' RACE and 3' RACE. (D) Relative *LncEDCH1* expression in polyadenylated RNA and total RNA (n = 4). (E and F) Relative *LncEDCH1* expression during the proliferation and differentiation of chicken primary myoblasts (CPMs) isolated from WRR (E) (n = 4) and XH chicken (F) (n = 4). (G and H) Tissue expression profiles of *LncEDCH1* in 7-week-old WRR (G) (n = 4) and XH chicken (H) (n = 4). The horizontal axis and vertical axis indicate different tissues and their relative expression values, respectively. (I and J) The distribution of *LncEDCH1* in the cytoplasm and nuclei of CPMs was determined by qPCR (I) (n = 2) and semi-quantitative PCR (J) (n = 4). *GAPDH* and *U6* served as cytoplasmic and nuclear localization controls, respectively. (K) RNA *in situ* hybridization of *LncEDCH1* in CPM. Special FISH probes against *LncEDCH1* were modified by Cy3 (red). The nucleus was stained by DAPI (blue). (L) Western blot analysis of the coding ability of *LncEDCH1* (n = 1). The potential ORFs of *LncEDCH1* were cloned into the pcDNA3.1-3xFLAG-C vector. CPMs transfected with β -actin-3xFLAG were used as a positive control (PC) and untransfected CPMs were used as a negative control (NC). In (L), the numbers shown below the bands are folds of band intensities relative to control. Band intensities were quantified by ImageJ and normalized to *GAPDH*. Data are expressed as a fold change relative to the control. Results are presented as mean \pm SEM. In (A), (B), and (D), the statistical significance of differences between means was assessed using an independent-sample t-test (**p < 0.01).

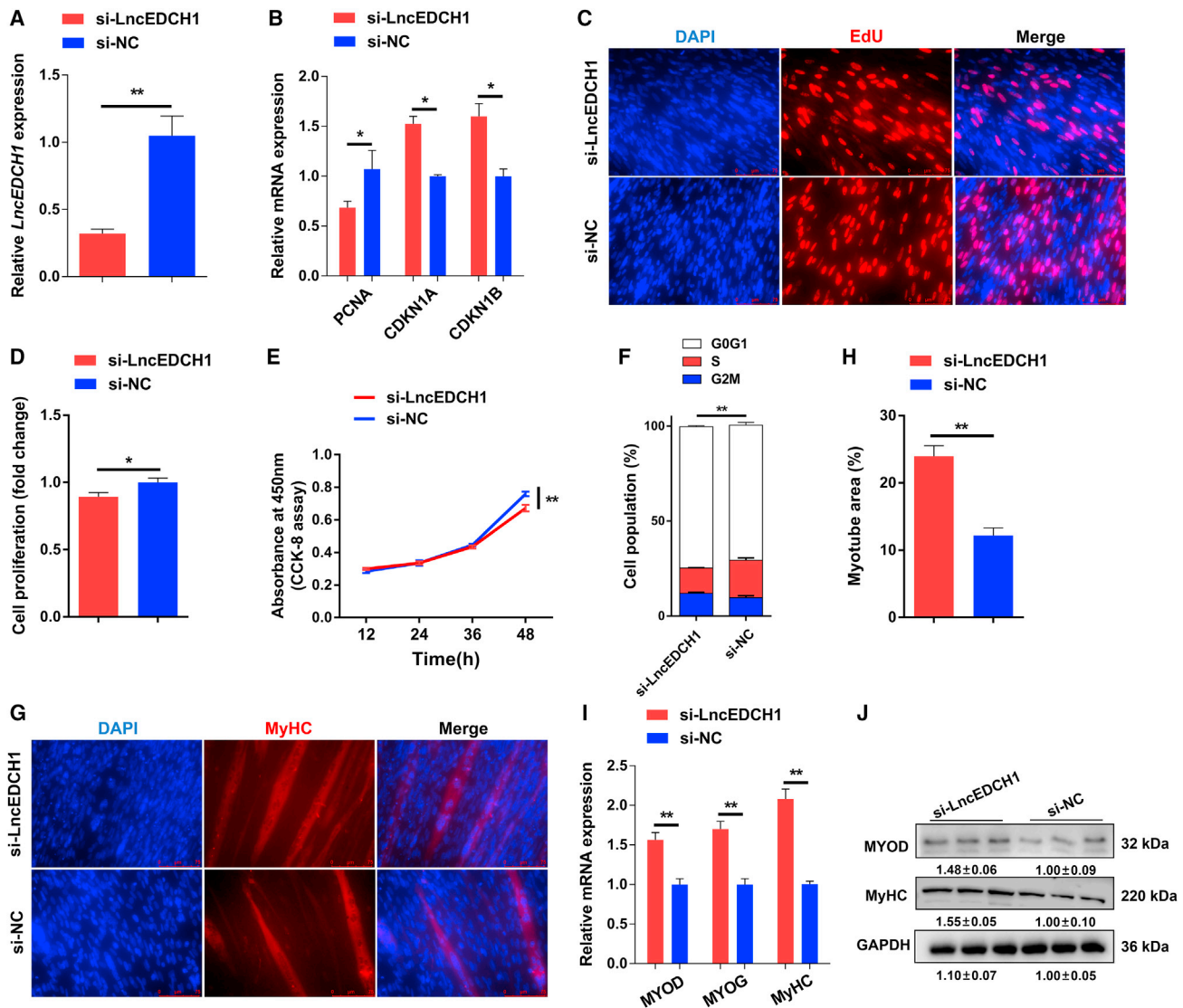


Figure 2. *LncEDCH1* interference suppresses myoblast proliferation but facilitates myogenic differentiation

(A) Relative *LncEDCH1* expression with *LncEDCH1* interference *in vitro* ($n = 6$). (B) Relative mRNA levels of several cell cycle genes with *LncEDCH1* interference ($n = 6$). (C) The proliferation of transfected CPMs was assessed by 5-ethynyl-2'-deoxyuridine (EdU) incorporation ($n = 3$). (D) Proliferation rate of myoblasts after the interference of *LncEDCH1* ($n = 3$). (E) CCK-8 assays were performed in CPMs with *LncEDCH1* interference ($n = 6$). (F) Cell cycle analysis of myoblasts after the interference of *LncEDCH1* ($n = 4$). (G and H) MyHC immunostaining (G) ($n = 3$) and myotube area (%) (H) ($n = 3$) of CPMs transfected with *LncEDCH1* interference. Cells were differentiated for 72 h after transfection. (I and J) Relative mRNA (I) ($n = 6$) and protein (J) ($n = 3$) expression levels of myoblast differentiation marker genes with *LncEDCH1* interference. In (J), the numbers shown below the bands are folds of band intensities relative to control. Band intensities were quantified by ImageJ and normalized to GAPDH. Data are expressed as a fold change relative to the control. Results are shown as mean \pm SEM. In (A), (B), (D–F), (H), and (I), the statistical significance of differences between means was assessed using an independent-sample t test (* $p < 0.05$; ** $p < 0.01$).

increased the total areas of myotubes (Figures 2G and 2H). Moreover, the results of qPCR and western blotting showed that expressions of myoblast differentiation marker genes (such as *MYOD*, *MYOG*, and *MyHC*) were upregulated with *LncEDCH1* inhibition (Figures 2I and 2J). In contrast, *LncEDCH1* overexpression repressed myoblast differentiation and downregulated the expression of myoblast differentiation marker genes (Figures S3G–S3J). Taken together, these data

indicated that *LncEDCH1* promotes myoblast proliferation and suppresses myoblast differentiation.

***LncEDCH1* accelerates fatty acid oxidation, reduces lipid deposition, and promotes TCA cycle in skeletal muscle**

To verify whether *LncEDCH1* is involved in the development of skeletal muscle *in vivo*, we injected the gastrocnemius muscle of 1-day-old

chicks with lentivirus-mediated *LncEDCH1* knockdown (Lv-sh*LncEDCH1*) or lentivirus-mediated *LncEDCH1* overexpression (Lv-*LncEDCH1*) (Figures 3A and S3A). *LncEDCH1* knockdown significantly reduced mitochondrial content, inhibited the fatty acid oxidation (FAO) rate, and facilitated the accumulation of free fatty acid (FFA) and triglyceride (TG), while its overexpression increased mitochondrial content and promoted FAO (Figures 3B–3D and S4B–S4D). Meanwhile, knockdown of *LncEDCH1* downregulated FAO-related genes such as *CPT1* and mitochondrial content regulators such as *PGC1 α* , as well as upregulating key genes involved in fatty acid synthesis (such as *FASN* and *ACC*) (Figures 3E and 3F). In contrast, overexpression of *LncEDCH1* showed opposite results (Figures S4E and S4F), indicating that *LncEDCH1* promotes FAO and inhibits lipid deposition.

Mitochondria are the central energy producers in cells due to their ability to generate numerous ATP from metabolizing fatty acids and the glycolytic product pyruvate through the TCA cycle.^{33,34} Given that knockdown of *LncEDCH1* reduced the content of mitochondria (Figure 3B), we further performed a central carbon metabolic profiling to study the regulation of *LncEDCH1* on skeletal muscle metabolism. The result of hierarchical clustering analysis (HCA) clearly separated controls and *LncEDCH1* knockdown (Figure 3G and Table S2). For example, compared with control, glycolytic metabolites such as glucose 6-phosphate and fructose 6-phosphate were significantly increased with *LncEDCH1* knockdown (Figure 3H and Table S2). In the meantime, metabolites of the TCA cycle, including citric acid and *cis*-aconitic acid, were significantly reduced (Figure 3H and Table S2). Altogether, our results indicated that *LncEDCH1* decreases the end products of glycolysis and elevates metabolites of the TCA cycle by promoting mitochondrial function, leading to reduction of lipid metabolites (Figure 3I).

***LncEDCH1* induces slow-twitch muscle phenotype and inhibits muscle atrophy**

The occurrence and transformation of myofiber types are regulated by a variety of factors, which are closely related to the mechanism of muscle metabolism.^{35–37} Recent studies have found that skeletal muscle can be remodeled by activating signaling pathways to reprogram gene expression and sustain muscle performance.³⁸ Compared with glycolytic myofibers (fast-twitch), the oxidative (slow-twitch) myofibers have more myoglobin and mitochondria, as well as higher activity of oxidative metabolic enzymes.^{39,40} Given that *LncEDCH1* mediated the flux of glycolysis and TCA cycle (Figure 3I), we speculate that *LncEDCH1* may function in the transformation of myofiber type by regulating muscle metabolism. *LncEDCH1* knockdown reduced the content of glycogen and ATP in gastrocnemius, whereas its overexpression promoted the accumulation of glycogen and ATP (Figures 4A, 4B, S5A, and S5B). Moreover, knockdown of *LncEDCH1* enhanced the activity of lactic dehydrogenase (LDH) and suppressed the activity of succinate dehydrogenase (SDH) (Figure 4C). On the contrary, *LncEDCH1* overexpression decreased glycolytic capacity and elevated oxidative capacity of skeletal muscle (Figure S5C). The expression levels of glycogenolytic and glycolytic genes (such as

HK1, *PGAM1*, *PYGL*, and *PGK1*) were further tested, whereby it was found that knockdown of *LncEDCH1* upregulated glycogenolytic and glycolytic genes (Figure 4D). Contrastingly, opposite results were shown with *LncEDCH1* overexpression (Figure S5D), suggesting that *LncEDCH1* impeded the glycolysis process and repressed skeletal muscle glycolysis. *LncEDCH1* knockdown led to the upregulation of fast-twitch myofiber genes (such as *SOX6*, *TNNC2*, and *TNNT3*) and inhibited the expression of slow-twitch myofiber genes such as *TNNC1* and *TNNT1* (Figure 4E). More importantly, the results of immunohistochemistry showed that *LncEDCH1* knockdown promoted the expression level of MYH1A/fast-twitch protein and suppressed the expression level of MYH7B/slow-twitch protein (Figures 4F and 4G). By contrast, overexpression of *LncEDCH1* improved the expression of slow-twitch myofiber genes and slow-twitch protein level, and drove the transformation of fast-twitch to slow-twitch myofibers (Figures S5E–S5G).

Numerous studies have found that glycolytic myofibers are more susceptible to atrophy compared with the oxidative myofibers.^{41,42} There was a significant decrease in muscle mass and mean cross-sectional area (CSA) with *LncEDCH1* knockdown in gastrocnemius, while the opposite result occurred upon *LncEDCH1* overexpression (Figures 4H–4J and S5H–S5J), suggesting that *LncEDCH1* is involved in muscle atrophy. Balanced autophagy flux in skeletal muscle is critical for the overall health of an organism. Maintaining basal autophagy flux is essential to clear damaged organelles or recycle macromolecules in muscles during metabolic stress.⁴³ mTOR is a master growth regulator that senses and integrates diverse nutritional and environmental cues and has been reported to modulate autophagy flux.^{44,45} To further explore the regulatory mechanism of *LncEDCH1* in reducing muscle atrophy, we tested the mTOR-mediated autophagy pathway. *LncEDCH1* knockdown upregulated the expression level of *SQSTM1*, whereas it suppressed autophagy-related genes such as *ULK1* and *MAP1LC3B* (Figure 4K). In the meantime, the phosphorylation level of mTOR was promoted and accompanied by a decrease in LC3BII content with *LncEDCH1* knockdown in gastrocnemius (Figure 4L). Conversely, *LncEDCH1* overexpression inhibited mTOR signaling and activated autophagy (Figures S5K and S5L), suggesting that *LncEDCH1* may alleviate muscle atrophy by increasing basal autophagy flux.

***LncEDCH1* interacts with SERCA2 protein to enhance SERCA2 activity**

To explore the molecular mechanism of *LncEDCH1* function in skeletal muscle development, we performed RNA pull-down coupled with mass spectrometry to identify its endogenous binding proteins. A total of 282 proteins were found to specifically bind to *LncEDCH1* (Table S3). Gene ontology (GO) and Kyoto Encyclopedia of Genes and Genomes (KEGG) enrichment analysis of these RNA-binding proteins revealed that they are mainly involved in metabolic pathways, calcium signaling pathways, and carbon metabolism (Figures S6A and S6B). Among these, SERCA2, which was previously reported to be involved in mitochondrial metabolism and muscle development in skeletal muscle,^{14,46–48} was identified specifically

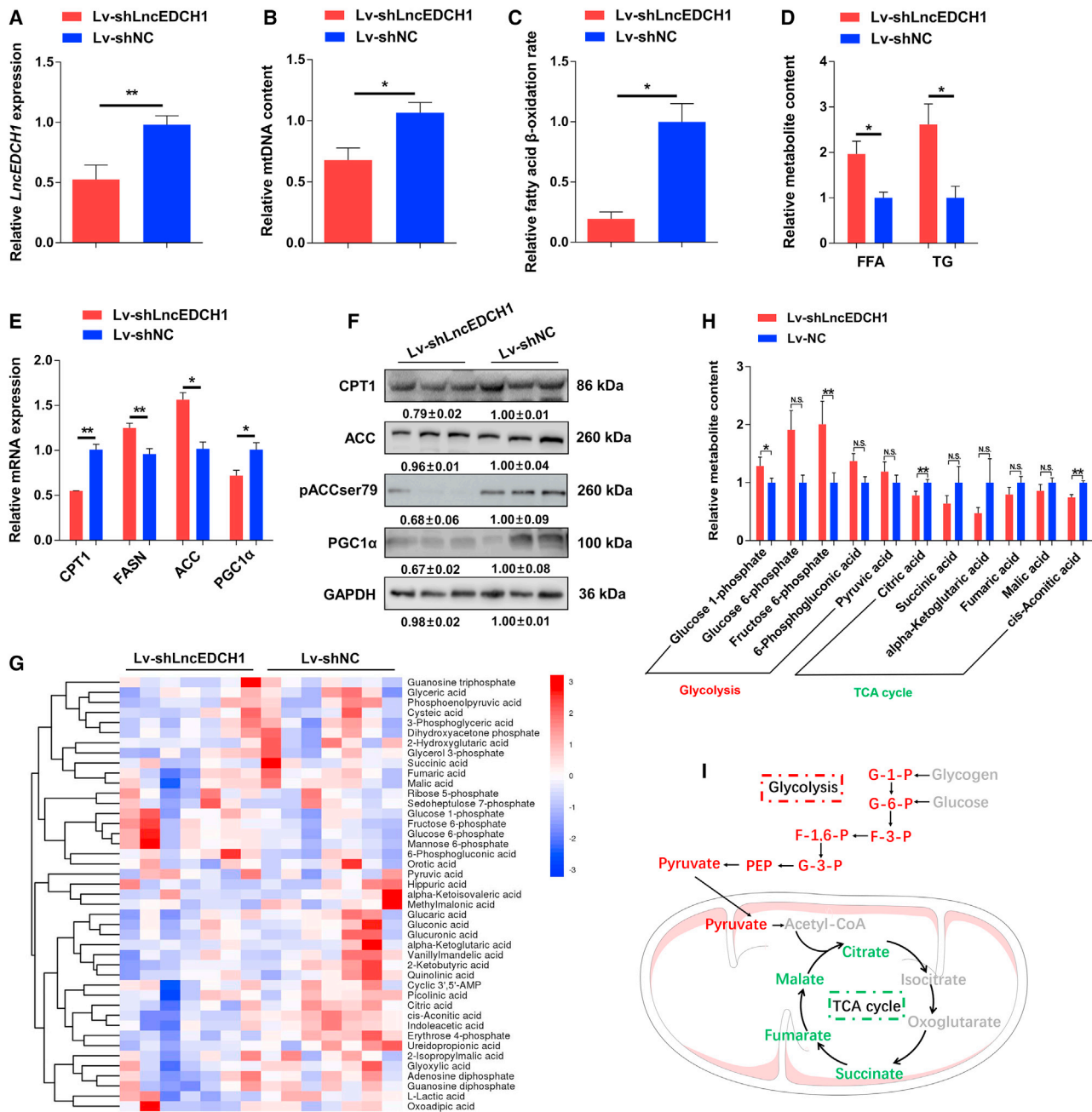


Figure 3. *LncEDCH1* knockdown restrains fatty acid oxidation and tricarboxylic acid cycle in skeletal muscle

(A) Relative *LncEDCH1* expression in gastrocnemius after infection with lentivirus-mediated *LncEDCH1* knockdown (Lv-shLncEDCH1) or negative control (Lv-shNC) (n = 6). (B) Relative mtDNA content in *LncEDCH1* knockdown gastrocnemius (n = 4). (C) Relative fatty acid β -oxidation rate with *LncEDCH1* interference in gastrocnemius (n = 4). (D) Relative free fatty acid (FFA) and triglyceride (TG) content in gastrocnemius with *LncEDCH1* knockdown (n = 4). (E and F) Relative mRNA (E) (n = 4) and protein (F) (n = 3) expression levels of fatty acid oxidation or synthesis-related genes in gastrocnemius with *LncEDCH1* interference. (G) Hierarchical clustering analysis of metabolites in gastrocnemius with interference *LncEDCH1* (n = 7). The colors indicate the relative levels in the *LncEDCH1* knockdown or control group. (H) Relative metabolite content of glycolysis and tricarboxylic acid (TCA) cycle in gastrocnemius with *LncEDCH1* knockdown (n = 7). (I) Schematic diagram of metabolic pathways of glycolysis and TCA cycle affected by *LncEDCH1* knockdown in the gastrocnemius. Upregulated metabolites are shown in red and the downregulated metabolites are shown in green. In (F), the numbers shown below the bands are folds of band intensities relative to control. Band intensities were quantified by ImageJ and normalized to GAPDH. Data are expressed as fold change relative to the control. Results are shown as mean \pm SEM. In (A–E) and (H), the statistical significance of differences between means was assessed using paired t tests (*p < 0.05; **p < 0.01; N.S., no significant difference).

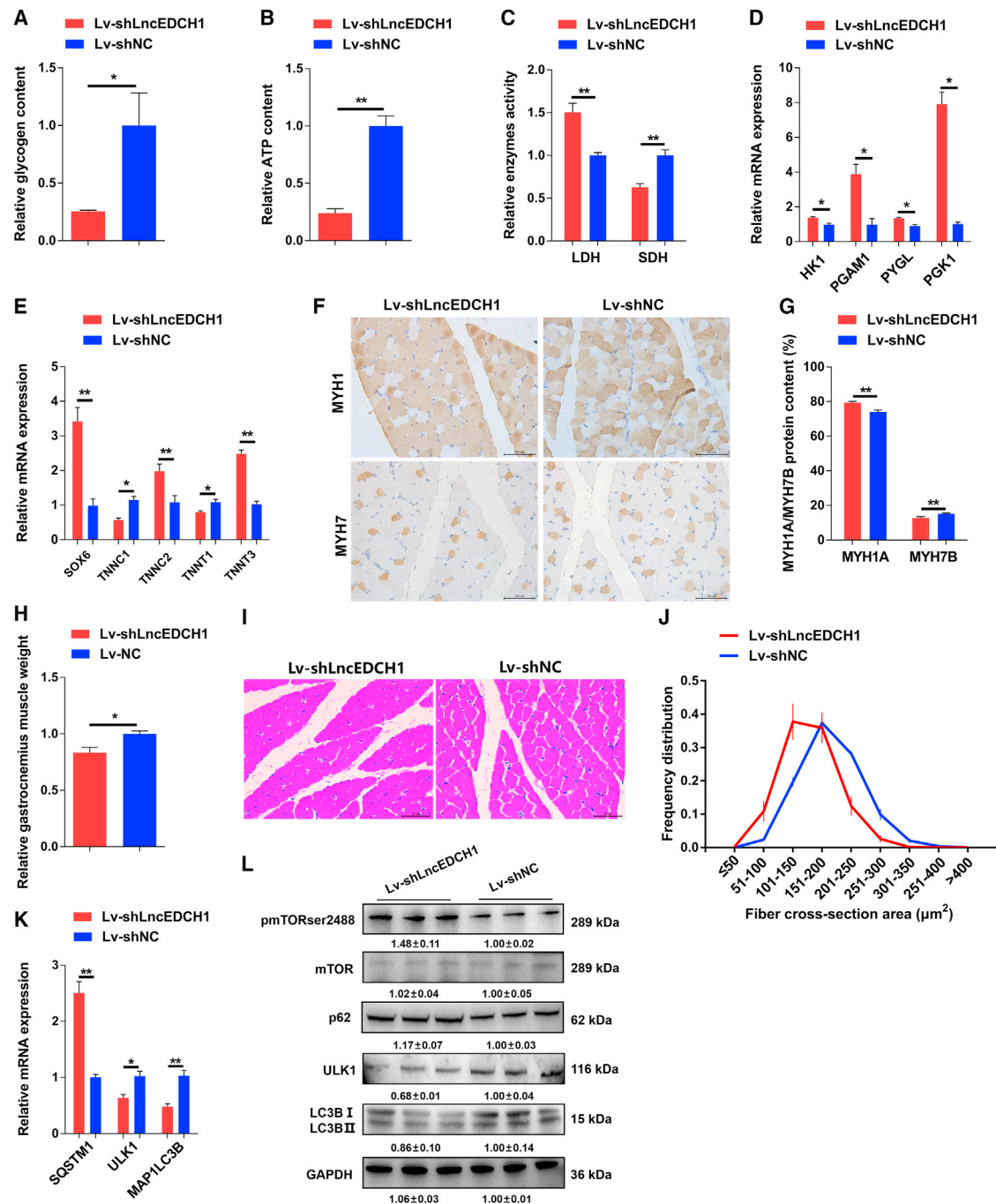


Figure 4. Knockdown of *LncEDCH1* activates fast-twitch muscle phenotype and induces muscle atrophy

(A) Relative glycogen content in *LncEDCH1* knockdown gastrocnemius ($n = 4$). (B) Relative ATP content in gastrocnemius with *LncEDCH1* interference ($n = 4$). (C) Relative enzyme activity of lactic dehydrogenase (LDH) and succinate dehydrogenase (SDH) in gastrocnemius infected with *LncEDCH1* knockdown ($n = 4$). (D) Relative mRNA expression levels of glycogenolytic and glycolytic genes in *LncEDCH1* knockdown gastrocnemius ($n = 4$). (E) Relative mRNA expression levels of several fast/slow-twitch myofiber genes in *LncEDCH1* knockdown gastrocnemius ($n = 4$). (F and G) Immunohistochemistry analysis of MYH1/MYH7 (F) ($n = 4$) and MYH1/MYH7 protein content (G) ($n = 4$) in gastrocnemius with knockdown of *LncEDCH1*. (H) Relative gastrocnemius muscle weight after infection with lentivirus-mediated *LncEDCH1* knockdown ($n = 6$). (I and J) H&E staining (I) ($n = 4$) and frequency distribution of fiber CSA (J) ($n = 4$) in *LncEDCH1* knockdown gastrocnemius. (K and L) Relative mRNA expression of autophagy-related genes (K) ($n = 6$) and the protein (L) ($n = 3$) expression levels of mTOR signaling in gastrocnemius with *LncEDCH1* interference. In (L), the numbers shown below the bands are folds of band intensities relative to control. Band intensities were quantified by ImageJ and normalized to GAPDH. Data are expressed as fold change relative to the control. Results are shown as mean \pm SEM. In (A–E), (G–H), and (K), the statistical significance of differences between means was assessed using paired t tests (* $p < 0.05$; ** $p < 0.01$).

bind to *LncEDCH1* (Table S3). To further corroborate this result, we performed RNA immunoprecipitation (RIP) and verified the interaction between *LncEDCH1* and SERCA2 protein (Figure 5A). To determine the functional motifs of *LncEDCH1* corresponding to SERCA2 binding, we constructed a series of truncated *LncEDCH1* fragments. However, unlike the full-length *LncEDCH1*, none of the truncated fragments could physically bind to SERCA2 (Figures 5B and 5C), suggesting that the complete RNA structure is essential for the molecular function of *LncEDCH1*. This interaction of *LncEDCH1* and SERCA2 was also confirmed by their same subcellular distribution pattern as shown by *in situ* RNA hybridization and SERCA2 immunofluorescence staining (Figure 5D).

With the observation that *LncEDCH1* directly interacts with SERCA2 protein, we further analyzed the effect of *LncEDCH1* on SERCA2. Overexpression and knockdown of *LncEDCH1* did not change the mRNA expression level of SERCA2 both *in vivo* and *in vitro* (Figures S7A–S7D). The protein expression level and activity of SERCA2 were increased with *LncEDCH1* overexpression, while *LncEDCH1* knockdown suppressed SERCA2 protein expression and SERCA2 activity (Figures 5E–5L). Meanwhile, rescue experiments, which were performed by *LncEDCH1* interference and SERCA2 overexpression, reduced suppression of SERCA2 activity (Figure 5M). Considering that *LncEDCH1* regulated SERCA2 protein expression and activity, but did not affect SERCA2 mRNA level, we speculated that *LncEDCH1* may be involved in the regulation of SERCA2 protein stability. Cycloheximide (CHX) is a bacterial toxin that can inhibit protein biosynthesis. Treatment with CHX decreased the expression of SERCA2 protein (Figure 5N). More importantly, overexpression of *LncEDCH1* relieved the decline of SERCA2 protein expression induced by CHX (Figure 5N), implying that *LncEDCH1* interacts with SERCA2 protein to maintain SERCA2 protein stability and increase SERCA2 activity.

***LncEDCH1* regulates Ca^{2+} homeostasis and activates the AMPK pathway to improve mitochondrial efficiency**

As the sarcoplasmic/ER calcium ATPase, SERCA2 was well known to regulate calcium transport from cytosol to ER to maintain Ca^{2+} homeostasis.¹⁹ Given that *LncEDCH1* interacts with SERCA2 protein to enhance SERCA2 activity, we conducted several experiments to evaluate the effect of *LncEDCH1* on Ca^{2+} homeostasis. Fluo-8-AM, a calcium indicator, was used to investigate the changes of free Ca^{2+} concentration intracellularly. Changes in cytosolic calcium were recorded when calcium transport from cytosol to ER was blocked by thapsigargin, a SERCA inhibitor. The amplitude of peak Ca^{2+} transient was calculated according to the equation $(F - F_0)/F_0$, where F represents the maximum value of a Ca^{2+} transient and F_0 represents Ca^{2+} level immediately before the onset of a Ca^{2+} transient. *LncEDCH1* interference reduced the maximum intensity of Fluo-8-AM and the area of the intensity change curve after treatment with 20 μM thapsigargin (Figures 6A–6C). Conversely, overexpression of *LncEDCH1* increased ER calcium levels (Figures S8A–S8C). Ionomycin can cause calcium release from most intracellular stores and is an effective calcium ionophore. Meanwhile, results similar to those upon thapsigargin treatment were observed with the addition

of 10 μM ionomycin (Figures 6D–6F and S8D–S8F). Next, the basal cytosolic calcium concentration was measured by using Fura-2 AM. Interference of *LncEDCH1* increased the basal cytosolic calcium concentration, whereas cytosolic calcium was reduced with *LncEDCH1* overexpression (Figures 6G and S8G). Furthermore, SERCA2 overexpression partially alleviated the decrease in ER calcium level caused by *LncEDCH1* interference (Figures 6H–6J), indicating that *LncEDCH1* regulates Ca^{2+} homeostasis by modulating SERCA2.

Numerous studies have shown that mitochondria and ER are physically and functionally interconnected to maintain the homeostasis of cytosolic calcium.^{20,21} ER stress can induce mitochondrial dysfunction, leading to insulin resistance.²² To investigate the role of *LncEDCH1* in mitochondria, we measured mitochondrial content and function after *LncEDCH1* inhibition and overexpression in CPMs. *LncEDCH1* interference decreased mitochondrial DNA (mtDNA) content accompanied by a decline of mitochondrial membrane potential (Figures 6K and 6L). Meanwhile, ROS production was significantly increased after *LncEDCH1* inhibition (Figure 6M). Inversely, overexpression of *LncEDCH1* upregulated mitochondrial content and enhanced mitochondrial function (Figures S8H–S8J). The activities of mitochondrial electron transport chain (ETC) complexes I, II, and V were repressed after transfection with *LncEDCH1* small interfering RNA (siRNA), whereas overexpression of *LncEDCH1* promoted activities of ETC complexes I, II, and V (Figures 6N–6P and S8K–S8M). In addition, cellular mitochondrial activities including oxygen consumption rate (OCR), basal and maximal mitochondrial respiration, and ATP production were suppressed with *LncEDCH1* inhibition (Figures 6Q and 6R). Meanwhile the opposite result was observed with *LncEDCH1* overexpression (Figures S8N and S8O), illustrating that *LncEDCH1* promotes mitochondria biogenesis.

Calcineurin is a calmodulin-dependent, calcium-activated, serine/threonine protein phosphatase that reportedly mediates multiple signaling cascades in response to changes in cellular calcium ions.^{49–51} As the main signal pathway regulating mitochondrial biogenesis, the AMPK-dependent pathway has recently been reported to be negatively regulated by calcineurin.^{52–54} Given that *LncEDCH1* regulated Ca^{2+} homeostasis and improved mitochondrial efficiency, we further assessed the calcineurin-mediated AMPK pathway. Inhibition of *LncEDCH1* upregulated the protein level of calcineurin, whereas calcineurin was reduced with *LncEDCH1* overexpression (Figures 6S and S8P). Moreover, the phosphorylation of AMPK and cAMP response element-binding protein (CREB) were suppressed after *LncEDCH1* interference, whereas the AMPK/CREB/peroxisome proliferator-activated receptor γ coactivator 1 α (PGC-1 α) pathway was activated upon *LncEDCH1* overexpression (Figures 3F, 6S, S4F, and S8P), demonstrating that *LncEDCH1* regulates Ca^{2+} homeostasis to activate the AMPK pathway, thereby improving mitochondrial efficiency.

The function of *LncEDCH1* depends on the regulation of SERCA2 to a certain extent

SERCA2 was highly expressed in breast and leg muscle and upregulated during myoblast differentiation (Figures S9A and S9B),

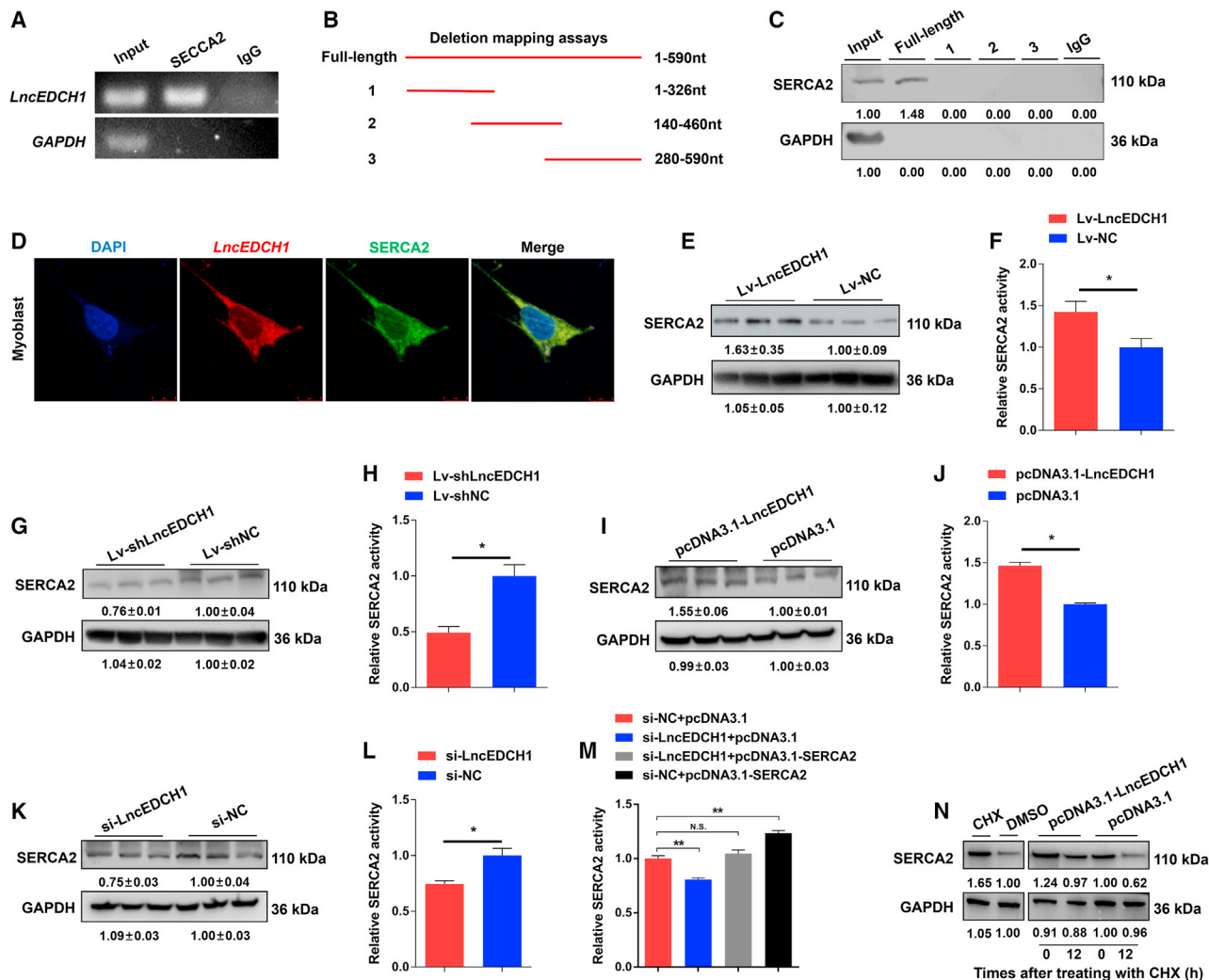


Figure 5. *LncEDCH1* interacts with SERCA2 and enhances Ca^{2+} -ATPase activity

(A) *LncEDCH1* interacts with SERCA2 protein were determined by RNA immunoprecipitation (RIP). (B and C) The interaction of full-length and truncated *LncEDCH1* (base pairs 1–590, 140–460, and 280–590) (B) with SERCA2 protein was determined by RNA pull-down (C). (D) RNA FISH and immunofluorescence staining showed that *LncEDCH1* co-localized with SERCA2 in CPMs. Magnification: 40 \times . (E–H) Protein expression levels of SERCA2 (E and G) ($n = 3$) and relative SERCA2 activity (F and H) ($n = 4$) after *LncEDCH1* overexpression or knockdown *in vitro*. (I–L) Protein expression levels of SERCA2 (I and K) ($n = 3$) and relative SERCA2 activity (J and L) ($n = 4$) after *LncEDCH1* overexpression or knockdown *in vivo*. (M) Relative SERCA2 activity induced after co-transfection with the listed nucleic acids in CPMs ($n = 3$). (N) Protein expression level of SERCA2 in *LncEDCH1* overexpressed myoblast was analyzed after incubation with the protein synthesis inhibitor cycloheximide (CHX; 25 $\mu\text{g}/\text{mL}$) ($n = 1$). In (C), (E), (G), (I), (K), and (N), the numbers shown below the bands are folds of band intensities relative to control. Band intensities were quantified by ImageJ and normalized to GAPDH. Data are expressed as fold change relative to the control. Results are presented as mean \pm SEM. In (F), (H), (J), (L), and (M), the statistical significance of differences between means was assessed using an independent-sample t test (F and H), paired t test (F and H), and ANOVA followed by Dunnett's test (M) (* $p < 0.05$; ** $p < 0.01$; N.S., no significant difference).

implying that it may play an important role in skeletal muscle development. Subcellular location annotation showed that SERCA2 protein exists in the ER (Figure S9C), consistent with our results (Figure 5D). To explore the potential biological functions of SERCA2 in myogenesis, we performed a series of experiments *in vivo*. SERCA2 overexpressed promoted myoblast proliferation and inhibited myoblast differentiation. On the contrary, interference of SERCA2 inhibited the proliferation of myoblasts and promoted the differentia-

tion of myoblasts (Figures S10A–S10T), which is similar to *LncEDCH1* in function.

Given the expression and functional relationship between *LncEDCH1* and SERCA2, we further verified the role of SERCA2 on *LncEDCH1*-mediated skeletal muscle development. Crucially, the regulatory effects of *LncEDCH1* knockdown were weakened after SERCA2 overexpression (Figures 7A–7H),

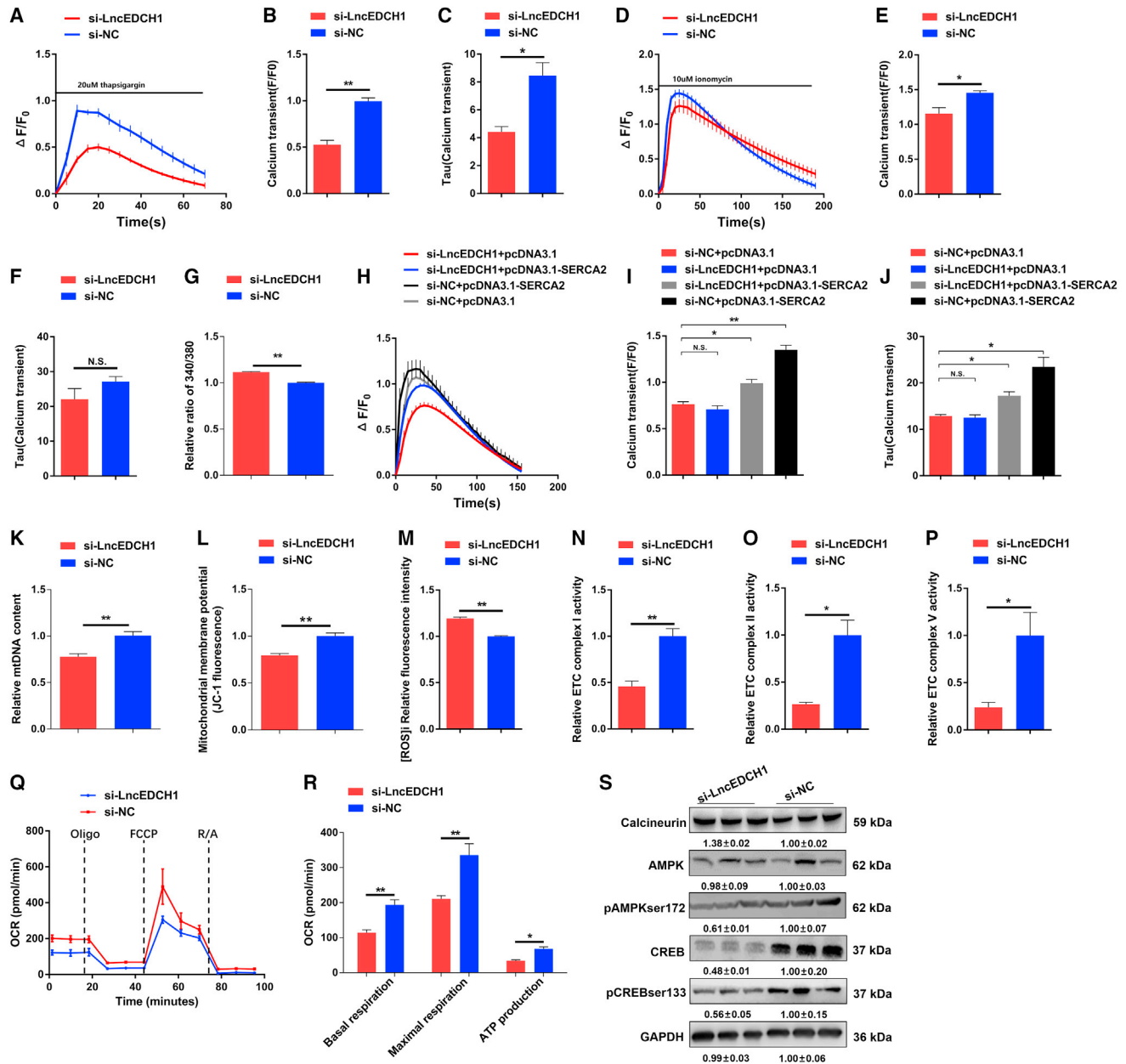
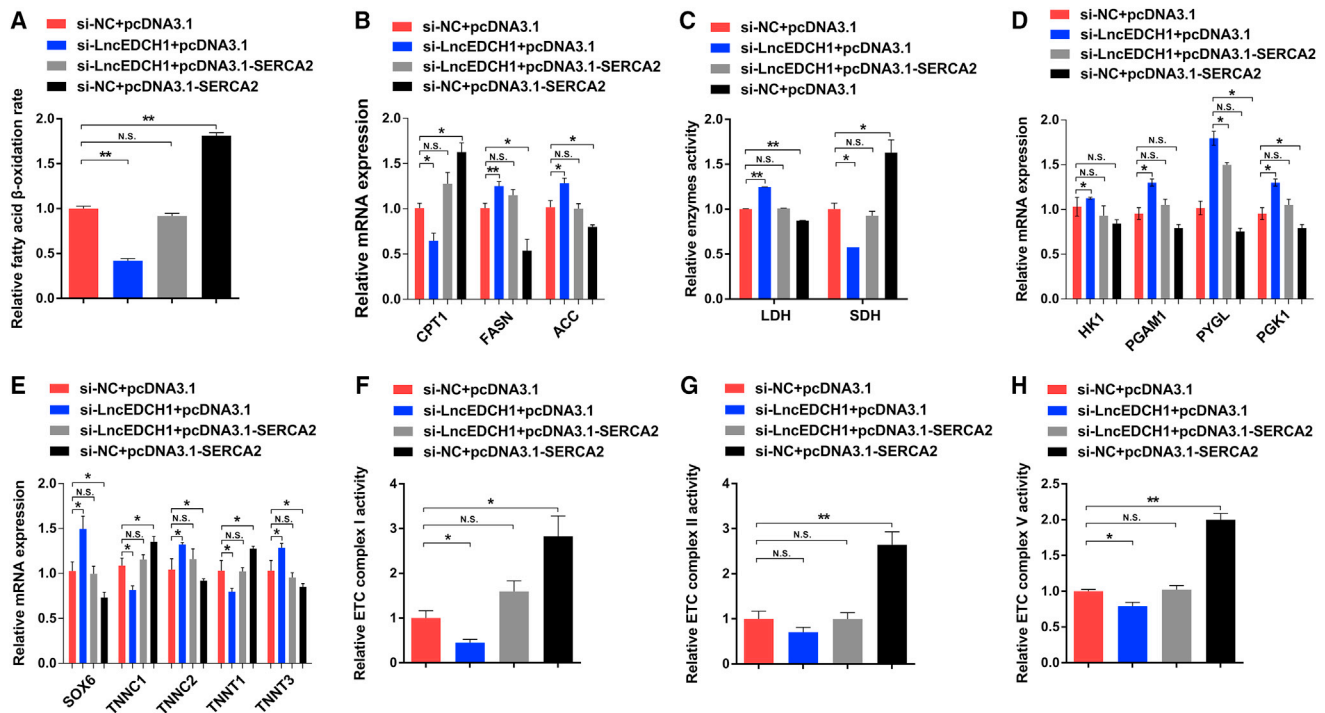


Figure 6. *LncEDCH1* interference destroys Ca^{2+} homeostasis and inactivates the AMPK pathway to reduce mitochondrial efficiency

(A–C) After treatment with 20 μ M thapsigargin, change in Fluo-8-AM fluorescence intensity ($F - F_0/F_0$) with time (A) ($n = 4$), maximum fluorescence intensity in (A) and (B) ($n = 4$), and areas under the curves (AUC) in (A) and (C) ($n = 4$) with *LncEDCH1* interference *in vitro*. (D–F) Treatment with 10 μ M ionomycin evoked change in Fluo-8-AM fluorescence intensity (D) ($n = 4$), the maximum fluorescence intensity in (D) and (E) ($n = 4$), and AUC in (D) and (F) ($n = 4$) after interference of *LncEDCH1*. (G) Relative basal cytosolic calcium level with *LncEDCH1* interference ($n = 6$). (H–J) Treatment with 10 μ M ionomycin evoked change in Fluo-8-AM fluorescence intensity (H) ($n = 3$), the maximum fluorescence intensity in (H) and (I) ($n = 3$), and AUC in (H) and (J) ($n = 3$) induced after co-transfection with the listed nucleic acids. (K–M) Relative mtDNA content (K) ($n = 5$), mitochondrial membrane potential (L) ($n = 6$), and intracellular ROS ([ROS]) (M) ($n = 4$) with *LncEDCH1* interference *in vitro*. (N–P) Relative enzyme activity of ETC complexes I (N) ($n = 3$), II (O) ($n = 3$), and V (P) ($n = 3$) with *LncEDCH1* inhibition in CPMs. (Q and R) Oxygen consumption rate (OCR) (Q) ($n = 5$), and basal respiration, maximal respiration, and ATP production (R) ($n = 5$) of myoblasts after interference of *LncEDCH1*. (S) Protein expression levels of calcineurin and AMPK signaling after the interference of *LncEDCH1* *in vitro* ($n = 3$). In (S), the numbers shown below the bands are folds of band intensities relative to control. Band intensities were quantified by ImageJ and normalized to GAPDH. Data are expressed as fold change relative to the control. Results are presented as mean \pm SEM. In (B), (C), (E–G), (K–P), and (R), the statistical significance of differences between means was assessed using an independent-sample t test. In (I) and (J), ANOVA followed by Dunnett's test was used (* $p < 0.05$; ** $p < 0.01$; N.S., no significant difference).



hinting that SERCA2 is indispensable to the function of *LncEDCH1*.

DISCUSSION

Myogenesis is a complex process that is finely tuned and controlled by a series of myogenic regulatory factors.^{43,55} These factors can regulate myoblasts to withdraw from the cell cycle, express muscle-specific genes, and prevent the expression of other cell- or tissue-specific genes. It is worth noting that recently, lncRNAs have also been demonstrated to function in myogenesis.^{31,56,57} *LncEDCH1* is an lncRNA that is differentially expressed between hypertrophic broiler and lean Chinese native breed and was identified by our previous RNA-seq data. In this study, we found that *LncEDCH1* is specifically enriched in skeletal muscle, and its transcriptional activity is positively regulated by transcription factor SP1. Functional studies demonstrated that *LncEDCH1* promoted myoblast proliferation but inhibited myoblast differentiation.

Molecular decoy is one of the main molecular mechanisms for an lncRNA to function. This refers to the fact that lncRNA directly binds to RNA or protein molecules, thereby activating or blocking the role and signal pathway of these molecules.⁵⁸ Here, SERCA2, a key ER Ca^{2+} -ATPase that regulates the calcium transport from

cytosol to ER, was found to specifically bind to *LncEDCH1*. *LncEDCH1* interacts with SERCA2 to enhance the stability of SERCA2 protein, thus increasing SERCA2 activity and strengthening ER calcium storage.

Skeletal muscle is a major player in regulating glucose uptake, lipid storage, and energy balance, which can maintain systemic energy homeostasis in response to various metabolic stresses.⁵⁹ As the main organelle of energy metabolism, mitochondria modulate metabolic processes including TCA cycle, ATP production, and amino acid catabolism, and are closely related to the development of skeletal muscle.^{60,61} In the current study, we found that *LncEDCH1* reduced cytosolic calcium to inhibit calcineurin, which causes activation of the AMPK pathway and promotes mitochondrial efficiency.

Autophagy is a highly conserved homeostatic process carrying out degradation of cytoplasmic components including damaged organelles, toxic protein aggregates, and intracellular pathogens.⁶² It has come to light that excess autophagy promotes extensive muscle wasting that affects tissue mass, muscle strength, and myofiber regeneration.⁶³ However, muscle-specific *Atg7* knockout mice have been reported to exhibit muscle loss and dysfunction, hinting that

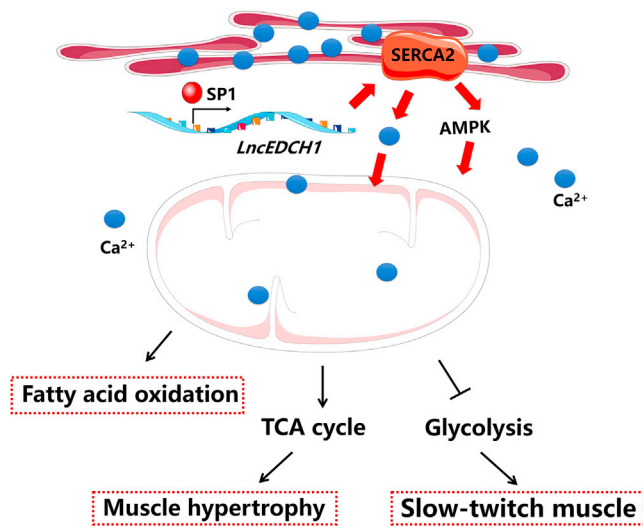


Figure 8. Model of *LncEDCH1* interacts with SERCA2 to improve mitochondrial efficiency, thus promoting intramuscular fatty acid oxidation as well as activating slow-twitch muscle phenotype and inhibiting muscle atrophy.

autophagy is required to maintain muscle mass.⁶⁴ Recently, the enhancement of autophagy and the promotion of mitochondrial function have also been found to alleviate muscle atrophy.⁶⁵ Here, we found that *LncEDCH1* activated autophagy by inhibiting mTOR signaling. *LncEDCH1* reduces intramuscular fat deposition, as well as activating slow-twitch muscle phenotype and inhibiting muscle atrophy, which potentially lends credence to its function in autophagy and mitochondrial biogenesis.

In conclusion, we demonstrated that *LncEDCH1* can bind with SERCA2 to modulate SERCA2 activity. *LncEDCH1* maintained ER Ca²⁺ homeostasis and improved mitochondrial efficiency to reduce intramuscular fat deposition, activate slow-twitch muscle phenotype, and relieve muscle atrophy (Figure 8). Our study shows that *LncEDCH1* could be an effective regulator for the treatment of energy metabolism and muscle atrophy.

MATERIALS AND METHODS

Animals and ethics statement

Chinese native breeds (XH chickens) were used for the *in vivo* experiment in this study. For construction of animal models of *LncEDCH1* overexpression and knockdown, sample group lentivirus was injected into the left gastrocnemius and control group lentivirus was injected into the right gastrocnemius at a dosage of 1×10^6 IU/mL (at the age of 1, 4, and 8 days). Fourteen days after the initial injection, chick gastrocnemius samples were collected. The use of animals was approved by conformed to “The Instructive Notions with Respect to Caring for Laboratory Animals” issued by the Ministry of Science and Technology of the People’s Republic of China, and approved by the Institutional Animal Care and Use Committee at the South China Agricultural University (approval ID: 2020-C036).

Cell culture and transfection

CPMs were isolated from E11 chicken leg muscles as previously described⁶⁶ and cultured in Roswell Park Memorial Institute (RPMI)-1640 medium (Gibco, USA) with 20% fetal bovine serum (Gibco).

All transient transfections were performed using Lipofectamine 3000 reagent (Invitrogen, USA) according to the manufacturer’s instructions.

RACE

The full-length of *LncEDCH1* was amplified by using a SMARTer RACE cDNA Amplification Kit (Clontech, Japan), following the manufacturer’s instructions.

RNA FISH

RNA fluorescence *in situ* hybridization (FISH) experiments were performed using an lncRNA FISH Kit (Guangzhou RiboBio, Guangzhou, China) according to the manufacturer’s instructions. In brief, the cells were incubated with the RNA probes in hybridization buffer overnight at 37°C. The cells were washed three times with saline-sodium citrate buffer, stained with 4’,6-diamidino-2-phenylindole (DAPI) for 10 min at room temperature, and examined using a fluorescence microscope.

Luciferase reporter assay

Different fragments of the *LncEDCH1* promoter were cloned into a pGL3-basic luciferase reporter vector (Addgene, USA), and the constructed luciferase reporter vectors were transfected into CPMs in a 96-well plate. The luciferase assay was performed using the Dual-Luciferase Reporter Assay System (Promega, USA) following the manufacturer’s instructions.

CCK-8, EdU, and flow cytometry assays

A TransDetect CCK kit (TransGen Biotech, China), an EdU Apollo In Vitro Imaging Kit (RiboBio, China), and a Cell Cycle Analysis Kit (Thermo Fisher Scientific, USA) were used for CCK-8, EdU, and flow cytometry assay, respectively, according to the manufacturers’ protocols.

RNA extraction, cDNA synthesis, and real-time qPCR

Total RNA was extracted using TRIzol reagent (TaKaRa, Japan) following the manufacturer’s protocol. A PARIS Kit (Ambion, USA) was used to harvest the cytoplasmic and nuclear cell lysates. A PrimeScript RT Reagent Kit with gDNA Eraser (Perfect Real Time) (TaKaRa, Japan) was used to synthesize cDNA. An iTaq Universal SYBR Green Supermix Kit (Toyobo, Japan) was used for cDNA quantification, according to the manufacturer’s protocol. All primers for RT-PCR and real-time qPCR are listed in Table S4.

Plasmid construction and RNA oligonucleotides

For FLAG fusion protein construction, six ORFs of *LncEDCH1* were amplified and cloned into the pcDNA3.1-3xFLAG-C vector. For *LncEDCH1* and *SERCA2* overexpression plasmid construction, the full-length sequence *LncEDCH1* and the *SERCA2* coding sequence

were amplified by PCR and cloned into a pcDNA3.1 vector (Promega).

For construction of viral vectors, the full-length sequence of *LncEDCH1* was amplified and then cloned into a pLVX-mCMV-ZsGreen-IRES-Puro vector (Addgene). Short hairpin RNA (shRNA) against *LncEDCH1* was designed by Shanghai Hanbio Biotechnology and subcloned into the pLVX-shRNA2-Puro vector (Addgene).

LncEDCH1 is an lncRNA molecule mainly present in the cytoplasm; the siRNAs that were used for the specific knockdown of *LncEDCH1* and *SERCA2* (NCBI: NM_001271973.1) were designed and synthesized by Guangzhou RiboBio.

Immunofluorescence, immunohistochemistry and hematoxylin and eosin staining

Immunofluorescence was performed using anti-MyHC (B103; DHSB, USA; 2.5 µg/mL), and images were captured using a fluorescence microscope (DMI8; Leica, Germany). The area of cells labeled with anti-MyHC was measured and calculated as previously described.²⁹

Immunohistochemistry was carried out using an SP-POD Kit (SP0041; Solarbio, China) with primary antibodies including anti-MYH1 (F59, DHSB, 1:100) and anti-MYH7 (S58, DHSB, 1:300).

Hematoxylin and eosin (H&E) staining was performed using muscle tissues embedded in paraffin and cut into 4-µm-thick transverse sections. Subsequently, the sections were stained with H&E.

Western blot analysis

Western blot analysis was performed as previously described.⁶⁶ The primary antibodies used were anti-FLAG (AF519, Beyotime, 1:1,000), anti-MYOD (ABP53067, Abbkine, 1:500), anti-MyHC (B103, DHSB, 0.5 µg/mL), anti-SERCA2 (NB100-237, Novus, 1:2,000), anti-ACC (PA5-17564, Thermo Fisher Scientific, 1:1,000), anti-pACCSer80 (orb315750, Biorbyt, 1:500), anti-CPT1 (bs-23779R, Bioss, 1:500), anti-pmTORSer2488 (#5536, CST, 1:1,000), anti-mTOR (bs-1992R, Bioss, 1:500), anti-ULK1 (bs-3602R, Bioss, 1:500), anti-LC3B (NB100-2220, Novus, 2.0 µg/mL), anti-P62 (18420-1-AP, Proteintech, 1:1,000), anti-CREB (bs-0035R, Bioss, 1:500), anti-pCREBSer133 (ab32096, Abcam, 1:5,000), anti-AMPK (bs-1115R, Bioss, 1:500), anti-pAMPKser712 (ABN-PAB12602, Abnova, 1:2,000), anti-Calceineurin (#2614S, CST, 1:1,000), anti-PGC-1α (66369-1-Ig, Proteintech, 1:5,000), and anti-GAPDH (60004-1-Ig, Proteintech, 1:5,000). ProteinFind goat anti-mouse IgG(H+L), HRP conjugate (HS201-01, TransGen, 1:1,000) and ProteinFind goat anti-rabbit IgG(H+L), HRP conjugate (HS101-01, TransGen, 1:500) were used as secondary antibodies.

mtDNA content and FAO rate assay

Total DNA was extracted using a Tissue DNA Kit (D3396, Omega Biotek, USA) following the manufacturer's protocol. The amount of mitochondrial DNA was determined by quantification of cytochrome *c* oxidase subunit II (COX2). The nuclear-encoded *β-globin* gene

was used as internal control. Primers used in the study can be found in Table S4.

The mitochondria of myoblast and gastrocnemius were isolated using a Cell/Tissue Mitochondria Isolation Kit (C3601/C3606, Beyotime, China) and then subjected to FAO rate assay with a Colorimetric Fatty Acid Oxidation Rate Assay Kit (HL50679, Haling, China), according to the manufacturer's protocol.

Central carbon metabolic profiling

The gastrocnemius samples (n = 7) of *LncEDCH1* knockdown were used for metabolite extraction and then subjected to high-performance ion exchange liquid chromatography (HPIC)-tandem mass spectrometry analysis. The HPIC separation was carried out using a Thermo Scientific Dionex ICS-6000 HPIC System (Thermo Fisher Scientific). An AB SCIEX 6500 QTRAP+ triple quadrupole mass spectrometer (AB Sciex, USA), equipped with electrospray ionization interface, was applied for assay development.

Metabolic HCA was performed using Cluster3.0 software as previously described.⁶⁷

Metabolite and enzyme activities assays

Content of TG, FFA, ATP, and glycogen as well as enzyme activity of LDH and SDH in skeletal muscle were measured using commercially available kits (BC0625, BC0595, BC0305, BC0345, BC0685, BC0955, respectively; Solarbio, China), according to the manufacturer's instructions.

RNA pull-down assay and RIP assay

Biotinylated RNAs were harvested by using a Ribo RNAmix-T7 biotin-labeled transcription kit (RiboBio, China). A Pierce Magnetic RNA-Protein Pull-Down Kit (Thermo Fisher Scientific) was used in RNA-protein pull-down experiments according to the manufacturer's instructions. The eluted products were identified by mass spectrometry with a Q Exactive mass spectrometer (Thermo Fisher) or western blot. Differentially expressed genes were subjected to enrichment analysis of GO functions and KEGG pathways.

RIP was performed using the Magna RIP RNA-Binding Protein Immunoprecipitation Kit (Millipore, USA) according to the manufacturer's instructions. The antibody used for RIP assays was anti-SERCA2 (NB100-237, Novus, 1:50).

SERCA2 activity measurement

The activity of SERCA2 was assessed by a colorimetric ATPase assay kit (A070-4-2, Nanjing Jiancheng Bioengineering Institute, China). Protein concentration was measured by the BCA method (P0012, Beyotime, China). ATPase activity was normalized by protein content.

Intracellular calcium and intracellular Ca²⁺ transient measurement

At 48 h after transfection, the CPMs were incubated with a 5 µM concentration of the acetoxymethyl ester form of Fura 2 (Fura 2-AM,

Beyotime, China) for 30 min at 37°C. The fluorescence emission (510 nm) was detected using a Fluorescence/Multi-Detection Microplate Reader (BioTek, USA) at 340 nm and 380 nm excitation. Data for ratio fluorescence were normalized to the basal fluorescence.

For the ionomycin- and thapsigargin-evoked calcium release assay, the CPMs were incubated with 5 mM Fluo-8 AM (21081, AAT, USA) for 60 min at 37°C in the dark. After washing three times with HL buffer, the HL buffer was replaced by calcium-free HL buffer containing 2 mM EGTA instead of 1.8 mM CaCl_2 . Thapsigargin (10 μM) (T9033, Sigma, USA) or ionomycin (20 μM) (S1672, Beyotime, China) in calcium-free HL buffer was used to stimulate Ca^{2+} release. Time-lapse images were recorded by a Lycka Live Cell Microscope. The calcium signal was presented as the mean of the relative change in fluorescence intensity normalized to baseline intensity ($F - F_0/F_0$).

Mitochondrial membrane potential, ROS concentration, and mitochondrial ETC activity assay

Mitochondrial membrane potential, ROS concentration, and activities of mitochondrial ETC I, II, and V were measured using commercially available kits (C2006 and S0033S, Beyotime, China; BC0515, BC3235, and BC1445, Solarbio, China), according to the manufacturer's instructions.

Mitochondrial respiration assay

The OCR of transfected myoblasts were measured using a Seahorse XF Cell Mito Stress Test Kit (103015, Agilent Technologies, CA, USA) and by a Seahorse XF96 Extracellular Flux Analyzer (Agilent Technologies) following the manufacturer's protocol.

Statistical analysis

In this study, all experiments were repeated at least three times, and results were representative of mean \pm SEM. Where applicable, the statistical significance of the data was tested using an independent-sample t test or ANOVA followed by Dunnett's test. The types of tests and the p values, when applicable, are indicated in the figure legends.

SUPPLEMENTAL INFORMATION

Supplemental information can be found online at <https://doi.org/10.1016/j.omtn.2021.12.004>.

ACKNOWLEDGMENTS

This work was supported by the Natural Scientific Foundation of China (U1901206, 31802051, and 31761143014), Local Innovative and Research Teams Project of Guangdong Province (2019BT02N630), Ten-Thousand Talents Program (W03020593), and China Agricultural Research System (CARS-41-G03).

AUTHOR CONTRIBUTIONS

Q.N., X.Z., and H.L. conceived and designed the study. B.C. and M.M. performed the experiments, interpreted the data, and wrote the paper. J.Z., Z.W., S.K., and Z.Z. performed the experiments. L.L., J.Z., J.L.,

and Y.W. interpreted the data. All authors read and approved the final manuscript.

DECLARATION OF INTERESTS

The authors declare no competing interests.

REFERENCES

- Rai, M., and Demontis, F. (2016). Systemic nutrient and stress signaling via myokines and myometabolites. *Annu. Rev. Physiol.* 78, 85–107.
- Ibrahim, A., Neinast, M., and Arany, Z.P. (2017). Myobolites: muscle-derived metabolites with paracrine and systemic effects. *Curr. Opin. Pharmacol.* 34, 15–20.
- Janssen, I., Heymsfield, S.B., Wang, Z.M., and Ross, R. (2000). Skeletal muscle mass and distribution in 468 men and women aged 18–88 yr. *J. Appl. Physiol.* 89, 81–88.
- Bowen, T.S., Schuler, G., and Adams, V. (2015). Skeletal muscle wasting in cachexia and sarcopenia: molecular pathophysiology and impact of exercise training. *J. Cachexia Sarcopenia Muscle* 6, 197–207.
- Godfrey, R., and Quinlivan, R. (2016). Skeletal muscle disorders of glycogenolysis and glycolysis. *Nat. Rev. Neurol.* 12, 393–402.
- Sartorelli, V., and Fulco, M. (2004). Molecular and cellular determinants of skeletal muscle atrophy and hypertrophy. *Sci. STKE* 2004, e11.
- Jagoe, R.T., and Goldberg, A.L. (2001). What do we really know about the ubiquitin-proteasome pathway in muscle atrophy? *Curr. Opin. Clin. Nutr. Metab. Care* 4, 183–190.
- Thomson, D.M. (2018). The role of AMPK in the regulation of skeletal muscle size, hypertrophy, and regeneration. *Int. J. Mol. Sci.* 19, 3125.
- Zanou, N., and Gailly, P. (2013). Skeletal muscle hypertrophy and regeneration: interplay between the myogenic regulatory factors (MRFs) and insulin-like growth factors (IGFs) pathways. *Cell. Mol. Life Sci.* 70, 4117–4130.
- Blaauw, B., Schiaffino, S., and Reggiani, C. (2013). Mechanisms modulating skeletal muscle phenotype. *Compr. Physiol.* 3, 1645–1687.
- Yamada, Y., Namba, K., and Fujii, T. (2020). Cardiac muscle thin filament structures reveal calcium regulatory mechanism. *Nat. Commun.* 11, 153.
- Borowiec, A.S., Bidaux, G., Pigat, N., Goffin, V., Bernichtein, S., and Capiod, T. (2014). Calcium channels, external calcium concentration and cell proliferation. *Eur. J. Pharmacol.* 739, 19–25.
- Wang, S.F., Liu, L.F., Wu, M.Y., Cai, C.Z., Su, H., Tan, J., Lu, J.H., and Li, M. (2017). Baicalein prevents 6-OHDA/ascorbic acid-induced calcium-dependent dopaminergic neuronal cell death. *Sci. Rep.* 7, 8398.
- Berridge, M.J. (2016). The inositol trisphosphate/calcium signaling pathway in health and disease. *Physiol. Rev.* 96, 1261–1296.
- Lasa-Elgarresta, J., Mosqueira-Martin, L., Naldaiz-Gastesi, N., Saenz, A., Lopez, D.M.A., and Vallejo-Illarramendi, A. (2019). Calcium mechanisms in limb-girdle muscular dystrophy with CAPN3 mutations. *Int. J. Mol. Sci.* 20, 4548.
- Vallejo-Illarramendi, A., Toral-Ojeda, I., Aldanondo, G., and Lopez, D.M.A. (2014). Dysregulation of calcium homeostasis in muscular dystrophies. *Expert Rev. Mol. Med.* 16, e16.
- Hadrevi, J., Barbe, M.F., Ortenblad, N., Frandsen, U., Boyle, E., Lazar, S., Sjogaard, G., and Sogaard, K. (2019). Calcium fluxes in work-related muscle disorder: implications from a rat model. *Biomed. Res. Int.* 2019, 5040818.
- Bohner, K.R., McMillan, J.D., and Kumar, A. (2018). Emerging roles of ER stress and unfolded protein response pathways in skeletal muscle health and disease. *J. Cell. Physiol.* 233, 67–78.
- Stammers, A.N., Susser, S.E., Hamm, N.C., Hlynsky, M.W., Kimber, D.E., Kehler, D.S., and Duhamel, T.A. (2015). The regulation of sarco(endo)plasmic reticulum calcium-ATPases (SERCA). *Can. J. Physiol. Pharmacol.* 93, 843–854.
- Leem, J., and Koh, E.H. (2012). Interaction between mitochondria and the endoplasmic reticulum: implications for the pathogenesis of type 2 diabetes mellitus. *Exp. Diabetes Res.* 2012, 242984.

21. Rieusset, J. (2011). Mitochondria and endoplasmic reticulum: mitochondria-endoplasmic reticulum interplay in type 2 diabetes pathophysiology. *Int. J. Biochem. Cell Biol.* 43, 1257–1262.
22. Lim, J.H., Lee, H.J., Ho, J.M., and Song, J. (2009). Coupling mitochondrial dysfunction to endoplasmic reticulum stress response: a molecular mechanism leading to hepatic insulin resistance. *Cell Signal.* 21, 169–177.
23. Lee, J.T. (2012). Epigenetic regulation by long noncoding RNAs. *Science* 338, 1435–1439.
24. Cabili, M.N., Trapnell, C., Goff, L., Koziol, M., Tazon-Vega, B., Regev, A., and Rinn, J.L. (2011). Integrative annotation of human large intergenic noncoding RNAs reveals global properties and specific subclasses. *Genes Dev.* 25, 1915–1927.
25. Djebali, S., Davis, C.A., Merkel, A., Dobin, A., Lassmann, T., Mortazavi, A., Tanzer, A., Lagarde, J., Lin, W., Schlesinger, F., et al. (2012). Landscape of transcription in human cells. *Nature* 489, 101–108.
26. Lu, L., Sun, K., Chen, X., Zhao, Y., Wang, L., Zhou, L., Sun, H., and Wang, H. (2013). Genome-wide survey by ChIP-seq reveals YY1 regulation of lincRNAs in skeletal myogenesis. *EMBO J.* 32, 2575–2588.
27. Wang, L., Zhao, Y., Bao, X., Zhu, X., Kwok, Y.K., Sun, K., Chen, X., Huang, Y., Jauch, R., Esteban, M.A., et al. (2015). LncRNA Dum interacts with Dnmts to regulate Dppa2 expression during myogenic differentiation and muscle regeneration. *Cell Res.* 25, 335–350.
28. Zhu, M., Liu, J., Xiao, J., Yang, L., Cai, M., Shen, H., Chen, X., Ma, Y., Hu, S., Wang, Z., et al. (2017). Lnc-mg is a long non-coding RNA that promotes myogenesis. *Nat. Commun.* 8, 14718.
29. Ma, M., Cai, B., Jiang, L., Abdalla, B.A., Li, Z., Nie, Q., and Zhang, X. (2018). lncRNA-Six1 is a target of miR-1611 that functions as a ceRNA to regulate Six1 protein expression and fiber type switching in chicken myogenesis. *Cells* 7, 243.
30. Zhang, Z.K., Li, J., Guan, D., Liang, C., Zhuo, Z., Liu, J., Lu, A., Zhang, G., and Zhang, B.T. (2018). Long noncoding RNA lncMUMA reverses established skeletal muscle atrophy following mechanical unloading. *Mol. Ther.* 26, 2669–2680.
31. Cai, B., Li, Z., Ma, M., Zhang, J., Kong, S., Abdalla, B.A., Xu, H., Jebessa, E., Zhang, X., Lawal, R.A., et al. (2021). Long noncoding RNA SMUL suppresses SMURF2 production-mediated muscle atrophy via nonsense-mediated mRNA decay. *Mol. Ther. Nucleic Acids* 23, 512–526.
32. Li, Z., Cai, B., Abdalla, B.A., Zhu, X., Zheng, M., Han, P., Nie, Q., and Zhang, X. (2019). lncIRS1 controls muscle atrophy via sponging miR-15 family to activate IGF1-PI3K/AKT pathway. *J. Cachexia Sarcopenia Muscle* 10, 391–410.
33. Zuo, H., and Wan, Y. (2019). Metabolic reprogramming in mitochondria of myeloid cells. *Cells* 9, 5.
34. Wallace, D.C. (2012). Mitochondria and cancer. *Nat. Rev. Cancer* 12, 685–698.
35. Schiaffino, S., Sandri, M., and Murgia, M. (2007). Activity-dependent signaling pathways controlling muscle diversity and plasticity. *Physiology* (Bethesda) 22, 269–278.
36. Wang, T., Xu, Y.Q., Yuan, Y.X., Xu, P.W., Zhang, C., Li, F., Wang, L.N., Yin, C., Zhang, L., Cai, X.C., et al. (2019). Succinate induces skeletal muscle fiber remodeling via SUNC1 signaling. *EMBO Rep.* 20, e47892.
37. Yang, X., Brobst, D., Chan, W.S., Tse, M., Herlea-Pana, O., Ahuja, P., Bi, X., Zaw, A.M., Kwong, Z., Jia, W.H., et al. (2019). Muscle-generated BDNF is a sexually dimorphic myokine that controls metabolic flexibility. *Sci. Signal.* 12, eaau1468.
38. Bassel-Duby, R., and Olson, E.N. (2006). Signaling pathways in skeletal muscle remodeling. *Annu. Rev. Biochem.* 75, 19–37.
39. Schiaffino, S., and Reggiani, C. (2011). Fiber types in mammalian skeletal muscles. *Physiol. Rev.* 91, 1447–1531.
40. Koutakis, P., Weiss, D.J., Miserlis, D., Shostrom, V.K., Papoutsis, E., Ha, D.M., Carpenter, L.A., McComb, R.D., Casale, G.P., and Pipinos, I.I. (2014). Oxidative damage in the gastrocnemius of patients with peripheral artery disease is myofiber type selective. *Redox Biol.* 2, 921–928.
41. Li, J.B., and Goldberg, A.L. (1976). Effects of food deprivation on protein synthesis and degradation in rat skeletal muscles. *Am. J. Physiol.* 231, 441–448.
42. Matsakas, A., and Patel, K. (2009). Skeletal muscle fibre plasticity in response to selected environmental and physiological stimuli. *Histol. Histopathol.* 24, 611–629.
43. Joseph, A.M., Adhietty, P.J., and Leeuwenburgh, C. (2016). Beneficial effects of exercise on age-related mitochondrial dysfunction and oxidative stress in skeletal muscle. *J. Physiol.* 594, 5105–5123.
44. Braun, T., and Gautel, M. (2011). Transcriptional mechanisms regulating skeletal muscle differentiation, growth and homeostasis. *Nat. Rev. Mol. Cell Biol.* 12, 349–361.
45. Saxton, R.A., and Sabatini, D.M. (2017). mTOR signaling in growth, metabolism, and disease. *Cell* 168, 960–976.
46. Tan, Y., Mui, D., Toan, S., Zhu, P., Li, R., and Zhou, H. (2020). SERCA overexpression improves mitochondrial quality control and attenuates cardiac microvascular ischemia-reperfusion injury. *Mol. Ther. Nucleic Acids* 22, 696–707.
47. Qaisar, R., Bhaskaran, S., Ranjit, R., Sataranatarajan, K., Premkumar, P., Huseman, K., and Van Remmen, H. (2019). Restoration of SERCA ATPase prevents oxidative stress-related muscle atrophy and weakness. *Redox Biol.* 20, 68–74.
48. Gailly, P. (2002). New aspects of calcium signaling in skeletal muscle cells: implications in Duchenne muscular dystrophy. *Biochim. Biophys. Acta* 1600, 38–44.
49. Rusnak, F., and Mertz, P. (2000). Calcineurin: form and function. *Physiol. Rev.* 80, 1483–1521.
50. Molkenkin, J.D., Lu, J.R., Antos, C.L., Markham, B., Richardson, J., Robbins, J., Grant, S.R., and Olson, E.N. (1998). A calcineurin-dependent transcriptional pathway for cardiac hypertrophy. *Cell* 93, 215–228.
51. Tan, W.Q., Wang, J.X., Lin, Z.Q., Li, Y.R., Lin, Y., and Li, P.F. (2008). Novel cardiac apoptotic pathway: the dephosphorylation of apoptosis repressor with caspase recruitment domain by calcineurin. *Circulation* 118, 2268–2276.
52. Reznick, R.M., Zong, H., Li, J., Morino, K., Moore, I.K., Yu, H.J., Liu, Z.X., Dong, J., Mustard, K.J., Hawley, S.A., et al. (2007). Aging-associated reductions in AMP-activated protein kinase activity and mitochondrial biogenesis. *Cell Metab.* 5, 151–156.
53. He, H., Liu, X., Lv, L., Liang, H., Leng, B., Zhao, D., Zhang, Y., Du, Z., Chen, X., Li, S., et al. (2014). Calcineurin suppresses AMPK-dependent cytoprotective autophagy in cardiomyocytes under oxidative stress. *Cell Death Dis.* 5, e997.
54. Wang, Y., Xie, C., Diao, Z., and Liang, B. (2017). Calcineurin antagonizes AMPK to regulate lipolysis in *Caenorhabditis elegans*. *Molecules* 22, 1062.
55. Buckingham, M., and Rigby, P.W. (2014). Gene regulatory networks and transcriptional mechanisms that control myogenesis. *Dev. Cell* 28, 225–238.
56. Wang, S., Jin, J., Xu, Z., and Zuo, B. (2019). Functions and regulatory mechanisms of lncRNAs in skeletal myogenesis, muscle disease and meat production. *Cells* 8, 1107.
57. Luo, H., Lv, W., Tong, Q., Jin, J., Xu, Z., and Zuo, B. (2021). Functional non-coding RNA during embryonic myogenesis and postnatal muscle development and disease. *Front. Cell. Dev. Biol.* 9, 628339.
58. Wang, K.C., and Chang, H.Y. (2011). Molecular mechanisms of long noncoding RNAs. *Mol. Cell.* 43, 904–914.
59. Zurlo, F., Larson, K., Bogardus, C., and Ravussin, E. (1990). Skeletal muscle metabolism is a major determinant of resting energy expenditure. *J. Clin. Invest.* 86, 1423–1427.
60. Boengler, K., Kosiol, M., Mayr, M., Schulz, R., and Rohrbach, S. (2017). Mitochondria and ageing: role in heart, skeletal muscle and adipose tissue. *J. Cachexia Sarcopenia Muscle* 8, 349–369.
61. Boncompagni, S., Pozzer, D., Viscomi, C., Ferreira, A., and Zito, E. (2020). Physical and functional cross talk between endo-sarcoplasmic reticulum and mitochondria in skeletal muscle. *Antioxid. Redox Signal.* 32, 873–883.
62. Mizushima, N., Levine, B., Cuervo, A.M., and Klionsky, D.J. (2008). Autophagy fights disease through cellular self-digestion. *Nature* 451, 1069–1075.
63. Jokl, E.J., and Blanco, G. (2016). Disrupted autophagy undermines skeletal muscle adaptation and integrity. *Mamm. Genome* 27, 525–537.
64. Masiero, E., Agatea, L., Mammucari, C., Blaauw, B., Loro, E., Komatsu, M., Metzger, D., Reggiani, C., Schiaffino, S., and Sandri, M. (2009). Autophagy is required to maintain muscle mass. *Cell Metab.* 10, 507–515.


65. Shen, S., Liao, Q., Liu, J., Pan, R., Lee, S.M., and Lin, L. (2019). Myricanol rescues dexamethasone-induced muscle dysfunction via a sirtuin 1-dependent mechanism. *J. Cachexia Sarcopenia Muscle* 10, 429–444.
66. Cai, B., Ma, M., Chen, B., Li, Z., Abdalla, B.A., Nie, Q., and Zhang, X. (2018). MiR-16-5p targets SESN1 to regulate the p53 signaling pathway, affecting myoblast proliferation and apoptosis, and is involved in myoblast differentiation. *Cell Death Dis.* 9, 367.
67. Ding, L., Yang, X., Tian, H., Liang, J., Zhang, F., Wang, G., Wang, Y., Ding, M., Shui, G., and Huang, X. (2018). Seipin regulates lipid homeostasis by ensuring calcium-dependent mitochondrial metabolism. *EMBO J.* 37, e97572.

RESEARCH

Open Access



circPTPN4 regulates myogenesis via the miR-499-3p/NAMPT axis

Bolin Cai^{1,2}, Manting Ma^{1,2}, Zhen Zhou^{1,2}, Shaofen Kong^{1,2}, Jing Zhang^{1,2}, Xiquan Zhang^{1,2} and Qinghua Nie^{1,2*} 

Abstract

Background: Circular RNAs (circRNAs) are a novel class of endogenous ncRNA, which widely exist in the transcriptomes of different species and tissues. Recent studies indicate important roles for circRNAs in the regulation of gene expression by acting as competing endogenous RNAs (ceRNAs). However, the specific role of circRNAs in myogenesis is still poorly understood. In this study, we attempted to systematically identify the circRNAs involved in myogenesis and analyze the biological functions of circRNAs in chicken skeletal muscle development.

Results: In total, 532 circRNAs were identified as being differentially expressed between pectoralis major (PEM) and soleus (SOL) in 7-week-old Xinghua chicken. Among them, a novel circRNA (novel_circ_002621), generated by *PTPN4* gene, was named *circPTPN4* and identified. *circPTPN4* is highly expressed in skeletal muscle, and its expression level is upregulated during myoblast differentiation. *circPTPN4* facilitates the proliferation and differentiation of myoblast. Moreover, *circPTPN4* suppresses mitochondria biogenesis and activates fast-twitch muscle phenotype. Mechanistically, *circPTPN4* can function as a ceRNA to regulate *NAMPT* expression by sponging *miR-499-3p*, thus participating in AMPK signaling.

Conclusions: *circPTPN4* functions as a ceRNA to regulate *NAMPT* expression by sponging *miR-499-3p*, thus promoting the proliferation and differentiation of myoblast, as well as activating fast-twitch muscle phenotype.

Keywords: Chicken, *CircPTPN4*, Circular RNA, *MiR-499-3p*, Myogenesis, *NAMPT*, The transformation of myofiber

Background

Chicken is the second most consumed meat in China, and the meat production performance of chicken determines its commercial value. While increasing the yield, improving the quality of chicken is the direction that poultry breeders have been working hard on. Recently, it has come to light that the composition of myofiber types has an important relationship with muscle quality [1, 2]. The discovery of genetic regulatory factors involved in

skeletal muscle development is of great significance to chicken production.

Gene is the carrier of genetic information, carrying various biological processes of life. The product, such as peptide or protein molecules, plays a key role in it [3]. However, protein-encoding genes only account for a small portion (~2%) of the genome, while more than 98% of the genomic loci are transcribed to non-coding RNAs (ncRNAs) [4]. Skeletal muscle is the largest tissue in the body, which comprises about 40% of the total body mass. The development of skeletal muscle is closely related to growth and health, and is directly regulated by multiple genetic factors. Noticeably, recent studies have found that ncRNAs play critical roles in it [5, 6].

* Correspondence: nqinghua@scau.edu.cn

¹State Key Laboratory for Conservation and Utilization of Subtropical Agro-Bioresources, Lingnan Guangdong Laboratory of Agriculture, College of Animal Science, South China Agricultural University, Guangzhou 510642, Guangdong, China

²Guangdong Provincial Key Lab of Agro-Animal Genomics and Molecular Breeding, and Key Laboratory of Chicken Genetics, Breeding and Reproduction, Ministry of Agriculture, Guangzhou 510642, Guangdong, China



© The Author(s). 2022 **Open Access** This article is licensed under a Creative Commons Attribution 4.0 International License, which permits use, sharing, adaptation, distribution and reproduction in any medium or format, as long as you give appropriate credit to the original author(s) and the source, provide a link to the Creative Commons licence, and indicate if changes were made. The images or other third party material in this article are included in the article's Creative Commons licence, unless indicated otherwise in a credit line to the material. If material is not included in the article's Creative Commons licence and your intended use is not permitted by statutory regulation or exceeds the permitted use, you will need to obtain permission directly from the copyright holder. To view a copy of this licence, visit <http://creativecommons.org/licenses/by/4.0/>. The Creative Commons Public Domain Dedication waiver (<http://creativecommons.org/publicdomain/zero/1.0/>) applies to the data made available in this article, unless otherwise stated in a credit line to the data.

Circular RNAs (circRNAs) are a novel class of endogenous ncRNA with a covalently closed loop, which widely exist in the transcriptomes of different species and tissues [7, 8]. Compared with linear RNA (such as long noncoding RNA), circRNA has higher structural stability and conservation. It is becoming increasingly clear that circRNAs can widely be involved in a series of biological processes by acting as a miRNA sponge, participating in regulating the expression of its own linear RNA in different ways, coding protein, and deriving pseudogenes [9–12]. Although, more and more circRNAs have been found by high-throughput sequencing, the mechanism of circRNA regulation involved in skeletal muscle development is still poorly understood.

MicroRNAs (miRNAs) are endogenous noncoding single-stranded RNA molecules of 18–22 nt long that are capable of degrading or inhibiting target mRNAs by perfect or imperfect pairing with the 3' untranslated region (3' UTR) of the target mRNA to regulate post-transcriptional gene expression [13, 14]. Recent study has found that *miR-499-3p* could suppress retinal cell proliferation while promote apoptosis to induce diabetic retinopathy by enhancing activation of the TLR4 signaling pathway [15]. In pigs, the expression of *ssc-miR-499-3p* was significantly correlated to the expression of myoglobin and pH, prompting its potential regulatory role in skeletal muscle fiber transformation and meat quality traits [16]. However, the exact biological function of *miR-499-3p* in skeletal muscle development has not been reported yet.

Nicotinamide phosphoribosyltransferase (*NAMPT*) is the rate-limiting enzyme which catalyzes the conversion of nicotinamide and phosphoribosyl-pyrophosphates to nicotinamide mononucleotide in the mammalian nicotinamide adenine dinucleotide (NAD⁺) synthetic salvage pathway [17, 18]. Recently, numerous studies have indicated that *NAMPT* is able to modulate processes involved in the pathogenesis of obesity and related disorders by influencing the oxidative stress response, apoptosis, lipid and glucose metabolism, inflammation and insulin resistance [19]. But little is known about how *NAMPT* functions in skeletal muscle development.

In this study, to systematically identify the circRNAs involved in skeletal muscle development, pectoralis major (PEM) and soleus (SOL) in 7-week-old Xinghua chicken were used for circRNA sequencing (circRNA-seq). Based on this result, a novel circRNA (novel_circ_002621), generated by the *PTPN4* gene, was identified and named *circPTPN4*. *circPTPN4* is highly expressed in skeletal muscle, and its expression upregulates with myoblast differentiation. Functional studies demonstrated that *circPTPN4* promotes the proliferation and differentiation of myoblast, as well as activates the fast-twitch muscle phenotype. Furthermore, the mechanistic

investigation revealed that *circPTPN4* can function as a competing endogenous RNA (ceRNA) by sponging *miR-499-3p*, thus regulating the expression of *NAMPT* to mediate the AMPK signaling.

Methods

Ethics statement

All animal experimental protocols were conformed to “The Instructive Notions with Respect to Caring for Laboratory Animals” issued by the Ministry of Science and Technology of the People’s Republic of China, and approved by the Institutional Animal Care and Use Committee at the South China Agricultural University (approval ID: 2021-C018).

Animals and cells

Seven-week-old Xinghua female chickens were hatched from the Avian Farm of South China Agricultural University (Guangzhou, China). The chickens were euthanized, and organs and tissues were collected after rapid dissection, then immediately frozen in liquid nitrogen and stored at – 80 °C.

Chicken primary myoblasts (CPMs) were isolated from leg muscles of E11 (11-embryonic-day-old) chicken and cultured as previously described [20]. Firstly, the muscle tissues were dissected away from the skin and bone, and then homogenized in a petri dish. To release single cells, the suspension was digested with pancreatin for 20 min at 37 °C. After neutralization with complete medium, single cells were collected by centrifugation at 500 × g. Subsequently, serial plating was performed to enrich primary myoblasts and eliminate fibroblasts. Primary myoblasts were cultured in Roswell Park Memorial Institute (RPMI)-1640 medium (Gibco, MD, USA) with 20% FBS, 1% nonessential amino acids, and 0.2% penicillin/streptomycin. The purity of isolated primary myoblasts was verified by immunofluorescence (Fig. S1).

To induce myogenic differentiation, the growth medium was removed and replaced with differentiation medium (RPMI-1640 medium [Gibco, MD, USA] containing 2% horse serum) after myoblasts achieved 90% cell confluence.

Circular RNA sequencing (circRNA-seq)

The pectoralis major (PEM; which is mainly composed of fast-twitch fibers) and soleus (SOL; which has higher proportion of slow muscle fibers) of 7-week-old Xinghua chicken were used for circRNA-seq. After extraction, total RNAs were treated with RNase R to degrade the linear RNAs, and purified using RNeasy MinElute Cleanup Kit (Qiagen, Walldorf, Germany). Next, strand-specific library was constructed using VAHTS Total RNA-seq (H/M/R) Library Prep Kit for Illumina following the manufacturer’s instructions. Briefly, ribosome

RNAs were removed to retain circRNAs. The enriched circRNAs were fragmented into short fragments by using fragmentation buffer and reverse transcribed into cDNA with random primers. Second-strand cDNA were synthesized by DNA polymerase I, RNase H, dNTP (dUTP instead of dTTP) and buffer. Next, the cDNA fragments were purified with VAHTSTM DNA Clean Beads, end repaired, poly(A) added, and ligated to Illumina sequencing adapters. Then UNG (Uracil-N-Glycosylase) was used to digest the second-strand cDNA. The digested products were purified with VAHTSTM DNA Clean Beads, PCR amplified, and sequenced using Illumina HiSeq™ 2500 by Gene Denovo Biotechnology Co. (Guangzhou, China). The raw data of circRNA-seq were deposited in the Sequence Read Archive (SRA) database under accession no. PRJNA751251.

Parental genes of differentially expressed circRNAs were subjected to enrichment analysis of Gene Ontology (GO) functions and Kyoto Encyclopedia of Genes and Genomes (KEGG) pathways.

Validation of circRNA

The circRNAs were validated using PCR with divergent and convergent primers as previously described [21]. To confirm the junction sequence of circRNAs, PCR products of divergent primers were gel purified and submitted for Sanger sequencing at Tsingke Biotechnology Co., Ltd. (Beijing, China). To check the sensitivity of circRNA to RNase R, quantitative PCR was also performed using RNA samples with and without RNase R treatment. Primers used for the validation of circRNA are summarized in Table S1.

RNA extraction, cDNA synthesis, and quantitative real-time PCR

Total RNA was extracted by using the TRIzol reagent (TaKaRa, Otsu, Japan), following the manufacturer's protocol. Nuclear and cytoplasmic RNA fractionation was performed by using the Paris kit (Ambion, Life Technologies, Carlsbad, CA, USA) as recommended by the supplier. The PrimeScript RT Reagent Kit with gDNA Eraser (Perfect Real Time) (TaKaRa, Otsu, Japan) was used to synthesize cDNA. Quantitative real-time PCR was performed as described before [22]. And primers used for quantitative real-time PCR are listed in Table S1.

Plasmid construction and RNA oligonucleotides

For pGL3 luciferase reporter vectors construction, the active region of *PTPN4* gene promoter containing FOXA2 binding site and FOXA2 binding site mutant were amplified and cloned into the pGL3-Basic Vector (Promega, Madison, WI, USA) by using *XhoI* and *HindIII* restriction sites.

For *FOXA2* expression vectors construction, the coding sequence of *FOXA2* was amplified by PCR, and then subcloned into *HindIII* and *XhoI* restriction sites of the pcDNA3.1-3xFLAG-C vector or cloned into the expression plasmid pcDNA-3.1 (Promega, Madison, WI, USA) by using *HindIII* and *XhoI* restriction sites.

For *circPTPN4* overexpression vector construction, the linear sequence of *circPTPN4* was amplified and then subcloned into *EcoRI* and *BamHI* restriction sites of the pCD25-ciR vector (Genesee Biotech, Guangzhou, China) by using the Trelief™ SoSoo Cloning Kit (Tsingke Biotech, Beijing, China), following the manufacturer's protocol.

For pmirGLO dual-luciferase miRNA target reporter vector, the segment sequences of *circPTPN4* and *NAMP T* 3' untranslated region (UTR) that contained the putative *miR-499-3p* binding sequence were amplified by PCR, and then subcloned into *XhoI* and *Sall* restriction sites in the pmirGLO dual luciferase reporter vector (Promega, Madison, WI, USA). Mutant plasmids were generated by changing the binding site of *miR-499-3p* from GTGATGT to TGTCGTG.

miR-499-3p mimic, mimic negative control (NC), 3' end biotinylated *miR-499-3p* mimic, 3' end biotinylated mimic NC and small interfering RNA (siRNA) against *circPTPN4* were designed and synthesized by Guangzhou RiboBio (Guangzhou, China).

The primers and oligonucleotide sequences used in this study are listed in Tables S1 and S2.

Cell transfection

All transient transfections were performed with Lipofectamine 3000 reagent (Invitrogen, Carlsbad, CA, USA) according to manufacturer's directions.

Dual-luciferase reporter assay

Dual-luciferase reporter assays were performed as previously described [23, 24]. For promoter activity assay, the pGL3-basic vectors were co-transfected with pRL-TK as a control. Firefly and Renilla luciferase activities were measured at 48 h post-transfection using a Dual-GLO Luciferase Assay System Kit (Promega, Madison, WI, USA), following the manufacturer's instructions. Luminescence was measured by using a Fluorescence/Multi-Detection Microplate Reader (BioTek, Winooski, VT, USA) and firefly luciferase activities were normalized to Renilla luminescence in each well.

Chromatin immunoprecipitation (ChIP) assay

ChIP assay was performed by using the ChIP assay kit (Beyotime, Shanghai, China) as recommended by the supplier. Chromatin was immunoprecipitated with the DYKDDDDK Tag (D6W5B) rabbit monoclonal antibody (14,793, 1:50, Cell Signaling Technology, Inc., Boston,

USA). The relative quantity of the immunoprecipitated factor was calculated by qPCR.

5-Ethynyl-2'-deoxyuridine (EdU), flow cytometry, and cell counting kit-8 (CCK-8) assay

For the EdU assay, primary myoblasts seeded in 24-well plates were cultured to 50% density and then transfected. Forty-eight hours after transfection, the cells were fixed and stained with a C10310 EdU Apollo In Vitro Imaging Kit (RiboBio, China; 50 μ mol/L) as previously described [23]. A fluorescence microscope (DMi8; Leica, German) was used to capture three randomly selected fields to visualize the number of EdU-stained cells.

For the flow cytometry analysis of the cell cycle, myoblasts were seeded in 12-well plates. After 48 h transfection, the cultured cells in growth media were collected and fixed overnight in 70% ethanol at -20°C . Cells were analyzed by a BD AccuriC6 flow cytometer (BD Biosciences, San Jose, CA, USA) with the Cell Cycle Analysis Kit (Thermo Fisher Scientific, USA), and the data were processed using FlowJo software (7.6, Treestar Incorporated, Ashland, OR, USA).

For the CCK-8 assay, primary myoblasts were seeded in a 96-well plate and cultured in growth medium. After being transfected, the proliferation of the cell culture was monitored at 12 h, 24 h, 36 h, and 48 h using the TransDetect CCK (TransGen Biotech, Beijing, China) as recommended by the supplier. The data of absorbance at 450 nm were read by an iMark™ Microplate Absorbance Reader (Bio-Rad, California, USA).

Immunoblotting and immunofluorescence (IF)

Western blots were performed as previously described [20]. The primary antibodies used were anti-MyHC (B103, 0.5 μ g/mL, DHSB, Iowa City, IA, USA), anti-MYOD (ABP53067, 1:500, Abbkine, Wuhan, China), anti-MYH1A (F59, 0.5 μ g/mL, DHSB, Iowa City, IA, USA), anti-MYH7B (S58, 0.5 μ g/mL, DHSB, Iowa City, IA, USA), anti-NAMPT (bs-0272R, 1:500, Bioss, Beijing, China), anti-p-AMPK (ABN-PAB12602, 1:2000, Abnova, Taipei City, Taiwan, China), anti-AMPK (bs-1115R, 1:500, Bioss, Beijing, China), anti-PGC1 α (66369-1-Ig, 1:5000, Proteintech, IL, USA), and anti- β -Tubulin (A01030, 1:10,000, Abbkine, Wuhan, China). Protein-Find Goat Anti-Mouse IgG (H + L), HRP Conjugate (HS201-01, 1:1000, TransGen, Beijing, China) and Protein-Find Goat Anti-Rabbit IgG (H + L), HRP Conjugate (HS101-01, 1:500, TransGen, Beijing, China) were used as a secondary antibody.

Immunofluorescence were performed using anti-Desmin (bs-1026R, 1:100, Bioss, Beijing, China) and anti-MyHC (B103, 2.5 μ g/mL, DHSB, Iowa City, IA, USA), as previously described [20]. A fluorescence microscope (DMi8; Leica, Germany) was used to capture

three randomly selected fields to visualize the area labeled with anti-MyHC.

Mitochondrial DNA (mtDNA) content assay

Total DNA was extracted by using the Tissue DNA Kit (D3396, Omega, GA, USA) according to the manufacturer's instructions. The amount of mitochondrial DNA was determined by quantification of cytochrome c oxidase subunit II (*COX2*). The nuclear-encoded β -globin gene was used as internal controls. Primers used in this study can be found in the Table S1.

Mitochondrial membrane potential and reactive oxygen species (ROS) concentration assay

Mitochondrial membrane potential and ROS concentration were measured using the mitochondrial membrane potential assay kit with JC-1 (C2006, Beyotime, Shanghai, China) and reactive oxygen species assay kit (S0033S, Beyotime, Shanghai, China), according to the manufacturer's instructions.

Enzyme activities assays

The glycolytic capacity of myoblast was evaluated by the activity of lactic dehydrogenase (LDH), while the oxidative capacity of myoblast was evaluated by the activity of succinate dehydrogenase (SDH). Enzyme activities were measured by commercial assay kits (BC0685 and BC0955) that were purchased from Beijing Solarbio Science & Technology.

Biotin-coupled miRNA pull down assay

The 3' end biotinylated *miR-499-3p* mimic and mimic NC were transfected into CPMs in T75 cell culture bottle. At 48 h after transfection, the cells were harvested and then lysed in lysis buffer. The biotin-coupled RNA complex was pull down, and then isolated as previously described [25]. The abundance of *circPTPN4* and *NAMPT* in bound fractions was evaluated by quantitative PCR.

Statistical analysis

In this study, all experiments were repeated at least three times, and results were represented as mean \pm SEM. Where applicable, the statistical significance of the data was tested using independent sample *t*-test or ANOVA followed by Dunnett's test. The types of tests and the *P*-values, when applicable, are indicated in the figure legends.

Results

Characterization of circRNAs in fast-twitch and slow-twitch myofiber

In poultry, breast muscle is generally considered to be composed of fast-twitch myofibers, while the leg muscle has a higher proportion of slow-twitch fibers

[24, 26]. To systematically identify circRNAs involved in skeletal muscle development, we performed a circRNA-seq to analyze differentially expressed circRNAs between PEM (which is mainly composed of fast-twitch fibers) and SOL (which has higher proportion of slow muscle fibers) in 7-week-old Xinghua chicken. A total of 8882 circRNAs were detected,

which were mainly (more than 85%) distributed among chromosomes 1 to 15, and W (Fig. 1A). According to their genomic locus, we found most of them (~75%) originate from coding exon (Fig. 1B). The length distribution of those circRNAs is relatively concentrated, with most in the range of 0–2000 nt (Fig. 1C).

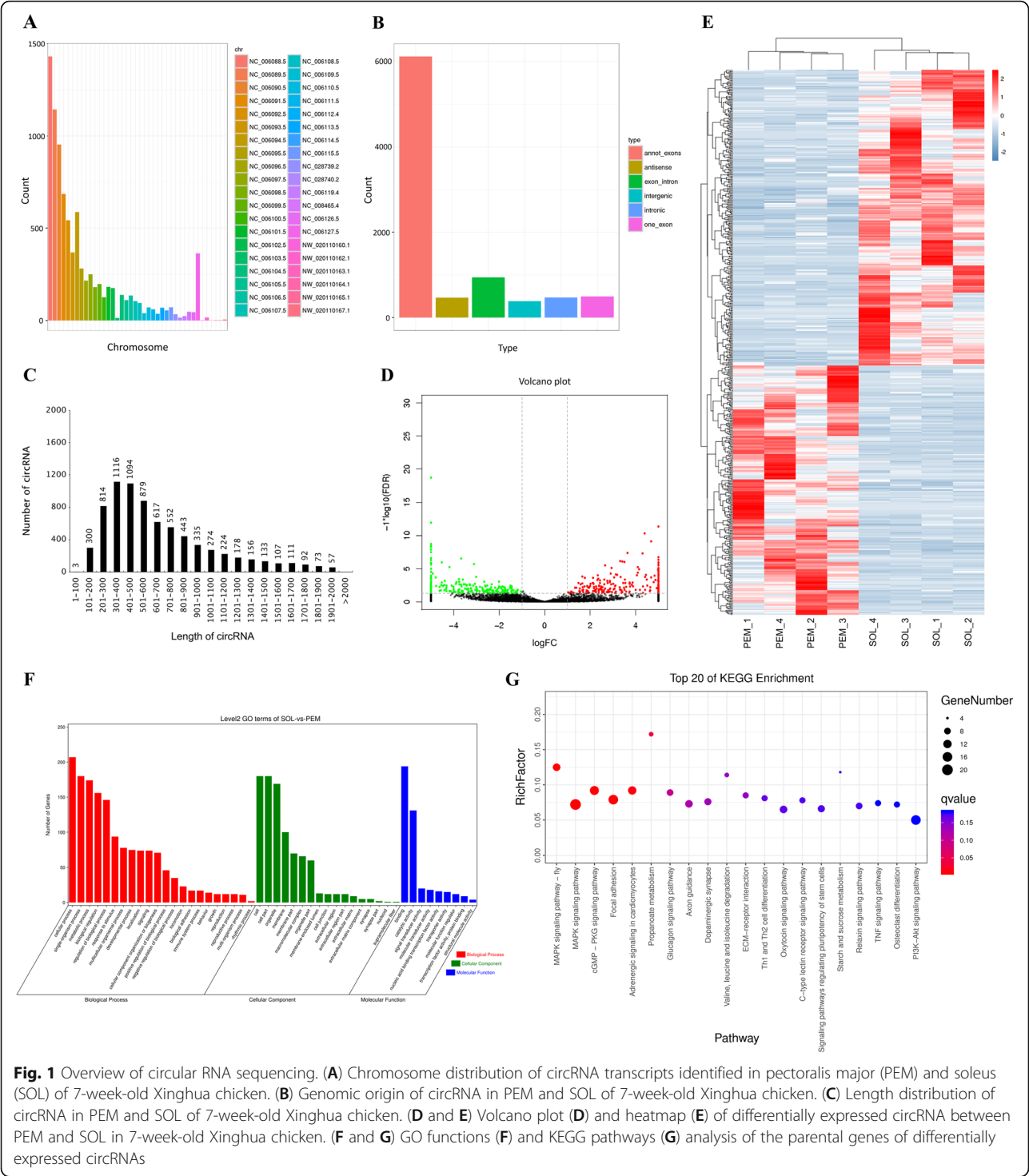


Fig. 1 Overview of circular RNA sequencing. **(A)** Chromosome distribution of circRNA transcripts identified in pectoralis major (PEM) and soleus (SOL) of 7-week-old Xinghua chicken. **(B)** Genomic origin of circRNA in PEM and SOL of 7-week-old Xinghua chicken. **(C)** Length distribution of circRNA in PEM and SOL of 7-week-old Xinghua chicken. **(D and E)** Volcano plot **(D)** and heatmap **(E)** of differentially expressed circRNA between PEM and SOL in 7-week-old Xinghua chicken. **(F and G)** GO functions **(F)** and KEGG pathways **(G)** analysis of the parental genes of differentially expressed circRNAs

In total, 532 circRNAs were identified as being differentially expressed between PEM and SOL in 7-week-old Xinghua chicken ($P < 0.05$; $|\log_2FC| > 1$) (Table S3). Among the differentially expressed circRNAs, 243

showed upregulation in PEM, while 289 were increased in SOL (Fig. 1D and E; Table S3). Recent studies have found that the biogenesis of circRNA can competes with pre-mRNA splicing, and intron or exon-intron circRNAs

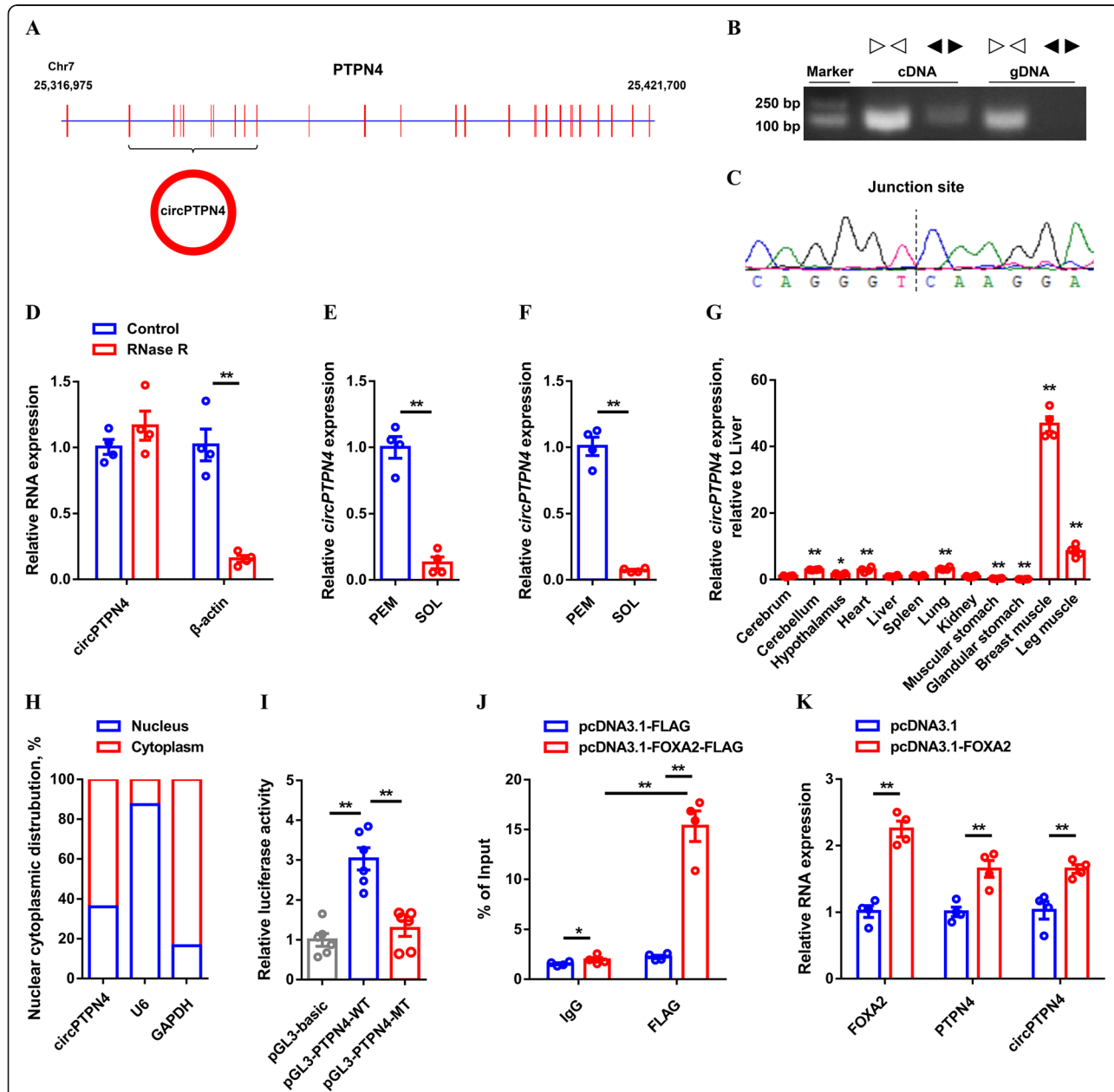
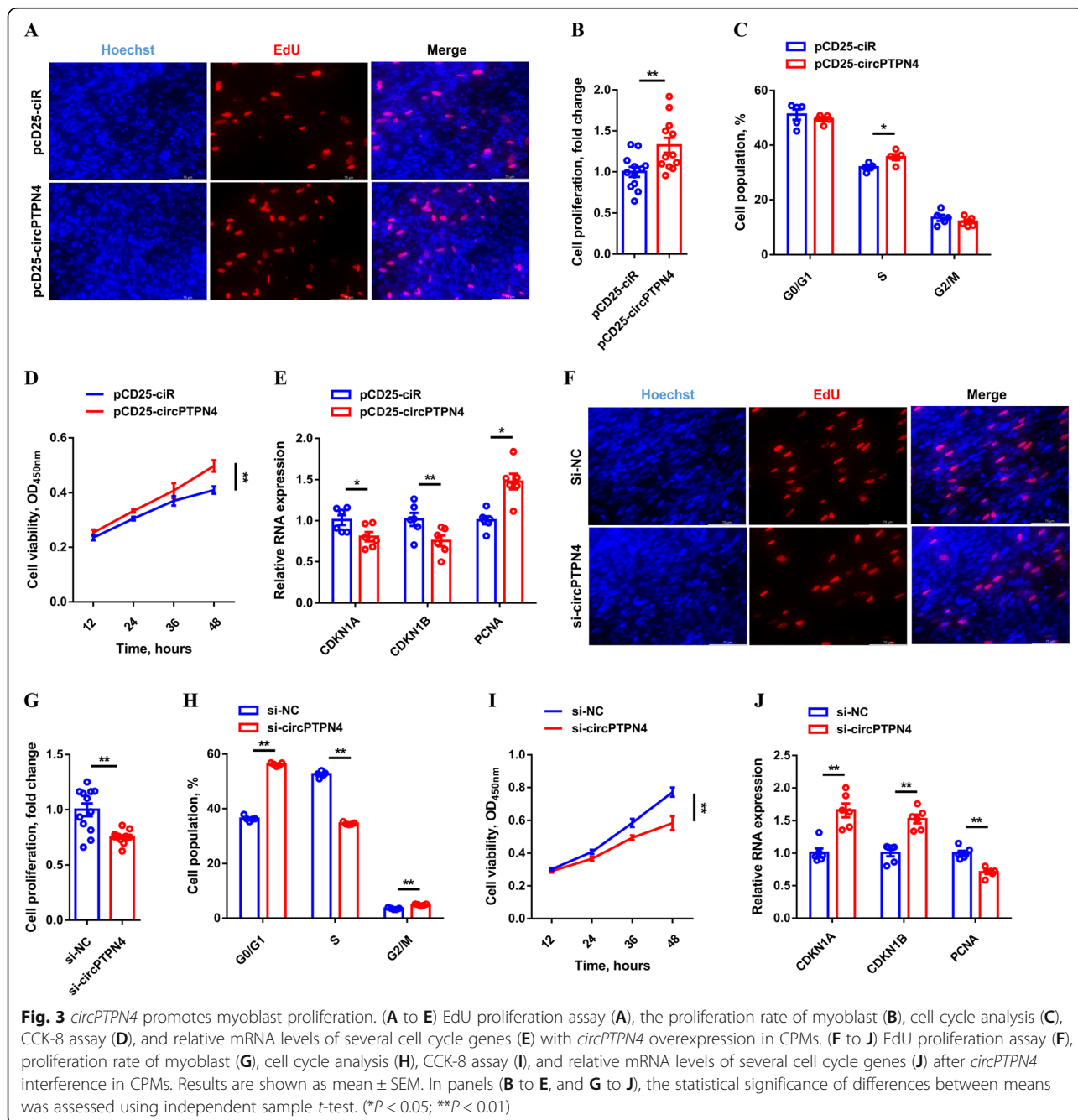


Fig. 2 Identification of *circPTPN4*. **(A)** Schematic image of *circPTPN4* derived from *PTPN4*. **(B)** Verification of *circPTPN4* by amplifying with divergent primers. **(C)** Sanger sequencing confirmed the back-splicing junction sequence of *circPTPN4*. **(D)** Relative *circPTPN4* and β -actin expression after treatment with RNase R. **(E and F)** Relative *circPTPN4* expression in pectoralis major (PEM) and soleus (SOL) of 7-week-old Xinghua chicken detected by RNA-seq **(E)** and qPCR **(F)**. **(G)** Tissue expression profiles of *circPTPN4*. The horizontal axis and vertical axis indicate different tissues and their relative expression values, respectively. **(H)** The distribution of *circPTPN4* in the cytoplasm and nuclei of chicken primary myoblast (CPM) was determined by qRT-PCR. GAPDH and U6 serve as cytoplasmic and nuclear localization controls, respectively. **(I)** The transcriptional activity of the *PTPN4* core promoter region. **(J)** Chromatin immunoprecipitation (ChIP) analysis of the binding capacity of FOXA2 to the *PTPN4* core promoter region. **(K)** Relative FOXA2, *circPTPN4* and *circPTPN4* expression with FOXA2 overexpression. Results are presented as mean \pm SEM. In panels **(D to H, and K)**, the statistical significance of differences between means was assessed using paired *t*-tests. In panels **(I and J)**, ANOVA followed by Dunnett's test was used. (* $P < 0.05$; ** $P < 0.01$)

can regulate the transcription of their parental gene [27–29]. Next, Gene Ontology (GO) and Kyoto Encyclopedia of Genes and Genomes (KEGG) enrichment analyses were performed for the parental genes of differentially expressed circRNAs. The results showed that these genes were mainly enriched in biological processes such as cellular process, metabolic process, and biological regulation, as well as participated in skeletal muscle development related pathways including MAPK signaling pathway, cGMP-PKG signaling pathway, PI3K-Akt signaling pathway, and so on (Fig. 1F and G).

circPTPN4 is a novel circRNA regulated by *FOXA2*

To further elucidate the regulation mechanism of circRNA involved in skeletal muscle development, a novel differentially expressed circRNA, *circPTPN4* (novel_circ_002621; which was derived from exon 2–10 of *PTPN4*, highly conserved in *Meleagris gallopavo*, *Numida meleagris* and *Anser cygnoides*) (Fig. 2A and S2; Table S4), was served as a candidate. Firstly, genomic DNA (gDNA) and cDNA were used for the PCR reaction with convergent and divergent primers to confirm the sequence and the junction of *circPTPN4*. A single distinct band with



the expected product size was only observed in cDNA samples (Fig. 2B), and the real existence was detected by Sanger sequencing (Fig. 2C). These results suggested that the presence of back-splicing junctions but not genomic rearrangement. Moreover, the RNase R tolerance test showed *circPTPN4* has more resistance than the linear mRNA control (Fig. 2D), which confirmed that *circPTPN4* is a real circRNA. Our circRNA-seq data showed *circPTPN4* was differentially expressed between PEM and SOL in 7-week-old Xinghua chicken (Fig. 2E). Similarly, the consistent result was found by quantitative PCR (qPCR) (Fig. 2F). *circPTPN4* was highly expressed in breast and leg muscle (Fig. 2G), implying that it may play an important role in skeletal muscle development.

In addition, cell-fractionation assays demonstrated that *circPTPN4* is mainly present in the cytoplasm of chicken primary myoblast (CPM) (Fig. 2H).

To explore the mechanism through which *circPTPN4* is regulated at the transcriptional level, we further analyzed the core promoter region of *PTPN4* (which is the parental gene of *circPTPN4*), and found a potential binding site for FOXA2 (−241 to −228 bp). Dual-luciferase reporter assay confirmed that the mutation of this site leads to a decrease of the transcriptional activity (Fig. 2I and S3A), while the transcriptional activity was increased with *FOXA2* overexpression (Fig. S3B). Moreover, results of a chromatin immunoprecipitation (ChIP) assay confirmed that FOXA2 could physically bind to the core

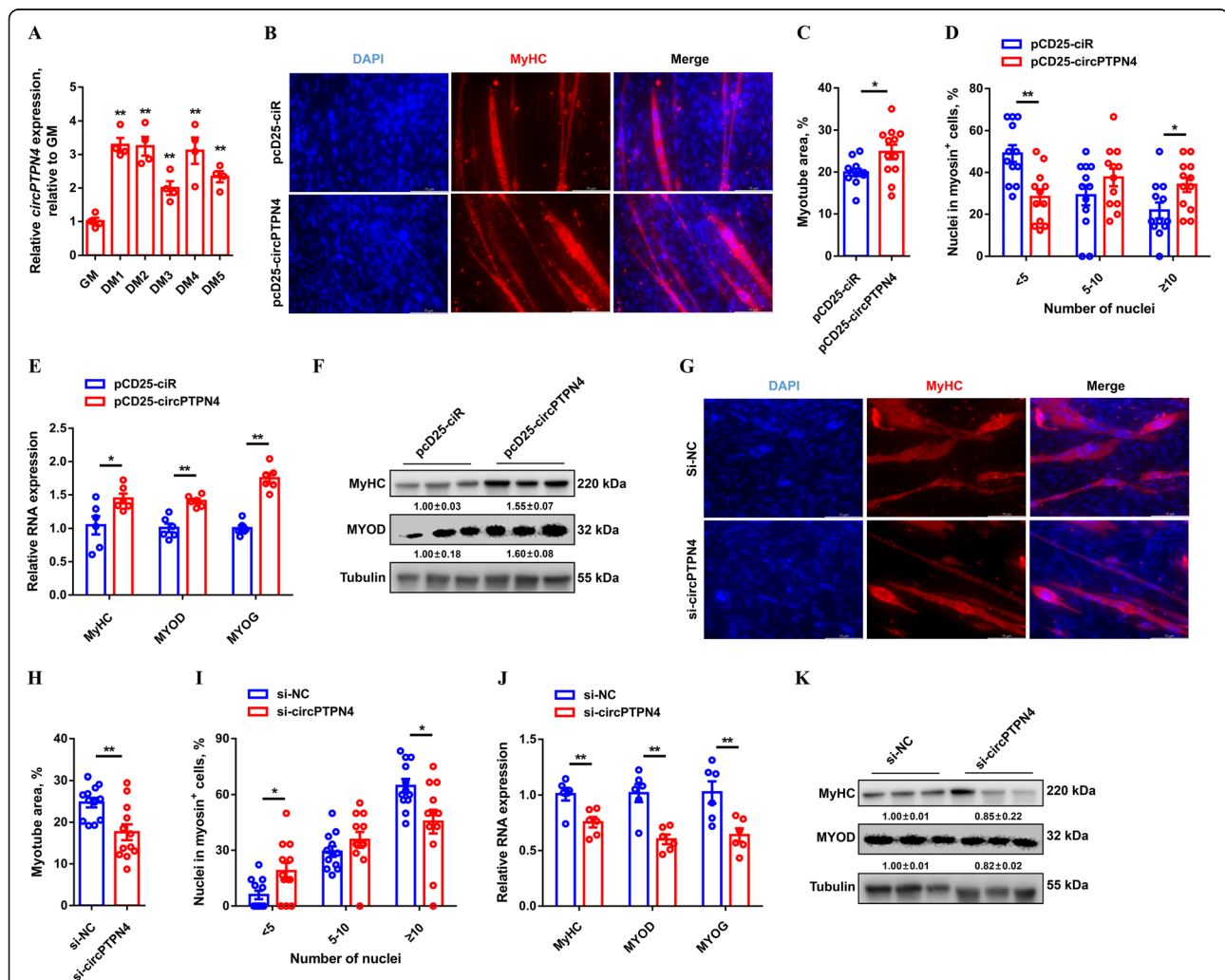


Fig. 4 *circPTPN4* induces myogenetic differentiation. (A) Relative *circPTPN4* expression during CPM differentiation. (B to F) MyHC immunostaining (B), myotube area (C), myoblast fusion index (D) and relative mRNA (E) and protein (F) expression levels of myoblast differentiation marker genes after overexpression of *circPTPN4*. (G to K) MyHC immunostaining (G), myotube area (H), myoblast fusion index (I) and relative mRNA (J) and protein (K) expression levels of myoblast differentiation marker genes with *circPTPN4* inhibition. In panels (F and K), the numbers shown below the bands were folds of band intensities relative to control. Band intensities were quantified by ImageJ and normalized to β -Tubulin. Data are expressed as a fold-change relative to the control. Results are shown as mean \pm SEM. In panels (A, C to E, and H to J), the statistical significance of differences between means was assessed using independent sample *t*-test. (**P* < 0.05; ***P* < 0.01)

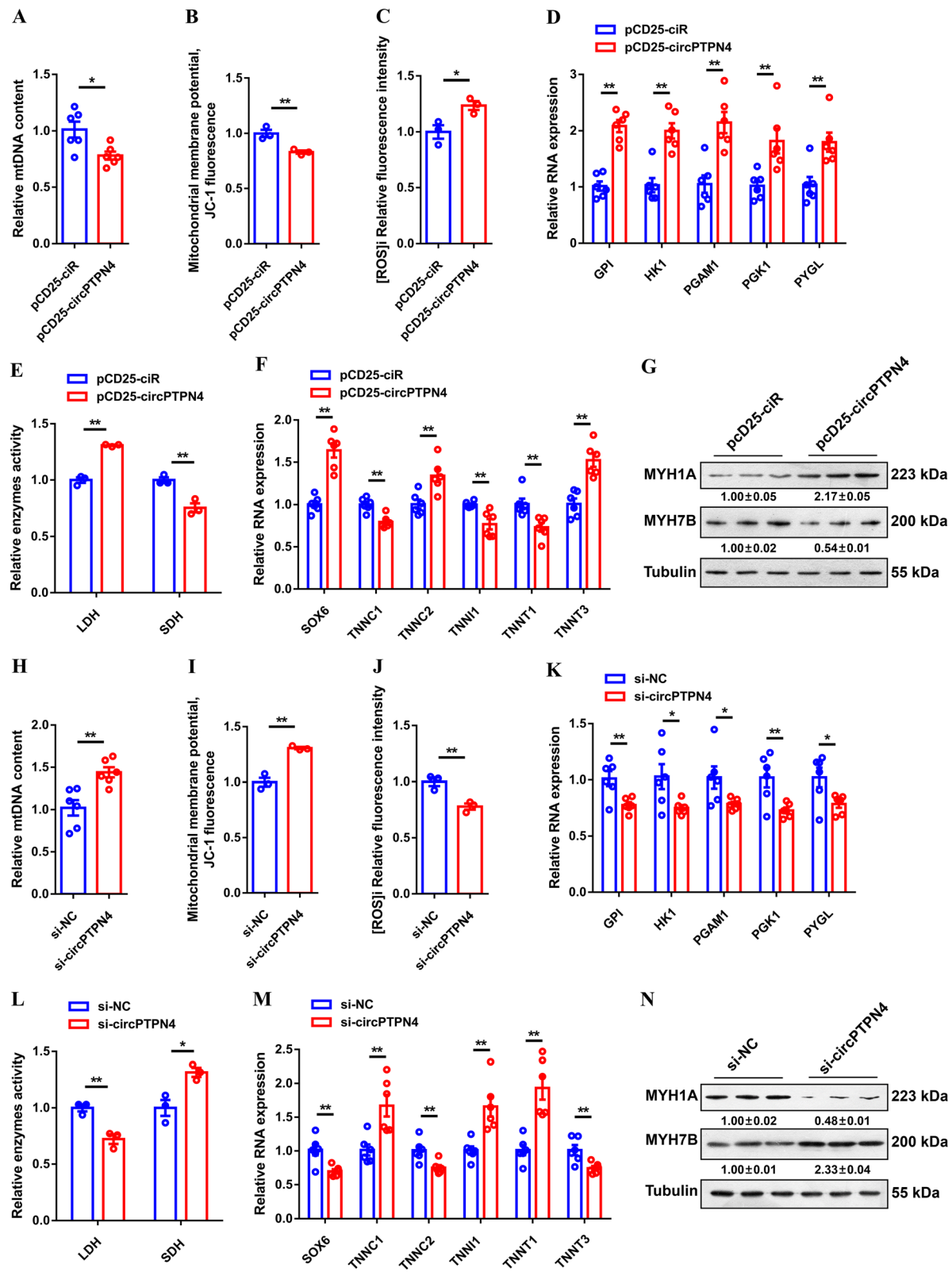


Fig. 5 (See legend on next page.)

(See figure on previous page.)

Fig. 5 *circPTPN4* represses mitochondria biogenesis and drives the transformation of slow-twitch to fast-twitch myofiber. (**A** to **G**) Relative mitochondrial DNA (mtDNA) content (**A**), mitochondrial membrane potential (**B**), reactive oxygen species (ROS) production (**C**), relative mRNA expression levels of glycogenolytic and glycolytic genes (**D**), relative enzymes activity of lactic dehydrogenase (LDH) and succinate dehydrogenase (SDH) (**E**), relative mRNA expression levels of several fast-/slow-twitch myofiber genes (**F**), and relative protein expression of MYH1A and MYH7B (**G**) in *circPTPN4* overexpression CPMs. (**H** to **N**) Relative mtDNA content (**H**), mitochondrial membrane potential (**I**), ROS production (**J**), relative mRNA expression levels of glycogenolytic and glycolytic genes (**K**), relative enzymes activity of LDH and SDH (**L**), relative mRNA expression levels of several fast-/slow-twitch myofiber genes (**M**), and relative protein expression of MYH1A and MYH7B (**N**) in CPMs with *circPTPN4* interference. In panels (**G** and **N**), the numbers shown below the bands were folds of band intensities relative to control. Band intensities were quantified by ImageJ and normalized to β -Tubulin. Data are expressed as a fold-change relative to the control. In all panels, results are shown as mean \pm SEM, the statistical significance of differences between means was assessed using independent sample *t*-test. (* $P < 0.05$; ** $P < 0.01$)

promoter of *PTPN4* (Fig. 2J). Overexpression of *FOXA2* upregulated the expression of *PTPN4* and *circPTPN4* (Fig. 2K). Collectively, these data revealed that *circPTPN4* is positively regulated by the *FOXA2*.

circPTPN4 facilitates the proliferation and differentiation of myoblast

In order to assess the function of *circPTPN4* in myogenesis, the overexpression vector of *circPTPN4* was constructed and transfected into CPM (Fig. S4A). The 5-ethynyl-2'-deoxyuridine (EdU) staining demonstrated that *circPTPN4* overexpression significantly increased EdU incorporation and promoted myoblast proliferation (Fig. 3A and B). Flow cytometric analysis and cell counting kit-8 (CCK-8) assay also showed that overexpression of *circPTPN4* significantly increased the number of S phase cells (Fig. 3C), and improved myoblast viability (Fig. 3D). Furthermore, *circPTPN4* overexpression repressed the expression level of cell cycle-inhibiting genes, including *CDKN1A* and *CDKN1B*, while increasing the expression level of cell cycle-promoting genes like *PCNA* (Fig. 3E). Conversely, the opposite result was observed by *circPTPN4* interference (Fig. 3F to J, and S4B), indicating that *circPTPN4* can facilitate myoblast proliferation.

circPTPN4 expression was upregulated with myogenic differentiation (Fig. 4A), which suggested that *circPTPN4* may be involved in the process of myoblast differentiation. To further investigate the potential function of *circPTPN4*, immunofluorescence staining was performed. Immunofluorescence staining showed that overexpression of *circPTPN4* increased the total areas of myotubes and induced myotube formation (Fig. 4B to D). In addition, the expressions level of myoblast differentiation marker genes, including *MyHC*, *MYOD*, and *MYOG* were significantly upregulated with *circPTPN4* overexpression (Fig. 4E and F). On the contrary, *circPTPN4* interference decreased the total areas of myotubes and inhibited myoblast fusion, as well as downregulated the expression of myoblast differentiation marker genes (Fig. 4G to K).

circPTPN4 suppresses mitochondria biogenesis and activates fast-twitch muscle phenotype

Skeletal muscle is a major player in regulating energy homeostasis [30, 31]. As the main organelle of energy metabolism, mitochondria are closely related to the development of skeletal muscle [32, 33]. Next, we evaluated mitochondrial content and function after overexpression and inhibition of *circPTPN4*. *circPTPN4* overexpression decreased mitochondrial DNA (mtDNA) content and was accompanied by a decline of mitochondrial membrane potential (Fig. 5A and B). Meanwhile, reactive oxygen species (ROS) production was significantly increased after *circPTPN4* overexpression (Fig. 5C). Inversely, *circPTPN4* inhibition increased mitochondrial content and enhanced mitochondrial function (Fig. 5H to J), illustrating that *circPTPN4* suppresses mitochondria biogenesis.

Skeletal muscle is comprised of heterogeneous myofibers that differ in their physiological and metabolic parameters [34]. Compared with slow-twitch (type I; oxidative) myofibers, fast-twitch (type II; glycolytic) myofibers have fewer mitochondria and higher activity of glycolytic metabolic enzymes [35, 36]. Given that *circPTPN4* is highly expressed in fast-twitch myofiber and repressed mitochondria biogenesis, we speculated that *circPTPN4* may function in the activation of fast-twitch muscle phenotype. As expected, overexpression of *circPTPN4* upregulated the expression of glycogenolytic and glycolytic genes (Fig. 5D). The activity of lactate dehydrogenase (LDH) was enhanced, while the activity of succinate dehydrogenase (SDH) was suppressed with *circPTPN4* overexpression (Fig. 5E). *circPTPN4* overexpression upregulated expressions of multiple fast-twitch myofiber genes like *SOX6*, *TNNC2* and *TNNT3*, while suppressed slow-twitch myofiber genes such as *TNNC1*, *TNNI1* and *TNNT1* (Fig. 5F). More importantly, western blot results showed that overexpression of *circPTPN4* promoted MYH1A/fast-twitch protein level and suppressed the expression level of MYH7B/slow-twitch protein (Fig. 5G). On the contrary, the glycolytic capacity of skeletal muscle was suppressed and

the slow-twitch muscle phenotype was induced with *circPTPN4* interference (Fig. 5K to N).

circPTPN4 interacts with *miR-499-3p* to upregulate *NAMPT* expression, thus inactivating AMPK signaling

In 2011, competitive endogenous RNAs (ceRNAs) were first reported as endogenous sponges that can affect the distribution of miRNAs on their targets, thereby imposing another novel layer of posttranscriptional regulation

[37]. Given that *circPTPN4* is mainly present in the cytoplasm, we hypothesized that *circPTPN4* may function as a ceRNA to exert its biological function. The target miRNAs and genes of *circPTPN4* were predicted on an RNAhybrid software. Interestingly, *miR-499-3p* was found to contain potential binding sites for both *circPTPN4* and *NAMPT* (Fig. 6A), suggesting that it may mediate the regulation of *NAMPT* expression by *circPTPN4*. Compared with PEM, the expression of *miR-*

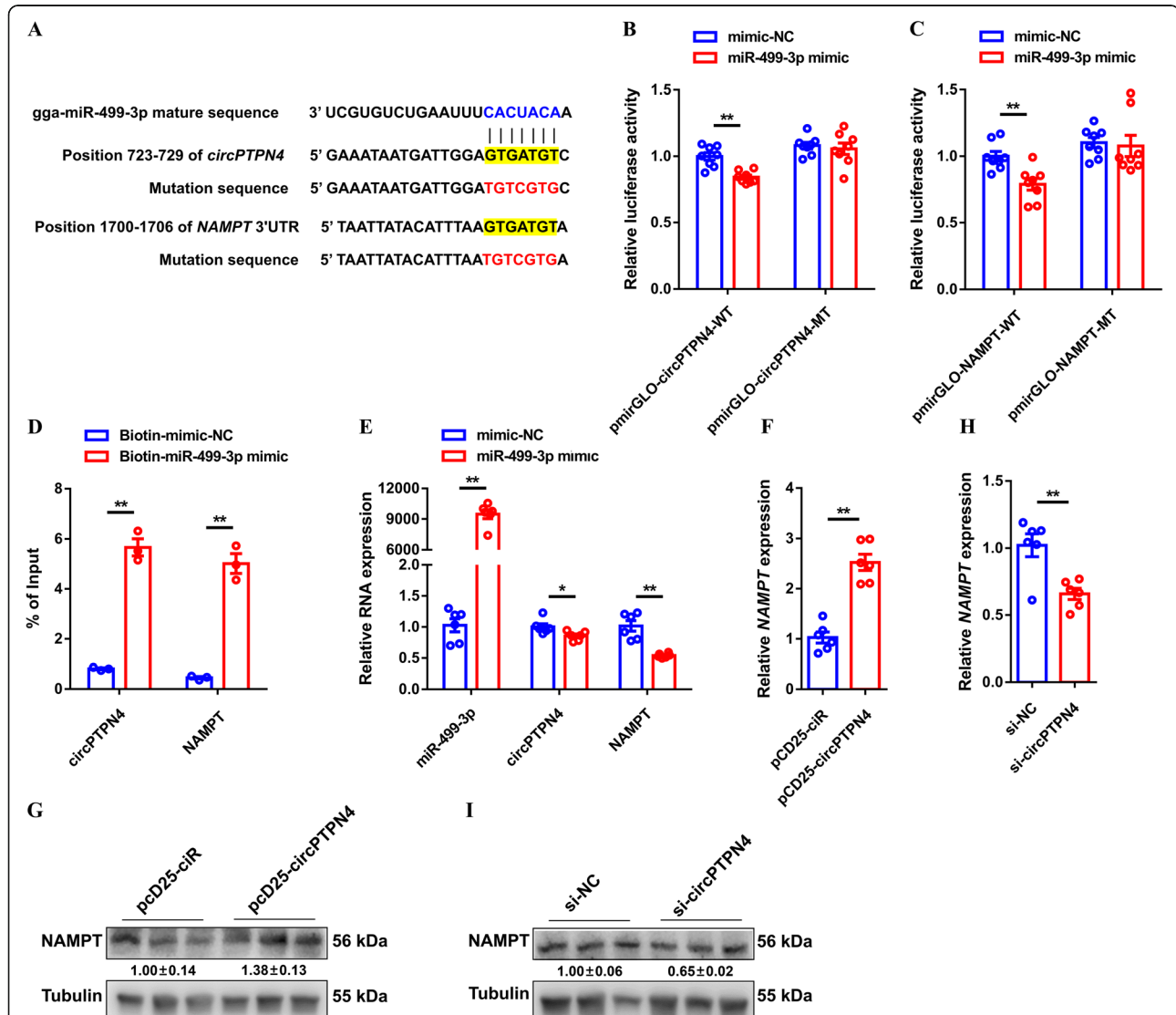
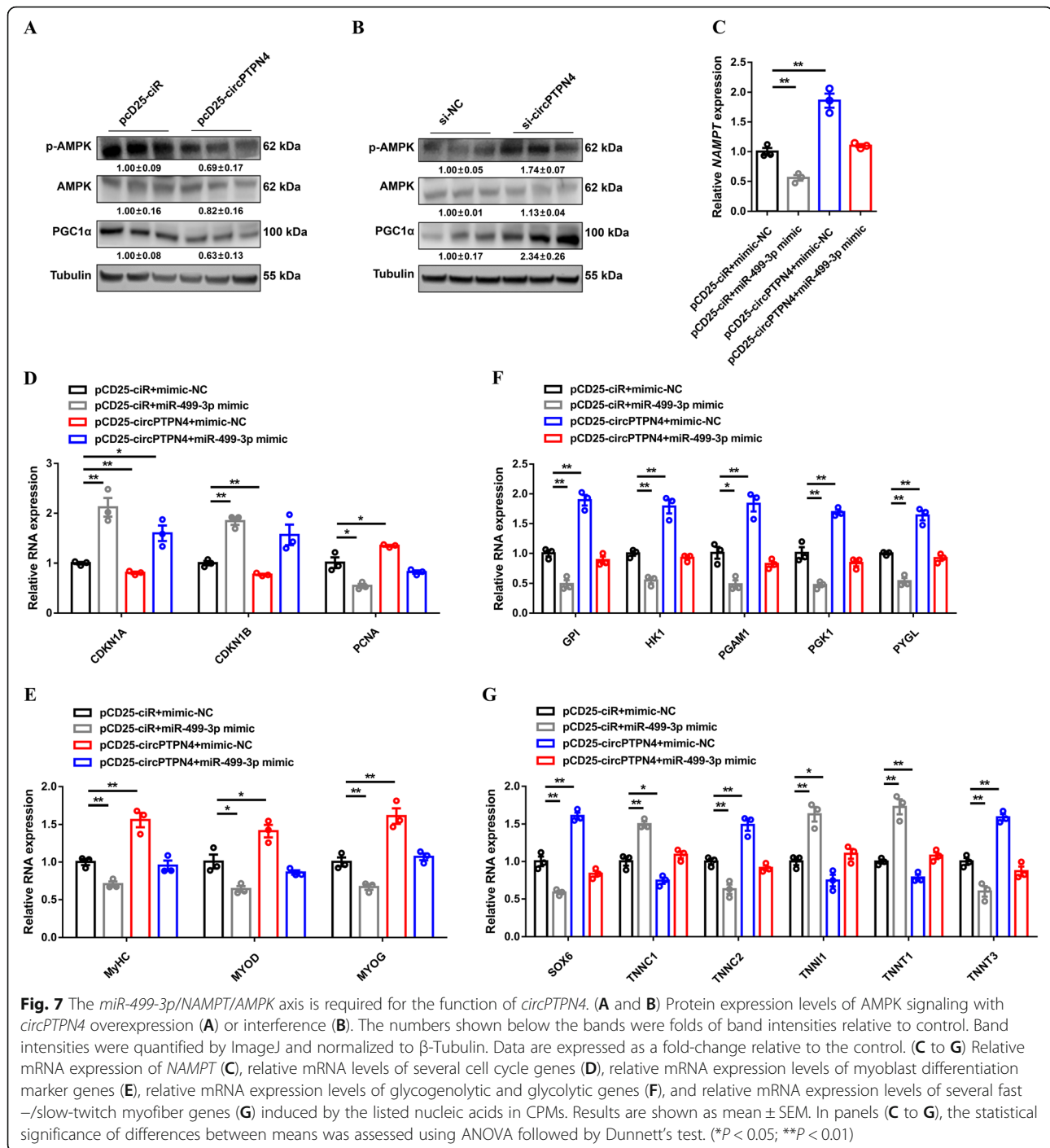


Fig. 6 *circPTPN4* functions as a competing endogenous RNA (ceRNA) to regulate *NAMPT* expression by sponging *miR-499-3p*. **(A)** The potential binding site of *miR-499-3p* in *circPTPN4* transcript and *NAMPT* 3' untranslated region (UTR). The mutant sequence in *miR-499-3p* binding site is highlighted in red. **(B and C)** Dual-luciferase reporter assay was conducted by co-transfecting the wild type or mutant: **(B)** *circPTPN4* and **(C)** *NAMPT* 3' UTR with a *miR-499-3p* mimic or mimic-negative control (NC). **(D)** The interaction of *miR-499-3p* with *circPTPN4* and *NAMPT* was determined by biotin-coupled miRNA pull down. **(E)** Relative *miR-499-3p*, *circPTPN4*, and *NAMPT* expression after overexpression of *miR-499-3p*. **(F and G)** Relative mRNA **(F)** and protein **(G)** expression levels of *NAMPT* with *circPTPN4* overexpression. **(H and I)** Relative mRNA **(H)** and protein **(I)** expression levels of *NAMPT* after *circPTPN4* interference. In panels **(G and I)**, the numbers shown below the bands were folds of band intensities relative to control. Band intensities were quantified by ImageJ and normalized to β -Tubulin. Data are expressed as a fold-change relative to the control. Results are presented as mean \pm SEM. In panels **(B to H)**, the statistical significance of differences between means was assessed using independent sample *t*-test. (**P* < 0.05; ***P* < 0.01)



499-3p is higher in SOL (Fig. S5A). In contrast, *NAMPT* is highly expressed in PEM (Fig. S5B), which is consistent with *circPTPN4*, further hinting that the interaction of *circPTPN4* with *miR-499-3p* and *NAMPT*. Dual-luciferase reporter assays were carried out to confirm whether *miR-499-3p* directly interact with *circPTPN4* and *NAMPT*. The results showed that *miR-499-3p* bind with both *circPTPN4* and the 3' UTR of *NAMPT* (Fig. 6B to C). Furthermore, the interaction of *miR-499-3p*

with *circPTPN4* and *NAMPT* was also verified by a biotin-coupled miRNA pull down assay (Fig. 6D). Overexpression of *miR-499-3p* repressed the expression of *circPTPN4* and *NAMPT* (Fig. 6E). More importantly, *circPTPN4* overexpression upregulated the mRNA and protein levels of *NAMPT*, whereas the expression of *NAMPT* was suppressed with *circPTPN4* interference (Fig. 6F-I), explaining the targeted regulation of *circPTPN4* on *NAMPT*.

Previous studies have shown that *NAMPT* is widely involved in a series of biological processes by inactivating AMPK signaling [38–40]. We further assessed the AMPK signaling and found that *circPTPN4* overexpression inhibited the phosphorylation of AMPK and down-regulated the expression of PGC1 α (Fig. 7A). Conversely, this pathway was activated with the interference of *circPTPN4* (Fig. 7B), suggesting that *circPTPN4* may participate in AMPK signaling by regulating *NAMPT*. Overexpression of *circPTPN4* alleviated the inhibitory effect of *miR-499-3p* on *NAMPT* expression (Fig. 7C). In addition, the regulatory effects of *circPTPN4* were weakened after *miR-499-3p* overexpression (Fig. 7D to G), indicating that the *miR-499-3p*/*NAMPT*/AMPK axis is required for the function of *circPTPN4*.

Discussion

Due to the low quantity and expressive abundance, circRNAs were once considered to be an abnormal splicing product of RNA or unique structure of pathogens, with less attention [41, 42]. However, recent studies have found that circRNA is universally present in archaea, suggesting that it may have important biological functions [43]. With the development of genome research, more and more circRNAs are found in various cells and tissues, which are widely present in eukaryotes [44–47]. In this study, a total of 532 circRNAs were identified as being differentially expressed between PEM and SOL in 7-week-old Xinghua chicken. Among them, a novel differentially expressed circRNA, *circPTPN4*, was served as a candidate. *circPTPN4* is highly expressed in fast-twitch myofiber, and its expression upregulates with myoblast differentiation, suggesting that it may play a significant role in skeletal muscle development.

Myogenesis is a process including myoblast proliferation, differentiation and myotube formation and is controlled by a series of myogenic regulatory factors. These factors can regulate myoblasts to withdraw from the cell cycle, express muscle-specific genes, and prevent the expression of other cell- or tissue-specific genes. Recently, it is worth noting that circRNAs have also been demonstrated to function in myogenesis [48–51]. Here, we found that *circPTPN4* promotes myoblast proliferation and induces myogenic differentiation.

Skeletal muscle is composed of different types of myofibers. Under certain conditions, different types of myofibers can be transformed. Previous studies have found that a total of 305 circRNAs were differentially expressed between the oxidative muscle sartorius compared and the glycolytic muscle pectoralis major in Chinese Qingyuan partridge chickens. Among them, *novel_circ_004282* and *novel_circ_002121* were speculated to play important roles in regulating oxidative myofibers by *PPP3CA* and *NFATC1* expression [52]. As a

transcriptional coactivator, PGC1 α is a downstream effector of AMPK signaling, has been found to regulate mitochondria biogenesis and the transformation of myofiber type [53–55]. In the current study, we found that *circPTPN4* decreases mtDNA content and suppresses mitochondria functions. Moreover, *circPTPN4* improves the glycolytic capacity of myoblast to activate fast-twitch muscle phenotype, demonstrating that *circPTPN4* is involved in the transformation of myofiber type by inactivating AMPK signaling.

Recently, a new pattern of gene expression has been come up with regarding the interaction of RNA transcripts, called ceRNA [37]. There is a great deal of researches indicated that circRNAs can function as ceRNAs to protect mRNAs by acting as molecular sponges for miRNAs, thereby modulating the depression of miRNA targets and imposing an additional level of post-transcriptional regulation [46, 49, 50]. In this study, using in silico analysis, we found *miR-499-3p* contains binding sites for *circPTPN4* and *NAMPT*. The interaction of *miR-499-3p* with *circPTPN4* and *NAMPT* was further validated by dual-luciferase reporter assay and biotin-coupled miRNA pull down assay. *circPTPN4*

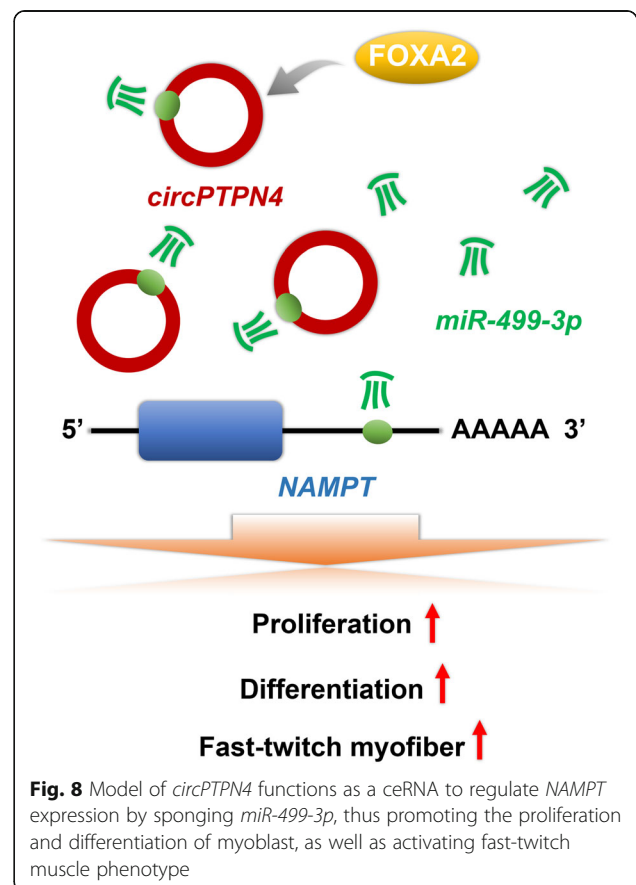


Fig. 8 Model of *circPTPN4* functions as a ceRNA to regulate *NAMPT* expression by sponging *miR-499-3p*, thus promoting the proliferation and differentiation of myoblast, as well as activating fast-twitch muscle phenotype

regulates *NAMPT* expression to function in AMPK signaling. In addition, our rescue experiment showed that the biological functions of *circPTPN4* were weakened with *miR-499-3p* overexpression, explaining that the *miR-499-3p/NAMPT* axis is required for the function of *circPTPN4*.

Conclusions

In conclusion, we demonstrated that *circPTPN4* is a novel circRNA, which is highly expressed in fast-twitch myofiber and is positively regulated by transcription factor FOXA2. Mechanistically, *circPTPN4* can function as a ceRNA to regulate *NAMPT* expression by sponging *miR-499-3p*, thus promoting the proliferation and differentiation of myoblast, as well as activating fast-twitch muscle phenotype (Fig. 8). Our findings provide a solid foundation for the understanding of the mechanisms and regulatory networks of myogenesis, and will contribute to the development of further research.

Abbreviations

CCK-8: Cell counting kit-8; ceRNA: Competing endogenous RNA; ChIP: Chromatin immunoprecipitation; circRNA: Circular RNA; CPMs: Chicken primary myoblasts; EdU: 5-Ethynyl-2'-deoxyuridine; gDNA: Genomic DNA; GO: Gene Ontology; IF: Immunofluorescence; KEGG: Kyoto Encyclopedia of Genes and Genomes; LDH: Lactic dehydrogenase; miRNA: MicroRNA; mtDNA: Mitochondrial DNA; *NAMPT*: Nicotinamide phosphoribosyltransferase; NC: Negative control; ncRNA: Noncoding RNA; PEM: Pectoralis major; ROS: Reactive oxygen species; SDH: Succinate dehydrogenase; siRNA: Small interfering RNA; SOL: Soleus; UTR: Untranslated region

Supplementary Information

The online version contains supplementary material available at <https://doi.org/10.1186/s40104-021-00664-1>.

Additional file 1.

Acknowledgements

Not applicable.

Authors' contributions

QN and XZ conceived and designed the study. BC and MM performed the experiments, interpreted the data and wrote the paper. ZZ, SK and JZ performed the experiments. All authors read and approved the final manuscript.

Funding

This work was supported by Local Innovative and Research Teams Project of Guangdong Province (2019BT02N630), the Natural Scientific Foundation of China (U1901206 and 31761143014), Guangzhou Science and Technology Key Project (202103000084), and China Agriculture Research System (CARS-41-G03).

Availability of data and materials

The data were exhibited in the main manuscript and supplemental materials.

Declarations

Ethics approval and consent to participate

All animal experimental protocols were conformed to "The Instructive Notions with Respect to Caring for Laboratory Animals" issued by the Ministry of Science and Technology of the People's Republic of China, and

approved by the Institutional Animal Care and Use Committee at the South China Agricultural University (approval ID: 2021-C018).

Consent for publication

Not applicable.

Competing interests

The authors declare that they have no conflict of interest.

Received: 10 August 2021 Accepted: 2 December 2021

Published online: 14 February 2022

References

- Lee SH, Joo ST, Ryu YC. Skeletal muscle fiber type and myofibrillar proteins in relation to meat quality. *Meat Sci.* 2010;86(1):166–70. <https://doi.org/10.1016/j.meatsci.2010.04.040>.
- Joo ST, Kim GD, Hwang YH, Ryu YC. Control of fresh meat quality through manipulation of muscle fiber characteristics. *Meat Sci.* 2013;95(4):828–36. <https://doi.org/10.1016/j.meatsci.2013.04.044>.
- Wilkins MR, Sanchez JC, Gooley AA, Appel RD, Humphrey-Smith I, Hochstrasser DF, et al. Progress with proteome projects: why all proteins expressed by a genome should be identified and how to do it. *Biotechnol Genet Eng Rev.* 1996;13(1):19–50. <https://doi.org/10.1080/02648725.1996.10647923>.
- Djebali S, Davis CA, Merkel A, Dobin A, Lassmann T, Mortazavi A, et al. Landscape of transcription in human cells. *Nature.* 2012;489(7414):101–8. <https://doi.org/10.1038/nature11233>.
- Xu M, Chen X, Chen D, Yu B, Li M, He J, et al. Regulation of skeletal myogenesis by microRNAs. *J Cell Physiol.* 2020;235(1):87–104. <https://doi.org/10.1002/jcp.28986>.
- Chen R, Lei S, Jiang T, Zeng J, Zhou S, She Y. Roles of lncRNAs and circRNAs in regulating skeletal muscle development. *Acta Physiol (Oxford).* 2020; 228(2):e13356. <https://doi.org/10.1111/apha.13356>.
- Memczak S, Jens M, Elefsinioti A, Torti F, Krueger J, Rybak A, et al. Circular RNAs are a large class of animal RNAs with regulatory potency. *Nature.* 2013;495(7441):333–8. <https://doi.org/10.1038/nature11928>.
- Rybak-Wolf A, Stottmeister C, Glazar P, Jens M, Pino N, Giusti S, et al. Circular RNAs in the mammalian brain are highly abundant, conserved, and dynamically expressed. *Mol Cell.* 2015;58(5):870–85. <https://doi.org/10.1016/j.molcel.2015.03.027>.
- Chen LL. The biogenesis and emerging roles of circular RNAs. *Nat Rev Mol Cell Biol.* 2016;17(4):205–11. <https://doi.org/10.1038/nrm.2015.32>.
- Dong R, Zhang XO, Zhang Y, Ma XK, Chen LL, Yang L. CircRNA-derived pseudogenes. *Cell Res.* 2016;26(6):747–50. <https://doi.org/10.1038/cr.2016.42>.
- Bach DH, Lee SK, Sood AK. Circular RNAs in cancer. *Mol Ther Nucleic Acids.* 2019;16:118–29. <https://doi.org/10.1016/j.omtn.2019.02.005>.
- Wu J, Qi X, Liu L, Hu X, Liu J, Yang J, et al. Emerging epigenetic regulation of circular RNAs in human cancer. *Mol Ther Nucleic Acids.* 2019;16:589–96. <https://doi.org/10.1016/j.omtn.2019.04.011>.
- Bartel DP. MicroRNAs: genomics, biogenesis, mechanism, and function. *Cell.* 2004;116(2):281–97. [https://doi.org/10.1016/s0092-8674\(04\)00045-5](https://doi.org/10.1016/s0092-8674(04)00045-5).
- Wahid F, Shehzad A, Khan T, Kim YY. MicroRNAs: synthesis, mechanism, function, and recent clinical trials. *Biochim Biophys Acta.* 2010;1803(11): 1231–43. <https://doi.org/10.1016/j.bbamcr.2010.06.013>.
- Liu X, Zhang Y, Liang H, Zhang Y, Xu Y. MicroRNA-499-3p inhibits proliferation and promotes apoptosis of retinal cells in diabetic retinopathy through activation of the TLR4 signaling pathway by targeting IFNA2. *Gene.* 2020;741:144539. <https://doi.org/10.1016/j.gene.2020.144539>.
- Jiang A, Yin D, Zhang L, Li B, Li R, Zhang X, et al. Parsing the microRNA genetics basis regulating skeletal muscle fiber types and meat quality traits in pigs. *Anim Genet.* 2021;52(3):292–303. <https://doi.org/10.1111/age.13064>.
- Samal B, Sun Y, Stearns G, Xie C, Suggs S, McNiece I. Cloning and characterization of the cDNA encoding a novel human pre-B-cell colony-enhancing factor. *Mol Cell Biol.* 1994;14(2):1431–7. <https://doi.org/10.1128/mcb.14.2.1431-1437.1994>.
- Imai S. Nicotinamide phosphoribosyltransferase (Namppt): a link between NAD biology, metabolism, and diseases. *Curr Pharm Des.* 2009;15(1):20–8. <https://doi.org/10.2174/138161209787185814>.
- Garten A, Schuster S, Penke M, Gorski T, de Giorgis T, Kiess W. Physiological and pathophysiological roles of NAMPT and NAD metabolism. *Nat Rev Endocrinol.* 2015;11(9):535–46. <https://doi.org/10.1038/nrendo.2015.117>.

20. Cai B, Ma M, Chen B, Li Z, Abdalla BA, Nie Q, et al. MiR-16-5p targets SESN1 to regulate the p53 signaling pathway, affecting myoblast proliferation and apoptosis, and is involved in myoblast differentiation. *Cell Death Dis.* 2018; 9(3):367. <https://doi.org/10.1038/s41419-018-0403-6>.
21. Jeck WR, Sorrentino JA, Wang K, Slevin MK, Burd CE, Liu J, et al. Circular RNAs are abundant, conserved, and associated with ALU repeats. *RNA.* 2013; 19(2):141–57. <https://doi.org/10.1261/rna.035667.112>.
22. Cai B, Li Z, Ma M, Zhang J, Kong S, Abdalla BA, et al. Long noncoding RNA SMUL suppresses SMURF2 production-mediated muscle atrophy via nonsense-mediated mRNA decay. *Mol Ther Nucleic Acids.* 2021;23:512–26. <https://doi.org/10.1016/j.omtn.2020.12.003>.
23. Cai B, Li Z, Ma M, Wang Z, Han P, Abdalla BA, et al. LncRNA-Six1 encodes a micropeptide to activate six1 in cis and is involved in cell proliferation and muscle growth. *Front Physiol.* 2017;8:230. <https://doi.org/10.3389/fphys.2017.00230>.
24. Ma M, Cai B, Jiang L, Abdalla BA, Li Z, Nie Q, et al. LncRNA-Six1 is a target of miR-1611 that functions as a ceRNA to regulate six1 protein expression and fiber type switching in chicken myogenesis. *Cells.* 2018;7(12):243. <https://doi.org/10.3390/cells7120243>.
25. Orom UA, Lund AH. Isolation of microRNA targets using biotinylated synthetic microRNAs. *Methods.* 2007;43(2):162–5. <https://doi.org/10.1016/j.ymeth.2007.04.007>.
26. Li L, Liu HH, Xu F, Si JM, Jia J, Wang JW. MyoD expression profile and developmental differences of leg and breast muscle in Peking duck (*Anas platyrhynchos Domestica*) during embryonic to neonatal stages. *Micron.* 2010;41(7):847–52. <https://doi.org/10.1016/j.micron.2010.04.016>.
27. Zhang Y, Zhang XO, Chen T, Xiang JF, Yin QF, Xing YH, et al. Circular intronic long noncoding RNAs. *Mol Cell.* 2013;51(6):792–806. <https://doi.org/10.1016/j.molcel.2013.08.017>.
28. Ashwal-Fluss R, Meyer M, Pamudurti NR, Ivanov A, Bartok O, Hanan M, et al. CircRNA biogenesis competes with pre-mRNA splicing. *Mol Cell.* 2014;56(1): 55–66. <https://doi.org/10.1016/j.molcel.2014.08.019>.
29. Li Z, Huang C, Bao C, Chen L, Lin M, Wang X, et al. Exon-intron circular RNAs regulate transcription in the nucleus. *Nat Struct Mol Biol.* 2015;22(3): 256–64. <https://doi.org/10.1038/nsmb.2959>.
30. Zurlo F, Larson K, Bogardus C, Ravussin E. Skeletal muscle metabolism is a major determinant of resting energy expenditure. *J Clin Invest.* 1990;86(5): 1423–7. <https://doi.org/10.1172/JCI114857>.
31. Ibrahim A, Neinast M, Arany ZP. Myobolites: muscle-derived metabolites with paracrine and systemic effects. *Curr Opin Pharmacol.* 2017;34:15–20. <https://doi.org/10.1016/j.coph.2017.03.007>.
32. Boengler K, Kosiol M, Mayr M, Schulz R, Rohrbach S. Mitochondria and ageing: role in heart, skeletal muscle and adipose tissue. *J Cachexia Sarcopenia Muscle.* 2017;8(3):349–69. <https://doi.org/10.1002/jcsm.12178>.
33. Boncompagni S, Pozzer D, Visconti C, Ferreiro A, Zito E. Physical and functional cross talk between Endo-sarcoplasmic reticulum and mitochondria in skeletal muscle. *Antioxid Redox Signal.* 2020;32(12):873–83. <https://doi.org/10.1089/ars.2019.7934>.
34. Bassel-Duby R, Olson EN. Signaling pathways in skeletal muscle remodeling. *Annu Rev Biochem.* 2006;75(1):19–37. <https://doi.org/10.1146/annurev.biochem.75.103004.142622>.
35. Schiaffino S, Reggiani C. Fiber types in mammalian skeletal muscles. *Physiol Rev.* 2011;91(4):1447–531. <https://doi.org/10.1152/physrev.00031.2010>.
36. Koutakis P, Weiss DJ, Miserlis D, Shostrom VK, Papoutsis E, Ha DM, et al. Oxidative damage in the gastrocnemius of patients with peripheral artery disease is myofiber type selective. *Redox Biol.* 2014;2:921–8. <https://doi.org/10.1016/j.redox.2014.07.002>.
37. Salmena L, Poliseno L, Tay Y, Kats L, Pandolfi PP. A ceRNA hypothesis: the Rosetta stone of a hidden RNA language? *Cell.* 2011;146(3):353–8. <https://doi.org/10.1016/j.cell.2011.07.014>.
38. Schuster S, Penke M, Gorski T, Gebhardt R, Weiss TS, Kiess W, et al. FK866-induced NAMPT inhibition activates AMPK and downregulates mTOR signaling in hepatocarcinoma cells. *Biochem Biophys Res Commun.* 2015; 458(2):334–40. <https://doi.org/10.1016/j.bbrc.2015.01.111>.
39. Tateishi K, Iafate AJ, Ho Q, Curry WT, Batchelor TT, Flaherty KT, et al. Myc-driven glycolysis is a therapeutic target in glioblastoma. *Clin Cancer Res.* 2016;22(17):4452–65. <https://doi.org/10.1158/1078-0432.CCR-15-2274>.
40. Nacarelli T, Lau L, Fukumoto T, Zundell J, Fatkhutdinov N, Wu S, et al. NAD(+) metabolism governs the proinflammatory senescence-associated secretome. *Nat Cell Biol.* 2019;21(3):397–407. <https://doi.org/10.1038/s41556-019-0287-4>.
41. Kos A, Dijkema R, Arnberg AC, van der Meide PH, Schellekens H. The hepatitis delta (delta) virus possesses a circular RNA. *Nature.* 1986;323(6088): 558–60. <https://doi.org/10.1038/323558a0>.
42. Cocquerelle C, Mascres B, Hetuin D, Bailleul B. Mis-splicing yields circular RNA molecules. *FASEB J.* 1993;7(1):155–60. <https://doi.org/10.1096/fasebj.7.1.7678559>.
43. Danan M, Schwartz S, Edelheit S, Sorek R. Transcriptome-wide discovery of circular RNAs in Archaea. *Nucleic Acids Res.* 2012;40(7):3131–42. <https://doi.org/10.1093/nar/gkr1009>.
44. Salzman J, Gawad C, Wang PL, Lacayo N, Brown PO. Circular RNAs are the predominant transcript isoform from hundreds of human genes in diverse cell types. *PLoS One.* 2012;7(2):e30733. <https://doi.org/10.1371/journal.pone.0030733>.
45. Werfel S, Nothjunge S, Schwarzmayr T, Strom TM, Meitinger T, Engelhardt S. Characterization of circular RNAs in human, mouse and rat hearts. *J Mol Cell Cardiol.* 2016;98:103–7. <https://doi.org/10.1016/j.yjmcc.2016.07.007>.
46. Zhang L, Liu X, Che S, Cui J, Ma X, An X, et al. Endometrial epithelial cell apoptosis is inhibited by a ciR8073-miR181a-Neurotensin pathway during embryo implantation. *Mol Ther Nucleic Acids.* 2019;14:262–73. <https://doi.org/10.1016/j.omtn.2018.12.005>.
47. Jiang R, Li H, Yang J, Shen X, Song C, Yang Z, et al. CircRNA profiling reveals an abundant circFUT10 that promotes adipocyte proliferation and inhibits adipocyte differentiation via sponging let-7. *Mol Ther Nucleic Acids.* 2020; 20:491–501. <https://doi.org/10.1016/j.omtn.2020.03.011>.
48. Chen B, Yu J, Guo L, Byers MS, Wang Z, Chen X, et al. Circular RNA circHIPK3 promotes the proliferation and differentiation of chicken myoblast cells by sponging miR-30a-3p. *Cells.* 2019;8(2):177. <https://doi.org/10.3390/cells8020177>.
49. Peng S, Song C, Li H, Cao X, Ma Y, Wang X, et al. Circular RNA SNX29 sponges miR-744 to regulate proliferation and differentiation of myoblasts by activating the Wnt5a/ca (2+) signaling pathway. *Mol Ther Nucleic Acids.* 2019;16:481–93. <https://doi.org/10.1016/j.omtn.2019.03.009>.
50. Shen X, Zhang X, Ru W, Huang Y, Lan X, Lei C, et al. CircINSR promotes proliferation and reduces apoptosis of embryonic myoblasts by sponging miR-34a. *Mol Ther Nucleic Acids.* 2020;19:986–99. <https://doi.org/10.1016/j.omtn.2019.12.032>.
51. Yue B, Yang H, Wu J, Wang J, Ru W, Cheng J, et al. CircSVIL regulates bovine myoblast development by inhibiting STAT1 phosphorylation. *Sci China Life Sci.* 2021. <https://doi.org/10.1007/s11427-020-1908-2>.
52. Ju X, Liu Y, Shan Y, Ji G, Zhang M, Tu Y, et al. Analysis of potential regulatory lncRNAs and circRNAs in the oxidative myofiber and glycolytic myofiber of chickens. *Sci Rep.* 2021;11(1):20861. <https://doi.org/10.1038/s41598-021-00176-y>.
53. Lin J, Wu H, Tarr PT, Zhang CY, Wu Z, Boss O, et al. Transcriptional co-activator PGC-1 alpha drives the formation of slow-twitch muscle fibres. *Nature.* 2002;418(6899):797–801. <https://doi.org/10.1038/nature00904>.
54. Ventura-Clapier R, Garnier A, Veksler V. Transcriptional control of mitochondrial biogenesis: the central role of PGC-1alpha. *Cardiovasc Res.* 2008;79(2):208–17. <https://doi.org/10.1093/cvr/cvn098>.
55. Zhang GM, Guo YX, Deng MT, Wan YJ, Deng KP, Xiao SH, et al. Effect of PPARGC1A on the development and metabolism of early rabbit embryos in vitro. *Mol Reprod Dev.* 2019;86(11):1758–70. <https://doi.org/10.1002/mrd.23269>.

Ready to submit your research? Choose BMC and benefit from:

- fast, convenient online submission
- thorough peer review by experienced researchers in your field
- rapid publication on acceptance
- support for research data, including large and complex data types
- gold Open Access which fosters wider collaboration and increased citations
- maximum visibility for your research: over 100M website views per year

At BMC, research is always in progress.

Learn more biomedcentral.com/submissions



LncEDCH1 g.1703613 T>C regulates chicken carcass traits by targeting *miR-196-2-3p*

Rongshuai Yuan,^{*,†,1} Bolin Cai,^{*,†,1} Manting Ma,^{*,†} Changbin Zhao,^{*,†} Yuanrong Xian,^{*,†} Qinghua Nie,^{*,†} Xiquan Zhang,^{*,†} and Dexiang Zhang^{*,†,2}

^{*}State Key Laboratory of Livestock and Poultry Breeding, Guangdong Laboratory for Lingnan Modern Agriculture, College of Animal Science, South China Agricultural University, Guangzhou, China; and [†]Guangdong Provincial Key Lab of Agro-Animal Genomics and Molecular Breeding, Key Laboratory of Chicken Genetics, Breeding and Reproduction, Ministry of Agriculture and Rural Affairs, National-Local Joint Engineering Research Center for Livestock Breeding, Guangzhou, China

ABSTRACT Single nucleotide polymorphisms (SNPs) are valuable genetic markers that can provide insights into the genetic diversity and variation within chicken populations. In poultry breeding, SNP analysis is widely utilized to accelerate the selection of desirable traits, improving the efficiency and effectiveness of chicken breeding programs. In our previous research, we identified an association between *LncEDCH1* and muscle development. To further investigate its specific mechanism, we conducted SNP detection and performed genotyping, linkage disequilibrium, and haplotype analysis. Our research findings indicate that 16 SNPs in the *LncEDCH1*. Among these SNPs, g.1703497 C>T and g.1704262 C>T were significantly associated with breast muscle weight percentage, g.1703497 C>T and g.1703613 T>C were significantly associated with leg weight percentage, and g.1703497 C>T, g.1703589

T>C, g.1703613 T>C, g.1703636 C>A, g.1703768 T>C, g.1704079 C>T, g.1704250 T>C, g.1704253 G>A were significantly associated with skin yellowness. Two haplotype blocks composed of 6 SNPs that were significantly associated with wing skin yellowness, breast skin yellowness, full-bore weight, and carcass weight percentage. Furthermore, through dual-luciferase reporter assays, biotin-coupled miRNA pull-down assays, 5-ethynyl-2'-deoxyuridine (EDU) assays, immunofluorescence, and quantitative real-time polymerase chain reaction (qPCR), it has been confirmed that *miR-196-2-3p* inhibits the expression of *LncEDCH1* directly by binding to *LncEDCH1* g.1703613T>C, thereby achieving indirect regulation of muscle development. These findings provide valuable molecular markers for chicken molecular breeding and broaden our understanding of the regulatory mechanisms.

Key words: *LncEDCH1*, *miR-196-2-3p*, single nucleotide polymorphism, carcass trait, chicken

2024 Poultry Science 103:103412

<https://doi.org/10.1016/j.psj.2023.103412>

INTRODUCTION

The demand for meat products, especially for chicken meat, is continuously increasing, driven by population growth. However, the purchase of live chickens for consumption was restricted by the Chinese government after the avian influenza (AI) virus outbreak in 2013 (Cui et al., 2022). In response to consumer demand for fresh and safe food, the sale of chilled chicken is on the rise. Especially, carcass traits are the most visual traits

of chilled chickens, and they directly influence consumers' choices. Consumers often judge the meat quality and quality of chickens by observing their carcass appearance characteristics. For example, bright, uniform skin yellowness is generally considered to be associated with tender, flavorful, and nutritious chicken meat (Hussein et al., 2019). However, assessing carcass traits in chickens can only be done postslaughter, making it difficult to incorporate these measurements into breeding programs for production purposes.

Long noncoding RNAs (lncRNAs) are a class of non-coding RNA molecules with more than 200 nucleotides in length that play an important role in gene regulation and cellular processes (Wilusz et al., 2009). lncRNAs are involved in key processes such as transcriptional regulation, epigenetic modification and cell signaling by interacting with DNA, RNA or proteins (Mercer et al., 2008). lncRNA has been found to be associated with

© 2023 The Authors. Published by Elsevier Inc. on behalf of Poultry Science Association Inc. This is an open access article under the CC BY-NC-ND license (<http://creativecommons.org/licenses/by-nc-nd/4.0/>).

Received July 1, 2023.

Accepted December 26, 2023.

¹These authors contributed equally to this work.

²Corresponding author: zhangdexiang0001@sina.com

chicken muscle development. For example, *LncIRS1* acts as a competitive inhibitor for *miR-15* family members, modulating *IRS1* expression to enhance skeletal muscle myogenesis and regulate atrophy (Li et al., 2019). *LncEDCH1* promotes muscle atrophy reduction by interacting with *SERCA2* and improving mitochondrial function (Cai et al., 2022a). *LncRNA SMARCD3-OT1* drives muscle hypertrophy and facilitates the transition to fast-twitch fiber type by enhancing *SMARCD3* expression (Zhang et al., 2022).

Single nucleotide polymorphism (SNP) is a form of genetic variation in which the sequence of bases at a single nucleotide position in the genome varies (Brookes, 1999). Due to the high polymorphism and wide distribution of SNPs in the genome, they are widely used in genetic research, disease association studies and the resolution of individual differences (Sachidanandam et al., 2001). Marker-assisted selection (MAS) has been widely used for selection and breeding of chickens for carcass traits (Yang et al., 2022; Zhao et al., 2023; Zhou et al., 2023).

MicroRNAs (miRNAs) are transcribed from genomic DNA and undergo a series of processing steps to produce mature small noncoding RNA molecules that play an important role in post-transcriptional gene regulation (Lee et al., 1993). The primary function of miRNAs is to regulate gene expression through binding to complementary sequences in messenger RNA (mRNA) molecules. This binding leads to the degradation of the target mRNA or inhibits its conversion to protein (Bartel, 2004). miRNAs have been recognized for their interactions with long noncoding RNAs in various biological processes (Ulitsky, 2018). Recent studies have revealed the crucial role of miRNAs in regulating chicken skeletal muscle development (Cai et al., 2022b; Ma et al., 2022). However, the impact of miRNA targeting of lncRNA polymorphic sites on phenotypic traits remains vastly understudied. In a recent study, it was discovered that the *lnc-LAMC2-1:1* SNP rs2147578 was found to play a role in promoting the progression of colorectal adenocarcinoma (COAD) by targeting the *miR-216a-3p/HMGB3* pathway (Ji et al., 2022). This finding contributes to our understanding of the complex interplay between genetic variations in lncRNA, miRNA regulation, and phenotypic traits.

In this study, we hypothesized that *LncEDCH1* plays an important role in carcass traits in chickens, then investigated SNPs of *LncEDCH1* and performed association and linkage disequilibrium and haplotype analysis with carcass traits in chickens. In addition, to gain insight into the regulatory mechanism, we predicted g.1703613 T>C-binding miRNAs associated with muscle development and validated the regulatory mechanism by dual-luciferase reporter assays, biotin-coupled miRNA pull-down assays, EDU assays, immunofluorescence, and qPCR to verify the regulatory mechanism between the miRNA and lncRNA. These results suggest that g.1703613 T>C of *LncEDCH1* is a potential molecular marker for chicken molecular breeding and is regulated by *miR-196-2-3p*.

MATERIALS AND METHODS

Ethics Statement

The animal experiment in this study strictly followed the guidelines and approval of the Institutional Animal Care and Use Committee at the South China Agricultural University (approval ID: 2021-f074). Every effort was made to minimize animal suffering.

Experimental Animals and Measurement of Traits

A crossbreeding approach was employed between the Chinese indigenous spotted chicken line and the Chinese indigenous yellow chicken to generate F1 individuals. Subsequently, 15 pairs of F1 individuals were selected to establish full-sib families for the production of F2 individuals. The F2 individuals were raised until they reached 80 d of age. Following this, the 410 F2 individuals were slaughtered using standard procedures. Before slaughter, blood samples were collected and stored at -20°C .

The measured carcass traits included subcutaneous fat thickness (SFT), intermuscular fat width (IFW), full-bore weight (FBW), half-bore weight (HBW), abdominal fat weight (AFW), leg weight (LW), breast muscle weight (BMW), body weight (BW), shank length (SL), shank girth (SG), carcass weight (CW), BMW percentage, LW percentage, AFW percentage, HBW percentage, FBW percentage, CW percentage, wing skin yellowness (WSY), buttock skin yellowness (BSY), abdominal skin yellowness (ASY), pectoral skin yellowness (PSY), leg skin yellowness (LSY), shin skin yellowness (SSY), abdominal fat yellowness (AFY).

Cell Culture and Transfection

Chicken primary myoblasts (CPMs) were isolated from leg muscles of 11-embryonic-day-old (E11) chicken and cultivated with Dulbecco's modified Eagle's medium (Gibco, Grand Island, NY) supplemented with 20% fetal bovine serum (Gibco) and 0.2% penicillin/streptomycin (Gibco) in a humidified atmosphere with 5% CO_2 at 37°C .

All transient transfections were performed with Lipofectamine 3000 reagent (Invitrogen, Carlsbad, CA) according to the manufacturer's directions.

Genomic DNA Extraction, PCR Amplification

The Genomic DNA was extracted from sample blood of 413 individuals using E.Z.N.A. SQ Blood DNA Kit (Omega, GA) according to the manufacturer's protocol. The concentration of DNA samples and optical density (OD) value of 260/280 were detected using a Nanodrop 2000c spectrophotometer (Thermo, Waltham, MA). The primers were designed using Primer 5, then synthesized by Beijing Tsingke Biotechnology Co., Ltd.

Table 1. Primer sequences.

Gene	Primers sequence (5'–3')	Product length (bp)	Temperature (°C)	Usage	Chromosome position
<i>LncEDCH1</i>	F: CTGGCAGCAAACCTCACG	935	58	PCR and Sanger sequencing	Chr25 Sbjct:1703431-1703448
	R: ACCGTCCCTCCCAGACACTC				Chr25 Sbjct 1704346-1704365
	F: CTGGAGGGCTATGCGATAT	115	56	qPCR	Chr25 Sbjct:1703501-1703519
	R: GGAGCAGCAGAGCAAGAA				Chr25 Sbjct:1703405-1703422
β -actin	F: GATATTGCTGCGCTCGTTG	178	56	qPCR	Chr14 Sbjct:4183894-4183876
	R: TTCAGGGTCAGGATACCTCTTT				Chr14 Sbjct:4183380-4183401

(Beijing, China). The information about the primers used is shown in Table 1. PCR was performed in a total volume of 30 μ L including the following: 2 μ L DNA template, 15 μ L 2 \times Taq Plus MasterMix (CWBio, Beijing, China), 1 μ L forward and reverse primers each, and 11 μ L ddH₂O. The reaction procedure included initial denaturation at 94°C for 2 min; 34 cycles of denaturation at 94°C for 30 s, annealing at 58°C for 30 s, and extension at 72°C for 30 s; final extension at 72°C for 2 min. The amplified samples were sent to Tsingke Biotech Co., Ltd. for sequencing.

Plasmid Construction and RNA Oligonucleotides

For pmirGLO dual-luciferase miRNA target reporter vector, the segment sequences of *LncEDCH1* wild-type that contained the putative *miR-196-2-3p* binding sequence were amplified by PCR and then cloned into *XhoI* and *SalI* restriction sites in the pmirGLO dual luciferase reporter vector (Promega, Madison, WI). Mutant plasmids were generated by changing the binding site of *miR-196-2-3p* from GCTGTAG to GCCGTAG. The *LncEDCH1* segment, cloned into the pmirGLO dual luciferase reporter vector and with a length of 299 bp, is as follows: cagcagagcaagaag-gaaactgctggcagcaaacctcacgtgttcacaggtggaaagaact-
caaataatgaaccagaggtgctgcacctgatatcgcatagccctc-
cagctgctctgagtgtgctggtagaagcaccgcagctggttaagcgatgag-
cactgaggatgaggtcggtgcatggagcagggtggcatccaggggctgta-
gagctgtgtgcacggctggctgctgctgtagaacttgggg-
cacggtggtggcaggttgcaggtgcatgtgttctgagggcaggtctg.

miR-196-2-3p mimic, mimic NC, *miR-196-2-3p* inhibitor, and inhibitor NC were designed and synthesized by Guangzhou RiboBio (Guangzhou, China).

RNA Extraction, Complementary DNA (cDNA) Synthesis, and qRT-PCR

RNA was extracted from cells using RNAiso reagent (Takara, Shiga, Japan) according to the manufacturer's protocol. The concentration of RNA samples and OD value of 260/280 were detected using a Nanodrop 2000c spectrophotometer. cDNA was synthesized using HiScript Q-RT SuperMix for qPCR (+gDNA wiper) (Vazyme, Nanjing, China). ChamQ Universal SYBR qPCR Master Mix (Vazyme, Guangzhou, China) was used in RT-qPCRs run on a Bio-Rad CFX96 Real-Time Detection instrument (Bio-Rad, Hercules, CA)

according to the manufacturer's protocol. The chicken β -actin gene was used as an internal control for *LncEDCH1*, U6 was used as an internal control for *miR-196-2-3p*. Comparative 2^{−ΔΔCT} method was used to analyze the data from qRT-PCR. Primers used in qRT-PCR are listed in Table 1.

Dual-Luciferase Reporter Assay

Four combinations of wild-type vector (*LncEDCH1*-WT) + *miR-196-2-3p* mimic, wild-type vector (*LncEDCH1*-WT) + NC mimic, mutated vector (*LncEDCH1*-MT) + *miR-196-2-3p* mimic, mutated vector (*LncEDCH1*-MT) + NC mimic were cotransfected into the cell culture in 48-well plates. After 36 h transfection, a Dual-Glo Luciferase Assay System Kit (Promega, Madison, WI) was used to detect the firefly and Renilla luciferase activities following the manufacturer's protocol. The data were acquired by a fluorescence/multidetection microplate reader (BioTek, Winooski, VT).

Biotin-Coupled miRNA Pull Down Assay

The 3' end biotinylated *miR-196-2-3p* mimic and mimic NC were transfected into CPMs in T75 cell culture bottle. At 36 h after transfection, the cells were harvested and then lysed in lysis buffer. The biotin-coupled RNA complex was pull down and subsequently isolated. The abundance of *LncEDCH1* in bound fractions was evaluated by qPCR.

Overexpression and Inhibition Assay

miR-196-2-3p mimic, mimic NC, *miR-196-2-3p* inhibitor, and inhibitor NC were transfected into the CPMs cell culture in 24-well plates. The *miR-196-2-3p* mimic and mimic NC were designated as the overexpression group, while the inhibitor and inhibitor NC were designated as the inhibition group. After 36 h transfection, qPCR was employed to assess the expression of *miR-196-2-3p* and *LncEDCH1* in the overexpression group. The expression of *LncEDCH1* was evaluated in the inhibition group.

5-Ethynyl-2'-Deoxyuridine (EdU) and Flow Cytometry Assay

For the EdU assay, primary myoblasts seeded in 12-well plates were cultured to 70% density and then

transfected. Forty-eight hours after transfection, the cells were fixed and stained with a C10310 EdU Apollo In Vitro Imaging Kit (RiboBio, China; 50 μ mol/L). A fluorescence microscope (DMi8; Leica, German) was used to capture 4 randomly selected fields to visualize the number of EdU-stained cells.

For the flow cytometry analysis of the cell cycle, myoblasts were seeded in 12-well plates. After 48 h transfection, the cultured cells in growth media were collected and fixed overnight in 70% ethanol at -20°C . Cells were analyzed by a BD AccuriC6 flow cytometer (BD Biosciences, San Jose, CA) with the Cell Cycle Analysis Kit (Thermo Fisher Scientific), and the data were processed using FlowJo software (7.6, Treestar Incorporated, Ashland, OR).

Statistics and Analysis

DNASTAR software (DNASTAR, Inc., Madison, WI) was employed for SNP genotyping analysis. Microsoft Excel (Microsoft Corporation, Redmond, WA) was employed to perform calculations for SNP analysis, including SNP counts, allele frequencies, genotype frequency differences (P values), Hardy-Weinberg equilibrium (HWE) P values, observed heterozygosity, expected heterozygosity, and polymorphic information content.

Linkage disequilibrium analysis (LD) between SNPs was performed using Haploview software (Broad Institute of MIT and Harvard, Cambridge, UK) (Barrett et al., 2005). The analysis of haplotype types and their frequencies was conducted using PHASE2.1 software (Stephens and Scheet, 2005). Due to missing phenotypic data in certain individuals, the number of counts for each SNP may vary.

In SPSS 24 software (SPSS Inc., Chicago, IL), a mixed linear model was employed to perform association analysis between SNPs and phenotypic traits, as well as between haplotypes and phenotypic traits. The analytical model used is as follows:

$$Y + \mu + G + H + e$$

Y : phenotypic values of carcass traits, μ : the overall population mean, G : the fixed effect of genotype or haplotype, H : the fixed effect of hatch, e : random residual error. Correction for multiple comparisons was performed using the Bonferroni method.

RESULTS

Single Nucleotide Polymorphisms and Genotyping of *LncEDCH1*

The *LncEDCH1* gene was amplified using PCR, followed by Sanger sequencing of the PCR products. Subsequently, genotype classification and data analysis were carried out for all individuals based on the obtained sequencing results. As shown in Figure 1, due to the limitations of Sanger sequencing, which permits single-

direction sequencing of only 800 base pairs (bp), it is necessary to perform bidirectional sequencing. Perform forward sequencing for the first 8 SNPs and reverse sequencing for the last 8 SNPs.

We examined 16 SNPs through statistical sequencing peak map analysis and identified 3 different genotypes. The 16 SNP sites of *LncEDCH1* detected in this study were NC_052556.1: g.1703497,C>T (SNP1), NC_052556.1: g.1703547,C>T (SNP2), NC_052556.1: g.1703589 T>C (SNP3), NC_052556.1: g.1703613 T>C (SNP4), NC_052556.1: g.1703615 T>C (SNP5), NC_052556.1: g.1703636 C>A (SNP6), NC_052556.1: g.1703768 T>C (SNP7), NC_052556.1: g.1703785 T>C (SNP8), NC_052556.1: g.1704079 C>T (SNP9), NC_052556.1: g.1704174 A>G (SNP10), NC_052556.1: g.1704235 A>G (SNP11), NC_052556.1: g.1704250 T>C (SNP12), NC_052556.1: g.1704253 G>A (SNP13), NC_052556.1: g.1704261 G>A (SNP14), NC_052556.1: g.1704262 C>T (SNP15), NC_052556.1: g.1704276 T>C (SNP16). Utilizing the statistical results, as shown in Table 2. We determined the genotype frequency and allele frequency for these 16 SNPs. The allele obtained from the database was designated as the wild type, while the mutant allele obtained through sequencing and screening was classified as the mutant type. In the 8 SNPs of SNP2, SNP3, SNP9, SNP10, SNP12, SNP13, SNP14, and SNP15 the frequency of wild-type alleles is greater than that of mutant alleles. In the SNPs of SNP1, SNP6, SNP8, and SNP16, the distribution of the 3 genotypes is relatively close. However, the frequency of wild-type alleles of SNP4, SNP5, SNP7, and SNP11 is less than that of mutant allele frequency. In order to elucidate the specific genetic mechanisms underlying these observed results, we also calculated and analyzed a series of additional parameters. HWE analyses were performed for each SNP using the chi-square test. The results of the analysis indicate that only SNP2 is consistent with the HWE. The observed heterozygosity (H_o) for all SNPs was found to be lower than the expected heterozygosity (H_e). Based on the polymorphism information content (PIC) analysis, the results indicate that SNP1, SNP4, SNP6, SNP7, SNP8, SNP10, SNP11, SNP12, SNP13, SNP14, and SNP15 exhibit PIC values between 0.25 and 0.5, suggesting intermediate levels of polymorphism. On the other hand, SNP2, SNP3, SNP5, and SNP15 exhibit PIC values lower than 0.25, indicating lower levels of polymorphism.

Association Analysis of SNPs in *LncEDCH1* With Chicken Traits

To investigate the correlation between the screened SNPs and various traits, we conducted an association analysis by examining the *LncEDCH1* genotype information about 24 specific traits. As shown in Table 3. The results reveal significant associations between specific SNPs and skin yellowness. Among the SNPs related to skin yellowness, SNP1, SNP3, SNP4, SNP6, SNP7,

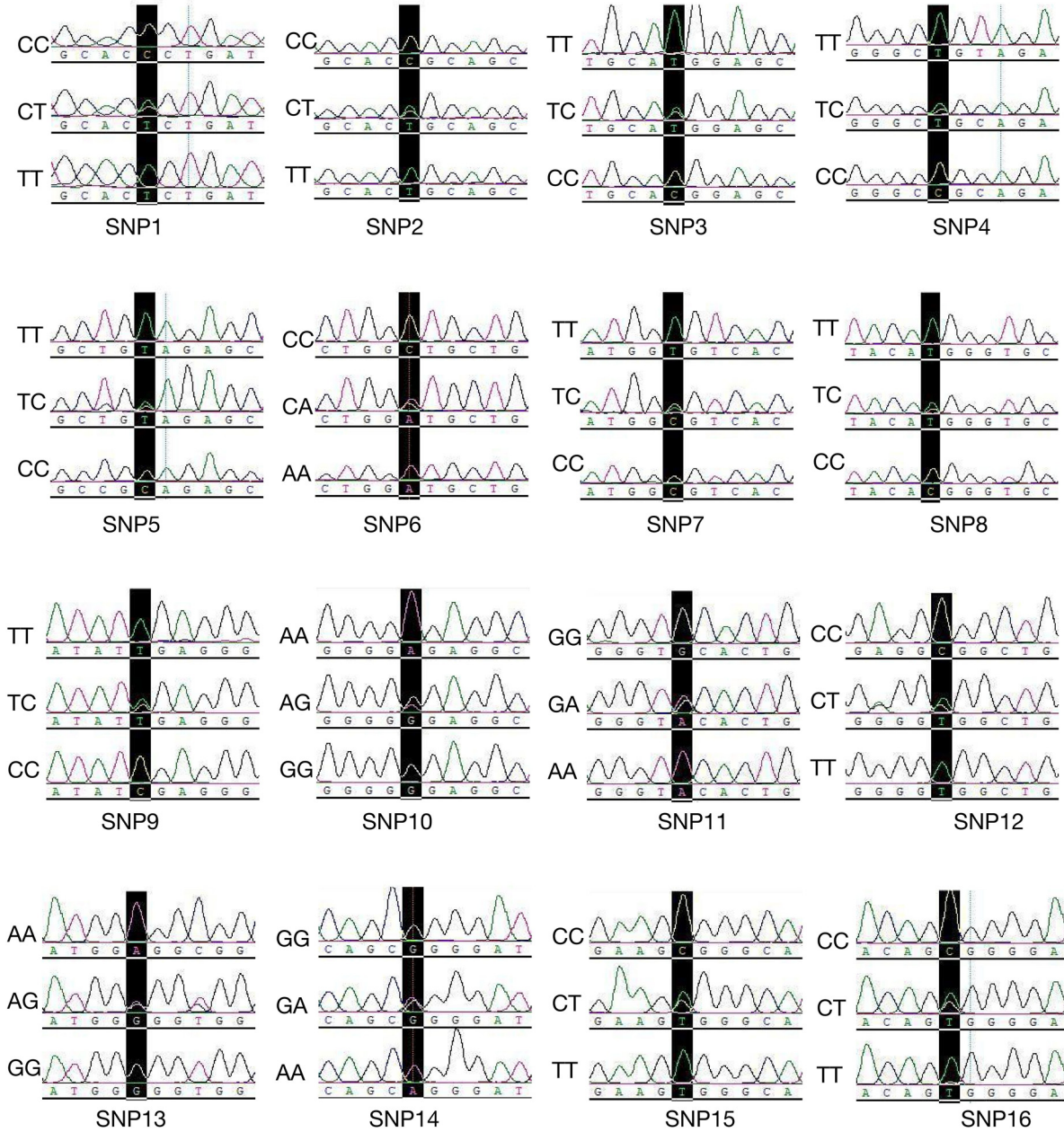


Figure 1. The peak maps of all 3 genotypes of SNPs. SNP1: NC_052556.1 g.1703497 C>T, SNP2: NC_052556.1 g.1703547 C>T, SNP3: NC_052556.1 g.1703589 T>C, SNP4: NC_052556.1 g.1703613 T>C, SNP5: NC_052556.1 g.1703615 T>C, SNP6: NC_052556.1 g.1703636 C>A, SNP7: NC_052556.1 g.1703768 T>C, SNP8: NC_052556.1 g.1703785 T>C, SNP9: NC_052556.1 g.1704079 C>T, SNP10: NC_052556.1 g.1704174 A>G, SNP11: NC_052556.1 g.1704235 A>G, SNP12: NC_052556.1 g.1704250 T>C, SNP13: NC_052556.1 g.1704253 G>A, SNP14: NC_052556.1 g.1704261 G>A, SNP15: NC_052556.1 g.1704262 T>C, SNP16: NC_052556.1 g.1704276 C>T.

SNP9, SNP12, and SNP13 showed significant correlations with PSY. SNP9 and SNP13 exhibited significant associations with LSY. SNP6 demonstrated a significant correlation with WSY, while SNP9 showed a significant association with ASY. Furthermore, significant correlations were observed in the association analysis between SNPs and other carcass traits. SNP4 and SNP6 were found to be significantly associated with AFW. SNP1 showed significant associations with BMWP and LWP. SNP4 exhibited a significant correlation with LWP. SNP15 showed a significant association with BMWP. Additionally, SNP3 demonstrated a significant correlation with SL, while SNP7 showed a significant association with IFW.

LD and Haplotype Analysis of SNPs in *LncEDCH1*

Using the Haploview software, we analyzed the LD among the 16 SNPs. The LD maps, generated based on D' and r^2 , are depicted in Figure 2. We identified 2 distinct LD blocks based on r^2 ($r^2 > 0.33$). SNP1, SNP4, and SNP7 were found to be part of block 1, while block 2 included SNP12, SNP13, and SNP15. Then, the haplotype types and their frequencies within each LD block were analyzed using the PHASE2.1 software. As shown in Table 4, block 1 has 8 haplotypes including H1, H2, H3, H4, H5, H6, H7, and H8. Block 2 has 7 haplotypes including H9, H10, H11, H12, H13, H14, and H15. To

Table 2. The genotype frequency, allele frequency, and diversity parameters.

SNPs	Genotype	Genotype number	Genotype frequency	Allele	Allele frequency	Pw ¹	Ho ²	He ³	PIC ⁴
NC_052556.1: g.1703497 C>T (SNP1)	CC	103	0.252	C	0.403	0.000	0.301	0.481	0.365
	CT	123	0.301	T	0.597				
	TT	182	0.446						
NC_052556.1: g.1703547 C>T (SNP2)	CC	287	0.710	C	0.834	0.106	0.248	0.277	0.238
	CT	100	0.248	T	0.166				
	TT	17	0.042						
NC_052556.1: g.1703589 C>T (SNP3)	TT	325	0.804	T	0.885	0.000	0.161	0.204	0.183
	CT	65	0.161	C	0.115				
	CC	14	0.035						
NC_052556.1: g.1703613 C>T (SNP4)	TT	88	0.217	T	0.365	0.000	0.296	0.463	0.356
	CT	120	0.296	C	0.635				
	CC	198	0.488						
NC_052556.1: g.1703615 C>T (SNP5)	TT	24	0.059	T	0.106	0.000	0.094	0.189	0.171
	CT	38	0.094	C	0.894				
	CC	344	0.847						
NC_052556.1: g.1703636 C>T (SNP6)	CC	90	0.222	C	0.369	0.000	0.296	0.466	0.357
	CA	120	0.296	A	0.631				
	AA	196	0.483						
NC_052556.1: g.17033768 C>T (SNP7)	TT	68	0.169	T	0.256	0.000	0.174	0.381	0.309
	CT	70	0.174	C	0.744				
	CC	264	0.657						
NC_052556.1: g.1703785 C>T (SNP8)	TT	103	0.255	T	0.458	0.001	0.406	0.496	0.373
	CT	164	0.406	C	0.542				
	CC	137	0.339						
NC_052556.1: g.1704079 C>T (SNP9)	CC	267	0.720	G	0.822	0.000	0.205	0.293	0.250
	CT	76	0.205	A	0.178				
	TT	28	0.075						
NC_052556.1: g.1704174 C>T (SNP10)	AA	234	0.613	T	0.757	0.000	0.288	0.368	0.301
	AG	110	0.288	C	0.243				
	GG	38	0.099						
NC_052556.1: g.1704235 C>T (SNP11)	AA	46	0.120	T	0.186	0.000	0.131	0.303	0.257
	AG	50	0.131	C	0.814				
	GG	286	0.749						
NC_052556.1: g.1704250 C>T (SNP12)	TT	210	0.550	A	0.668	0.000	0.236	0.444	0.345
	TC	90	0.236	G	0.332				
	CC	82	0.215						
NC_052556.1: g.1704253 C>T (SNP13)	GG	196	0.513	C	0.641	0.000	0.257	0.460	0.354
	GA	98	0.257	T	0.359				
	AA	88	0.230						
NC_052556.1: g.1704261 C>T (SNP14)	GG	230	0.602	C	0.694	0.000	0.183	0.425	0.335
	GA	70	0.183	T	0.306				
	AA	82	0.215						
NC_052556.1: g.1704262 C>T (SNP15)	CC	358	0.955	A	0.967	0.000	0.024	0.064	0.062
	CT	9	0.024	G	0.033				
	TT	8	0.021						
NC_052556.1: g.1704276 C>T (SNP16)	TT	149	0.390	A	0.547	0.000	0.314	0.496	0.373
	TC	120	0.314	G	0.453				
	CC	113	0.296						

¹P value: the χ^2 test of Hardy–Weinberg equilibrium, P value >0.05 means it is in Hardy Weinberg equilibrium.

²Ho: observed heterozygosity.

³He: expected heterozygosity.

⁴PIC: polymorphism information content, PIC > 0.5 means high polymorphism, 0.25 < PIC < 0.5 means intermediate polymorphism, PIC < 0.25 means low polymorphism.

investigate the association between haplotype combinations and traits, we excluded haplotypes with a frequency of less than 5%. Following this, a comprehensive joint analysis was performed to explore the relationship between these retained haplotypes and the traits. The association results show that the haplotype of block 1 is significantly associated with HBW, CWP, WSY, and PSY, the results are presented in Table 5.

LncEDCH1 Is Targeted by *miR-196-2-3p*

Previous studies have found that *LncEDCH1* is associated with muscle development and that miRNA regulates lncRNA (Hou et al., 2020; Cai et al., 2022a). In this

study, we identified SNP4 in *LncEDCH1* that are associated with muscle development. Our decision to focus on SNP4 reflects our interest in understanding the role of this particular genetic marker in the context of muscle development, without exploring other SNPs. Using RNAhybrid to predict the binding of miRNA to SNP4, *miR-196-2-3p* was found to bind to the T allele of SNP4 (Figure 3A, B). To confirm whether *miR-196-2-3p* directly targets SNP4 of *LncEDCH1*, dual-luciferase reporter assay and biotin-coupled miRNA pull down assay were performed. The results showed that *miR-196-2-3p* could perfectly bind with *LncEDCH1* (Figure 3C, D). More importantly, *miR-196-2-3p* over-expression 40,000 times significantly decreased the level of *LncEDCH1*, whereas the expression of *LncEDCH1*

Table 3. Association analysis of *LncEDCH1* SNPs with traits.

SNPs	Traits	Genotype			Available sample	P value
		Wild type	Heterozygote	Mutant type		
NC_052556.1: g.1703497 C>T (SNP1)	PSY	7.13 ± 2.18B (CC = 88)	7.52 ± 2.07 (CT = 110)	8.17 ± 2.27A (TT = 160)	358	0.0010
	BMWP (%)	8.47 ± 0.76b (CC = 97)	8.47 ± 0.8a (CT = 113)	8.7 ± 0.81a (TT = 168)	378	0.0230
	LWP (%)	17.57 ± 0.76 (CC = 97)	17.68 ± 0.92a (CT = 113)	17.42 ± 0.92b (TT = 168)	378	0.0446
NC_052556.1: g.1703589 C>T (SNP3)	SL (mm)	69.64 ± 20.05bB (CC = 11)	76.73 ± 5.93aA (CT = 59)	75.14 ± 6.22a (TT = 295)	365	0.0074
	PSY	6.17 ± 2.29b (CC = 13)	7.39 ± 2.41 (CT = 60)	7.85 ± 2.15a (TT = 285)	358	0.0130
NC_052556.1: g.1703613 C>T (SNP4)	AFW (g)	38.72 ± 20.19 (CC = 184)	33.35 ± 20.24b (CT = 111)	40.47 ± 20.02a (TT = 82)	377	0.0288
	PSY	7.98 ± 2.15a (CC = 176)	7.7 ± 2.31 (CT = 105)	7.14 ± 2.19b (TT = 77)	358	0.0211
	LWP (%)	17.41 ± 0.87b (CC = 185)	17.69 ± 1a (CT = 111)	17.6 ± 0.7 (TT = 82)	378	0.0205
NC_052556.1: g.1703636 C>T (SNP6)	AFW (g)	35.84 ± 20.14b (AA = 182)	36.21 ± 19.08 (AC = 111)	42.91 ± 21.5a (CC = 84)	377	0.0199
	WSY	4.45 ± 2.09a (AA = 170)	3.92 ± 1.78 (AC = 112)	3.79 ± 1.91b (CC = 76)	358	0.0187
	PSY	8.06 ± 2.31a (AA = 170)	7.52 ± 2.16 (AC = 112)	7.24 ± 2.03b (CC = 76)	358	0.0154
NC_052556.1: g.17033768 C>T (SNP7)	IMF (mm)	27.65 ± 9.93A (CC = 246)	23.3 ± 9.28B (CT = 65)	26.75 ± 10.41 (TT = 66)	377	0.0087
	PSY	7.93 ± 2.25a (CC = 232)	7.17 ± 2.23b (CT = 65)	7.46 ± 2 (TT = 61)	358	0.0305
NC_052556.1: g.1704079 C>T (SNP9)	AFY	6.94 ± 2.13 (CC = 273)	7.5 ± 2.37a (CT = 68)	6.13 ± 2.47b (TT = 28)	333	0.0185
	PSY	7.47 ± 2.1B (CC = 273)	8.41 ± 2.45A (CT = 68)	8.13 ± 2.16 (TT = 28)	333	0.0047
	LSY	2.35 ± 2.13b (CC = 273)	3.11 ± 2.41a (CT = 68)	2.48 ± 1.86 (TT = 28)	333	0.0398
NC_052556.1: g.1704250 C>T (SNP12)	PSY	7.84 ± 2.29 (CC = 71)	8.25 ± 2.15a (CT = 83)	7.42 ± 2.16b (TT = 179)	333	0.014053
NC_052556.1: g.1704253 C>T (SNP13)	PSY	7.87 ± 2.22 (AA = 76)	8.13 ± 2.19a (AG = 93)	7.41 ± 2.18b (GG = 164)	333	0.030876
	LSY	2.29 ± 2.19b (AA = 76)	3.03 ± 2.18a (AG = 93)	2.32 ± 2.15a (GG = 164)	333	0.0409
NC_052556.1: g.1704262 C>T (SNP15)	BMWP (%)	8.58 ± 0.81 (GG = 358)	7.97 ± 0.77b (GA = 9)	9.03 ± 0.6a (AA = 8)	375	0.0221

Abbreviations: AFW, abdominal fat weight; ASY, abdominal skin yellowness; BMWP, breast muscle weight percentage; HBW, half-bore weight; IMF, intermuscular fat width; LSY, leg skin yellowness; LWP, leg weight percentage; PSY, pectoral skin yellowness; SL, shank length; WSY, wing skin yellowness. Different lowercase letters indicate significant differences in means ($P < 0.05$), different capital letters indicate highly significant differences in means ($P < 0.001$), and the same letters indicate insignificant differences in means ($P > 0.05$).

was upregulated with the inhibition of *miR-196-2-3p* (Figure 3E, F). In conclusion, *miR-196-2-3p* directly targets and regulate *LncEDCH1*. Importantly, through miRBase, we predicted the binding of *miR-196-2-3p* to the genes MAPK8 and MFN2, which play crucial roles in muscle development (Figure 3G, H).

Furthermore, we investigated the association between SNP4 alleles and *LncEDCH1* expression in chicken muscle. The results indicate that the expression level of *LncEDCH1* is highest when the SNP4 is TT (Figure 3I).

miR-196-2-3p Inhibits Proliferation and Promotes Differentiation of Myoblasts

In order to investigate the potential involvement of *miR-196-2-3p* in muscle development, I conducted

inhibition and overexpression assay to assess its impact on the proliferation and differentiation of myoblasts. EdU assays demonstrated that overexpression *miR-196-2-3p* decreased EdU incorporation and repressed myoblast proliferation (Figure 4A, B). Flow cytometric analysis also showed that overexpression of *miR-196-2-3p* significantly decreased the number of S phase cells (Figure 4C). Furthermore, *miR-196-2-3p* overexpression increased the expression level of cell cycle-inhibiting genes, including *CDKN1A* and *CDKN1B*, while repressing the expression level of cell cycle-promoting genes like *PCNA* (Figure 4D). Conversely, the opposite result was observed by *miR-196-2-3p* inhibition (Figure 4E–H), indicating that *miR-196-2-3p* can inhibit myoblast proliferation.

Further exploration of *miR-196-2-3p*'s role in myoblast differentiation showed that overexpression of *miR*-

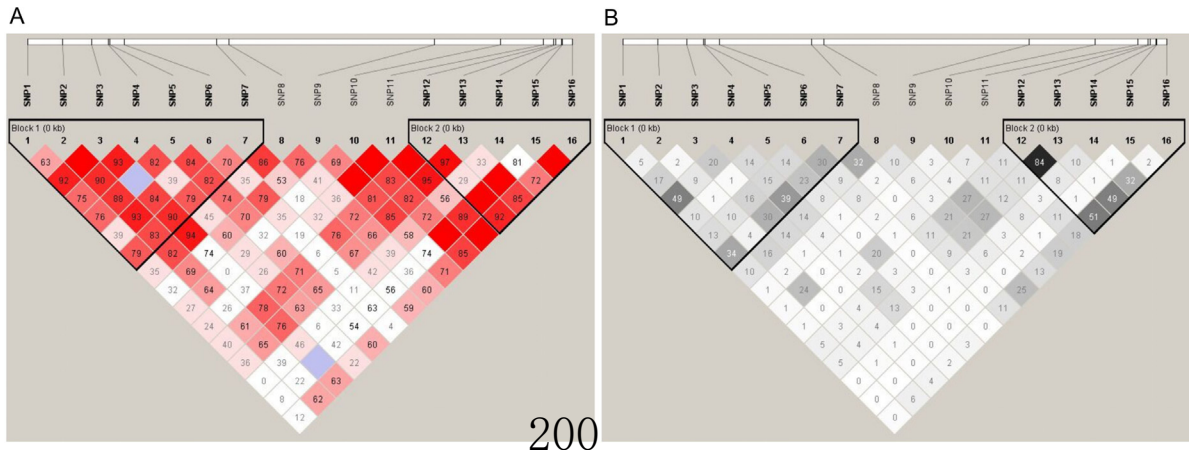


Figure 2. Linkage disequilibrium analysis of SNPs of *LncEDCH1*. (A) LD analysis based on D' . $D' = 1$ indicates full linkage. (B) LD analysis based on r^2 . $r^2 > 0.33$ indicates strong linkage.

Table 4. Haplotype composition of the linkage regions.

Block	Haplotype	SNPs			Haplotype frequency
		g.1703497 C>T	g.1703613 T>C	g.1703768 T>C	
Block1	H1	C	T	T	0.215
	H2	C	T	C	0.101
	H3	C	C	T	0.015
	H4	C	C	C	0.072
	H5	T	T	T	0.012
	H6	T	T	C	0.035
	H7	T	C	T	0.014
	H8	T	C	C	0.536
Block2	Haplotype	g.1704250 T>C	g.1704253 G>A	g.1704276 T>C	Haplotype frequency
		H9	T	G	0.525
		H10	T	G	0.113
		H11	T	A	0.013
		H12	T	A	0.019
		H13	C	G	0.005
		H14	C	A	0.013
		H15	C	A	0.311

Table 5. Association analysis of Haplotype combinations of *LncEDCH1* SNPs with trait.

Traits	Haplotype combinations	Mean \pm SEM	Haplotype combinations	Mean \pm SEM
SFT	(H1, H1)	3.88 \pm 1.21	(H9, H9)	3.71 \pm 1.28
	(H1, H2)	3.5 \pm 1.38	(H9, H10)	3.6 \pm 0.99
	(H1, H8)	3.61 \pm 1.31	(H9, H15)	4.09 \pm 1.46
	(H2, H2)	3.75 \pm 1.09	(H10, H10)	4.11 \pm 1.29
	(H2, H4)	4.02 \pm 0.84	(H10, H15)	3.68 \pm 1.32
	(H2, H8)	3.84 \pm 1.78	(H15, H15)	3.77 \pm 1.33
	(H4, H4)	3.77 \pm 1.26		
	(H4, H8)	4.74 \pm 0.1		
IMF	(H8, H8)	3.97 \pm 1.41		
	(H1, H1)	27.5 \pm 9.31	(H9, H9)	26.16 \pm 10.27
	(H1, H2)	16.52 \pm 11.97	(H9, H10)	24.78 \pm 10.27
	(H1, H8)	24.26 \pm 9.25	(H9, H15)	24.59 \pm 10.07
	(H2, H2)	25.09 \pm 6.12	(H10, H10)	28.25 \pm 7.86
	(H2, H4)	36.59 \pm 8.92	(H10, H15)	29.59 \pm 8.89
	(H2, H8)	27.93 \pm 9	(H15, H15)	28.56 \pm 10.2
	(H4, H4)	26.21 \pm 10.56		
FBW	(H4, H8)	30.23 \pm 9.64		
	(H8, H8)	27.88 \pm 10.32		
	(H1, H1)	1253.01 \pm 156.9	(H9, H9)	1260.83 \pm 166.07
	(H1, H2)	1183.5 \pm 210.64	(H9, H10)	1317.32 \pm 160.42
	(H1, H8)	1262.79 \pm 160.52	(H9, H15)	1246.03 \pm 150.72
	(H2, H2)	1288.98 \pm 145.59	(H10, H10)	1326.83 \pm 141.07
	(H2, H4)	1307.4 \pm 140.42	(H10, H15)	1307.83 \pm 112.63
	(H2, H8)	1307.47 \pm 160.59	(H15, H15)	1271.32 \pm 169.34
HBW	(H4, H4)	1286.9 \pm 164.06		
	(H4, H8)	1129.65 \pm 81.11		
	(H8, H8)	1264.05 \pm 164.69		
	(H1, H1)	1505.79 \pm 182.42b	(H9, H9)	1506.52 \pm 191.31
	(H1, H2)	1412.73 \pm 244.09	(H9, H10)	1571.77 \pm 188.55
	(H1, H8)	1509.57 \pm 183.41b	(H9, H15)	1489.56 \pm 173.39
	(H2, H2)	1541.21 \pm 171.25	(H10, H10)	1582.7 \pm 164.55
	(H2, H4)	1564.6 \pm 156.98	(H10, H15)	1570.96 \pm 125.95
AFW	(H2, H8)	1559.19 \pm 178.32	(H15, H15)	1517.98 \pm 199.7
	(H4, H4)	1530.57 \pm 190.71a		
	(H4, H8)	1363.4 \pm 119.08		
	(H8, H8)	1508.36 \pm 193.15b		
	(H1, H1)	42.79 \pm 21.03	(H9, H9)	36.02 \pm 22.26
	(H1, H2)	28.57 \pm 24.19	(H9, H10)	35.44 \pm 19.54
	(H1, H8)	33 \pm 20.17	(H9, H15)	36.19 \pm 15.93
	(H2, H2)	42.91 \pm 15	(H10, H10)	37.72 \pm 16.09
	(H2, H4)	45.68 \pm 17.38	(H10, H15)	48.43 \pm 14.62
	(H2, H8)	38.35 \pm 25.94	(H15, H15)	37.42 \pm 21.18
	(H4, H4)	32.48 \pm 20.55		
	(H4, H8)	31.8 \pm 22.63		
	(H8, H8)	40.08 \pm 20.12		
	(H1, H1)	219 \pm 29.24	(H9, H9)	222.57 \pm 31.9
	(H1, H2)	206.43 \pm 38.59	(H9, H10)	232.43 \pm 28.7
	(H1, H8)	224.74 \pm 31.89	(H9, H15)	218.67 \pm 29.28
	(H2, H2)	228.22 \pm 25.8	(H10, H10)	233.37 \pm 31.19

(continued)

Table 5 (Continued)

Traits	Haplotype combinations	Mean \pm SEM	Haplotype combinations	Mean \pm SEM
LW	(H2, H4)	226.55 \pm 21.92	(H10, H15)	225.84 \pm 21.4
	(H2, H8)	228.98 \pm 30.83	(H15, H15)	221.1 \pm 30.92
	(H4, H4)	226.11 \pm 34.48		
	(H4, H8)	196.55 \pm 21.85		
	(H8, H8)	219.7 \pm 30.83		
	(H1, H1)	106.74 \pm 18.33	(H9, H9)	107.08 \pm 18.37
	(H1, H2)	102.17 \pm 6.15	(H9, H10)	113.63 \pm 14.2
	(H1, H8)	106.69 \pm 17.32	(H9, H15)	107.53 \pm 17.38
	(H2, H2)	109.36 \pm 18.96	(H10, H10)	116.6 \pm 14.83
	(H2, H4)	109.1 \pm 15.17	(H10, H15)	113.46 \pm 13.84
BMW	(H2, H8)	111.32 \pm 13.75	(H15, H15)	108.68 \pm 17.21
	(H4, H4)	109.11 \pm 16.42		
	(H4, H8)	94.85 \pm 0.78		
	(H8, H8)	109.81 \pm 17.89		
	(H1, H1)	3.4 \pm 1.65b	(H9, H9)	3.93 \pm 1.95
	(H1, H2)	2.81 \pm 1.53	(H9, H10)	5.29 \pm 3.11
	(H1, H8)	4.11 \pm 1.92	(H9, H15)	4.21 \pm 2.1
	(H2, H2)	4.61 \pm 2.18	(H10, H10)	4.21 \pm 2.12
	(H2, H4)	5.05 \pm 3.2	(H10, H15)	3.36 \pm 1.45
	(H2, H8)	3.57 \pm 1.52	(H15, H15)	4.27 \pm 1.66
WSY	(H4, H4)	3.77 \pm 1.27		
	(H4, H8)	6.24 \pm 1.38a		
	(H8, H8)	4.37 \pm 2.06		
	(H1, H1)	6.1 \pm 1.98	(H9, H9)	6.78 \pm 2.09
	(H1, H2)	5.41 \pm 1.61	(H9, H10)	7.04 \pm 2.45
	(H1, H8)	7.3 \pm 2.02	(H9, H15)	7.19 \pm 2.34
	(H2, H2)	6.99 \pm 2.16	(H10, H10)	6.86 \pm 2.09
	(H2, H4)	7.13 \pm 2.53	(H10, H15)	7.07 \pm 1.72
	(H2, H8)	7.09 \pm 2.62	(H15, H15)	7.35 \pm 2.32
	(H4, H4)	6.97 \pm 2.28		
BSY	(H4, H8)	9.32 \pm 0.84		
	(H8, H8)	7.07 \pm 2.13		
	(H1, H1)	5.94 \pm 2.57	(H9, H9)	6.9 \pm 2.03
	(H1, H2)	5.83 \pm 1.79	(H9, H10)	7.24 \pm 2.15
	(H1, H8)	7.34 \pm 1.57	(H9, H15)	7.14 \pm 2.71
	(H2, H2)	7.25 \pm 2.37	(H10, H10)	7.73 \pm 2.25
	(H2, H4)	7 \pm 1.42	(H10, H15)	6.21 \pm 2.36
	(H2, H8)	6.66 \pm 2.16	(H15, H15)	6.6 \pm 2.37
	(H4, H4)	6.42 \pm 2.15		
	(H4, H8)	7.17 \pm 2.32		
ASY	(H8, H8)	7.08 \pm 2.35		
	(H1, H1)	7.02 \pm 2.33	(H9, H9)	7.28 \pm 2.27
	(H1, H2)	4.53 \pm 4.48b	(H9, H10)	7.5 \pm 2.22
	(H1, H8)	7.4 \pm 2.06	(H9, H15)	8.09 \pm 2.52
	(H2, H2)	7.14 \pm 2.63	(H10, H10)	7.38 \pm 2.47
	(H2, H4)	7.29 \pm 1.65	(H10, H15)	8.26 \pm 1.35
	(H2, H8)	7.74 \pm 2.35	(H15, H15)	7.8 \pm 2.37
	(H4, H4)	7.11 \pm 1.6		
	(H4, H8)	10.8 \pm 2.38a		
	(H8, H8)	8.1 \pm 2.17		
PSY	(H1, H1)	2.39 \pm 2.03	(H9, H9)	2.21 \pm 2.11
	(H1, H2)	0.95 \pm 2.17	(H9, H10)	2.68 \pm 2.49
	(H1, H8)	2.08 \pm 1.99	(H9, H15)	2.91 \pm 2.22
	(H2, H2)	3.55 \pm 2.44	(H10, H10)	3.31 \pm 2.16
	(H2, H4)	3.42 \pm 4.1	(H10, H15)	3.6 \pm 2.54
	(H2, H8)	2.59 \pm 2.23	(H15, H15)	2.26 \pm 2.24
	(H4, H4)	2.13 \pm 1.49		
	(H4, H8)	3.54 \pm 0.16		
	(H8, H8)	2.69 \pm 2.15		
	(H1, H1)	6.87 \pm 2.73	(H9, H9)	7.29 \pm 2.97
LSY	(H1, H2)	7.88 \pm 5.73	(H9, H10)	8.01 \pm 3.37
	(H1, H8)	6.56 \pm 2.67	(H9, H15)	6.51 \pm 3.02
	(H2, H2)	7.62 \pm 2.16	(H10, H10)	7.16 \pm 2.33
	(H2, H4)	7.23 \pm 1.93	(H10, H15)	8.34 \pm 3.83
	(H2, H8)	7.51 \pm 2.93	(H15, H15)	7.09 \pm 2.59
	(H4, H4)	6.71 \pm 1.98		
	(H4, H8)	9.26 \pm 2.09		
	(H8, H8)	7.31 \pm 3.13		
	(H1, H1)	11.49 \pm 6.37	(H9, H9)	11.63 \pm 6.46
	(H1, H2)	17.71 \pm 5.37	(H9, H10)	14.11 \pm 5.47
SSY	(H1, H8)	11.52 \pm 6.58	(H9, H15)	11.32 \pm 6.53
	(H2, H2)	11 \pm 5.72	(H10, H10)	12.02 \pm 5.65
	(H2, H4)	10.15 \pm 9.97	(H10, H15)	10.11 \pm 3.61
	(H2, H8)	11.05 \pm 5.94	(H15, H15)	12.02 \pm 6.07

(continued)

Table 5 (*Continued*)

Traits	Haplotype combinations	Mean \pm SEM	Haplotype combinations	Mean \pm SEM
BW	(H4, H4)	12.87 \pm 7.43		
	(H4, H8)	3.85 \pm 5.44		
	(H8, H8)	11.51 \pm 5.83		
	(H1, H1)	1875.23 \pm 207.74	(H9, H9)	1884.46 \pm 217.19
	(H1, H2)	1751.67 \pm 328.42	(H9, H10)	1964 \pm 231.04
	(H1, H8)	1892.91 \pm 221.79	(H9, H15)	1873.31 \pm 213.42
	(H2, H2)	1908.33 \pm 195.65	(H10, H10)	1975.45 \pm 201.9
	(H2, H4)	1960 \pm 144.74	(H10, H15)	1954.38 \pm 170.49
	(H2, H8)	1948.26 \pm 210.12	(H15, H15)	1918.58 \pm 236.2
	(H4, H4)	1949.05 \pm 216.64		
	(H4, H8)	1730 \pm 155.56		
	(H8, H8)	1889.09 \pm 232.58		
	(H1, H1)	74 \pm 11.45	(H9, H9)	75.69 \pm 7.46
	(H1, H2)	76.62 \pm 3	(H9, H10)	74.06 \pm 14.61
SL	(H1, H8)	76.26 \pm 6.22	(H9, H15)	75.32 \pm 5.93
	(H2, H2)	76.36 \pm 4.99	(H10, H10)	77.27 \pm 3.85
	(H2, H4)	73.32 \pm 3.48	(H10, H15)	72.83 \pm 5.5
	(H2, H8)	73.87 \pm 14.87	(H15, H15)	75.59 \pm 5.22
	(H4, H4)	77.72 \pm 6.21		
	(H4, H8)	72.65 \pm 0.44		
	(H8, H8)	74.67 \pm 4.48		
	(H1, H1)	11.65 \pm 1.13	(H9, H9)	11.8 \pm 0.94
	(H1, H2)	12.54 \pm 0.85	(H9, H10)	12.12 \pm 1.27
	(H1, H8)	12.04 \pm 0.98	(H9, H15)	11.88 \pm 1.02
SG	(H2, H2)	11.79 \pm 0.88	(H10, H10)	12.12 \pm 0.9
	(H2, H4)	12.24 \pm 0.87	(H10, H15)	11.96 \pm 0.84
	(H2, H8)	12.01 \pm 1.39	(H15, H15)	12.02 \pm 0.92
	(H4, H4)	11.95 \pm 0.82		
	(H4, H8)	12.95 \pm 1.6		
	(H8, H8)	11.84 \pm 0.85		
	(H1, H1)	1616.15 \pm 334.31	(H9, H9)	1651.97 \pm 252.88
	(H1, H2)	1636.67 \pm 151.77	(H9, H10)	1680 \pm 399.2
	(H1, H8)	1677.36 \pm 208.08	(H9, H15)	1629.44 \pm 286.65
	(H2, H2)	1684.67 \pm 182.32	(H10, H10)	1756.36 \pm 191.32
CW	(H2, H4)	1730 \pm 152.1	(H10, H15)	1740 \pm 148.13
	(H2, H8)	1650.48 \pm 411.37	(H15, H15)	1683.58 \pm 230.13
	(H4, H4)	1661.82 \pm 260.76		
	(H4, H8)	1525 \pm 134.35		
	(H8, H8)	1670.5 \pm 216.91		
	(H1, H1)	8.49 \pm 0.82	(H9, H9)	8.48 \pm 0.88
	(H1, H2)	8.75 \pm 1.02	(H9, H10)	8.67 \pm 0.9
	(H1, H8)	8.44 \pm 0.82	(H9, H15)	8.62 \pm 0.81
	(H2, H2)	8.46 \pm 0.88	(H10, H10)	8.78 \pm 0.58
	(H2, H4)	8.34 \pm 0.69	(H10, H15)	8.68 \pm 0.8
BMWP	(H2, H8)	8.55 \pm 0.74	(H15, H15)	8.55 \pm 0.73
	(H4, H4)	8.48 \pm 0.68		
	(H4, H8)	8.42 \pm 0.54		
	(H8, H8)	8.68 \pm 0.79		
	(H1, H1)	17.48 \pm 0.75	(H9, H9)	17.65 \pm 0.92
	(H1, H2)	17.43 \pm 0.51	(H9, H10)	17.66 \pm 0.72
	(H1, H8)	17.78 \pm 0.85	(H9, H15)	17.55 \pm 0.94
	(H2, H2)	17.72 \pm 0.6	(H10, H10)	17.55 \pm 0.64
	(H2, H4)	17.35 \pm 0.62	(H10, H15)	17.28 \pm 0.89
	(H2, H8)	17.53 \pm 1.11	(H15, H15)	17.4 \pm 0.8
LWP	(H4, H4)	17.54 \pm 0.91		
	(H4, H8)	17.37 \pm 0.69		
	(H8, H8)	17.38 \pm 0.89		
	(H1, H1)	3.26 \pm 1.52	(H9, H9)	2.82 \pm 1.63
	(H1, H2)	3.15 \pm 2.52	(H9, H10)	2.8 \pm 1.56
	(H1, H8)	2.67 \pm 1.67	(H9, H15)	2.88 \pm 1.17
	(H2, H2)	3.31 \pm 1.25	(H10, H10)	2.75 \pm 1.27
	(H2, H4)	3.54 \pm 1.41	(H10, H15)	3.75 \pm 1.19
	(H2, H8)	2.99 \pm 1.85	(H15, H15)	2.95 \pm 1.63
	(H4, H4)	2.26 \pm 1.47		
AFWP	(H4, H8)	2.75 \pm 1.81		
	(H8, H8)	3.16 \pm 1.44		
	(H1, H1)	80.21 \pm 2.16	(H9, H9)	80.02 \pm 2.32
	(H1, H2)	80.43 \pm 1.39	(H9, H10)	79.96 \pm 2.36
	(H1, H8)	80.1 \pm 2.57	(H9, H15)	79.65 \pm 2.17
	(H2, H2)	80.08 \pm 2.49	(H10, H10)	80.34 \pm 2.04
	(H2, H4)	79.71 \pm 2.13	(H10, H15)	80.45 \pm 1.85
	(H2, H8)	79.8 \pm 1.5	(H15, H15)	79.21 \pm 3.02
	(H4, H4)	77.72 \pm 0.99		
	(H4, H8)	78.82 \pm 0.2		
HBWP	(H8, H8)	79.85 \pm 2.12		

(continued)

Table 5 (Continued)

Traits	Haplotype combinations	Mean \pm SEM	Haplotype combinations	Mean \pm SEM
FBWP	(H1, H1)	66.75 \pm 2.46	(H9, H9)	66.98 \pm 2.53
	(H1, H2)	67.3 \pm 0.41	(H9, H10)	67 \pm 2.15
	(H1, H8)	66.92 \pm 2.61	(H9, H15)	66.56 \pm 2.23
	(H2, H2)	67.05 \pm 2.89	(H10, H10)	67.4 \pm 2.33
	(H2, H4)	66.58 \pm 2.3	(H10, H15)	66.94 \pm 1.55
	(H2, H8)	66.9 \pm 2.58	(H15, H15)	66.33 \pm 2.8
	(H4, H4)	65.42 \pm 3.31		
	(H4, H8)	65.35 \pm 1.19		
	(H8, H8)	66.91 \pm 2.14		
	(H1, H1)	88.34 \pm 4.87a	(H9, H9)	88.42 \pm 3.25
CWP	(H1, H2)	87.3 \pm 2.81	(H9, H10)	88.39 \pm 2.59
	(H1, H8)	88.63 \pm 2.41a	(H9, H15)	88.13 \pm 3.28
	(H2, H2)	88.26 \pm 1.95	(H10, H10)	88.78 \pm 1.5
	(H2, H4)	88.2 \pm 1.31	(H10, H15)	89.06 \pm 1.59
	(H2, H8)	88.49 \pm 2.05a	(H15, H15)	87.65 \pm 4.4
	(H4, H4)	85.02 \pm 7.02b		
	(H4, H8)	88.16 \pm 0.16		
	(H8, H8)	88.38 \pm 2.32a		

Abbreviations: AFW, abdominal fat weight; AFWP, abdominal fat weight percentage; AFY, abdominal fat yellowness; ASY, abdominal skin yellowness; BMW, breast muscle weight; BMWP, breast muscle weight percentage; BSY, buttock skin yellowness; BW, body weight; CW, carcass weight; CWP, carcass weight percentage; FBW, full-bore weight; FBWP, full-bore weight percentage; HBW, half-bore weight; HBWP, half-bore weight percentage; IFW, intermuscular fat width; LSY, leg skin yellowness; LW, leg weight; LWP, leg weight percentage; PSY, pectoral skin yellowness; SG, shank girth; SL, shank length; SSY, shin skin yellowness; WSY, wing skin yellowness. Different lowercase letters indicate significant differences in means ($P < 0.05$), different capital letters indicate highly significant differences in means ($P < 0.001$), and the same letters indicate insignificant differences in means ($P > 0.05$).

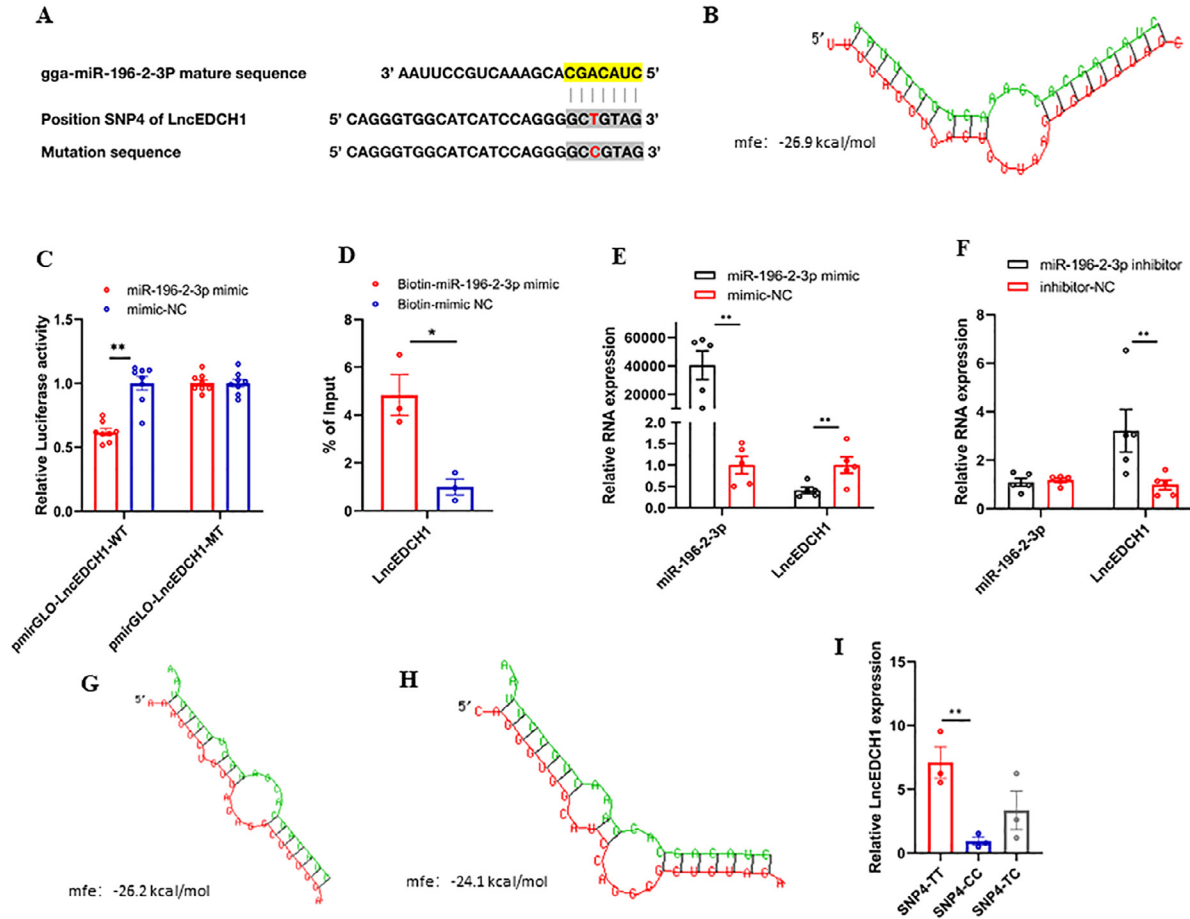


Figure 3. Identification of SNP4 of *LncEDCH1* as a direct target of *miR-196-2-3p*. (A) The original potential binding site of *miR-196-2-3p* in *LncEDCH1*, the mutant sequence resulting from the mutated binding site of *miR-196-2-3p* in *LncEDCH1* (SNP4). (B) The potential interaction model between *miR-196-2-3p* and *LncEDCH1* from RNAhybrid. (C) Luciferase assay was conducted by cotransfecting wild-type or mutant *LncEDCH1* SNP4 with *miR-196-2-3p* mimic or mimic-negative control (NC). (D) The interaction of *miR-196-2-3p* with *LncEDCH1* was determined by biotin-coupled miRNA pull down. (E) The relative expression levels of *miR-196-2-3p* and *LncEDCH1* in *miR-196-2-3p* overexpression group. (F) The relative expression levels of *miR-196-2-3p* and *LncEDCH1* in *miR-196-2-3p* inhibition group. (G) The potential interaction model between *miR-196-2-3p* and MAPK8 from RNAhybrid. (H) The potential interaction model between *miR-196-2-3p* and MFN2 from RNAhybrid. (I) The expression of *LncEDCH1* in chicken muscle varies with different SNP4 alleles. In panels (A-I), results are presented as mean \pm SEM and paired t tests were used to assess the statistical significance of differences between means. (** $P < 0.01$).

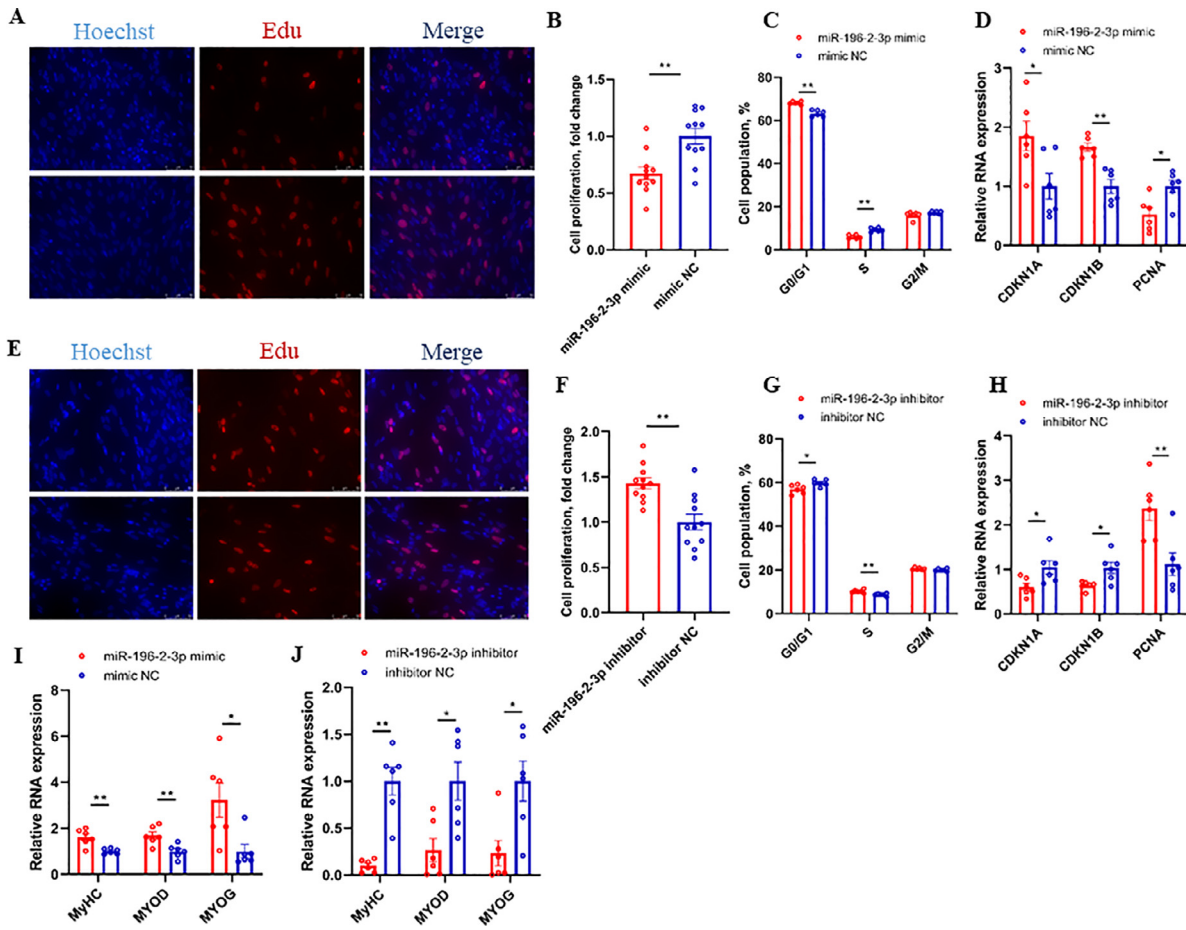


Figure 4. *miR-196-2-3p* inhibits proliferation and promotes differentiation of myoblasts. (A–D) EdU proliferation assay (A), the proliferation rate of myoblast (B), cell cycle analysis (C), and relative mRNA levels of several cell cycle genes (D) with *miR-196-2-3p* overexpression in CPMs. (E–H) EdU proliferation assay (E), the proliferation rate of myoblast (F), cell cycle analysis (G), and relative mRNA levels of several cell cycle genes (H) with *miR-196-2-3p* inhibition in CPMs. (I) Relative mRNA expression levels of myoblast differentiation marker genes with *miR-196-2-3p* overexpression in CPMs. (J) Relative mRNA expression levels of myoblast differentiation marker genes with *miR-196-2-3p* inhibition in CPMs.

196-2-3p upregulated the expression of myoblast differentiation marker genes, including MyHC, MYOD, and MYOG (Figures 4I). In contrast, *miR-196-2-3p* inhibition downregulated the expression of myoblast differentiation marker genes (Figures 4J). In summary, these findings indicate that *miR-196-2-3p* promotes myoblast differentiation while suppressing myoblast proliferation.

DISCUSSION

Carcass traits and skin yellowness have always been important breeding criteria in poultry production. These traits not only influence the visual appeal and consumer acceptance of poultry products but also impact their market value and economic profitability. Traditionally, breeding programs relied on phenotypic selection to improve these traits. However, with advancements in genetic research, there is a growing recognition of the importance of genetic polymorphisms in driving desirable phenotypic variations (Chang et al., 2012). Recent studies have revealed a close association between *LncEDCH1* and chicken muscle development (Cai et al., 2022a). Given its potentially important role, we decided to study the polymorphisms and regulatory mechanisms of *LncEDCH1*.

In the absence of migration, mutation, natural selection, and assortative mating, a population can achieve Hardy-Weinberg equilibrium (Wigginton et al., 2005). In this study, under the presence of mutation, SNP2 was found to be in HWE, suggesting a dynamic equilibrium where various factors potentially counterbalance each other. None of the other loci were found to be in HWE, which could be attributed to the outcomes of artificial selection. In addition, The HO being lower than the expected HE for all SNPs suggests a deviation from HWE, indicating the occurrence of selection or inbreeding in the population (Fenster et al., 2018). Due to the breeders' aim to consistently pass on favorable traits to offspring, Ho gradually decreases and the traits become more stable after selection. Based on the analysis of PIC and the association between SNPs and carcass traits, it can be concluded that SNP1 and SNP4 exhibit high levels of genetic variation, indicating significant potential for selection.

Population genetic principles show us that variation in populations is inherently structured into haplotypes (Clark, 2004). Individual SNP-based polymorphism analysis may not capture the potential interactions between underlying genetic loci. Therefore, we conducted LD and haplotype analysis to explore potential relationships between genetic markers. Based on the

fact that r^2 is less influenced by sample size or allele frequency, and considering r^2 values greater than 0.33 as indicative of closely linked loci (Ardlie et al., 2002; Weiss and Clark, 2002). This study revealed that haplotype combination H4H8 is dominant in skin yellowness, while H2H4 and H2H8 are dominant in carcass traits.

In this study, we found a significant correlation between SNP4 of *LncEDCH1* and AFW, PSY, and LWP. Furthermore, we discovered that *miR-196-2-3p* exerts a regulatory role in muscle development by targeting SNP4. Interestingly, some of these predicted genes are associated with muscle development. For instance, RAC2 is potentially involved in the modulation of cell proliferation through the regulation of the PAKs/MAPK8 pathway, which can influence the growth of chickens (Zhang et al., 2021). Mfn2 plays a role in controlling the levels of mitochondrial complex I proteins and respiratory functions in both myogenic progenitor cells and myofibers (Luo et al., 2021). This additional evidence supports the notion that *miR-196-2-3p* plays a significant role in regulating muscle development.

CONCLUSIONS

In summary, we observed significant associations between 9 SNPs and 1 block within *LncEDCH1* and carcass traits as well as skin yellowness. SNP1, SNP3, SNP4, SNP6, SNP7, SNP9, SNP12, and SNP13 showed significant correlations with skin yellowness. SNP4 and SNP6 were found to be significantly associated with AFW. SNP1 showed significant associations with BMWP and LWP. SNP4 exhibited a significant correlation with LWP. SNP15 showed a significant association with BMWP. Additionally, SNP3 demonstrated a significant correlation with SL, while SNP7 showed a significant association with IFW. Additionally, the block showed significant associations with WSY, PSY, HBWP, and CWP. Furthermore, SNP4 of *LncEDCH1*, associated with muscle development, is targeted by *miR-196-2-3p* and regulated by it. Subsequently, we can employ direct sequencing of this locus or integrate it into the QTL structure on a chip. These methods can facilitate marker-assisted breeding, accelerating the process of variety improvement.

ACKNOWLEDGMENTS

This work was supported by the Project of the Seed Industry Revitalization of Department of Agriculture (2022-XPY-00-004), Rural Affairs of Guangdong Province (2022-XPY-05-001), and Guangdong Basic and Applied Basic Research Foundation (2021A1515111069 and 2023A1515010096).

DISCLOSURES

The authors declare no conflict of interest.

REFERENCES

- Ardlie, K. G., L. Kruglyak, and M. Seielstad. 2002. Patterns of linkage disequilibrium in the human genome. *Nat. Rev. Genet.* 3:299–309.
- Barrett, J. C., B. Fry, J. Maller, and M. J. Daly. 2005. Haploview: analysis and visualization of LD and haplotype maps. *Bioinformatics* 21:263–265.
- Bartel, D. P. 2004. MicroRNAs: genomics, biogenesis, mechanism, and function. *Cell* 116:281–297.
- Brookes, A. J. 1999. The essence of SNPs. *Gene* 234:177–186.
- Cai, B., M. Ma, J. Zhang, Z. Wang, S. Kong, Z. Zhou, L. Lian, J. Zhang, J. Li, Y. Wang, H. Li, X. Zhang, and Q. Nie. 2022a. *LncEDCH1* improves mitochondrial function to reduce muscle atrophy by interacting with SERCA2. *Mol. Ther. Nucleic Acids* 27:319–334.
- Cai, B., M. Ma, Z. Zhou, S. Kong, J. Zhang, X. Zhang, and Q. Nie. 2022b. circPTPN4 regulates myogenesis via the miR-499-3p/NAMPT axis. *J. Anim. Sci. Biotechnol.* 13:2.
- Chang, M.-T., Y.-S. Cheng, and M.-C. Huang. 2012. A novel non-synonymous SNP of the COLX gene and its association with duck reproductive traits. *Mol. Cell. Probes* 26:204–207.
- Clark, A. G. 2004. The role of haplotypes in candidate gene studies. *Genet. Epidemiol.* 27:321–333.
- Cui, B., L. D.-L. Wang, X. Chen, M. Y. Xu, J. Ke, and Y. Tian. 2022. Chicken meat taste preferences, perceived risk of human infection with avian influenza virus, and self-reported chicken meat consumption in China. *Prev. Vet. Med.* 203:105658.
- Fenster, C. B., J. D. Ballou, M. R. Dudash, M. D. B. Eldridge, R. Frankham, R. C. Lacy, K. Ralls, and P. Sunnucks. 2018. Conservation and genetics. *Yale J. Biol. Med.* 91:491–501.
- Hou, Z.-H., X.-W. Xu, X.-Y. Fu, L.-D. Zhou, S.-P. Liu, and D.-M. Tan. 2020. Long non-coding RNA MALAT1 promotes angiogenesis and immunosuppressive properties of HCC cells by sponging miR-140. *Am. J. Physiol.-Cell Physiol.* 318:C649–C663.
- Hussein, E. O. S., G. M. Suliman, A. N. Al-Owaimer, S. H. Ahmed, A. M. Abudabos, M. E. Abd El-Hack, A. E. Taha, I. M. Saadeldin, and A. A. Swelum. 2019. Effects of stock, sex, and muscle type on carcass characteristics and meat quality attributes of parent broiler breeders and broiler chickens. *Poult. Sci.* 98:6586–6592.
- Ji, F., Z. Yao, C. Liu, S. Fu, B. Ren, Y. Liu, L. Ma, J. Wei, and D. Sun. 2022. A novel lnc-LAMC2-1:1 SNP promotes colon adenocarcinoma progression by targeting miR-216a-3p/HMGB3. *Heliyon* 8:e12342.
- Lee, R. C., R. L. Feinbaum, and V. Ambros. 1993. The *C. elegans* heterochronic gene lin-4 encodes small RNAs with antisense complementarity to lin-14. *Cell* 75:843–854.
- Li, Z., B. Cai, B. A. Abdalla, X. Zhu, M. Zheng, P. Han, Q. Nie, and X. Zhang. 2019. *LncIRS1* controls muscle atrophy via sponging miR-15 family to activate IGF1-PI3K/AKT pathway. *J. Cachexia Sarcopen. Muscle* 10:391–410.
- Luo, N., F. Yue, Z. Jia, J. Chen, Q. Deng, Y. Zhao, and S. Kuang. 2021. Reduced electron transport chain complex I protein abundance and function in Mfn2-deficient myogenic progenitors lead to oxidative stress and mitochondria swelling. *FASEB J.* 35.
- Ma, M., B. Cai, S. Kong, Z. Zhou, J. Zhang, X. Zhang, and Q. Nie. 2022. PPARGC1A is a moderator of skeletal muscle development regulated by miR-193b-3p. *Int. J. Mol. Sci.* 23:9575.
- Mercer, T. R., M. E. Dinger, S. M. Sunkin, M. F. Mehler, and J. S. Mattick. 2008. Specific expression of long noncoding RNAs in the mouse brain. *Proc. Natl. Acad. Sci.* 105:716–721.
- Sachidanandam, R., D. Weissman, S. C. Schmidt, J. M. Kakol, L. D. Stein, G. Marth, S. Sherry, J. C. Mullikin, B. J. Mortimore, D. L. Willey, S. E. Hunt, C. G. Cole, P. C. Coggill, C. M. Rice, Z. Ning, J. Rogers, D. R. Bentley, P.-Y. Kwok, E. R. Mardis, R. T. Yeh, B. Schultz, L. Cook, R. Davenport, M. Dante, L. Fulton, L. Hillier, R. H. Waterston, J. D. McPherson, B. Gilman, S. Schaffner, W. J. Van Etten, D. Reich, J. Higgins, M. J. Daly, B. Blumenstiel, J. Baldwin, N. Stange-Thomann, M. C. Zody, L. Linton, E. S. Lander, and D. Altshuler. 2001. A map of human genome sequence variation containing 1.42 million single nucleotide polymorphisms. *Nature* 409:928–933.

- Stephens, M., and P. Scheet. 2005. Accounting for decay of linkage disequilibrium in haplotype inference and missing-data imputation. *Am. J. Hum. Genet.* 76:449–462.
- Ulitsky, I. 2018. Interactions between short and long noncoding RNAs. *FEBS Lett.* 592:2874–2883.
- Weiss, K. M., and A. G. Clark. 2002. Linkage disequilibrium and the mapping of complex human traits. *Trends Genet.* 18:19–24.
- Wigginton, J. E., D. J. Cutler, and G. R. Abecasis. 2005. A note on exact tests of Hardy-Weinberg equilibrium. *Am. J. Hum. Genet.* 76:887–893.
- Wilusz, J. E., H. Sunwoo, and D. L. Spector. 2009. Long noncoding RNAs: functional surprises from the RNA world. *Genes Dev.* 23:1494–1504.
- Yang, X., Y. Xian, Z. Li, Z. Wang, and Q. Nie. 2022. G0S2 gene polymorphism and its relationship with carcass traits in chicken. *Animals* 12:916.
- Zhang, J., B. Cai, M. Ma, S. Kong, Z. Zhou, X. Zhang, and Q. Nie. 2022. LncRNA SMARCD3-OT1 promotes muscle hypertrophy and fast-twitch fiber transformation via enhancing SMARCD3×4 expression. *Int. J. Mol. Sci.* 23:4510.
- Zhang, G., P. Wu, K. Zhou, M. He, X. Zhang, C. Qiu, T. Li, T. Zhang, K. Xie, G. Dai, and J. Wang. 2021. Study on the transcriptome for breast muscle of chickens and the function of key gene RAC2 on fibroblasts proliferation. *BMC Genomics* 22:1–15.
- Zhao, C., B. Hu, Z. Zhang, Q. Luo, Q. Nie, X. Zhang, and H. Li. 2023. Detection of CD36 gene polymorphism associated with chicken carcass traits and skin yellowness. *Poult. Sci.* 102:102691.
- Zhou, Z., D. Cai, G. Wei, B. Cai, S. Kong, M. Ma, J. Zhang, and Q. Nie. 2023. Polymorphisms of CRELD1 and DNAJC30 and their relationship with chicken carcass traits. *Poult. Sci.* 102:102324.

***PPM1J* regulates meat quality feature and glycerophospholipids composition in broiler by modulating protein dephosphorylation**



Manting Ma^{1,4}, Xin Yang^{2,3,4}, Yanan Zhang¹, Shuang Wang¹, Chenglong Jin¹, Weiguang Xia¹, Wei Chen¹, Bolin Cai^{2,3} ✉ & Chuntian Zheng¹ ✉

The quality of broiler meat affects consumers' purchasing decisions. Numerous studies have shown that phosphorylation of proteins in muscle can affect muscle quality. Here, metabolomics and transcriptomics were used to systematically identify the genetic regulation of differences in meat flavor among different broiler. By constructing the meat flavor-related metabolite-gene networks, we identified that protein phosphatase magnesium/manganese-dependent 1J (*PPM1J*), which is known to regulate a range of biological processes by modulating reversible protein phosphorylation, was a differentially expressed gene with the highest connectivity to meat flavor-related metabolites. Gain- and loss-of-function analysis revealed that *PPM1J* induced muscular atrophy, improved meat quality and regulated the composition of glycerophospholipids. More importantly, phosphoproteome and metabolome results found that *PPM1J* participates in the regulation of meat quality feature and glycerophospholipids composition by catalyzing protein dephosphorylation. Our study provides a basis for further understanding the molecular mechanism of meat quality feature and glycerophospholipids composition in broiler.

Poultry meat represents the most consumed meat product, and its consumption continues to grow in both developed and developing countries¹. Compared with other livestock, broilers have lower rearing costs and higher production efficiency². According to the growth rate of chickens, broilers can be divided into fast-growing (FG) broilers and slow-growing (SG) broilers. FG broilers are preferred by producers for their high feed efficiency, meat yield and slaughter rate³. However, SG broiler meat is considered to have a better flavor than FG broiler meat⁴. For consumers, the quality of broiler meat affects their purchasing decision⁵. With the improvement of living standards, the demand for quality meat products is also increasing. There is no doubt that it is imperative to understand the molecular mechanism of meat flavor formation.

In the last decades, proteomics has been widely used to elucidate mechanisms and explore biomarkers that determine meat quality⁶.

Recently, protein posttranslational modification (PTM), which regulates structures and functions of proteins in living tissues, has also been reported to play important roles in meat quality^{4,7}. Phosphorylation is one of the first reported and most commonly PTMs. Notably, it has been found that protein phosphorylation negatively affects meat tenderness, color and water holding capacity (WHC)^{8,9}. Proteins phosphorylation in the glycolysis pathway is believed to lead to pale, soft, and exudative (PSE)-like meat in broiler¹⁰. Moreover, AMP-activated protein kinase (AMPK) phosphorylation was significantly positively correlated with AMP/ATP ratio, droplet loss, and cooking loss of meat¹¹. Protein phosphatase magnesium/manganese-dependent 1J (*PPM1J*) belongs to the metal-dependent protein phosphatase family, which is well known to involved in regulating diverse cellular functions, such as cell cycle control, cell differentiation, immune responses, and cell metabolism, by modulating reversible protein

¹Institute of Animal Science, Guangdong Academy of Agricultural Sciences, State Key Laboratory of Swine and Poultry Breeding Industry, Key Laboratory of Animal Nutrition and Feed Science in South China, Ministry of Agriculture and Rural Affairs, Guangdong Key Laboratory of Animal Breeding and Nutrition, Guangzhou, China. ²State Key Laboratory of Swine and Poultry Breeding Industry, Lingnan Guangdong Laboratory of Agriculture, College of Animal Science, South China Agricultural University, Guangzhou, China. ³Guangdong Provincial Key Lab of Agro-Animal Genomics and Molecular Breeding, and Key Laboratory of Chicken Genetics, Breeding and Reproduction, Ministry of Agriculture, Guangzhou, China. ⁴These authors contributed equally: Manting Ma, Xin Yang

✉ e-mail: bolincai@scau.edu.cn; zhengcht@163.com

phosphorylation¹². Recent studies have shown that PPM phosphatase family facilitated adipogenesis and fat accumulation through dephosphorylation of PPAR γ ¹³.

In this study, metabolome based on mass spectrometry and transcriptome were performed to construct key metabolite-gene networks involved in the formation of meat flavor by using Guangming-2 (GM2, FG broilers, which is a white-feathered broiler autonomous bred by Chinese) and Xinghua chicken (XH, SG broilers, which is a Chinese native breed with yellow-feather). Based on the above results, *PPM1J*, which is one of the genes with the highest connectivity of meat flavor-related metabolites, was selected as a candidate. Here, to study the role of *PPM1J* in meat flavor formation, lentivirus-mediated *PPM1J* overexpression or knockdown animal model were constructed. Non-target metabolomic and phosphoproteomic analysis were further performed to explore its molecular mechanism. Our study reveals a model in which protein phosphatase regulates meat flavor formation by mediating protein dephosphorylation, and will contribute to the development of further studies.

Results

The regulatory network governing meat flavor formation in different broilers

To explore the differences in meat flavor of different broiler breeds, GM2 and XH at marketing age were selected for the further study. H&E staining analysis was performed to analyze the differences in myofiber cross-sectional area in breast muscle of GM2 (GM2-B) and of XH (XH-B). The breast muscle of GM2 exhibited a higher proportion of large myofibers (>1000 μm^2) compared to XH (Fig. 1A, B).

To identify the differences in chemical composition of muscle of different broiler breeds, metabolomics analysis by UHPLC-Q-TOF-MS/MS technology was performed in GM2-B and XH-B. The OPLS-DA model evaluation parameters (R^2Y , Q^2) obtained after 7 cycles interactive verification are listed in Supplementary Table S1. Both R^2Y and Q^2 are greater than 0.93 (Supplementary Table S1), indicating that this model is stable and reliable. Meanwhile, as the permutation retention gradually decreased, the R^2 and Q^2 of the random models gradually reduced (Supplementary Fig. S1A, B), explaining that there was no over-fitting in the original model and a distinct difference in the metabolite composition between GM2-B and XH-B. We screened out differential metabolites with $VIP > 1$, $FC > 1.5$ or $FC < 0.67$, and P value < 0.05 . A total of 254 different metabolites were identified, of which 84 metabolites were up-regulated and 170 metabolites were down-regulated in GM2-B (Fig. 1C, D; Supplementary Table S2). KEGG pathway analysis of differential metabolites was performed to identify significantly enriched metabolic pathways. A total of 77 metabolic pathways involving 184 different metabolites were identified. These metabolic pathways are mainly enriched in biosynthesis of amino acids, aminoacyl-tRNA biosynthesis, and neuroactive ligand-receptor interaction (Supplementary Fig. S2A). The differential metabolic pathways were also analyzed by differential abundance (DA) analysis. 20 metabolic pathways were captured, including 8 pathways (like beta-Alanine metabolism, aminoacyl-tRNA biosynthesis, and pyrimidine metabolism) were up-regulated (>0.5 DA score, red) (Supplementary Fig. S2B).

To further determine the genetic factors associated with muscle chemical composition, RNA-Seq was used to analyze gene expression changes between GM2-B and XH-B. Totally, 1766 (851 up-regulated while 915 were down-regulated) differential expression genes (DEGs) were identified (Fig. 1E, F; Supplementary Table S3). GO enrichment analysis were performed to determine the function of these DEGs. The top 3 enriched terms were multicellular organismal process, acid secretion, and cell periphery (Supplementary Fig. S2C). To explore the molecular pathways involved in these DEGs, KEGG enrichment analysis were also performed. The DEGs were mainly enriched in neuroactive ligand-receptor interaction, calcium signaling pathway, and inflammatory mediator regulation of TRP channels (Supplementary Fig. S2D).

Correlation analysis of the metabolome and transcriptome were performed, and the variations of differential metabolites and DEGs in

and XH-B comparison were illustrated by nine-quadrant diagrams, with $|R| > 0.80$ and $P < 0.05$ (Fig. 1G). 2538 positive metabolite-gene connections and 3647 negative metabolite-gene connections were identified. (Fig. 1H). Comparing the differences in meat flavor-related metabolite in different breeds, we found that 8 amino acids and nucleotides (Methionine, Glycine, Histidine, Leucine, Phenylalanine, Tyrosine, Hypoxanthine, Inosine, and Inosine 5'-monophosphate) were up-regulated in GM2-B, while only Lysine content was decreased (Fig. 1H). The connections between meat flavor-related differential metabolites and the top 30 DEGs were analyzed to identify the key genetic factors involved in the formation of meat flavor (Fig. 1I). The meat-flavor-related metabolite-gene networks comprised 20 gene-metabolite connections ($|R| > 0.8$, $P < 0.05$) among 8 genes and 6 metabolites was constructed (Fig. 1J). And the top 3 genes with the most connectivity were *PPM1J*, *ELN*, and *CCDC92B* (Fig. 1J).

PPM1J regulates muscle development and meat quality feature

PPM1J, which is one of the most differential expressed gene with the highest connectivity of meat flavor-related metabolites was found (Fig. 2A–C), implied that *PPM1J* is probably associated with meat flavor formation. Tissue expression profile found that *PPM1J* was highly expressed in breast muscle, leg muscle, and heart (Fig. 2D). To analyze the potential function of *PPM1J*, we used the SOPMA software to predict its secondary structure. The result showed that alpha helix, beta turn, extended strand, and random coil accounted for 24.46%, 4.24%, 14.34% and 54.95% of the *PPM1J* protein, respectively (Fig. 2E). In addition, molecular phylogenetic analysis revealed chicken *PPM1J* protein has a large genetic distance with mammals, whereas mainly conserved in *Aves* (such as *Coturnix japonica* and *Meleagris gallopavo*) (Fig. 2F).

To prepare efficient *PPM1J* overexpression and knockdown lentivirus, *PPM1J* overexpression vector was constructed and specific siRNA against *PPM1J* were synthesized. The qPCR results showed that these vector and RNA oligonucleotide could significantly overexpress and inhibit the expression of *PPM1J* in CPM (Fig. 3A and Supplementary Fig. S3A), suggesting that they can be used for lentivirus production. Subsequently, lentivirus-mediated *PPM1J* overexpression (Lv-*PPM1J*) and lentivirus-mediated *PPM1J* knockdown (Lv-sh*PPM1J*) animal models were constructed through targeted injection (Fig. 3B and Supplementary Fig. S3B).

Previous studies have established a strong correlation between the muscle fiber characteristics (including myofiber cross-sectional area (CSA) and diameter) and tenderness of meat^{14,15}. Firstly, we analyzed the function of *PPM1J* on muscle fiber characteristics. The results shown that *PPM1J* overexpression increased the proportion of small myofiber ($\leq 1000 \mu\text{m}^2$) (Supplementary Fig. S3C, D). Inversely, the proportion of large myofiber ($>1000 \mu\text{m}^2$) was raised with *PPM1J* knockdown (Fig. 3C, D), indicating that *PPM1J* regulates myofiber CSA. To explore the regulatory mechanism of *PPM1J* on muscle development, we further detected the genes associated with ubiquitin-proteasome system (UPS) after *PPM1J* overexpression and knockdown. The results demonstrated that overexpression of *PPM1J* upregulated the expression level of *ATROGIN1* and *MURF1*, while the opposite result occurred upon *PPM1J* knockdown (Fig. 3E and Supplementary Fig. S3E). Furthermore, immunofluorescence staining was also performed to investigate the potential function of *PPM1J* in myoblast differentiation. The results showed that suppression of *PPM1J* increased the total areas of myotubes, while myotube formation was reduced with *PPM1J* overexpression (Fig. 3F, G and Supplementary Fig. S3F, G). Given that *PPM1J* function in muscle development, we also analyzed the biological effect of *PPM1J* in meat-quality performance. Overexpression of *PPM1J* decreased the shear force, but significantly increased the WHC and IMF content of breast muscle (Supplementary Fig. S3H–J). On the contrary, shear force was increased while WHC and IMF content were decreased after *PPM1J* knockdown (Fig. 3H–J), indicating that *PPM1J* improves meat quality feature.

PPM1J regulates meat flavor-related metabolites

Given that *PPM1J* is one of the most differential expressed gene with the highest connectivity of meat flavor-related metabolites, we performed

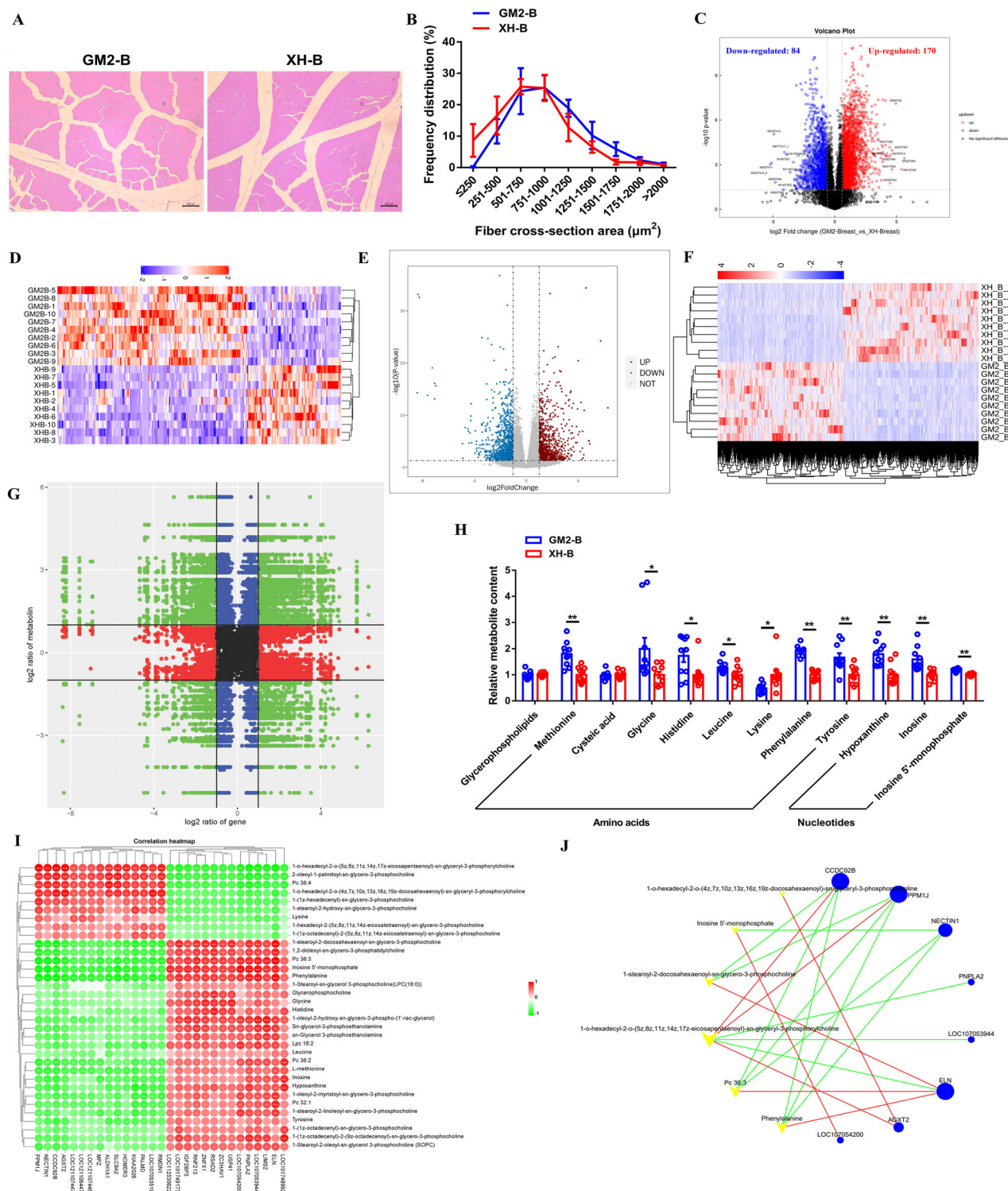


Fig. 1 | Identification of muscle characteristics in breast muscle of GM2 and XH. H&E staining (A) and frequency distribution of fiber cross-section area (B) in breast muscle of GM2 (GM2-B) and breast muscle of XH (XH-B) comparison. The volcano plot (C) and hierarchical clustering analysis (D) of differential metabolites in GM2-B and XH-B comparison. The volcano plot (E) and hierarchical clustering analysis (F) of DEGs in GM2-B and XH-B comparison. G Nine-quadrant diagrams show the correlation of metabolites (obtained from metabolome) and genes (identified from transcriptome) in GM2-B and XH-B comparison. H Relative meat flavor-related

metabolite content in GM2-B and XH-B comparison. I Correlation heatmap of meat flavor-related differential metabolites and the top 30 differential expressed genes in GM2-B and XH-B comparison. K Regulatory network between screened differential metabolites top 30 DE genes and the top 30 differential expressed genes in GM2-B and XH-B comparison. In panels B and H, results are shown as mean \pm SEM. Statistical significance of differences between means was assessed using independent sample *t*-test. (* $P < 0.05$; ** $P < 0.01$).

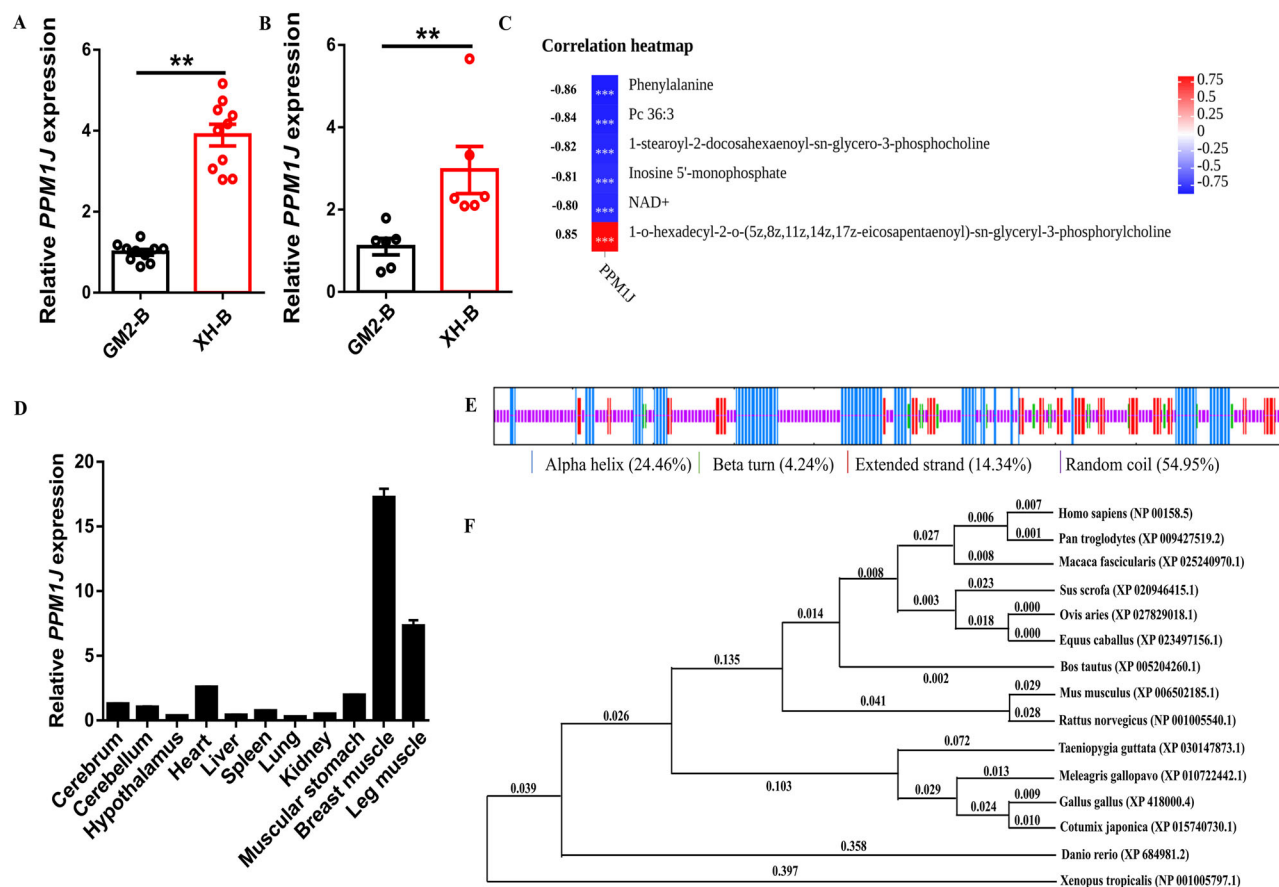


Fig. 2 | Identification of chicken *PPM1J*. Relative *PPM1J* expression in breast of Guangming-2 chicken and Xinhua chicken detected by RNA-seq (A) and qPCR (B). C Correlation analysis of *PPM1J* and meat flavor related metabolites. D Tissue expression profiles of *PPM1J*. The horizontal axis and vertical axis indicate different tissues and their relative expression values, respectively. E Secondary structure of

PPM1J protein predicted by SOPMA software (https://npsa-prabi.ibcp.fr/cgi-bin/npsa_automat.pl?page=npsa_sopma.html). F Phylogenetic tree of chicken *PPM1J* aligned amino acid sequences was analyzed by using MEGA 11 software. Results are presented as mean \pm SEM. In panels A and B, statistical significance of differences between means was assessed using paired *t*-tests. (* $P < 0.05$; ** $P < 0.01$).

metabolome to inquire about the metabolite landscapes in *PPM1J* knock-down muscle. OPLS-DA models were conducted, and results of OPLS-DA analysis showed that these comparisons could be clearly distinguished, indicating that these models are stable and reliable (Fig. 4A). We screened out differential metabolites with VIP > 1, and P -value < 0.05. Respectively, 75 metabolites were found to be downregulated, while 42 were upregulated. (Fig. 4B, C and Supplementary Table S4). According to their chemical taxonomy attribution information, the categories with the most differential metabolites are lipids and lipid-like molecules (25.89%), organic acids and derivatives (20.54%) and benzenoids (15%) (Fig. 4D). Among them, the content of meat flavor related metabolites, such as 1-stearoyl-2-docosahexaenoyl-sn-glycero-3-phosphocholine, glycine and hypoxanthine were significantly up-regulated with *PPM1J* knockdown (Fig. 4E). Inversely, 1-o-hexadecyl-2-o-(5z,8z,11z,14z,17z-eicosapentaenoyl)-sn-glyceryl-3-phosphorylcholine and anserine were significantly downregulated in *PPM1J* knockdown muscle (Fig. 4E). KEGG pathway analysis was used to extract biological pathways associated with these identified differential metabolites. The results showed that differential metabolites were mainly related to the ABC transporters, valine, leucine and isoleucine biosynthesis and starch and sucrose metabolism (Fig. 4F).

PPM1J mediates protein dephosphorylation in muscle

Recently, numerous studies have found that phosphorylation of proteins affects meat quality^{9,16}. *PPM1J* is well known to regulate reversible protein phosphorylation¹², suggested that it may exert its biological function by mediating protein dephosphorylation. To explore the molecular mechanism of *PPM1J* function in meat flavor formation, quantitative

phosphoproteomic analysis using 4D-labfree labeling was performed in *PPM1J* knockdown muscle. A total of 3372 phosphosites mapped onto 2903 phosphopeptides corresponding to 1279 phosphoproteins were identified (Fig. 5A). Among the 1279 phosphoproteins, 61.16% of the proteins have more than two phosphorylation sites (Fig. 5B). The length distribution of phosphorylated peptides and the molecular weight distribution of phosphoproteins were further analyzed (Fig. 5C, D). The results showed that the phosphorylated site distribution in *PPM1J* knockdown muscle is very diverse. Among the 3372 phosphorylation sites, 2692 (79.84%) occurred at Ser, 619 (18.36%) occurred at Thr, and 61 (1.79%) occurred at Tyr residues (Fig. 5E).

To reveal the differential abundance of phosphopeptides (DAPs) in *PPM1J* knockdown muscle, phosphopeptides with a FC > 2 or < 0.5 and a P -value < 0.05 were identified. Volcano plots and hierarchical cluster analysis were performed, and 33 phosphopeptides with differential abundance were identified (Fig. 5F, G). Specifically, 18 phosphopeptides were up-regulated, while 15 were down-regulated. (Fig. 5F, G; Supplementary Table S5). Meanwhile, 61 phosphopeptides were found to specifically peculiar in the *PPM1J* knockdown group, while 46 phosphopeptides were only present in the control group (Supplementary Table S6).

Most of the up-regulated phosphopeptides are associated with actin binding and muscle development-related proteins, such as Titin (TTN), Obscurin (OBSCN) and troponin T (TNNT3) (Supplementary Table S6). Moreover, RICTOR (an important component of mTORC2 kinase) and heat shock protein family members (like HSPD1 and HSPB1) was specifically phosphorylated after *PPM1J* knockdown, suggesting that *PPM1J* may regulate meat quality feature by mediating protein phosphorylation. GO

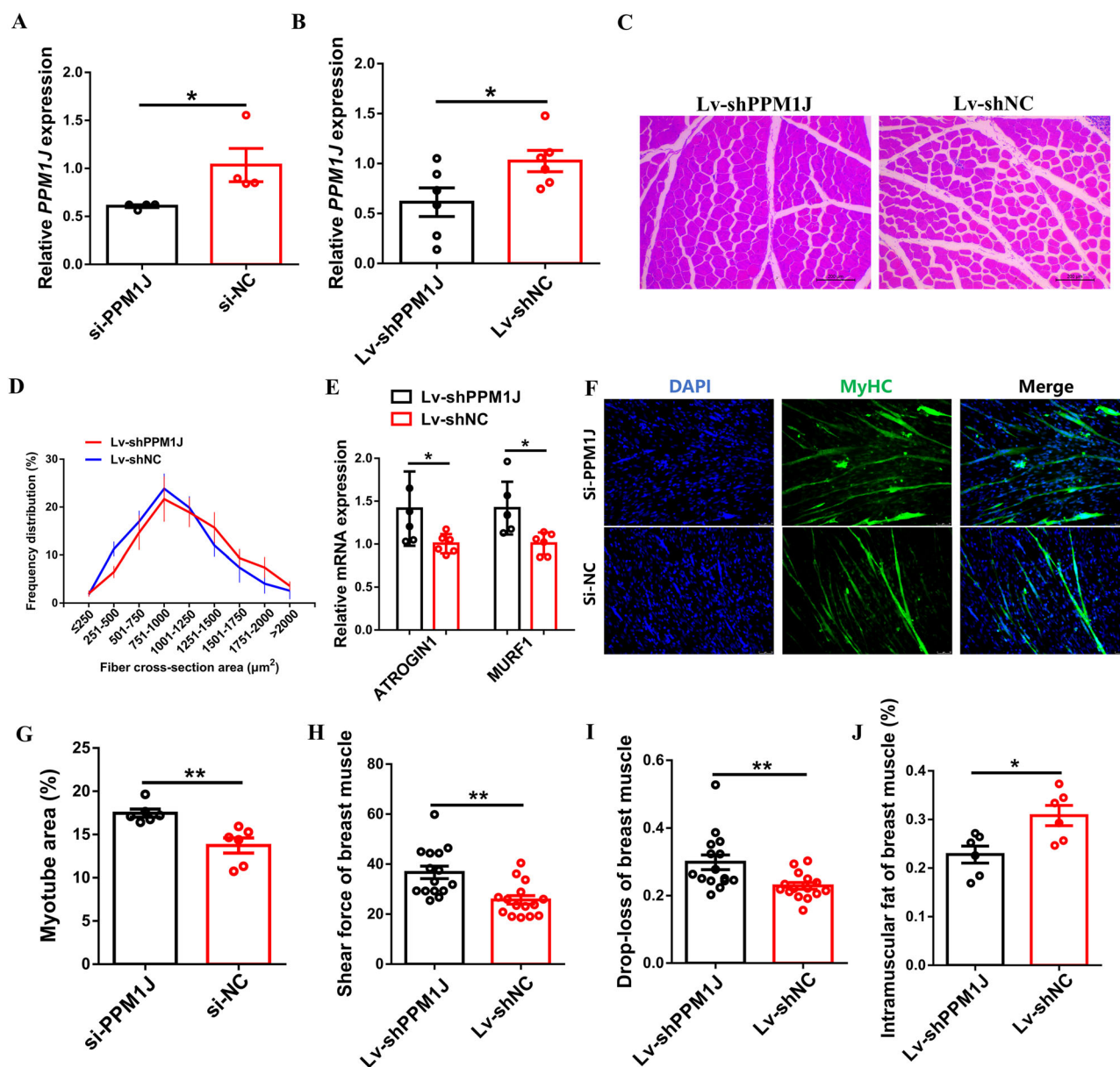


Fig. 3 | *PPM1J* regulate muscle development and meat quality feature. A Relative *PPM1J* expression with *PPM1J* interference in CPMs. B-E. Relative *PPM1J* mRNA expression (B), H&E staining (C), frequency distribution of fiber cross-section area (CSA) (D), and relative *ATROGIN1* and *MURF1* expression (E) in breast muscle with infection of lentivirus-mediated *PPM1J* knockdown (Lv-shPPM1J); MyHC

immunostaining (F), myotube area (%) (G) of CPMs transduced with *PPM1J* interference. Shear force (H), Drop-loss (I), and IMF (J) in breast muscle with *PPM1J* knockdown. In panels (A, B, E and G–J), results are shown as mean ± SEM, statistical significance of differences between means was assessed using paired *t*-tests (A, B, and G–J) and independent sample *t*-tests (E). (**P* < 0.05; ***P* < 0.01).

enrichment analyses were performed to identify the functional terms of these DAPs (Fig. 5H). According to biological processes, the most significantly enriched proteins were involved in positive regulation of cytokine production, regulation of cytokine production, and cytokine production (Fig. 5H). In addition, the major cellular components were related to sarcomere, contractile fiber, myofibril. Moreover, KEGG pathway analysis was performed. Vascular smooth muscle contraction, MAPK signaling pathway and tight junction were the most enriched pathways associated with the DAPs. (Fig. 5G).

Analysis of regulatory network of *PPM1J* regulating meat flavor formation

To investigate whether *PPM1J* participates in the formation of meat flavor through mediated protein phosphorylation, we analyzed the co-enrichment pathways of DAPs and differential metabolites. The results showed that

DAPs and differential metabolites are mainly co-enriched in metabolic pathways, including fructose and mannose metabolism, galactose metabolism, and methane metabolism (Fig. 6A). The correlation heat maps of DAPs and differential metabolites were further analyzed, considering only those with $|R| > 0.80$ and $P < 0.05$ (Fig. 6B). Further analysis of the nine-quadrant diagram showed the changes of DAPs and differential metabolites. 145 positive metabolite-DAPs connections and 5 negative metabolite-DAPs connections were identified (Fig. 6C).

Given that the expression of *PPM1J* is correlated with the content of glycerophospholipids (like 1-stearoyl-2-docosahexaenoyl-sn-glycero-3-phosphocholine and 1-o-hexadecyl-2-o-(5z,8z,11z,14z,17z-eicosapentaenoyl)-sn-glycerol-3-phosphorylcholine), and that knockdown of *PPM1J* regulates the contents of these glycerophospholipids (Figs. 2C and 4E), we further scanned differentially abundant phosphoproteins which are associated with these glycerophospholipids. Excitingly, we found that MYLK4,

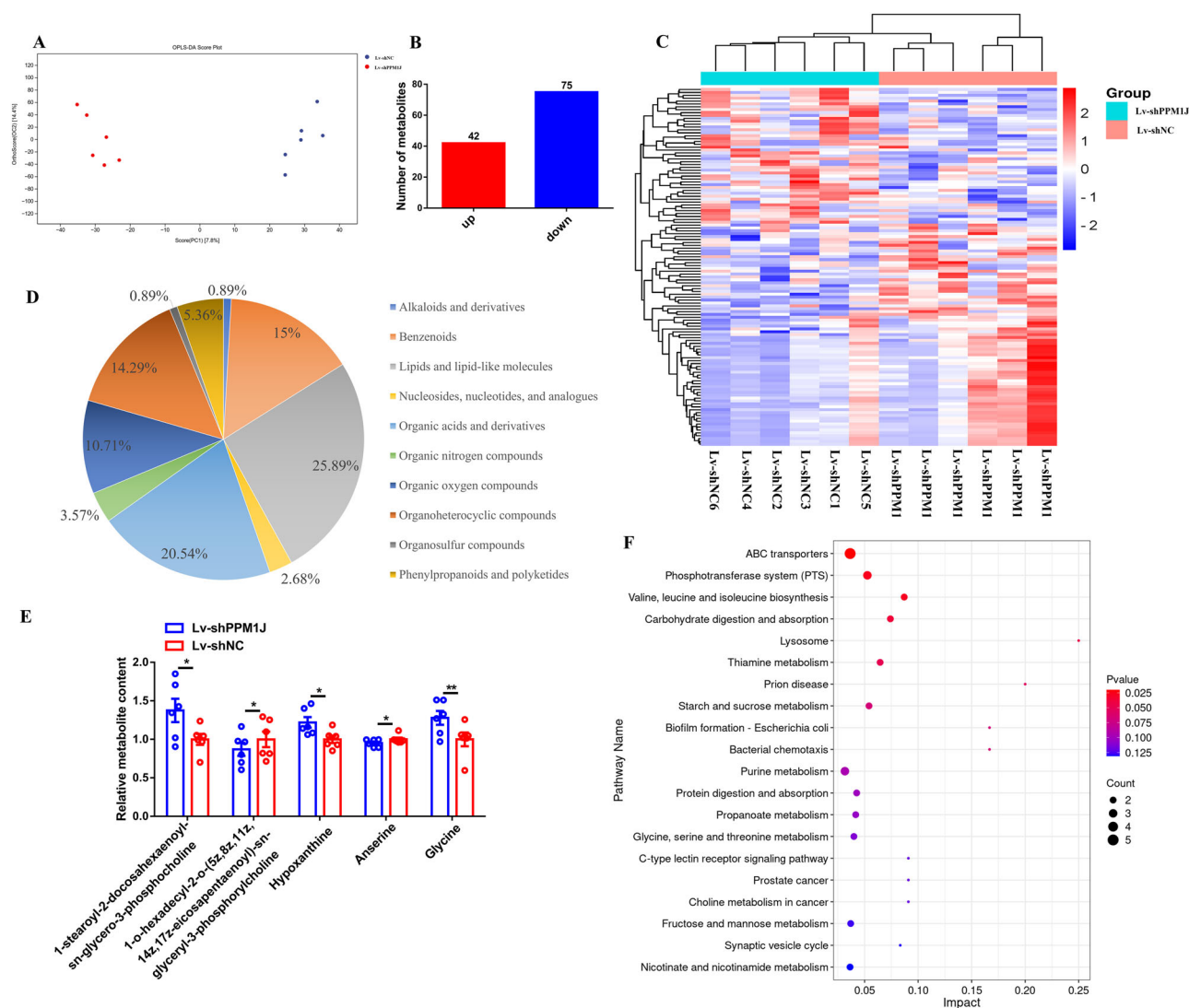


Fig. 4 | Analysis of metabolome in muscle of *PPM1J* knockdown. A–D The OPLS-DA score scatter plots result of the positive and negative ion mode in *PPM1J* knockdown muscle. **B–F** Statistics (**B**), heatmap (**C**), chemical taxonomy (**D**) of differential metabolites in *PPM1J* knockdown muscle. **E** Relative meat flavor-related

metabolite content in *PPM1J* knockdown muscle. **F** KEGG pathway analysis of differential metabolites in *PPM1J* knockdown muscle. In panel **E**, results are shown as mean + SEM, statistical significance of differences between means was assessed using paired *t*-tests. (**P* < 0.05; ***P* < 0.01).

AAK1, and SYNPO2L, which are specifically phosphorylated in *PPM1J* knockdown muscle, were highly correlated with the content of 1-stearoyl-2-docosahexaenoyl-sn-glycero-3-phosphocholine (Fig. 6D). Moreover, DUSP27 (which is a specific phosphorylated protein in *PPM1J* knockdown muscle) and DDI2 (which is up-regulate phosphorylated with *PPM1J* knockdown) were found negatively correlated with the content of 1-o-hexadecyl-2-o-(5z,8z,11z,14z,17z-eicosapentaenoyl)-sn-glycyl-3-phosphorylcholine (Fig. 6E). In consideration of *PPM1J* functions as a protein phosphatase that can catalytic protein dephosphorylation, we infer that *PPM1J* may regulate the composition of glycerophospholipids by modulating the phosphorylation level of MYLK4, AAK1, SYNPO2L, DUSP27 and DDI2.

Discussions

With the improvement of living standards, consumers' demand for broiler meat flavor is increasing. Compared to yellow feather broilers, white feather broilers are FG broilers with higher breast muscle rate. However, the rapid growth of broilers has been identified as the main cause of meat quality issues¹⁷. Moreover, SG broiler is considered to have a better meat quality compare to FG broiler^{4,18}. Skeletal muscle is the main component of poultry meat and is made up of myofibers. The diameter and density of myofibers

have been reported to influence meat tenderness on a tissue level, serving as a crucial indicator for the evaluation of muscle tenderness¹⁹. In this study, we found that breast muscle in GM2 have larger myofiber diameter than XH, suspecting that the difference in cross-sectional area may contributed to variations of meat flavor between GM2 and XH.

Amino acids have many nutritional and physiological functions, which affect the nutritional value and taste of meat²⁰. Different amino acids have different tastes, generally can be classified as sweet, sour, salty, bitter, umami, and tasteless^{21,22}. Except for lipids and free amino acids, nucleotides also play important roles in imparting unique aroma and taste properties to meat products^{22,23}. In this study, we found numerous bitter or sour amino acids (such as Histidine, Leucine, Methionine, Phenylalanine, and Tyrosine), hypoxanthine and inosine were increased, whereas Lysine (which is sweet) was reduced in breast muscle of GM2, indicated that there were significant differences in muscle flavor related metabolites between different breeds.

Discovery of genetic regulatory factors involved in formation of meat flavor is of great significance to broiler production. To systematically identify the genetic regulation of differences in meat flavor among different broiler, we integrate metabolome and transcriptome data, and constructed key meat flavor-related metabolite-gene networks, 20 metabolite-gene connections among 6 metabolites and 8 genes were identified. *PPM1J* has

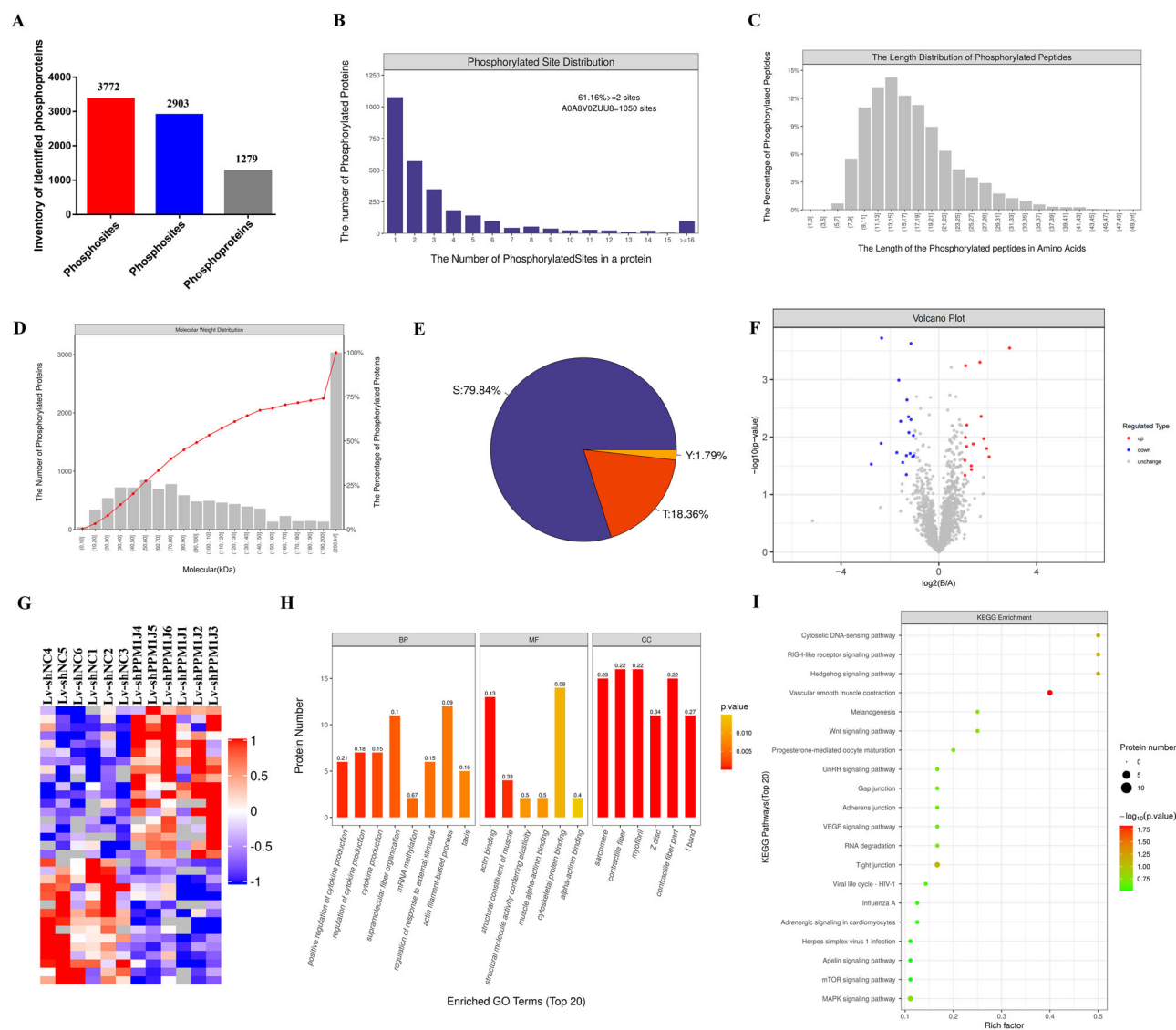


Fig. 5 | Analysis of phosphoproteome in muscle of *PPM1J* knockdown. **A** Number of phosphosites, phosphopeptides, and phosphoproteins detected in *PPM1J* knockdown muscle. **B** Distribution and number of phosphosites matched to phosphoproteins in *PPM1J* knockdown muscle. **C** The length distribution of phosphorylated peptides in *PPM1J* knockdown muscle. **D** The molecular weight

distribution of phosphoproteins in *PPM1J* knockdown muscle. **E** Distribution of the amino acid residues for all detected phosphosites in *PPM1J* knockdown muscle. Volcano plot (**F**), hierarchical clustering analysis (**G**), GO terms analysis (**H**) and KEGG pathways analysis (**I**) of DAPs in *PPM1J* knockdown muscle.

been reported to play important roles in metabolism and disease by mediating protein phosphorylation^{24,25}. Here, we found that *PPM1J* is one of the genes with the highest connectivity of meat flavor-related metabolites. *PPM1J* overexpression reduced the cross-sectional area of myofibers. Ubiquitin-specific peptidase 10 (USP10) functions as a deubiquitinating enzyme that inhibits the ubiquitin-proteasome system (UPS) degradation pathway. Previous study revealed that phosphorylation of USP10 inhibits the USP degradation pathway by enhancing protein stability and inhibiting muscle atrophy²⁶. Interestingly, we observed that USP10 is specifically phosphorylated in the breast muscles with *PPM1J* knockdown, indicating that *PPM1J* may mitigate muscle atrophy by modulating USP10 phosphorylation. The diameter and density of myofibers are closely related to muscle tenderness. In meat-quality traits, overexpression of *PPM1J* reduces muscle shear force, which means better tenderness. Tenderness can most likely be attributed to IMF content and WHC²⁷. *PPM1J* increases the content of IMF and WHC in the muscles, suggesting that it may contribute significantly to better tenderness. Lipids could produce flavor precursor

compounds through the lipolysis and oxidation²⁸. Moreover, phospholipids are a major component of intramuscular fat, which is related to such as juiciness, flavor and tenderness. Here, we found *PPM1J* knockdown reduced the content of 1-o-hexadecyl-2-o-(5z,8z,11z,14z,17z-eicosapentaenoyl)-sn-glycerol-3-phosphorylcholine, while promoted the accumulation of 1-stearoyl-2-docosahexaenoyl-sn-glycerol-3-phosphocholine, explained that *PPM1J* enhances muscle tenderness through the regulation of glycerophospholipid composition in muscle. Previous studies indicated that water-soluble compounds with taste or tactile properties, such as hypoxanthine and certain amino acids are associated with bitterness, while anserine is known to produce umami²⁹. Here, *PPM1J* knockdown significantly promoted hypoxanthine levels and decreased the content of anserine, suggested that *PPM1J* is helpful to improve meat flavor. The *ELN* gene encodes tropoelastin which is used to generate elastic fibers that insure proper tissue elasticity³⁰. *ELN* has reported to be mainly expressed during early developmental stages, and its insufficiency predisposes to metabolic disease³⁰. Coiled-coil domain containing 92B (*CCDC92B*) belongs to the

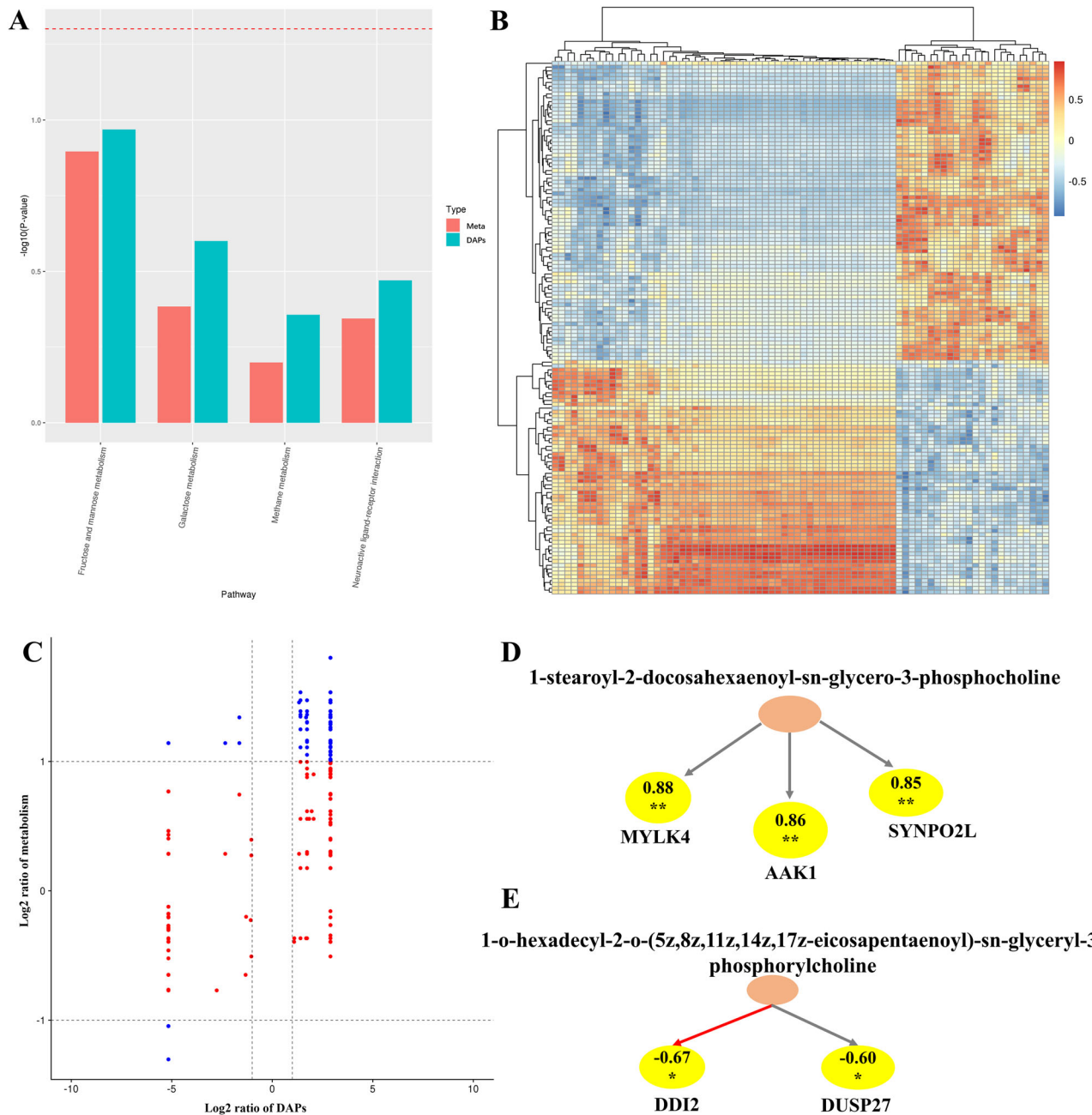


Fig. 6 | Correlation analysis of the phosphoproteome and metabolomes. **A** DAPs (identified from phosphorylomics) and metabolite differential co-enrichment pathway in *PPM1J* knockdown muscle. **B** Correlation heatmap of DAPs and differential metabolites (obtained from metabolome) in *PPM1J* knockdown muscle. **C** Nine-quadrant diagrams show the correlation of differential metabolites and

DAPs in *PPM1J* knockdown muscle. **D–E** Regulatory network between glycerophospholipids (like 1-stearoyl-2-docosahexaenoyl-sn-glycero-3-phosphocholine ($|R| > 0.80$ and $P < 0.05$) (**D**) and 1-o-hexadecyl-2-o-(5z,8z,11z,14z,17z-eicosapentaenoyl)-sn-glyceryl-3-phosphorylcholine ($|R| > 0.60$ and $P < 0.05$) (**E**)) and DAPs in *PPM1J* knockdown muscle.

coiled-coil domain-containing protein family. Previous research has indicated that *CCDC* genes are associated with metabolic disorders and lipid metabolism³¹. Given that the expression of *ELN* and *CCDC92B* is mainly connect to glycerophospholipids, we speculated that they may function in meat flavor formation by modulating lipid metabolism.

Recently, numerous studies have reported that the phosphorylation of certain proteins negatively influences meat tenderness, color, and WHC^{9,32–34}. The heat shock protein (HSP) family is responsible for cell protection that involved in stress resistance and apoptotic signaling pathway. The high abundance of HSPs has the potential to delay meat aging, which negatively impacts meat tenderness^{35,36}. In the study, we found HSPB1 and HSPD1 are specifically phosphorylated in *PPM1J* knockdown

muscle. In addition, RICTOR, which plays a crucial role in mTOR kinase activity, was also found to be specifically phosphorylated after *PPM1J* knockdown, indicating that *PPM1J* may improve muscle tenderness by mediating protein dephosphorylation. As an important component of intramuscular fat, phospholipids make significant contributions to the flavor of meat. Here, we found *PPM1J* knockdown induced phosphorylation of MYLK4, AAK1, SYNPO2L, DUSP27, and DDI2, which are significantly correlated with the content of glycerophospholipids, suggesting that *PPM1J* modulates the phosphorylation level of proteins to regulate glycerophospholipids composition.

In conclusion, we demonstrated that *PPM1J* is one of the genes with the highest connectivity of meat flavor-related metabolites. *PPM1J*, which is

highly expressed in muscle, regulates meat quality feature and glycerophospholipids composition by mediating protein dephosphorylation. Our study reveals a model in which protein phosphatase regulates meat quality feature and glycerophospholipids composition, and will contribute to the development of further studies.

Materials and methods

Ethics statement

All animal experimental protocols were conformed to “The Instructive Notions with Respect to Caring for Laboratory Animals” issued by the Ministry of Science and Technology of the People’s Republic of China, and approved by the Institutional Animal Care and Use Committee at the South China Agricultural University (approval ID: 2021c008).

Animals and cell

GM-2 and XH chickens were purchased from JinKai Agriculture and Animal Husbandry Co., Ltd. and ZhiCheng Poultry Breeding Co., Ltd, respectively.

Chicken primary myoblasts (CPMs) were isolated from E11 chicken leg muscles as previously described³⁷, and cultured in Roswell Park Memorial Institute (RPMI)-1640 medium (Gibco, USA) with 20% fetal bovine serum (Gibco, USA).

RNA isolation, complementary DNA (cDNA) synthesis, and real-time (RT) PCR analysis

Total RNA was extracted from tissues or cells using RNAiso plus reagent (TaKaRa, Japan). cDNA synthesis was obtained by using a PrimeScript RT Reagent Kit with gDNA Eraser (Perfect Real Time) (Takara, Japan). Real-time quantitative PCR (qRT-PCR) reactions were performed on a QuantStudio 5 Real-Time PCR Systems (Thermo Fisher, Waltham, MA, USA) by using a ChamQ Universal SYBR qPCR Master Mix (Vazyme, China). All primers for RT-PCR and real-time qPCR are listed in Supplementary Table S7.

Plasmid construction and RNA oligonucleotides

For viral vectors constructed, the full-length sequence of *PPM1J* was amplified and then cloned into a pLVX-mCMV-ZsGreen-IRES-Puro vector (Addgene, USA).

The small interfering RNAs (siRNA) that were used for the specific knockdown of *PPM1J* were designed and synthesized by Guangzhou RiboBio Biotechnology Co., Ltd. In order to produce a large number of interfering fragments to construct *PPM1J* knockdown animal model, specific siRNA sequence was cloned into the pLVX-shRNA2-Puro vector (Addgene, USA).

Primer pairs for vector construction and the sequence of oligonucleotides are presented in Supplementary Tables S7 and S8.

All transient transfections were performed using Lipofectamine 3000 Reagent (Invitrogen, USA) according to the manufacturer’s instructions.

Lentivirus production and transduction

Lentivirus productions were performed as described before³⁷. Thirty Xinhua chickens of 14 weeks were randomly divided into two groups (n = 15) (1) experimental group: Lv-PPM1J and control group: Lv-NC, (2) experimental group: Lv-shPPM1J and control group: Lv-shNC. Chickens received thrice intramuscular doses of lentivirus (10^6 titers) in the breast muscle (at the age of 14, 15, and 16 weeks). Chickens at 17 weeks were euthanized according to the Chinese National Standard (GB/T 19478-2018). Briefly, before slaughter, chickens were fasted for 12 h but had free access to water. Subsequently, chickens were unconscious by electric shock and euthanized using exsanguination method. Muscles were collected after rapid dissection, then immediately frozen in liquid nitrogen and stored at -80°C .

Hematoxylin and eosin (HE) staining

HE staining were performed as described before³⁷.

Immunofluorescence

Immunofluorescence was performed using anti-MyHC (B103; DHSB, USA; 2.5 mg/mL), and images were captured using a fluorescence microscope (DMI8; Leica, Germany). The area of cells labeled with anti-MyHC was measured and calculated as previously described³⁷.

Meat-quality traits determination

Meat tenderness was measured by shear force using a C-LM4 digital tenderness meter (Tenovo, China). The muscles were cut into three pieces ($2.5 \times 1.0 \times 3.0 \text{ cm}^3$) to measure shear force at a speed of 1 mm/s. Each piece of data was measured three times, and the average value was taken as final value.

WHC was measured by drip loss. After removing the excess fat and fascia, muscles were cut into three pieces ($2.0 \times 1.0 \times 3.0 \text{ cm}^3$) to be weighed and stored in a plastic bag at 4°C for 24 h. The pieces were wiped dry and weighted to calculate drip loss.

Intramuscular fat (IMF) content was measured using a Soxtec automated analyzer (FOSS Analytical, Hillerød, Denmark). Grind 30 g breast muscle into meat batters and remove moisture by oven-drying at 110°C for 5 h. The routine Soxhlet extraction method was conducted to extract the total fat with petroleum ether, and IMF content was calculated. Each data was measured three times to take the average value.

RNA sequencing (RNA-seq)

For RNA-seq, total RNA was extracted from the breast tissue using TRIzol® Reagent according to the manufacturer’s instructions (Magen). RNA samples were detected based on the A260/A280 absorbance ratio with a Nanodrop ND-2000 system (Thermo Scientific, USA), and the RIN of RNA was determined by an Agilent Bioanalyzer 4150 system (Agilent Technologies, USA). Qualified samples were further used for library construction. Paired-end libraries were prepared using an ABclonal mRNA-seq Lib Prep Kit (ABclonal, China) following the manufacturer’s instructions. The library preparations were sequenced on an Illumina Novaseq 6000 and 150 bp paired-end reads were generated. The data generated from Illumina platform were used for bioinformatics analysis.

Enrichment analysis

The Gene Ontology (GO) analysis and Genes and Genomes (KEGG) enrichment analysis of differential genes were performed to explain the functional enrichment of differential genes and clarify the differences between samples at the gene function level. ClusterProfiler R software package was used for GO function enrichment and KEGG pathway enrichment analysis.

Metabolomics analysis by UHPLC-Q-TOF-MS/MS and data processing

Metabolomics analysis was performed using an UHPLC (1290 Infinity LC, Agilent Technologies) coupled to a quadrupole time-of-flight (AB Sciex TripleTOF 6600) in Shanghai Applied Protein Technology Co., Ltd. For HILIC separation, samples were analyzed using a $2.1 \text{ mm} \times 100 \text{ mm}$ ACQUITY UPLC BEH Amide $1.7 \mu\text{m}$ column (Waters, Ireland). The mobile phase in both ESI positive and negative modes consisted of A = 25 mM ammonium acetate and 25 mM ammonium hydroxide in water, along with B=acetonitrile. The gradient was 95% B for 0.5 min and was linearly reduced to 65% in 6.5 min, and then was reduced to 40% in 1 min and kept for 1 min, and then increased to 95% in 0.1 min, with a 3 min re-equilibration period employed.

The ESI source conditions were set as follows: Ion Source Gas1 (Gas1) as 60 psi, Ion Source Gas2 (Gas2) as 60 psi, curtain gas (CUR) as 30 psi, source temperature is 600°C , IonSpray Voltage Floating (ISVF) $\pm 5500 \text{ V}$. In MS only acquisition, the instrument was set to acquire over the m/z range 60–1000 Da, and the accumulation time for TOF MS scan was set at 0.20 s/spectra. In auto MS/MS acquisition, the instrument was set to acquire over the m/z range 25–1000 Da, and the accumulation time for product ion scan

was set at 0.05 s/spectra. The product ion scan was acquired using information dependent acquisition (IDA) with high sensitivity mode selected. The parameters were set as follows: the collision energy (CE) was fixed at 35 V with ± 15 eV; declustering potential (DP), 60 V (+) and -60 V (−); exclude isotopes within 4 Da, candidate ions to monitor per cycle is 10.

Protein extraction and digestion

The protein extraction (4%SDS, 100 mM Tris-HCl, 1 mM DTT, pH7.6) buffer was used for sample lysis and protein extraction. The amount of protein was quantified with the BCA Protein Assay Kit (Bio-Rad, USA). Protein digestion by trypsin was performed according to filter-aided sample preparation (FASP) procedure described by Matthias Mann.

Phosphopeptide enrichment and LC-MS/MS analysis

The enrichment of phosphopeptides was carried out using High-Select™ Fe-NTA Phosphopeptides Enrichment Kit according to the manufacturer's instructions (Thermo Scientific). After lyophilized, the phosphopeptides peptides were resuspended in 20 μ L loading buffer (0.1% formic acid). A reverse phase trap column (Thermo Scientific Acclaim PepMap100, 100 μ m \times 2 cm, nanoViper C18) was used to separate the samples, and the peptide fractions were analyzed using a Q Exactive HF mass spectrometer (Thermo Fisher Scientific, Waltham, USA).

LC-MS/MS analysis was performed on a timsTOF Pro mass spectrometer (Bruker, tims tof pro, Germany) that was coupled to Nanoelute (Bruker Daltonics, Germany) for 60 min. The peptides were loaded on a C18-reversed phase analytical column (homemade, 25 cm long, 75 μ m inner diameter, 1.9 μ m, C18) in buffer A (0.1% Formic acid) and separated with a linear gradient of buffer B (84% acetonitrile and 0.1% Formic acid) at a flow rate of 300 nL/min. The mass spectrometer was operated in positive ion mode. The mass spectrometer collected ion mobility MS spectra over a mass range of m/z 100–1700 and $1/k_0$ of 0.6 to 1.6, and then performed 10 cycles of PASEF MS/MS with a target intensity of 1.5k and a threshold of 2500. Active exclusion was enabled with a release time of 0.4 min.

Identification and quantitation of Phosphorylated proteins

The MS raw data for each sample were combined and searched using the MaxQuant software for identification and quantitation analysis. Trypsin with [D]P was chosen as the specific enzyme with a maximum of two missed cleavages per peptide. The precursor and fragment mass tolerances were set to 20 ppm and 0.05 Da, respectively. The database search parameters were oxidation (methionine), acetyl (protein N-terminus), and phosphorylation (serine, threonine, tyrosine) as variable modifications; carbamidomethyl (cysteine) as fixed modifications. The false discovery rate (FDR) was set at 1%. The NCBI_Gallus_gallus_159905_20230726.fasta was employed for this analysis.

Statistical analysis

In this study, at least three biological replicates were used for all experiments, and data were presented as means \pm standard error (SE). Where applicable, the statistical significance of the data was tested using independent sample *t*-test or paired *t*-test by using SPSS (version 19.0; SPSS, Chicago IL, USA), and $P < 0.05$ was considered statistically significant. Pearson's correlation analysis was given for correlation analysis, and $|R| > 0.80$ and $P < 0.05$ was considered statistically significant. The types of tests and the *P*-values, when applicable, were indicated in the Figure legends. The programs used for graphics and figures were GraphPad Prism (GraphPad Software Inc., USA).

Data availability

All data generated or analyzed during this study are included in this published article (and its supplementary information files). Additional data related to this paper may be available from the corresponding author on reasonable request.

References

- Fan, M. et al. Aroma Compounds in Chicken Broths of Beijing Youji and Commercial Broilers. *J. Agric. Food Chem.* **66**, 10242–10251 (2018).
- Dalle, Z. A., Gleeson, E., Franco, D., Cullere, M., & Lorenzo, J. M. Proximate Composition, Amino Acid Profile, and Oxidative Stability of Slow-Growing Indigenous Chickens Compared with Commercial Broiler Chickens. *Foods* **9**, 546 (2020).
- Dalle, Z. A. et al. Effect of “Wooden Breast” appearance on poultry meat quality, histological traits, and lesions characterization. *Czech J. Anim. Sci.* **62**, 51–57 (2017).
- Weng, K. et al. Fiber characteristics and meat quality of different muscular tissues from slow- and fast-growing broilers. *Poult. Sci.* **101**, 101537 (2022).
- Mir, N. A., Rafiq, A., Kumar, F., Singh, V. & Shukla, V. Determinants of broiler chicken meat quality and factors affecting them: a review. *J. Food Sci. Tec.* **54**, 2997–3009 (2017).
- Bjarnadottir, S. G., Hollung, K., Faergestad, E. M. & Veiseth-Kent, E. Proteome changes in bovine longissimus thoracis muscle during the first 48 h postmortem: shifts in energy status and myofibrillar stability. *J. Agric. Food Chem.* **58**, 7408–7414 (2010).
- Li, X. et al. Effects of protein posttranslational modifications on meat quality: A review. *Compr. Rev. Food Sci. F.* **20**, 289–331 (2021).
- Li, Z. et al. Quantitative phosphoproteomic analysis among muscles of different color stability using tandem mass tag labeling. *Food Chem.* **249**, 8–15 (2018).
- Chen, L. et al. Phosphorylation of myofibrillar proteins in post-mortem ovine muscle with different tenderness. *J. Sci. Food Agric.* **96**, 1474–1483 (2016).
- Xing, T. et al. Proteome Analysis Using Isobaric Tags for Relative and Absolute Analysis Quantitation (iTRAQ) Reveals Alterations in Stress-Induced Dysfunctional Chicken Muscle. *J. Agr. Food Chem.* **65**, 2913–2922 (2017).
- Xing, T., Xu, X. L., Zhou, G. H., Wang, P. & Jiang, N. N. The effect of transportation of broilers during summer on the expression of heat shock protein 70, postmortem metabolism and meat quality. *J. Anim. Sci.* **93**, 62–70 (2015).
- Kamada, R. et al. Metal-dependent Ser/Thr protein phosphatase PPM family: Evolution, structures, diseases and inhibitors. *Pharmacol. Therapeutics* **215**, 107622 (2020).
- Li, D. et al. WIP1 phosphatase is a critical regulator of adipogenesis through dephosphorylating PPARgamma serine 112. *Cell Mol. Life Sci.* **74**, 2067–2079 (2017).
- Baryshnikova, L. M., Croes, S. A. & von Bartheld, C. S. Classification and development of myofiber types in the superior oblique extraocular muscle of chicken. *Anat. Rec.* **290**, 1526–1541 (2007).
- Zhao, G. P. et al. Comparison of breast muscle meat quality in 2 broiler breeds. *Poult. Sci.* **90**, 2355–2359 (2011).
- Huang, H. et al. Gel-based phosphoproteomics analysis of sarcoplasmic proteins in postmortem porcine muscle with pH decline rate and time differences. *Proteomics* **11**, 4063–4076 (2011).
- Kuttappan, V. A., Hargis, B. M. & Owens, C. M. White striping and woody breast myopathies in the modern poultry industry: a review. *Poult. Sci.* **95**, 2724–2733 (2016).
- Devatkal, S. K., Naveena, B. M. & Kotaiah, T. Quality, composition, and consumer evaluation of meat from slow-growing broilers relative to commercial broilers. *Poult. Sci.* **98**, 6177–6186 (2019).
- An, J. Y. et al. Effect of myofiber characteristics and thickness of perimysium and endomysium on meat tenderness of chickens. *Poult. Sci.* **89**, 1750–1754 (2010).
- Owen, J. E. & Lawrie, R. A. The effect of an artificially induced high pH on the susceptibility of minced porcine muscle to undergo oxidative rancidity under frozen storage. *Int. J. Food Sci. Tec.* **10**, 169–180 (2010).

21. Schiffman, S. S., Sennewald, K. & Gagnon, J. Comparison of taste qualities and thresholds of D- and L-amino acids. *Physiol. Behav.* **27**, 51–59 (1981).
22. Dashdorj, D., Amna, T. & Hwang, I. Influence of specific taste-active components on meat flavor as affected by intrinsic and extrinsic factors: An overview. *Eur. Food Res. Technol.* **241**, 157–171 (2015).
23. Chen, J. N. et al. Integrated volatolomics and metabolomics analysis reveals the characteristic flavor formation in Chouguiyu, a traditional fermented mandarin fish of China. *Food Chem.* **418**, 135874 (2023).
24. He, Z. Y. et al. Gamma-H2AX upregulation caused by Wip1 deficiency increases depression-related cellular senescence in hippocampus. *Sci. Rep.* **6**, 34558 (2016).
25. Le Guezennec, X. et al. Wip1-dependent regulation of autophagy, obesity, and atherosclerosis. *Cell Met* **16**, 68–80 (2012).
26. Sun, L., Yu, J., Guinney, J., Qin, B. & Sinicrope, F. A. USP10 Regulates ZEB1 Ubiquitination and Protein Stability to Inhibit ZEB1-Mediated Colorectal Cancer Metastasis. *Mol. Cancer Res.* **21**, 578–590 (2023).
27. Wen, Y. et al. Analysis of the physical meat quality in partridge (*Alectoris chukar*) and its relationship with intramuscular fat. *Poult. Sci.* **99**, 1225–1231 (2020).
28. Xu, Y. et al. The contribution of autochthonous microflora on free fatty acids release and flavor development in low-salt fermented fish. *Food Chem.* **256**, 259–267 (2018).
29. Dashmaa, D., Touseef, A. & Inho, H. Influence of specific taste-active components on meat flavor as affected by intrinsic and extrinsic factors: an overview. *Eur. Food Res Technol.* **241**, 157–171 (2015).
30. Czarnecka-Herok, J. et al. A non-canonical role of ELN protects from cellular senescence by limiting iron-dependent regulation of gene expression. *Redox Biol.* **73**, 103204 (2024).
31. Kobayashi, S. et al. Identification of a new secretory factor, CCDC3/Favine, in adipocytes and endothelial cells. *Biochem Biophys. Res Commun.* **392**, 29–35 (2010).
32. Bowker, B. & Zhuang, H. Relationship between water-holding capacity and protein denaturation in broiler breast meat. *Poult. Sci.* **94**, 1657–1664 (2015).
33. Fritz, J. D., Mitchell, M. C., Marsh, B. B. & Greaser, M. L. Titin content of beef in relation to tenderness. *Meat Sci.* **33**, 41–50 (1993).
34. Ramanathan, R., Suman, S. P. & Faustman, C. Biomolecular Interactions Governing Fresh Meat Color in Post-mortem Skeletal Muscle: A Review. *J. Agr. Food Chem.* **68**, 12779–12787 (2020).
35. Ouali, A. et al. Revisiting the conversion of muscle into meat and the underlying mechanisms. *Meat Sci.* **74**, 44–58 (2006).
36. Takayama, S., Reed, J. C. & Homma, S. Heat-shock proteins as regulators of apoptosis. *Oncogene* **22**, 9041–9047 (2003).
37. Cai, B. et al. Long noncoding RNA SMUL suppresses SMURF2 production-mediated muscle atrophy via nonsense-mediated mRNA decay. *Mol. Ther. Nucleic Acids* **23**, 512–526 (2021).

Acknowledgements

This work was supported by National Key Research and Development Program of China (2022YFF1000201, 2022YFD1300502 and 2022YFD1300503), Natural Scientific Foundation of China (32302728), and Guangdong Basic and Applied Basic Research Foundation (2023A1515111031), and Science and Technology Program of Guangdong Academy of Agricultural Sciences (R2024YJ-YB3004), and State Key Laboratory of Swine and Poultry Breeding Industry (GDNKY-ZQQZ-K22).

Author contributions

C.Z. and B.C. conceived and designed the study. M.M. and X.Y. performed the experiments, interpreted the data and wrote the paper. Y.Z., C.J., S.W., W.X., and W.C. performed the experiments. All authors read and approved the final manuscript.

Competing interests

The authors declare no competing interests.

Additional information

Supplementary information The online version contains supplementary material available at <https://doi.org/10.1038/s41538-024-00335-1>.

Correspondence and requests for materials should be addressed to Bolin Cai or Chuntian Zheng.

Reprints and permissions information is available at <http://www.nature.com/reprints>

Publisher's note Springer Nature remains neutral with regard to jurisdictional claims in published maps and institutional affiliations.

Open Access This article is licensed under a Creative Commons Attribution-NonCommercial-NoDerivatives 4.0 International License, which permits any non-commercial use, sharing, distribution and reproduction in any medium or format, as long as you give appropriate credit to the original author(s) and the source, provide a link to the Creative Commons licence, and indicate if you modified the licensed material. You do not have permission under this licence to share adapted material derived from this article or parts of it. The images or other third party material in this article are included in the article's Creative Commons licence, unless indicated otherwise in a credit line to the material. If material is not included in the article's Creative Commons licence and your intended use is not permitted by statutory regulation or exceeds the permitted use, you will need to obtain permission directly from the copyright holder. To view a copy of this licence, visit <http://creativecommons.org/licenses/by-nc-nd/4.0/>.

© The Author(s) 2024, corrected publication 2025

四、科研成果

1. 1. 专利授权证书：与鸡屠体性状相关的CYP27A1单核苷酸多态性分子标记及应用

证书号第7217285号



专利公告信息

发明专利证书

发明名称：与鸡屠体性状相关的CYP27A1单核苷酸多态性分子标记及应用

专利权人：华南农业大学;清远市清城区动物卫生防疫中心
清远市清城区清远鸡研究院

地址：510610 广东省广州市天河区五山

发明人：蔡柏林;何彤;周震;聂庆华;林铎;蔡丹凤;郭素茵;罗雪辉

专利号：ZL 2024 1 0080416.2

授权公告号：CN 117904314 B

专利申请日：2024年01月19日

授权公告日：2024年07月23日

申请日时申请人：华南农业大学;清远市清城区动物卫生防疫中心
清远市清城区清远鸡研究院

申请日时发明人：蔡柏林;何彤;周震;聂庆华;林铎;蔡丹凤;郭素茵;罗雪辉

国家知识产权局依照中华人民共和国专利法进行审查，决定授予专利权，并予以公告。
专利权自授权公告之日起生效。专利权有效性及专利权人变更等法律信息以专利登记簿记载为准。

局长
申长雨

申长雨



1. 2. 专利授权证书：与鸡屠体性状相关的SERCA2基因分子标记及其应用

证书号第6508168号



发明专利证书

发 明 名 称：与鸡屠体性状相关的SERCA2基因分子标记及其应用

发 明 人：聂庆华;马曼婷;蔡柏林;孔少芬;周震

专 利 号：ZL 2022 1 1150774.3

专 利 申 请 日：2022年09月21日

专 利 权 人：华南农业大学

地 址：510640 广东省广州市天河区五山华南农业大学

授权公告日：2023年11月24日 授权公告号：CN 116334235 B

国家知识产权局依照中华人民共和国专利法进行审查，决定授予专利权，颁发发明专利证书并在专利登记簿上予以登记。专利权自授权公告之日起生效。专利权期限为二十年，自申请日起算。

专利证书记载专利权登记时的法律状况。专利权的转移、质押、无效、终止、恢复和专利权人的姓名或名称、国籍、地址变更等事项记载在专利登记簿上。



局长
申长雨

申长雨



1.3. 专利授权证书：一种应用于小白鸡青脚性状的分子检测方法及其应用

证书号第6471537号



发明专利证书

发 明 名 称：一种应用于小白鸡青脚性状的分子检测方法及其应用

发 明 人：聂庆华;孔少芬;蔡柏林;周震;蔡丹凤;徐海平

专 利 号：ZL 2022 1 1625745.8

专 利 申 请 日：2022年12月13日

专 利 权 人：华南农业大学

地 址：510640 广东省广州市天河区五山华南农业大学

授权公告日：2023年11月10日

授权公告号：CN 116287287 B

国家知识产权局依照中华人民共和国专利法进行审查，决定授予专利权，颁发发明专利证书并在专利登记簿上予以登记。专利权自授权公告之日起生效。专利权期限为二十年，自申请日起算。

专利证书记载专利权登记时的法律状况。专利权的转移、质押、无效、终止、恢复和专利权人的姓名或名称、国籍、地址变更等事项记载在专利登记簿上。



局长
申长雨

申长雨



1.4. 专利授权证书：与鸡屠体性状相关的CRELD1基因分子标记及应用

证书号第5472714号



发明专利证书

发明名称：与鸡屠体性状相关的 CRELD1 基因分子标记及应用

发明人：聂庆华;周震;蔡柏林;蔡丹凤;孔少芬;徐海平;马曼婷
张静

专利号：ZL 2022 1 0230893.3

专利申请日：2022 年 03 月 10 日

专利权人：华南农业大学

地址：510610 广东省广州市天河区五山

授权公告日：2022 年 09 月 23 日

授权公告号：CN 114438231 B

国家知识产权局依照中华人民共和国专利法进行审查，决定授予专利权，颁发发明专利证书并在专利登记簿上予以登记。专利权自授权公告之日起生效。专利权期限为二十年，自申请日起算。

专利证书记载专利权登记时的法律状况。专利权的转移、质押、无效、终止、恢复和专利权人的姓名或名称、国籍、地址变更等事项记载在专利登记簿上。



局长
申长雨

申长雨



第 1 页 (共 2 页)
222

其他事项参见续页

五、其他业绩

1.1. 第十七届“挑战杯”广东大学生课外学术科技作品竞赛一等奖



获奖证书

华南农业大学

黄炜辰、温琪、张兆烽、陈希凡、罗俊 同学：

你(们)的作品《优质肉鸡屠宰性状的分选标记开发与应用》在第十七届“挑战杯”广东大学生课外学术科技作品竞赛中荣获

一等奖

指导老师：聂庆华、陈宇栋、蔡柏林



2023年11月

Journal of Animal Science and Biotechnology

2023 Best Paper Award

This certificate is awarded to

**Bolin Cai, Manting Ma, Zhen Zhou, Shaofen Kong, Jing Zhang,
Xiquan Zhang and Qinghua Nie**

For the paper

circPTPN4 regulates myogenesis via the miR-499-3p/NAMPT axis

Journal of Animal Science and Biotechnology 2022 13:2



Chinese Association of
Animal Science and
Veterinary Medicine

Defa Li

Prof. Defa Li
Editor-in-Chief



Journal of Animal
Science and
Biotechnology